Wangari

A Swarm of Water Bombing UAVs

Design Synthesis Exercise

Group 03

2nd July 2019

Technische Universiteit Delft

Delft University of Technology

Challenge the future

Wangari

Design Synthesis Exercise Final Report

by

Group 03

Bachelor of Aerospace Engineering
at the Delft University of Technology.

Authors:	Patricia Apostol	4561821
	Kars ter Beek	4290399
	Wissam Chalabi	4454537
	Leanne van Dam	4601777
	Berend Eikelenboom	4538870
	Max Koster	4491343
	Mees van Löben Sels	4438132
	Geert van der Velde	4554515
	Luke de Waal	4560000
	Liesbeth Wijn	4567080
Supervised by:	Dr. C. D. Rans	Principal tutor
	Ir. M. J. Schuurman	Principal tutor
	Ir. D. van Baelen	Coach
	Dr. X. Wang	Coach

TU Delft Delft University of Technology

Preface

This is the final report in a series of four, concluding the Design Synthesis Exercise for group 03. During the DSE, ten students of the faculty of Aerospace Engineering at Delft University of Technology have investigated the feasibility of a proposed concept: Water bombing UAVs. This would not have been possible without the valuable help of many people.

First of all, we would like to express our deepest gratitude to our tutors Calvin Rans and Michiel Schuurman as well as our coaches Dirk van Baelen and Xuerui Wang for their guidance and constructive feedback throughout the entire project. The tremendous effort and time they invested into improving the quality of our work is much valued.

We would also like to express our gratitude to ir. P. C. Roling for helping us prepare models of the design and dr. C. A. Dransfeld for providing us with great tools to carry out the concept selection, as well as to greatly improve our presentations. Additionally, we would like to thank Nimmi Sreekumar for helping us make beautiful renders and images of our design.

Finally, we would like to thank the OSCC and OSSAs, especially M. Beukelaer, for helping us improve the quality of our work throughout the project and assisting us in our logistical needs during the DSE.

Group 03
"I'll be a hummingbird; I will do the best I can."
- Dr. Wangari Maathai

Executive Summary

Introduction

As the climate crisis worsens, wildfires are increasing drastically. Not only is this a major threat to the environmental well being of the planet, but it is causing significant tangible damage to communities across the world, both financially and in terms of endangering people's lives. The so-called "fire season" is no more, as wildfires are burning all year long. With this intensifying situation, firefighting authorities look to aerial firefighters for support. Ground crews cannot approach such intense fires easily, and they can certainly not do it quickly enough to contain aggressive fires before they spread beyond control.

A literature study was complemented by conversations with firefighting experts, including representatives of local fire brigades, to understand the main demands to be met by aerial firefighting aircraft. The main overarching concerns were flight crew safety and cost. The operational demands were clear; initial attack time was the most important parameter, followed by dropping capacity, which can be achieved either by frequent drops, or aircraft with larger tanks. In general, a minimum of $2500L$ is expected for any good firefighting aircraft, and some of the biggest water tankers carry over $10000L$ at once. In order to achieve a higher drop frequency, aircraft that can refill their tanks from natural bodies of water are advantageous. These can be amphibious scooping fixed-wing aircraft or helicopters that can hover and pick up water using a snorkel or a bucket. Additional features that could further improve aerial firefighting are the potential of night time firefighting, which currently is restricted due to safety concerns, potential improvements to the tactical approaches used to make fire containment more efficient, as well as transportability, which would allow aircraft to be deployed to other regions of the world at different times of the year.

This report presents the design of a fixed-wing amphibious scooping unmanned aerial vehicle (UAV), that can carry and drop up to $4500L$ of water, which it can mix with retardant if required. The UAV is named Wangari, in honour of the late Dr. Wangari Maathai who was the first African woman to win the Nobel Peace Prize, and the first environmentalist to do so. She started movements in Kenya that led to the planting of over 50 million trees across Central Africa while improving women's rights in the region. In this summary, the final design is described after a brief description of the process that led to it. Then, the performance parameters exclusively related to firefighting are discussed. Finally, a note on sustainability is followed by the conclusion and recommendations.

Concept Selection

A long concept selection process was undertaken to come to the final concept. The main highlights of the process are the choice for a fixed-wing aircraft over a helicopter, and the choice for a single engine aircraft over a twin engine concept. The former was decided mainly due to the highlighted importance of initial attack time. Upon talks with firefighting experts, it became clear that in the initial attack, every second counts. Since fixed-wing aircraft can achieve higher cruise speeds to arrive at the fire scene quicker, this ultimately led to the elimination of helicopters from the selection process. As for the single engine, it was ultimately chosen as it would be easier to detach wings off a single engine aircraft to achieve higher transportability, and a single engine was deemed sufficient to power and carry payloads higher than the minimum of $2500L$ making it also the more sustainable option.

Design Evolution

The outcome of the concept selection was a single engine fixed-wing aircraft. Nevertheless, subsequent analysis resulted in multiple design iterations. Initially, the engine was directly placed in the vertical tail of the aircraft. This configuration, however, provided one major setback. Given that it was a design requirement to have the aircraft inherently stable, the large moment created by the placement of the propeller in the vertical tail inhibited the UAV's natural in-flight stability. In order to solve this issue, it was then considered to move the propeller on top of the fuselage closer to the c.g. of the aircraft. From a control perspective this was an improvement. Placing the engine on a pylon however was structurally more challenging. Furthermore, in order to meet the transportability requirement, the engine as well as the wings would always have to be removed from the fuselage. The other major setback of having the engine together with the propeller on top of the fuselage stemmed from aerodynamics. After a first calculation of the additional lift the high lift devices were able to generate, it was concluded that in order to be competitive with the current market leaders in terms of low speed performance, an additional method of lift augmentation was required. In consultation with a propulsion expert[1], key to this additional lift generation lies in the placement of the propellers over the wing such that the wing can benefit from the increased lift due to the additional induced propeller slipstream velocity. Hence, the finalised design is a twin prop fixed-wing configuration. The engine is placed within the fuselage for ease of wing detachability.

Final Design

In line with targeting the desired design parameters of safety, fast initial attack, transportability, and dropping capacity, the finalised UAV design can be seen in Figure 1.

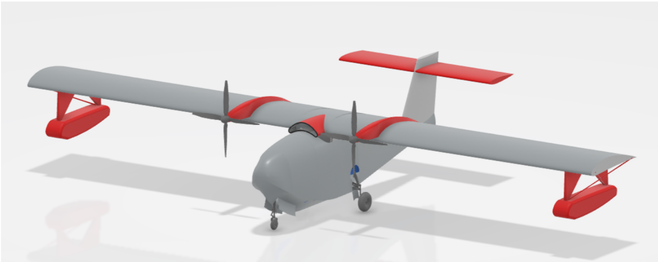

Figure 1: The final configuration of Wangari when stationary on land.

The twin-propeller fixed-wing UAV is powered by a single engine placed in the centre of the fuselage. In order to facilitate its scooping capability, and allow for enough clearance for the propellers, a high wing configuration was chosen. For stability during its water taxiing operations, retractable floats have been attached to the wing tips. Finally, Wangari possesses a full moving cruciform-tail, with the horizontal stabiliser placed in the wake of the propeller in order to benefit from the resultant velocity increase.

Transportability

UAVs are limited by extensive regulations in the zones where they can fly, especially across international borders. Given that a firefighting aircraft may be shared or used by several countries, this poses a high risk to its usability, even if it outperforms manned competitors. Therefore, a prime design driver for the UAV has been deployability.The wings and the horizontal tail of the UAV are detachable using a bolted connection to the fuselage. The ease of transportability is also reflected in the position of the engine within the fuselage to avoid a complex engine-removal process in disassembly. The modularity of the UAV enables two units to fit in the cargo hold of the A400M transport aircraft as seen in Figure 2. Additionally, the UAV fits in a standard extra tall ISO shipping container.

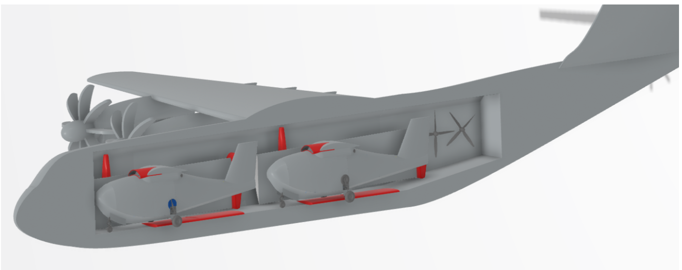

Figure 2: Two Wangari UAVs transported in an A400M.

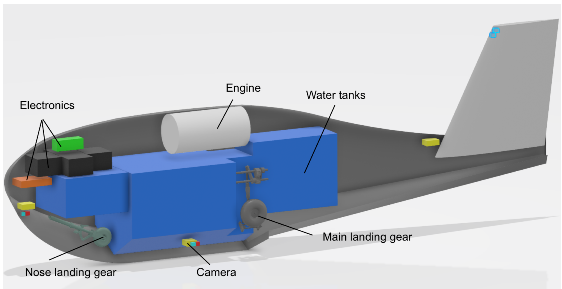

Figure 3: Overview of the internal layout.

Safety

As a UAV, safety risks for the pilots are already mitigated. Nonetheless, safety for those on the ground as well as for other aircraft within the airspace is important. The UAV is equipped with sensors and cameras forming a navigation system able to detect other UAVs as well as ground crew. Finally, an air attack aircraft is assumed to be on site of the fire, and is used to ensure connection when the link between the ground station and UAV is disturbed due to the harsh fire environment. In case this should also fail, any given UAV may communicate with the ground station via another approaching

[1] Joris Melkert, Lecturer, Flight Performance and Propulsion, TU Delft

UAV.

The aircraft shall be able to manage the harsh conditions of the firefighting mission. Hence, the materials selected are highly corrosion and heat resistant. The heat resistance is also crucial for the correct functioning of the equipment on board. As composites have great corrosion resistance, an epoxy S-glass fibre material in a sandwich panel with Nomex as core material is used for the hull structure. The wing is made of aluminium, not only for its superior fatigue performance in comparison to composites but also for its easily detectable damage before failure. In order to increase the corrosion resistance of the aluminium, a five layer coating is applied.

A final safety consideration may be taken into account in the float design. Allowing for the floats to be retractable reduces the risk of a float touching the water surface during the scooping manoeuvre at high speeds.

Internal Systems

The water and retardant tanks are the largest internal components of the UAV. They are shaped to allow for enough space to accommodate the main and nose landing gear. The nose gear retracts to an almost horizontal position into the fuselage whilst the main gear can vertically retract to an external position close to the water tanks. For longitudinal stability during flight, heavy components such as the batteries and electronics have been placed near the nose. A finalised internal layout is shown in Figure 3.

An engine powering the propellers is placed in the centre of the fuselage, slightly elevated into a nacelle and incorporates the generator in order to power the batteries during flight. The batteries can be used as a backup power system. The fuel tanks, providing the propellant for the engine, are not directly visible in Figure 3 as they have been placed as bladders directly in the wing, which improves their ease of removal in disassembly.

Finally, the UAV possesses an electro-hydraulic actuation system. control commands are sent electronically by the pilot to the actuator, which is equipped with an internal hydraulic system to provide the actuation force. This eliminates the need for a heavy, high power consuming hydraulic unit. The actuation system is fully designed with redundancy using both fail safe and safe life principles.

Flight Performance

The flight performance requirements of the Wangari UAV were based on its special and specific mission, firefighting. The driving performance factors that came forth from this were: Have a high a allowable load factor, have a high manoeuvrability have in general good performance at low speeds, and have a fast initial attack. The allowable load factors of the aircraft were sized to the maximum load factors allowed stated in CS23. Which resulted in the maximum manoeuvring loads being 4.4, and -1; and 6.8, and -2.6 when the gust loading are applied. Afterwards as basis for all flight performance calculations the airfoil was selected. The airfoil selected is the NACA 6415, and was chosen for its high $C_{l_{max}}$ of 1.6, low zero lift angle, and its relatively high $\frac{t}{c}$ ratio. The results of the flight performance analysis, after going through some iterations, can be seen in Table 1.

Table 1: Summary of the flight performance numbers.

V_{stall} [km/h]	123.5
V_{cruise} [km/h]	405
s_{TO} [m]	500
s_L [m]	500
RC [m/s]	>10

Next to this also the banking angles achievable were analysed and it was found that the UAV is able to sustain, and even climb at bank angles of up to 60 degrees.

Firefighting Performance

The Wangari UAV has been designed with a specific mission in mind, one where the distance from the base to the fire is $50km$ and the distance between the fire and the nearest water body $10km$. However this is the average mission, and the average missino is of course not always the mission that will be flown. Therefore also different missions were analysed. For different distances between airbase and fire the initial attack time was calculated for the CL-415, AT802 Fire Boss and

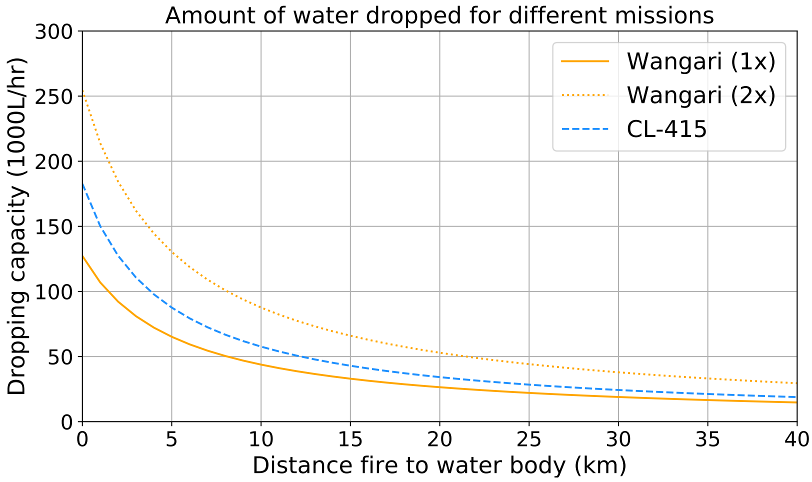

Figure 4: Amount of water dropped per hour for different distances between fire and water body.

the Wangari, refill time for different mission difference was also calculated for the same set of aircraft. From this analysis the conclusion can be drawn that the Wangari outperforms the other aircraft, independent of the mission distance. Next to the attack times also the dropping capacity of the CL-415 and the Wangari are compared in Figure 4. It can be seen in this figure that one CL-415 out performs one Wangari UAV, however it should be noted that one Wangari UAV costs about half of a CL-415, so for a fair comparison the performance of two Wangari UAVs is also plotted.

Payload capacity

The payload capacity of the UAV is $4500L$, however depending on the mission the UAV may start out with a payload of $2500L$ to take more fuel on board. This trade-off is advantageous to the total water dropped in the mission due to the extra mission time obtained because of the extra fuel on board. However just like the mission design the payload needs to be versatile to accommodate different missions. Taking off without any payload on board may be considered to have a more efficient cruise phase. Alternatively, the maximum amount of payload may be chosen at the beginning because the initial attack is the more important than the longevity of the mission.

Scooping

For acquiring the water payload, Wangari has two options, either filling the tanks via the overflow vents on land or by scooping. To recover when scooping, the UAV is designed to land on water. While scooping the UAV flies low above the water and exerts a scooping mechanism through which the water flows in the water tank. The scooping mechanism is comparable with the scooping mechanism used on the CL-415.

During the scooping the aircraft is stable and controllable due to its horizontal tail surface. The scooping mechanism adds a drag component to the downside of the fuselage, which adds a pitch-down moment on the UAV. As the size of the scooping mechanisms is not big ($0.0051 m^2$ per scooper), the added moment is negligible when compared to the moment when landing on the water. This is the determining case for the horizontal tail size.

Dropping

The dropping mechanism influences the properties of the containment line. Different dropping mechanisms exist nowadays, each having their advantages and disadvantages. The optimal dropping mechanism is determined to consist of a combination between a constant flow door and a pressurised system. The advantage of having a constant flow door is that the containment line on the ground will contain a constant volume of retardant per surface area. The advantage of having a pressurised system is that the line can be made wider, due to the velocity of the retardant when exiting the tank being higher, which means that the drop will be less affected by the wind. However, having an active pressurised system is heavy and requires a waiting delay of several minutes to pressurise the tank on the ground. To combine the advantages of those mechanisms, an innovative dropping method was designed. The technique consists of performing manoeuvres, to passively pressurise the retardant in the tank using the force of gravity, while also having sliding doors to keep the flow constant over time. After an analysis, the conclusion was that it is an efficient dropping technique.

The dropping of the retardant on the fire can have a disastrous effect on the stability and controllability of the UAV, if not assessed properly. In a few seconds, 50% of the MTOW is lost. However, the horizontal c.g. shift is limited to 7 millimetres, which means the consequences of dropping the payload on the stability is limited.

Firefighting Strategies

A fire simulation is in continuous development producing video simulations that show fire spreading behaviour. The simulation takes into account a range of parameters including wind direction and speed, elevation profile of the area, fire fuel availability and dryness, evaporation rates of dropped retardant, retardant effectiveness, and fire intensity. The fire simulation can be used to generate several fire scenario cases, which can be used to investigate firefighting tactics.

To investigate the usefulness of swarming, meaning the use of several smaller aircraft as opposed to fewer larger aircraft, for firefighting missions, two fire scenarios are set up and the performance of several UAVs is compared to the performance of fewer Canadair CL-415 aircraft. The CL-415 aircraft is used for comparison as it is considered the strongest competitor. Since the cost of one CL-415 is comparable to that of two Wangari UAVs, the comparison is done on that basis. Swarming was found to be extremely useful, especially in intense and aggressive fires.

Sustainability

The aforementioned passive dropping system goes directly in line with the sustainability considerations present throughout the entire design process. As an actively pressurised system would induce additional weight the system resulting in an increase in fuel consumption. Minimising the fuel consumption was also reflected in choosing a single engine over a twin engine aircraft. Sustainable materials were chosen for the components throughout the entire design. Finally, the UAV may also fit in a shipping container and not just the A400M cargo aircraft, in order to facilitate the possibility of more sustainable deployment.

Conclusion & Recommendations

The Wangari system has shown the potential of strategic firefighting, already outperforming the current market alternatives in fire simulations, by means of swarming and its innovative dropping capabilities.
At the current state the UAV is highly cost-competitive with the current market leaders such as the CL-415. A conservative estimate, based on the production and sales of 60 UAVs within 5 years, prices a single UAV at 10.63 million euros. This is just under half the price of a single CL-415, which is capable of delivering 6317L of suppressant. This gives the Wangari system a great advantage given that for the same cost, two Wangaris are capable of providing up to 1.5 times the payload.
The main risks going forward is the fact that the direct competitor is working on an update of their existing water bombing aircraft, potentially bringing strong competition for the UAV. Besides this, in terms of performance and maintenance the drivetrain induces risk for the UAV, as a complex drivetrain was created such that the UAV remains easily transportable. This concerned an engine inside of the fuselage, which means that it is hard to access for maintenance, and that it may have an impact on the performance of the instruments on board. Moreover, further investigation of the sloshing in the water tanks is needed as this could have hazardous effects on the stability of the UAV.
Based on the feasibility assessment of the current design, it is highly recommended to continue the design process of the Wangari system to introduce a more safe and strategic aerial firefighter to the world.

Contents

1 Introduction

In the current age of climate crisis, temperatures are rapidly rising, causing wildfires to ignite all over the world. This leads to more greenhouse gas emissions and further global temperature increase, the impacts of which are already witnessed across the world. Wangari Maathai, born in the remote village of Ihithe, Kenya, responded in 1977 already to the needs of rural African women who reported that their streams were drying up, their food supply was less secure, and they had to walk further and further to get firewood for fuel and fencing, by setting up the Green Belt Movement. A movement that strives to reduce the impact of climate change by saving forests. The Green Belt Movement reports that immediate human action is required to put out the wildfires and save the world from rising to even higher temperatures. Aerial support can be an invaluable resource in firefighting efforts. The majority of existing firefighting aircraft are, however, not designed specifically for this dangerous type of mission. Old military and agricultural aircraft have been converted to carry and drop fire suppressant, which causes them to operate far outside of their flight envelopes and hinders them from excelling at crucial aspects such as pilot safety, range, speed, and fire containment efficiency. Wangari Maathai, who became the first environmentalist to win the Nobel Peace Prize, and her Green Belt Movement have been an inspiration to the group to help reduce the impact of climate change by specifically designing an unmanned aerial vehicle for the firefighting mission. The objective of this project was therefore to develop a preliminary design that excels at the aforementioned crucial aspects and revolutionises aerial firefighting with innovations such as tactical swarm attacks, night firefighting, and passively pressurised fire retardant drops.

This report is written to provide insight into the feasibility of the amphibious design concept, named in honour of Dr. Wangari Maathai, to present the current state of the design, and make recommendations for future research. This is done using system engineering tools, qualitative analyses, preliminary design calculations and statistical models.

The report is divided into four parts. In part I, an analysis of the current aerial firefighting market is performed to establish the problem, needs and opportunities. Therefrom, the functionalities of the potential concepts have been determined and a final concept is selected. In part II, the selected concept is described in detail by analysing its flight and firefighting performance, for which an extensive fire simulation model was created to investigate the advantage of swarm firefighting. In part III, the described concept is evaluated in terms of mission and requirement compliance as well as reliability and sustainability. Finally, in part IV, recommendations for future design steps as well as a manufacturing plan and financial analysis are presented.

Part I

Project Definition

2
Aerial Firefighting Market Analysis

Wildfires have increased drastically in numbers over the past years as a result of climate change. Aerial firefighting can be an effective tool to help contain aggressive fires. However, current firefighting aircraft are failing to meet this need due to several factors, most of which are due to the fact that these aircraft were not originally designed for firefighting. The one exception is the Canadian CL-415 aircraft, but even this firefighting aircraft faces big challenges, such as the danger of operations for its flight crew, its limited cruise speed, and regulations that restrict it to operating only during the day. The UAV design can revolutionise aerial firefighting with regards to these parameters, as well as introduce the swarming strategy, meaning that several UAVs simultaneously dropping retardant can increase the effectiveness and success of missions in comparison to large aircraft dropping large amounts of retardant once at a time. This would favour stakeholders as endangered flight crew and inhabitants of fire prone areas, manufacturers and potential buyers such as governments, and ultimately all life on Earth as greenhouse emissions will be reduced.

2.1. State of Wildfires in 2019

The climate crisis is worsening beyond common perception. In 2018, the World Meteorological Organisation published a report [1], whereof the results cause great concern. Namely, the years 2015-2018 have been the warmest on record, with the trend continuing to deteriorate. This is clear to many populations who lately observed the effects of the crisis firsthand, through unprecedentedly hot summers, a drastic increase in heavy rain and flooding[1], and a shocking increase in forest fires, as shown in Figure 2.1 and Figure 2.2. These figures, provided by the EFFIS (European Forest Fire Information System), show the number of fires and the area burnt in the first half of 2019 in the EU, compared to the averages of the past decade (2008-2018). Not only do they highlight the increase in forest fires by more than eight times, they also show an important and concerning fact: the concept of "fire season" is coming to an end. Figure 2.1 shows that the number of fires in Europe in 2019 has already exceeded the maximum number of fires of the past decade in early March. Whereas in the past, such high numbers were only reached by the end of the fire season around October. Furthermore, whilst these figures show the average over the EU, the situation is much more severe in the most affected countries, France, Spain, and Romania. The seasonal trends of every country are made visible on the EFFIS website. [2] Although most wildfires are caused by negligence and human instigation, the trend is still attributed to the climate crisis, since the increasingly hot and dry weather eases the probabilities of wildfires to ignite and spread faster. [3]

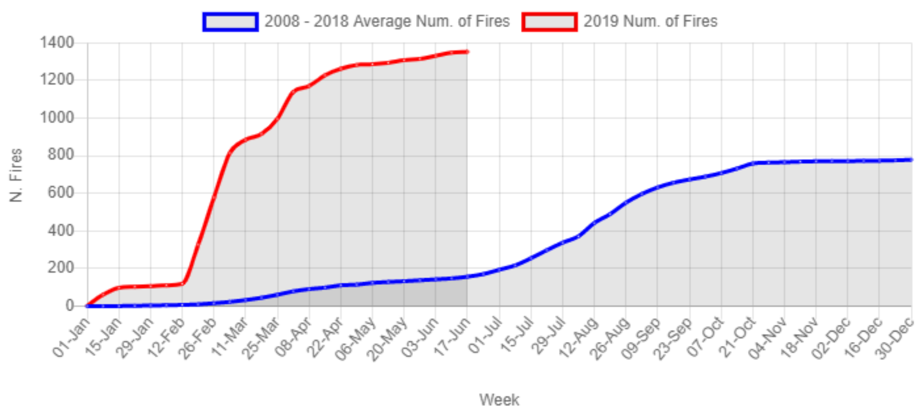

Figure 2.1: Number of wildfires in the EU larger than 30ha during the first half of 2019 in comparison to the average of the past decade (2008-2018).[2]

[1] https://www.theguardian.com/environment/2018/mar/21/flooding-and-heavy-rains-rise-50-worldwide-in-a-decade-figures-show [cited 18 June 2019]
[2] http://effis.jrc.ec.europa.eu/static/effis_current_situation/public/index.html [cited 17 June 2019]
[3] https://www.nationalgeographic.com/environment/natural-disasters/wildfires/ [cited 17 June 2019]

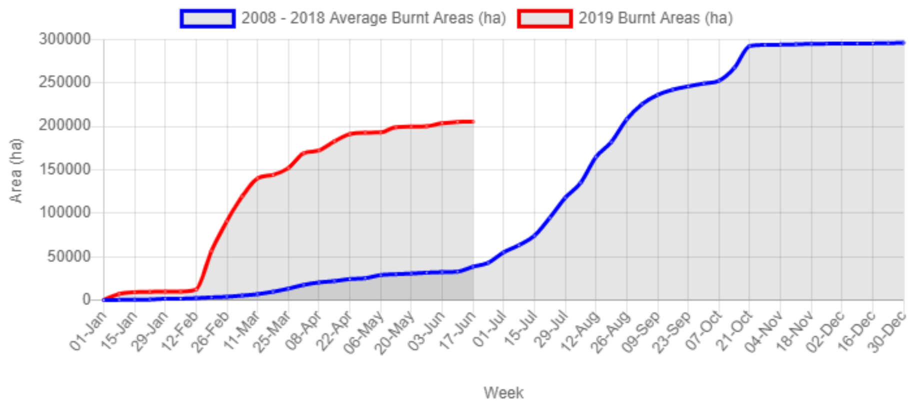

Figure 2.2: Total burnt area in the EU by wildfires larger than 30ha during the first half of 2019 in comparison to the average of the past decade (2008-2018).[2]

The wildfire crisis is not only severe in Europe. Unfortunately, it is intensifying around the world, as evidenced by the NASA satellite image in Figure 2.3.

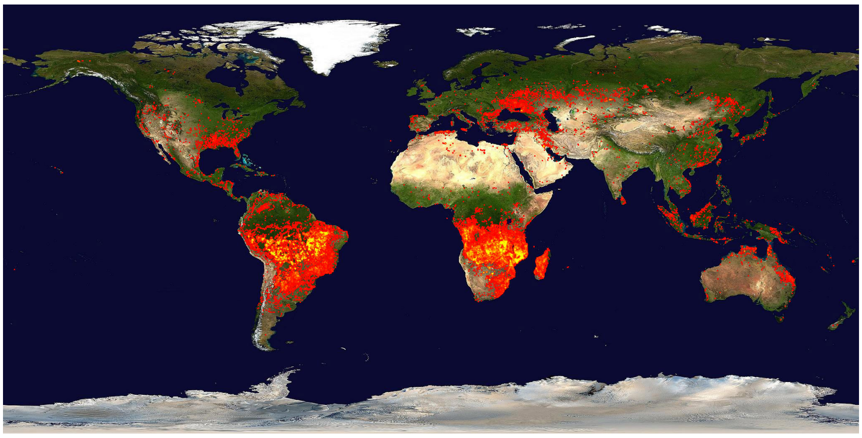

Figure 2.3: Spread of wildfires around the world.[4]

2.2. Aerial Firefighting Needs

National agencies are responding to the crisis with useful educational campaigns, to ensure that people are more cautious in hazardous areas and minimise the risk of igniting wildfires. Unfortunately, as demonstrated by the frequency of large fires in Figure 2.1, this is not enough and fire suppression efforts are still urgently needed. Ground crews are often too late to arrive at an aggressive fire or have difficulties in coming close enough to the fire in order to contain and extinguish it. For these reasons, aerial firefighting is an useful resource that many fire agencies rely on to reach far away fires quickly and try to contain them, as well as cool them down, such that the ground crew can more easily reach and control the fire. Before making decisions for a preliminary design, it is useful to study and understand the desired performance parameters of aerial firefighting aircraft. For this, a literature study was performed and complemented by interviews with several firefighting experts to gain insights into what is most needed. This resulted in the following desirable parameters:

Short initial attack time
Arriving at the fire as fast as possible is one of the most desirable parameters in any type of fire suppression effort. If the fire can be contained quickly, before it has had a chance to spread, it remains smaller and is, therefore, much easier to control. This saves areas of land from getting burnt as well as major costs associated with the potential escape and larger spread of the fire. The Forest Fire Danger Index (FFDI) in Figure 2.4 describes the severity of the fire based on its intensity and spread potential. Figure 2.4 shows that aerial firefighting support is most helpful when it has a shorter time

[4] `https://www.nasa.gov/images/content/484444main_firemap-2048x1024.jpg` [cited 26 June 2019]

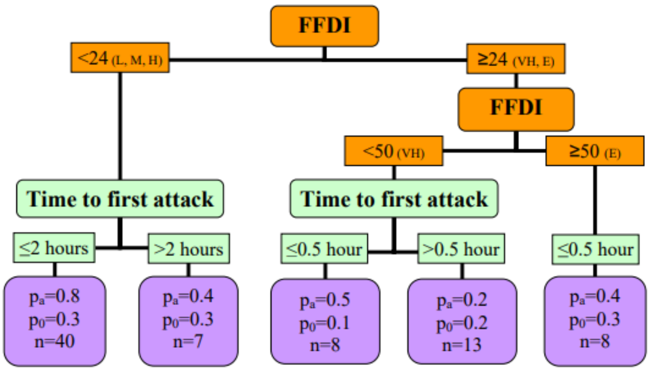

Figure 2.4: The probability of first attack success, using FFDI and time to first attack, with and without aerial firefighting [5].
L,M,H,VH,E: Low, Medium, High, Very High, Extreme categories of FFDI.
p_a: probability of first attack success with aerial suppression support.
p_0: probability of first attack success without aerial suppression support.
n: number of fires accounted for in each section.

to first attack. Namely, the probability of success increases from 0.3 to 0.8 when the time to first attack is within 2 hours for low, medium, and high danger fires; and from 0.1 to 0.5 when the time to first attack is within half an hour for very high danger fires. In conclusion, it is desirable for firefighting aircraft to be quickly deployable and have high speeds to reach the fire quickly.

Safety for flight crew

Aerial firefighting is a dangerous task. Pilots, an important group of stakeholders, are flying in an environment with limited visibility, frequent turbulence and difficulty to maintain balance amid wind gusts, and are expected to carry out dangerous manoeuvres, often in rocky terrain. After several drops, the limitations of human perception can tempt pilots to be less careful and perform more dangerous manoeuvres, or fly at dangerously low altitudes near the fire. In the United States alone, 78 fatalities from aerial firefighting were recorded between the years 2000-2013 [2]. These safety concerns have impactful implications on aerial firefighting services. One of the main compromises made, is to limit firefighting operation times. A pilot can only fly for a limited duration, and only during daytime when visibility is not restricted. This means that nightly aerial firefighting is rarely performed, which is a big loss to any firefighting unit since night time operations have many advantages. Temperatures are cooler and wind speeds are lower, making the fire easier to control [3]. Hence, water bombers can be even more effective in assisting ground crews to contain and extinguish the fire. The need for a firefighting aircraft that can operate at night time without exposing flight crews to the dangers associated with low visibility is pressing.

Ability to scoop water from natural water bodies

The frequency of drops is intuitively an important aspect of aerial firefighting. The ability of an aircraft to make more drops within a given time, can translate into faster containment or extinguishing of the fire. Large tankers make large drops of 10,000L or more, which is an impressive volume, but afterwards they have to return to the airbase, which may be far from the fire, in order to refill their retardant tanks. The flying back, refilling, and heading again to the fire is a time consuming mission. In fast spreading fires where seconds count, this is a serious limitation. Aircraft that have a capability to collect water from nearby water bodies have a clear advantage. Currently, two types of aircraft can do this. Helicopters are able to collect water by hovering and using a snorkel or a bucket, and seaplanes can scoop up water from large lakes by skimming the surface of the water body. Since helicopters have a serious disadvantage related to their initial attack, the importance of which is elaborated upon in Figure 2.4, the need can be narrowed down to an aircraft that can access as many water bodies as possible, and is able to collect water therefrom.

Ability to drop large volumes of suppressant

For any fire, a certain minimum amount of suppressant is needed to contain or extinguish it. Larger dropped volumes are therefore desirable. This can be achieved by having a large capacity in one aircraft, or by having an aircraft that is able to make more frequent drops to achieve the same amount of dropped suppressant per unit time.

Ability to make effective drops of suppressant

Naturally, more volume of suppressant is desirable and helpful in aerial firefighting. However, more volume does not necessarily mean more effective firefighting, resulting in smaller areas burnt. For instance, a large aircraft that cannot fly at low altitudes or at slow speeds during the drop, will be ineffective at aiming the drop at the right place. The liquid dropped may be dispersed over a large area, resulting in a low coverage level in L/m^2, which may not slow down or stop the fire from spreading. There are two types of dropping mechanisms that firefighting aircraft are currently equipped with. The first is a passive system, where a door on the bottom of the aircraft opens and the retardant is released, and the second is a pressurised dropping system where a heavier system is installed to actively push out the water. The first passive system is cheaper and lighter, but is wasteful and less effective, since the dispersal of the water dropped causes ineffective coverage levels on the ground. Whilst the second active system is more effective and sustainable in the sense that it does not waste the retardant, it is a heavier, more costly, and more energy consuming system. The need for a cheap and sustainable dropping system that is also effective at controlling retardant drops is yet to be met.

Sustainability
Firefighting is an emergency response field. If a house is on fire, it is more sustainable for the fire brigade overall to drive a truck to the house and put out the fire quickly, than take a bicycle to emit vehicle emissions, only to arrive to a burning neighbourhood. Similarly, the overarching sustainability issue in aerial firefighting is to have efficient aircraft that can arrive at the fire quickly, and are able to frequently drop large amounts of suppressant, and do so in an effective way such that the dropped liquid actually stops the fire from spreading and causing devastating damage to the environment. Since sustainability is at the centre of the aircraft mission, the focus is on highly performing aircraft rather than traditional interpretations of sustainable designs. For example, an electric aircraft that is powered by batteries may cause less greenhouse gas emissions but it will have a lower endurance. Hence, it will need to land to recharge batteries, all during valuable mission time whilst the fire is burning and causing comparatively massive emissions. Nonetheless, characteristics such as efficient engines that burn less fuel, reusable materials, effective dropping systems, and weight reducing measures that make the aircraft require less fuel, are all good examples of how even an emergency response vehicle can meet certain sustainability standards.

2.3. Competition

The main competition in aerial firefighters is the CL-415, currently the only fixed-wing aircraft specifically designed for firefighting missions. The CL-415, first produced by Canadair in 1991, classifies as a flying boat. It has a drop capacity of 6137 litres, which it can scoop up from water bodies in 12 seconds over a length of 1341 metres. Since 1991, 95 CL-415 have been delivered, its main customers being the governments of Canada, France and Italy. The unit price of a CL-415 is about 25 million euros.[4] Hence, to satisfy the main buying stakeholders, governments, the unit price of an equal or better performing system of Wangari UAVs must be lower than 25 million euro.
Other existing firefighting craft that could possible be competition are helicopters such as the Sikorsky S-64 Skycrane, having a capacity of 9463 litres, and the S-70 Firehawk, having a capacity of 7571 litres.

2.4. Side-markets

Apart from firefighting, the UAV can also be employed for other tasks. Its big water tank, large fuel capacity and therefore great endurance and range give it a wide variety of missions in which it can be put to use. The agricultural, cargo/disaster relief, and surveillance uses are the three cases that will be elaborated on.

2.4.1. Agricultural applications
As the UAV is equipped with a big water tank and varied dropping capabilities, the UAV can be put to use very well on agricultural tasks. Watering the crops with a UAV, which is able to control its drop pattern and able to refill on the nearest water source, makes it worthy competition to general agricultural aircraft. Next to watering the crops, it can also be used to apply pesticides or fertiliser to the crops. These common agricultural tasks can easily be performed by the UAV.

2.4.2. Cargo Transport
With an adjustment to the water tank, a cargo capacity of $4500L$ can be made available. This could be done by adding a door to the fuselage and water tank, through which the cargo can be loaded in. If the UAV has cargo transport capabilities, it could be put to use in disaster relief instances. In remote areas it can make use of its amphibious qualities and land on nearby bodies of water. A landing/take-off distance of around $600m$ opens up the possibility to land at smaller airfields, that bigger cargo aircraft have difficulty to land at. Having multiple UAVs opens up the possibility to deliver emergency products in a coordinated manner to an affected area.

2.4.3. Surveillance

Using the cameras equipped on the UAV it could be put to use very well for surveillance. It contains four normal cameras and four infrared (IR) cameras. This means, it has got great capability for remote surveillance and night operations. The IR cameras can also be put to use when looking for heat sources (e.g. people).

2.5. SWOT Analysis

To gain more insight in the market position of the UAV, a SWOT (Strengths, Weaknesses, Opportunities and Threats) analysis has been performed. The strengths and weaknesses are internal, based on the UAV; the opportunities and threats are based on external parameters, i.e., the market. The SWOT is visualised in Figure 2.5.

The strengths of the UAV can be summarised by its unmanned characteristics, its ability to vary the drop pattern, its great tank capacity and its transportability. Being a UAV is a strength as it reduces the chances of pilot fatalities incredibly. Moreover, the unmanned nature frees it from the need to adhere to limiting pilot flight time and g-force regulations, making it able to fly for a longer amount of time and perform more dangerous manoeuvres. By being transportable in an A400M, the deployable range of the UAV is increased, enabling it to move along with the fire season across the globe within the cargo compartment of the A400M.

Potential disadvantages consist of the fact that it needs a whole system to operate (e.g., the CL-415 does not need a ground station, just the air attack) and that a lag between the ground system and the UAV could result in loss of performance.

The main threat is the fact that there are little regulations established for (amphibious) UAVs yet, which could slow down the certification process, and, therefore, delay the development. Another threat could be that the follow up for the CL-415 is being developed, the CL-515. The CL-515 is directly based on an existing design, so the certification is likely to go more quickly than that of the UAV.

A major opportunity for the UAV is that, unfortunately, the demand for aerial firefighting is increasing but, therefore, also the budget of stakeholders for aerial firefighting aircraft is increasing.

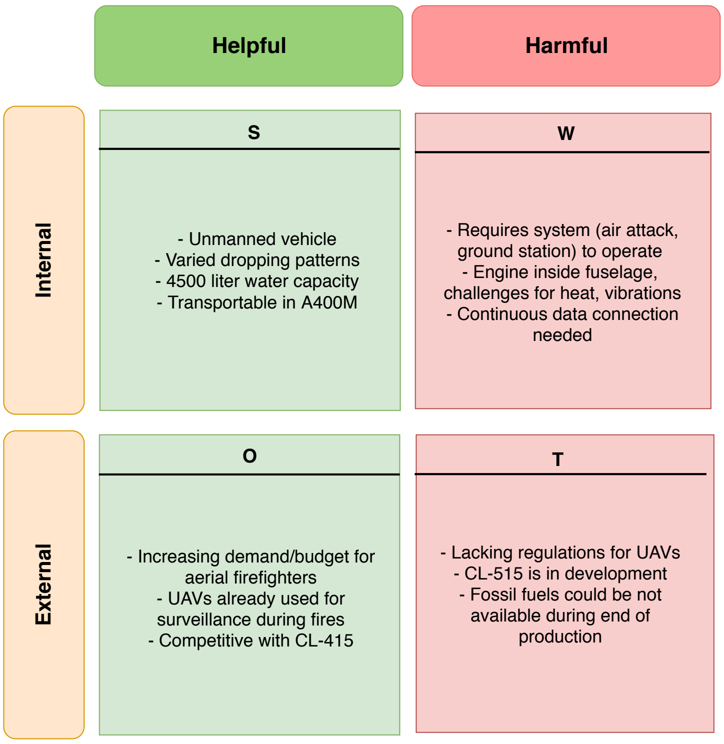

Figure 2.5: SWOT for the UAV based on the market analysis.

3
Problem Definition

Taking into account the previously established problems and needs in aerial firefighting, the following Mission Need Statement has been defined:

MNS : **"Tackle the need for a safe and strategic aerial firefighting system."**

The keywords in the MNS are *"safe"* and *"strategic"*. The goal is to make aerial firefighting safer by making the vehicle unmanned, and by this reducing pilot fatalities in firefighting. With the keyword "strategic", it is meant that extra development and research will be spent on how deploying multiple, smaller UAVs, which will have the opportunity to fly in swarms and strategically lay lines, will improve the efficiency of aerial firefighting. If successful, aerial firefighting will be significantly improved in terms of pilot fatalities.

For the project as a whole, a Project Objective Statement has been decided upon by the team:

POS : **"Design a UAV system that can more safely and strategically attack wildfires, within ten weeks by ten students, with the goal of winning the DSE Symposium."**

The team decided that winning the symposium is the ultimate goal of the project. Every major decision made, should be in consideration with this goal. Here again, the keywords are *"safely"* and *"strategically"*. The emphasis of the team will be on the strategic aspect. By using smaller aerial firefighter UAVs, firefighters should be able to contain the fire in a more strategic manner than with existing technology. Having the capability to quickly lay lines in a smart manner, is a big advantage of having multiple UAVs, hence, a focus of the project.

4
Functional Analysis

In the previous chapter a project objective has been defined. In this chapter, the requirements of the concept to meet the objectives have been analysed. This is done by firstly analysing the mission of the aerial firefighting UAV, which is found to be fulfilling the air tanker role in the containment of wildfires. From this mission analysis, functionalities of the UAV could be defined, of which the most important ones are found to be quickly arriving at a fire, scooping up water, and dropping suppressant. For the UAV to achieve these functionalities, requirements are set in addition to those set by the stakeholders, which mainly concerned transportability, safety and sustainability.

4.1. Purpose of Mission

Aircraft used for firefighting can take on different roles during the mission of fighting a wildfire. Two of the most common roles it can perform are those of the air attack and the air tanker. Whereas the air attack keeps an overview of the wildfire and all other aircraft involved, the air tanker is the aircraft that actually fights the wildfire. It is named air tanker, because it is the aircraft that is provided with a tank that can hold large quantities of fire suppressant which is eventually dropped at the location of the wildfire. It has been decided that the UAV will have the air tanker role. This decision has been made by the stakeholders and is thus to be adhered to. Although attention should also be payed to the air attack within the to be designed aerial firefighting system as a form of communication should be established. However, this will be in significantly less detail than the design of the air tanker UAV.

The air tanker can then again have two different purposes; it can either contain, or extinguish a wildfire. A decision had to be made before setting up the requirements, as both functions demand different capabilities of the UAV. Also, different concepts excel in different functions within an aerial firefighting mission. The concepts for the design of the air tanker will be further discussed in chapter 5.

Extinguishing a wildfire may seem like the most effective function to put out wildfires; the intensity of the fire is decreased by applying water directly to the fire. However, as the suppressant will be dropped directly above the fire, a large portion of the suppressant will have been evaporated by the time it can have an extinguishing effect on the fire. Also, an air tanker that extinguishes fire will have to be able to withstand more extreme flight conditions. For instance direct smoke and increased temperature will result in a decreased density of the air, resulting in a lowered performance of the aircraft.

Containing the fire will ensure that fire does not get past certain boundaries. This can be achieved by 'laying lines', dropping large amounts of suppressant in a line to slow down the spreading of the fire. The fire will then either be extinguished by the ground crew or will burn out itself. A disadvantage of containing the fire instead of extinguishing it, is, however, that the intensity of the fire is not lowered. Although this procedure sounds objectionable, ensuring that the fire does not grow is of greater importance and considered to be more effective [5]. This, and the less extreme flight conditions experienced during the containment of wildfires (smoke will still be present, but the temperature will be significantly lower than directly above the fire), has led to the decision of designing the UAV with a focus on containing wildfires.

The decision of ensuring that the UAV will be best at containing wildfires, rather than extinguishing them, is verified with the use of a fire simulation tool. It has been shown that indeed containing wildfires is more effective in the sense of lower evaporation rates and higher coverage levels. The exact workings of the simulation tool will be addressed in chapter 9.

The UAVs will fly within a system, which can differ in number of UAVs, ensuring that the system is highly adaptable to different sizes and intensities of wildfires. The purpose of letting the UAVs fly as part of a larger system is to drop the suppressant as strategically as possible, making use of each litre of suppressant dropped. This strategy will depend on the amount of suppressant the UAV can take along and how many UAVs are available. Further investigation is again done using the fire simulation.

The UAVs may also be able to operate more efficiently during general flight than current aerial firefighters as flying in formation to the fire will potentially result in a reduction of fuel used. This will allow for longer missions and/or a reduction of emissions by the UAVs.

4.2. Mission Functionalities

Determining the functions of the air tanker will lead to certain requirements that have to be met by the UAV. In order to assess these functions, a flight profile diagram has been established. This diagram can be found in Figure 4.1. Multiple phases throughout a single mission of the UAV are shown in the figure, in which the horizontal axis displays the distance covered during the mission and the vertical axis shows the altitude at which each phase is executed (note that the figure is not to scale). Each phase is numbered, a brief description of all phases is given in Table 4.1. Further explanation with regards to the specific altitudes and distances is discussed in section 7.3. The phases are distributed amongst three different parts of the flight: initial attack, refill, and back to base. Each mission will consist at least of the initial attack and back to base section. Depending on the number of refills needed, the refill part is present multiple times.

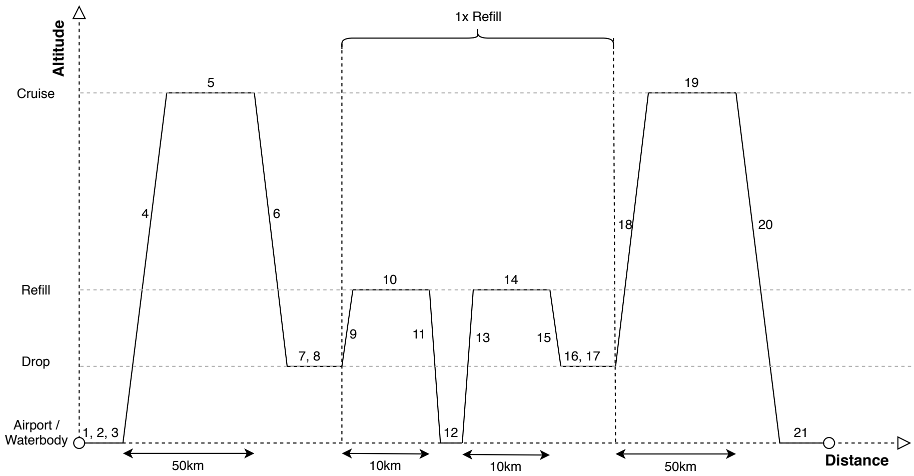

Figure 4.1: Flight profile diagram of Wangari, phases are described in Table 4.1. Note: the axes are not scaled.

Table 4.1: Description of flight phases visualised and numbered in Figure 4.1, phases are divided in three parts: initial attack, refill and back to base.

#	Description - Initial Attack
1	Engine start and warm-up
2	Taxi
3	Take-off
4	Climb to cruise altitude
5	Cruise to fire
6	Descent to drop location
7	Drop suppressant
8	Flight to climb location

#	Description - Refill
9	Climb to refill altitude
10	Cruise to water body
11	Descent to water body
12	Scoop up water
13	Climb to refill altitude
14	Cruise to fire
15	Descent to drop location
16	Drop suppressant
17	Flight to climb location

#	Description - Back to Base
18	Climb to cruise alitude.
19	Cruise to airport
20	Descent to ground
21	Landing, taxi and shut-down

From the flight profile diagram several abilities of the UAV can be determined. These follow from the different phases the UAV will go through, which have been summarised in a functional flow diagram, of which the top level is visible in Figure 4.2. The main aspects that should be taken care of when designing the UAV follow from the functional breakdown structure, visible in Figure 4.3, and flight profile diagram, and are proposed in the following part of this section.

Fast initial attack

As mentioned in section 2.2, the initial attack of an aerial firefighter is of utmost importance. The UAV should be readily available (possibly stored with fuel, retardant and water to save precious time), able to reach high cruise speeds (the faster, the better) and should be versatile enough such that it can operate for different kind of fires (carrying varying

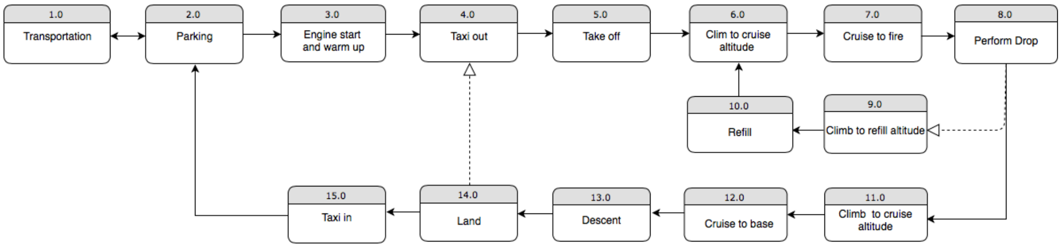

Figure 4.2: Top level of the functional flow diagram of the Wangari. Dotted line show an alternative flow path.

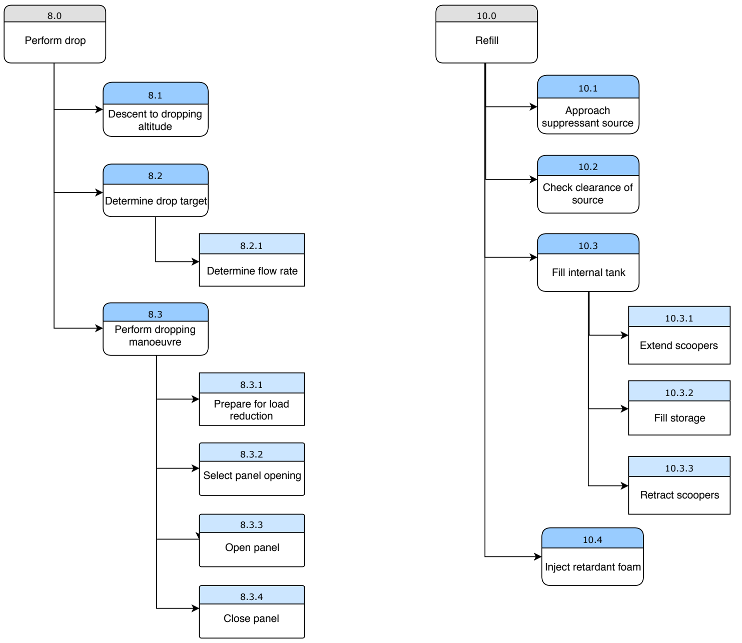

Figure 4.3: Functional breakdown structure of the two functions specific to aerial firefighting.

amounts of payload/fuel to enable fast initial attack). This aspect concerns phases 1 to 8 and especially phase 5: cruise to fire.

Dropping of suppressant
As phase 7, and also 16 within the refill iteration, indicate, the UAV should be able to drop suppressant. This has to be done in order to contain the fire as quick and efficient as possible. Thus, it is necessary to be able to drop the suppressant with a high accuracy, which can be achieved by dropping at low speed and at low altitude with a large enough volume of suppressant. This is required to acquire a high enough coverage level and minimise evaporation.

Withstand high load factors
To perform phases 7, 12 and 16, the UAV will have to withstand high load factors. These are mainly induced by the significant loss and gain of weight throughout the flight.

Extreme flight conditions
The UAV will, during phases 6-8 and 15-17, be within close proximity of the to be contained fire. It will have to perform under these conditions, which are certainly harsher than those in general aircraft missions. It will have to withstand the heat and smoke from the fire, and possible manoeuvre around high canopies/ground infrastructures.

Amphibious refilling
To ensure that the UAV does not have to return to base after phase 8 to collect a new load of water, it should be able to collect water at a water body. This is to save precious time on travelling back and forth to the airfield, as it has been

shown during preliminary research, that water bodies tend to be closer by than airports. Amphibious refilling will thus enable more efficient use of time and resources. In order to refill the water tank at a water body, the aircraft should be amphibious, such that it can float on the water if a landing must be performed during phase 12, or in case of emergency.

Land on small water bodies and short airfields
A logical result of being able to land on smaller bodies of water, is that more water bodies are available to scoop from. Reducing the landing and take-off distance will enable the UAV to scoop from a larger number of water sources than the competing aircraft.

Highly manoeuvrable
Phases 4, 9, 13 and 18 require a highly manoeuvrable aircraft. Especially during phase 13, as lakes and other water bodies are often surrounded by vegetation and thus require large turning angles in combination with climbing at a high rate. The manoeuvrability will also come into play when dropping the suppressant and flying around the fire, as an accurate drop is required.

Transportable
This aspect is not explicitly mentioned in the flight profile diagram, but will have a large influence on the availability of the UAV. Thus, in order to be able to supply the system across the globe, it should fit within a transportation aircraft.

4.3. Initial Design Requirements

Before a concept generation and trade-off can take place, it is important to identify the design requirements. Additionally, these requirements help in identifying risks in the detailed design phase. These will, however, be elaborated upon in chapter 6. Both the original stakeholder requirements as well as the subsequently generated performance requirements are driven by the goal of being cost competitive and outperforming some of the current existing firefighting aircraft, and more specifically the CL-415. Following the functional flow diagram, and in consultation with firefighting experts[1], in negotiation with the stakeholders a finalised set of requirements was established.

The requirements have been split up into four overarching categories related to cost, transportability, safety and general flight performance. It is important to note that at this stage in the design process, it was still unknown whether a rotary or fixed-wing aircraft would be carried to the detailed design phase. Therefore, within general water-dropping performance, it was decided to separate the requirements for the two types of aircraft. This separation seemed the most logical choice in preparation for the trade-off as it allowed for identifying key strengths, weaknesses, difficulties and potential risks carrying through to the detailed design phase for each concept.

As a complete requirements compliance matrix is presented in chapter 15 following the finalised design, only select key, driving and killer requirements, determined to have had a greater influence on the trade-off decision will be justified and presented in further detail in this section. Furthermore, chapter 15 will also present any additional requirements altered or added during the detailed design phase. To begin with, an explanation of the requirement abbreviations is presented below:

COST	Cost	**GRND**	Ground operations
PERF-TO	Take-off performance	**CMM**	Communications
PERF-CRUS	Cruise performance	**TRANS**	Transportability
PERF-BMB	Water bombing performance	**SFE**	Safety
PERF-MAN	Manoeuvring Performance	**SUS**	Sustainability
PERF-STAB	Stability performance	**STMAT-MAT**	Structures and materials - Materials
PERF-LND	Landing performance	**STMAT-ST**	Structures and materials - Structures
PERF-COLL	Retardant collecting performance	**SH**	Stakeholder

Requirements ending in -R and -F were considered as rotorcraft and fixed-wing specific, respectively. Additionally, the requirements have been identified as either key, driving or killer. Driving requirements are requirements that drive the design more than others and will have a major influence on the design of (sub)systems. They can often be directly linked to the project objective statement. Meanwhile, key requirements may be described as those which are of primary

[1] Duncan van de Laar, Head of Fire Department Rijswijk, The Netherlands, and Michael Gollner, Fire Safety Engineering Professor, University of Maryland, US

importance to the customer, whilst killer requirements are determined to drive the design to an unacceptable extent. The selected requirements for both rotary- and fixed-wing aircraft are summarised in Table 4.2.

Table 4.2: Main driving, key and killer requirements.

Reference	Requirement
AF-PERF-TO-01 $_{driving}$	The UAV shall be able to take off on water
AF-PERF-TO-02 $_{driving}$	The UAV shall be able to take off on ground
AF-PERF-LND-03 $_{driving}$	The UAV shall be able to land on ground
AF-PERF-LND-04-F $_{driving}$	The UAV shall be able to land on water
AF-PERF-CRUS-02-F $_{driving}$	The UAV shall have a cruise speed of at least 300km/h
AF-PERF-CRUS-02-R $_{driving}$	The UAV shall have a cruise speed of 200km/h
AF-PERF-01-F $_{driving}$	The UAV shall have a stall speed lower than 120km/h
AF-PERF-BMB-02 $_{driving}$	The UAV shall be able to carry out controlled drops
AF-PERF-MAN-01 $_{driving}$	The UAV shall be able to sustain load factors between -1g and 4g
AF-STMAT-MAT-01 $_{driving}$	The UAV shall be able to withstand temperatures of up to 130 degrees Celsius
AF-STMAT-MAT-02 $_{driving}$	The UAV shall have a lifetime of at least 20 years
AH-SH-SFE-02 $_{driving}$	The UAV shall be able to autonomously avoid ground crew and bystanders
AH-SH-SFE-03 $_{driving}$	The UAV shall be able to autonomously avoid other UAVs in formation flying
AH-SH-SFE-05 $_{driving}$	The UAV shall comply with flight safety regulations
AH-SH-SFE-06 $_{driving}$	The UAV shall avoid restricted airspace during autonomous flight
AF-CMM-01 $_{driving}$	The UAV shall be unaffected by smoke
AF-CMM-11 $_{driving}$	The UAV shall be able to fight fires at any time of the day
AF-TRNS-01 $_{key}$	At least two UAVs shall be able to fit in an A400M[2]
AF-COST-01 $_{key}$	A single UAV shall have a maximum cost of 11 million euro (based on half of CL-415)
AF-SH-SUS-01 $_{killer}$	The UAV shall not produce more than 70dB of noise

4.3.1. Driving requirements

Take-off and landing performance

The first four driving requirements present in the table relate to the take-off and landing performance of the aircraft. It is clear that the take-off and landing performance of the fixed-wing aircraft become a critical design aspect from both a water operations and deployment standpoint. During the trade-off process, these requirements emphasise the need of a complete hydrodynamic design and additional resource allocation in case such a fixed-wing design is chosen for the final design phase. Furthermore, a fixed-wing concept induces additional risks to be taken into account and mitigated by the design team related primarily to a knowledge gap as well as additional time constraints. In comparison, the rotorcraft requirements are purely limited to ground based take-off and landing operations. Instead, a single potential hydrodynamic focus arises related to the use of either a water pump or bucket for water operations, and thus the focus and resource allocation within the team may shift. Aside from restructuring the team, these performance requirements have been considered as key as they directly influence the general firefighting strategy and ultimate goal. The fixed-wing aircraft's water restrictions imply a direct limitation on accessible water bodies. Additionally, there may be constraints with regards to the bases from which the two aircraft types may be deployed/refuelled with the fixed-wing potentially being subject to higher constraints related to aspects such as a limited runway length.

Cruise and speed performance

The next two driving requirements are related to cruise speed. The two design targets of 200km/h and 300km/h for the rotary- and fixed-wing aircraft respectively were chosen based on currently existing competitors. In consultation with firefighting experts[1], it was found that initial response time was critical for firefighting efficiency and (rapid) containment. Rotorcraft are globally slower than fixed-wing aircraft, thus benefit of quick initial attack should be carefully weighed out against attack distances in the trade-off process. The cruise requirement is considered as driving as similarly to the aforementioned take-off and landing requirements, they play a crucial role in the developed firefighting strategy. Finally, in order to drop the fire as carefully as possible, it is important to design a fixed-wing aircraft with as low of a stall speed possible, competitive with that of the market leaders. As this stall speed requirement may be difficult to achieve

[2]The A400M cargo compartment has a volume of 17.71x4.00x3.85m^3.

for aircraft in comparison to being non existent for rotorcraft, it is again a requirement which must be taken into careful consideration within the concept selection process.

Water bombing and manoeuvring
A strong aspect of aerial firefighting is providing efficient dropping patterns. This is reflected in the aircraft's ability to provide controlled low altitude drops. It is then important to explore an efficient dropping system. In case of a fixed-wing aircraft, such an innovative controlled dropping mechanism may be coupled with the significant g-forces experienced by the aircraft during the dropping manoeuvre due to the large load released. Similar loads are experienced by the helicopter during the dropping phase, however, may differ depending on whether a bucket or helitank is used. Finally, these requirements are considered as driving as not only do they highlight additional structural considerations but also greatly impact the stability and control systems. These vary greatly between rotorcraft and fixed-wing aircraft and in turn each induce additional risks. Thus, assuring these requirements are met, is key during both the trade-off and final design phase in order to assure the most successful operation of the aircraft.

Materials
Unique to firefighting aircraft are the high air temperatures they may be subjected to during operations, especially, if the drops should be conducted as low as possible in order to minimise water and retardant evaporation. Other than the aerodynamic consequences this may have on the ability to generate lift, it is crucial that the chosen material should be able to cope with high (up to $130°C$) heat levels for extended periods of time. Moreover, as aerial firefighters remain operationally very expensive, ideally they should be designed for long lifetimes of at least 20 years. This is critical within both the trade-off as well as the material choice, especially with regards to fatigue and corrosion.

Safety and communications
A key underlying concept of an aerial unmanned firefighter lies within the removal of an on-board pilot and hence greatly decreased pilot risk. Other than complying with regulations, it is imperative the UAV must be able to ascertain the safety of the ground crew as well as other UAVs/manned aircraft within the airspace, during both solo flight and formation flying. Furthermore, a great impediment to manned aerial firefighters today is the inability to fight fires at night as well as reduced visibility due to the smoke. By meeting communications requirements, and designing an operations system which can function 24/7 and at slightly lower altitudes, the UAVs are expected to greatly outperform the current market leaders.

4.3.2. Key Requirements

Two key requirements are considered of importance to not just the stakeholders but the overall deployability and usability of the system. These relate to firstly the transportability requirement, and secondly the total cost of a single UAV. It is aimed that at least two of the UAVs should be transportable in an A400M aircraft. Meanwhile, as a swarm of UAVs is expected to be deployed in order to remain cost competitive with the current market leader (the CL-415), the goal is that a single UAV should be priced at around 1/3 of the current CL-415 market price.

Ascertaining the UAV transportability should not only ensure rapid fleet deployment but might also lead to decreased emissions during the deployment. Additionally, deploying the UAVs for a longer distance may mitigate the risks for UAV certification and access to civilian and military airspace. Despite this, this requirement may induce additional design as well as operations complexity due to assembly and disassembly. Thus, meeting it in an efficient manner will be key towards rapid initial attack as well as maximising stakeholder satisfaction.

Finally, key to stakeholder's satisfaction as well as the system's success is of course being cost competitive with the current market leaders. Not only should the design team aim at developing a cheaper product, but the team should convince the stakeholders the proposed design is able to outperform existing competitors for a similar or better price by establishing itself as one of the best if not the best potential aerial firefighting system.

4.3.3. Killer Requirements

The noise requirement initially imposed by the stakeholder is expected to drive the design to an unacceptable extent. Seeing that any type of electrical propulsion has been directly ruled out by the stakeholder due to the current limited performance of electrical propulsion systems and potentially large volume of batteries close to very high temperatures, it seems at this stage impossible to find a fossil fuel powered engine with a 70dB comparative noise level. Nevertheless, as this is a emergency vehicle expected to operate in remote areas, in an extreme situation, it has been assumed that noise pollution will not be a primary concern.

5
Concept Selection

A preliminary literature study informed the team on the general needs of aerial firefighting, and the desired characteristics of aircraft that are used for suppressing wildfires. Brainstorming sessions followed where several creative ideas were discussed. Design option trees like the one shown in Figure 5.1 were used to ultimately generate six concepts, which entered the trade-off process seen in Figure 5.2. The first trade-off led to the elimination of the blended wing body and double bubble concepts. The main reason for this was the team's approach to design a feasible and reliable aircraft given the existing and proven technology of today, since it is an emergency response aircraft. The second trade-off, which made use of a trade-off criteria matrix shown in Table 5.1, led to the elimination of helicopters after a meeting with a firefighting expert emphasised the importance of fast initial attack times. Given the helicopters' lower cruise speed they became less favourable. Finally, the third trade-off led to the choice for a single engine fixed-wing UAV with detachable high wings. This choice was motivated by several factors. Firstly, the concept is relatively small, which gives it a higher potential for transportability. This also has additional advantages such as more accessibility to water bodies from which it can scoop up water. Secondly, the single engine placement on the tail reduces the complexity of detachable wings. Upon discussing the design choice with firefighting professionals, it became clear that 2000L payload is perceived as low and ineffective. Evidently, water can evaporate when dispersed after a drop before reaching the ground. With such a low amount of water, the wasted portion becomes significant, and the effective portion insufficient. After choosing the single engine concept, negotiations with the stakeholders led to a new goal. The focus was placed on maximising the payload whilst maintaining the deployability and the advantages of swarming.

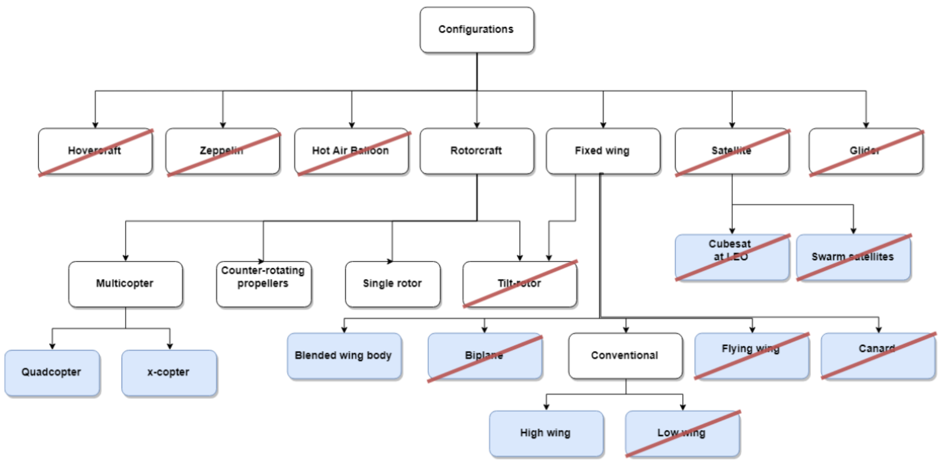

Figure 5.1: Design option tree for the general configuration of the design.

5.1. Sensitivity Analysis

A sensitivity analysis was performed during the trade-off process in order to consider the different missions the aircraft may perform. The concepts have different strengths and weaknesses which differ per mission. Different missions have different distances to the fire and to the water source. The remaining concepts were graded on the different criteria for each mission. Four general mission types were identified varying the distances from the fire to the base, and from the fire to the water source. The overall result was obtained for all different missions. The single engine concept was the most versatile as it scored the highest for all mission types. More detailed explanation of the process and all trade-off tables can be found in the preceding report [6].

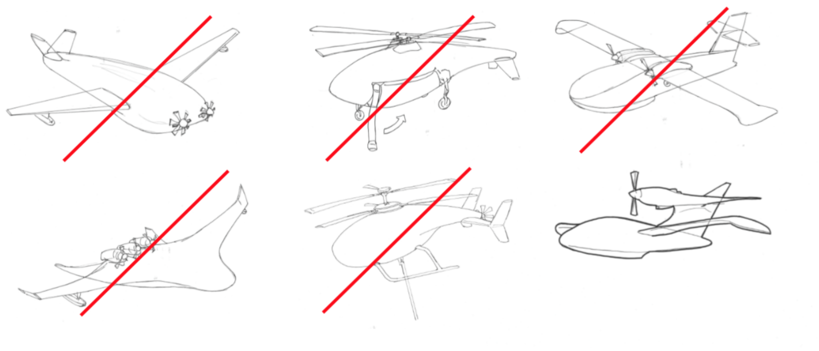

Figure 5.2: Concept selection results of the different trade-offs.

5.2. Risk analysis

Throughout the trade-off process, risks and their likelihoods were identified, and a plan to mitigate them in later stages of the project was decided upon. The full risk analysis is described in more detail in the preceding report [6]. Important risks that turned out to influence the direction of the design are summarised here.

- **The internal tank** associated with a fixed-wing concept poses a risk as the water inside the tank will slosh during flight and manoeuvres and cause potentially dangerous centre of gravity shifts. The risk was to be mitigated by ensuring to place the tank close to the centre of gravity of the whole aircraft, and to design an anti-sloshing mechanism within the tank. Both measures were implemented eventually, but should be investigated further in the future steps of this design.
- **Shadow dropping** is a phenomenon that occurs when an aircraft drops water on the ground at high speed. It means that the water is dispersed before it falls to the ground and is blocked by trees and other objects, such that it only covers the ground on one side of a tree and misses the other. If the water line laid by the selected fixed-wing, which can reach high speeds,t is not continuous, the fire will get through and the line will be ineffective. To mitigate this risk, the phenomenon had to be studied and a solution designed. This indeed became an important part of the project and the manoeuvres carried out by the aircraft whilst dropping were designed carefully to passively pressurise the drop and obtain the desired coverage level. This is described in chapter 8.
- **Placement of the engine** on the tail of the aircraft was expected to produce a pitch down moment. The mitigation strategy included studying the pitch down moment caused and how it influences the stability requirement to be inherently stable in flight and on water. Eventually, this risk was verified and the engine was moved forward.

Table 5.1: Criteria matrix used to conduct the second trade-off

Aspect	Weight	Weight (%)	Poor (1)	Marginal (2)	Satisfactory (3)	Good (4)	Excellent (5)
Transportability and assembly readiness	3.1	8.0	Cannot be transported in other vehicles	One or more units can be transported on cargo ships	One unit can be transported in an A400m	Two units can be transported in an A400m	More than two units can be transported in an A400m
Cruise speed	4.2	10.9	Can reach fire from base in over 6 min	Can reach fire from base within 6 minutes	Can reach fire from base within 4 minutes	Can reach fire from base within 2 minutes	Can reach fire from base within 1 minute
Rotation time	4.8	12.4	over 8 minutes	8 minutes or less	7 minutes or less	6 minutes or less	5 minutes or less
Mission time (Endurance)	5	13.0	less than 1 hour	between 1 and 2 hours	between 2 and 3 hours	between 3 and 4 hours	more than 4 hours
Base turn around time	3.6	9.3	more than 25 minutes	between 20 and 25 minutes	between 15 and 20 minutes	between 12 and 15 minutes	less than 12 min
Unit cost	3.3	8.6	More than 40 mil €/6000L	less than 40 mil €/6000L	less than 35 mil €/6000L	less than 30 mil €/6000L	Less than 25 mil €/6000L payload
Expected lifetime	3.75	9.7	less than 24000hr	more than 28000hr	more than 32000hr	more than 36000hr	more than 40000hr
Risk	4.06	10.5	Risks are hard to predict and mitigate	Risks are partly predictable and hard to mitigate	Risks are predictable and possible to mitigate	Risks are easy to predict and mitigate	-
Litres of water /fuel litre	3.25	8.4	<30	30	40	50	60+
Ability to do segmented/controlled drops	3.5	9.1	Unable to control drops	Able to do some form of controlled drop with marginal accuracy	Able to do limited variations of controlled drops with satisfactory accuracy	Able to do limited variations of controlled drops accurately	Able to do several variations of controlled drops accurately

Part II

Detailed Concept Description

6
Detail Design Overview

Within this chapter, an overview of the overall design as well as the risk and sustainability strategies that lead to the final design are given. This overview is intended to provide context and ease the understanding of the individual components described in detail in part II.

6.1. Design Summary

The Wangari aerial firefighting UAV design was driven by the requirements of quick global deployment, rapid initial attack and strategic attack capabilities. Out of these requirements, a fixed-wing concept, able to fight fires at any time of the day, was developed, which is illustrated in Figure 6.1 and Figure 6.2. The details of the concept selection process that lead to this configuration were previously covered in chapter 5. Here, an overview of the design features and how they link to major design requirements is made.

Wangari is a fixed-wing, twin prop aircraft driven by a single engine, which is placed within the centre of the fuselage in order to facilitate the UAV's transportability. To accommodate its water scooping capabilities, a high wing configuration has been chosen to allow for enough clearance for the propellers. For stability during water taxiing operations, deployable floats are attached to the wing tips. Additionally, the retraction capability allows for mitigating the risk of catching the water at high speeds during the scooping manoeuvre. For in-flight stability, Wangari possesses a cruciform tail, allowing the fully moving horizontal stabiliser to benefit from the increased velocity in the wake of the propellers.

Finally, in order to enhance its quick deployment capability, both the main wing and horizontal tail have been designed to be detachable. This allows for two UAVs to easily fit in the cargo hold of a standard transportation aircraft such as the A400M[1].

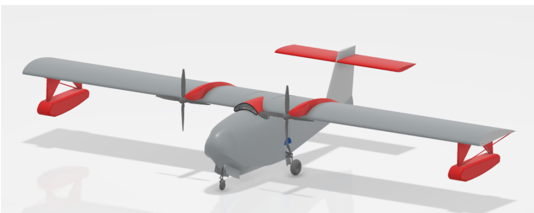

Figure 6.1: Wangari's final configuration when stationary on land.

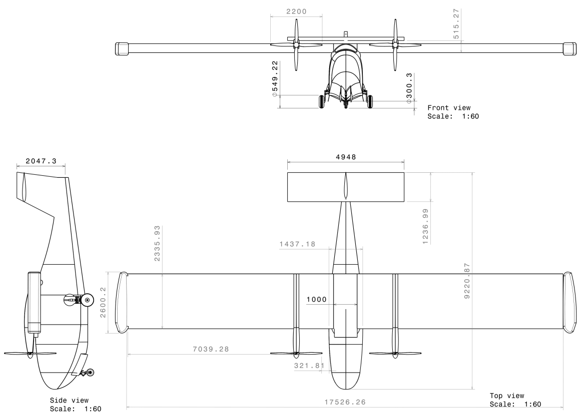

Figure 6.2: Technical drawing showing final dimensions of the UAV

6.1.1. Mass Budget

The mass budget used for performance calculations, based on Class II weight estimations and more detailed design calculations in the case of wing and communication devices, is presented in Table 6.1. To be noted is that for the fuel and payload, a minimum and maximum is given. This is due to the fact that fuel is used during the mission, resulting in an increase in the amount of payload Wangari can carry. The maximum amount of payload Wangari is 4500 kg of payload, or 4500 litres of water.

[1]The cargo hold of the A400M has a volume of 17.50x3.85x4.00m^3

Table 6.1: Preliminary mass budget.

	Weight [kg]		Weight [kg]
Empty		*Propulsion Total*	724
Structures Total	2357	Power	654
Wing	1106	Fuel System	70
Horizontal Tail	86.5		
Vertical Tail	29	**Payload**	
Fuselage	883	Min	0
Landing Gear	152.5	Max	4500
Floats	100		
Fixed Equipment Total	737	**Fuel**	
Batteries	288	Min	0
Flight Controls	250	Max	2700
IAE1	87		
Electrical System	112	Grand Total	9000

6.1.2. Propulsion

The UAV will be fitted with a newly developed GE T901 turbo-shaft engine developed as a successor to the commonly used T700. The engine will provide 50% more power then the T700 and is also presumed to be 25% more fuel efficient then the T700. Wangari will, therefore, have a maximum of $2,439 kW$ shaft power at its disposal. This power will be split into two driveshafts that will deliver the power to the propellers which are located on the wings for aerodynamic purposes. The propellers are relatively small, having a diameter of $2.2m$, due to the clearance required when scooping or landing on water. This small diameter of the blade has a large influence on the propeller efficiency, mainly at low speeds when the exit velocity of the propeller relative to the free-stream velocity is large. This is the main limiting factor in the low speed performance of the UAV. Nevertheless, the Wangari UAV will be able to generate an excess power of over $1,000 kW$ within almost every stage of its flight envelope, while weighing not more than $9,000 kg$.

6.1.3. Scooping and Dropping Mechanism

Arguably the most important part of the design are the scooping and dropping mechanisms. In a mission with a duration of four hours, Wangari can perform a drop 39 times, as described in section 8.1. During the dropping operation, the UAV has to sustain high manoeuvre and gust loads as well as a change in loading due to the weight loss. This change in loading can be harnessed during the dropping manoeuvre in order to provide a passive pressurised dropping system, thereby enhancing the firefighting performance. This dropping mechanism includes a sliding door which enables the remote pilot to control the flow rate at any given time. The inclusion of this innovative system is made with sustainability in mind, as pressurised dropping systems are heavy and will contribute to increased fuel consumption. By having a passively pressurised system for the main tank, an active pressurised system is only required for the smaller retardant tanks due to the substance's reaction with air. This will, however, be considerably smaller and provide less of a weight and cost penalty.

6.1.4. Internal Systems

Striving to design a quickly deployable UAV, transportable in general air carriers, the internal layout, illustrated in Figure 6.3, is kept as compact as possible. When filled, the water and retardant tanks form the heaviest internal component. Therefore, they have been placed around the c.g. and shaped to accommodate the main and nose landing gear. The nose gear retracts to an almost horizontal position into the fuselage while the main gear can vertically retract to a position close to the water tanks. For longitudinal stability during flight, the heavy components such as the batteries and electronics have been placed near the front. IR and visual cameras are placed at various positions within the UAV to allow the pilot to observe the fire.

In order to power the propellers, the engine has been placed in the centre of the fuselage slightly elevated into a nacelle and incorporates the generator in order to power the batteries during flight. The batteries of which are also used as a backup power system. Within the nacelle, a gear box and differential are placed transmitting the power through the driveshaft located in the wing to the gearboxes located within the small nacelle of each of the two propellers.

The fuel tanks are not directly visible in Figure 6.3 as they have been placed as bladders directly in the wing. Finally, the UAV possesses an electro-hydraulic actuation system. The command is send electronically by the pilot to the actuator equipped with an internal hydraulic system to provide the actuation force. This enabled the elimination of a heavy, high power consuming hydraulic unit.

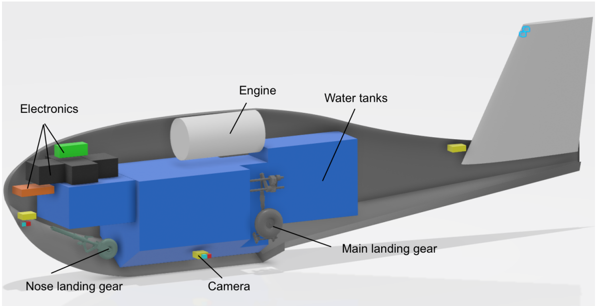

Figure 6.3: Overview of the internal layout. It must be noted that herein only the largest components are drawn.

6.2. Sustainability Strategy

The mission of Wangari is to fight the environmental problem of wildfires. Counteracting the increasing amount and impact of wildfires is in itself sustainable as greenhouse gases emitted by the fires are reduced and the impact on biodiversity lessened. The amount of emissions produced by the UAV are incomparably small to those produced by the wildfires. Thus, it is of utmost importance that the emissions done by the wildfires are limited. However, whilst optimising performance, the sustainability of the UAV shall not be neglected. Therefore, all design choices shall be made using a sustainability strategy. This strategy is built up in several clauses, key aspects of which are stated in the following.

Material Selection

Sustainability is one of the many things to consider during the selections of the material. Things to consider are the severity and method and location of production of the materials. Additionally, the materials selected shall be reusable or recyclable at the end-of-life of the system, this may be in complete different applications, as long as it is not discarded. Being sustainable is not only achieved by making sure degradable materials are used, it is also important to create something of the quality to be able to continue for a long time, thereby creating less waste. Thence, the UAV shall be designed such that it has an operational lifetime of at least 20 years, in which it is estimated to fly 40,000 hours. To achieve this lifetime, the fatigue life of materials shall be considered in the material selection process.

Development and Manufacturing

The sustainability strategy for the development and manufacturing is to limit the use of resources during this phase. These resources include time, money, materials and people. A philosophy like lean manufacturing could be adhered to. Also, after the UAVs are produced, tests will have to be performed. When these tests are designed, sustainability should be taken into account in the sense of limiting the number of destructive tests, to minimise the waste of materials and resources.

Retardant Choice

A retardant will be chosen to be mixed in with water to fight fires more efficiently. There are multiple types of retardants that are useful, each of them having positive and negative effects on the environment. The choice of retardant shall, therefore, not only depend on the improved efficiency of fighting wildfires it can generate but also on the environmental toxicity and fate. Additionally, the dropping shall be accurate enough to ensure that no retardant is accidentally dropped in areas not affected by the wildfire.

Pilot Training

Resources, both cost and materials, could be saved by training the pilots and others involved using a simulation. This would mean that the actual UAVs do not have to fly, thereby reducing the amount of fuel used to educate the people involved in the system, and also limiting the number of flight hours spent on performing an actual mission.

Finally, more conventional measures of sustainability will be researched, such as noise impact and NO_x and CO_2 emissions, which will be reflected upon in chapter 16.

6.3. Risk Mitigation Strategy

In a complex design as Wangari, risks are unavoidable. However, some of them can be anticipated and mitigated. In this section, the risks that were identified in the concept selection process and their mitigation strategy are discussed. From this it was concluded that mainly the requirement on transportability introduced risks into the design.

1. **Collisions during formation flying**: The mitigation strategy is to implement a collision avoidance system.
2. **Hitting objects due to flight at low altitude**: The mitigation strategy is to implement an avoidance system.
3. **UAV exceeding flight envelope**: The mitigation strategy is to design the UAV to withstand extreme load factors.

4. **Signal loss**: The mitigation strategy for this risk is to improve the communication system of the UAV system (so UAV, grounds station, air attack) by creating redundancies in the communication system, for example, the use of the air attacker aircraft as a relay in the communication.
5. **Smoke impacting flight performance**: The mitigation strategy is to include instruments, such as navigation and position instruments, heat sensors, and radars, as as well as redundant cameras that can be used for navigation. For reduction of the air quality due to smoke, filters can be installed in the engine air intake, and the engine should be tested for performance with lower amounts of oxygen.
6. **Water conditions impacting performance**: The strategy is to size the hull such that it is able to withstand waves up to a moderate sea-state. If the waves exceed this, the mitigation strategy is to fly to a lake instead.
7. **Wing tip caught in water during manoeuvring on water**: The mitigation strategy for this is to design a mechanism to ensure manoeuvring on water with the wings level and/or retractable floats.
8. **Scooping too much water**: The mitigation strategy is to place sensors to measure the payload intake and communicate this to the scooper retracting mechanism. Moreover, passive means shall be implemented to ensure the MTOW is not exceeded, this will be done by installing overflow vents.
9. **Corrosion of parts of aircraft**: To mitigate the risk of corroding parts, corrosion resistance shall be ensured in the selection of materials, either by selecting inherently corrosion resistance materials or by adding additional coatings to improve the corrosion resistance.
10. **Instability due to shift of centre of gravity**: The c.g. of the aircraft shall be created such that there is close to no shift of the c.g. in the longitudinal direction in the case of all and zero payload.
11. **Sloshing of suppressant within tank**: The mitigation is to implemented antis-sloshing baffles into the water tanks.
12. **Too large change in load factor due to dropping of suppressant**: The maximum allowable load factors before dropping for different amounts of retardant shall be calculated to mitigate this risk.
13. **Suppressant evaporation and shadow drops whilst dropping**: To optimise the dropping a passive pressurisation system is to be designed and a minimum of 2500L of suppressant shall be dropped per drop.

The identified risks have been summarised in risk maps before and after mitigation strategies are implemented, in Figure 6.4 and Figure 6.5, respectively.

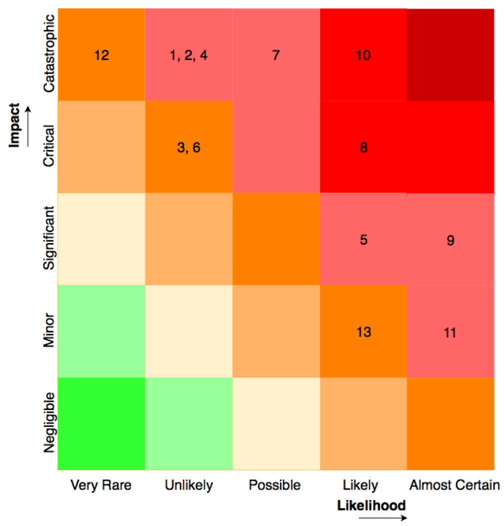

Figure 6.4: Risk map before mitigation.

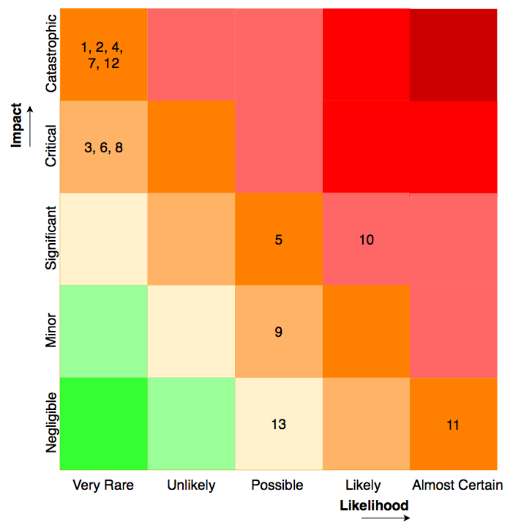

Figure 6.5: Risk map after mitigation.

Whilst many risk were already defined in the concept selection phase some new risks were introduced in the detailed design. The majority of these risks were due to the requirement on transportability that had to be met. These risks and their mitigation strategies are defined per component in chapter 10. Likely risks in the entire detail design phase are due to uncertainties of values or design choices. Therefore, a general mitigation strategy is defined as verification of the values, validation were possible and including a sensitivity analysis to determine the severity of the risk for the feasibility of the concept.

7
Flight Performance

Wangari is to be designed for the specific mission of firefighting. However, this mission results in a flight profile quite different compared to those of regular aircraft. The flight performance of Wangari is mainly based on its low speed performance due to the continuous low speed manoeuvres of dropping and scooping of the suppressant. A sustained cruise is often just a small part of its flight profile. In this chapter it can be observed that Wangari is designed to have excellent low speed performance.

7.1. Flight Envelope

In this section, the flight envelope of the Wangari UAV is presented. The flight envelope of Wangari contains load factors due to the dropping, scooping manoeuvres and the gusts from the fires. While these gusts and manoeuvres will not increase the maximum load factor compared to a normal flight envelope, the sheer number of gusts will be much higher. This leads to much more load cycles compared to general aviation aircraft which makes the Wangari more prone to fatigue. The flight envelope has been created using the aircraft parameters as stated in Table 7.1. In the determination of the aircraft load factors, references have been used from EASA[1] as there are currently insufficient regulations on amphibious UAVs. This reference has been used as a starting point for the design of the flight envelope. However, not all load factors could be determined using these regulations. Therefore, in the calculations of V$_{cruise}$, it was necessary to deviate from the given design specifications. In the design of the flight envelope, the following assumptions have been made:

- The aircraft is considered to be a utility aircraft.
- The maximum positive load factor is 4.4, the maximum negative load factor is $-0.4 \cdot n_{max}$. This is without taking gusts into account.
- Gust forces are assumed to be in vertical direction.
- Gusts due to fires are not excessive compared to regular loading cases for general utility aviation type aircraft. [7].
- $V_{dropping}$ is assumed to be at $n = 2.2$ which occurs at $51 m/s$, and $V_{scooping}$ is assumed to be at $1.1 \cdot V_{stall} = 38 m/s$.
- As no passengers are on board and the fuselage is not pressurised, V_{dive} can be removed from the flight envelope as this is not an important design paramter of the Wangari UAV system.
- V_{cruise} is at $0.9 \cdot V_{max}$.

In the calculation of the maximum experienced load factor during flight, Equation 7.1 was used. In this equation, the gust velocity u has been calculated using the CS23 regulation[1] resulting in a velocity of 17m/s. The flight envelope for Wangari at MTOW is illustrated in Table 7.1. The critical points are the maximum negative load factor of $n = -2.6$ and the maximum positive load factor of $n = 6.6$. Other important factors are those of dropping, $n = 5.9$, and scooping, $n = -1.8$. At empty weight and $700 kg$ of fuel, the maximum load factor will increase to $n = 8.1$ and negatively to a load factor of $n = -3.2$. Due to the lower wing loading in this scenario, this is not the most critical case for the wing loading of the UAV.

$$\delta n = \frac{\rho V C_{L_\alpha} u}{2 \frac{W}{S}} \tag{7.1}$$

7.2. Airfoil Selection

The shape of the airfoil is determined by some of the characteristics it needs to have. These characteristics are as follows:

- $C_{L_{max_{clean}}} = 1.5$
- High lift at low angle of attack
- Low structural weight

[1] `https://www.easa.europa.eu/download/general-aviation/documents-guidance-and-examples/ABCD-FE-01-00`[cited 7 june 2019]

Table 7.1: Table of main design parameters for the flight envelope

MTOW (kg)	9000
Surface Area (m^2)	40.8
Span (m)	17.5
Cord (m)	2.33
Pa (kW)	1626
V$_{stall}$ (m/s)	34.3
V$_{max}$ (m/s)	125
V$_{cruise}$ (m/s)	112.5
V$_{dropping}$ (m/s)	51
V$_{scooping}$ (m/s)	37.8
W/S (kg/m^2)	221

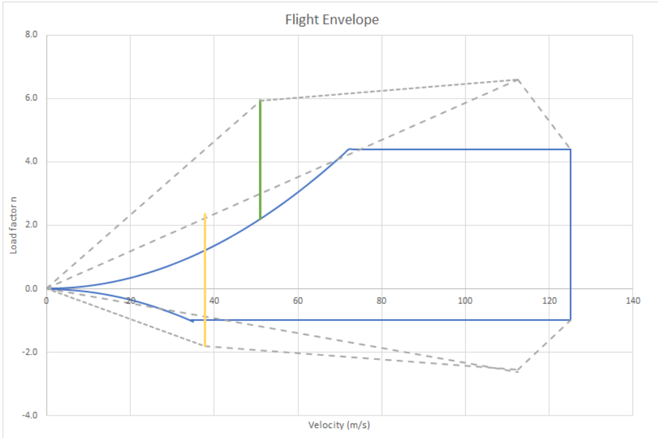

Figure 7.1: Flight Envelope for Wangari, the green line concerns the dropping manoeuvre and scooping is visualised by the yellow line.

From the second requirement, it can be concluded that the airfoil must have a low zero-lift angle, which is the angle at which the lift coefficient of the airfoil is equal to zero. This can be achieved with a high cambered airfoil. Furthermore, a low structural weight can be achieved by increasing the thickness of the airfoil, as this increases its mass moment of inertia. In this way, there is less need for structurally strengthening the airfoil compared to a thin airfoil, which decreases its overall weight.
Based on this, several airfoils were analysed using JavaFoil after which the NACA 6415 was selected due to its high $C_{l_{max}}$, low zero-lift angle and relatively high thickness. Its characteristics where then plotted and are presented in Figure 7.2 until Figure 7.4.

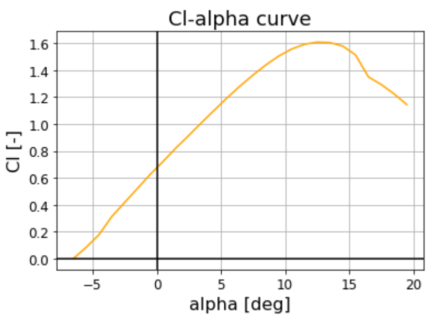

Figure 7.2: Cl-alpha curve of the NACA 6415

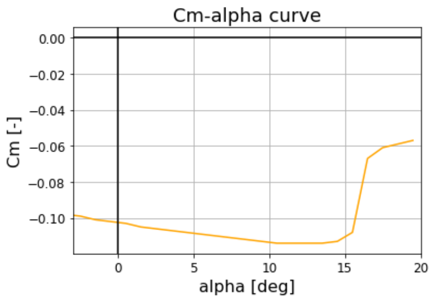

Figure 7.3: Cm-alpha curve of the NACA 6415 at quarter chord

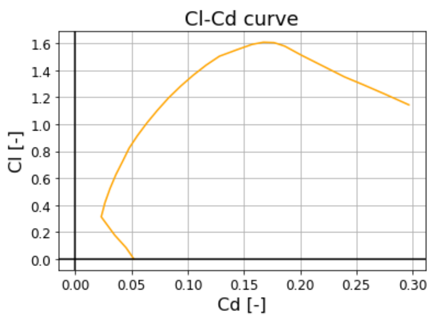

Figure 7.4: Cl-Cd curve of the NACA 6415

As can be seen from Figure 7.2, the $C_{l_{max}}$ of the NACA 6415 is slightly higher than the required $C_{l_{max}}$, at 1.6. Furthermore it is evident from Figure 7.2 and Figure 7.3 that the airfoil's stall angle of attack is around 14°. At this angle, the $C_{m_{ac}}$ is about -1.03 and the C_d is around 0.17, as can also be seen in Figure 7.3 and Figure 7.4.

7.3. Mission Specific Weights

This section is dedicated to specific weights of the aircraft during flight. The weights are divided in three groups: empty, fuel and payload weight. A first estimate of each of these weight components had been made earlier in the concept selection phase. However, this estimation was based on a flight profile diagram of a typical aircraft. As shown in section 4.2, the mission of Wangari is rather different from a typical mission. Thus, a new estimation had to be made in order to estimate fuel usage and duration of each phase of the flight, number of possible scoops and drops, and the firefighting ability of the UAV (amount of suppressant dropped per unit of time). Roskams method for class I weight estimation has been used throughout this section [8].

Design Mission
In order to design the UAV, a specific mission has been thought of. This allows for consistent comparisons and the establishment of a goal. The mission was specified as a wildfire located 50km away from the airfield, with a water body located

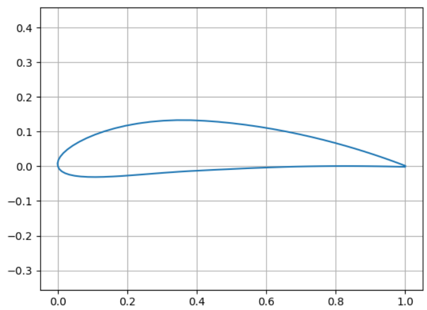

Figure 7.5: A plot of the coordinates of the NACA 6415

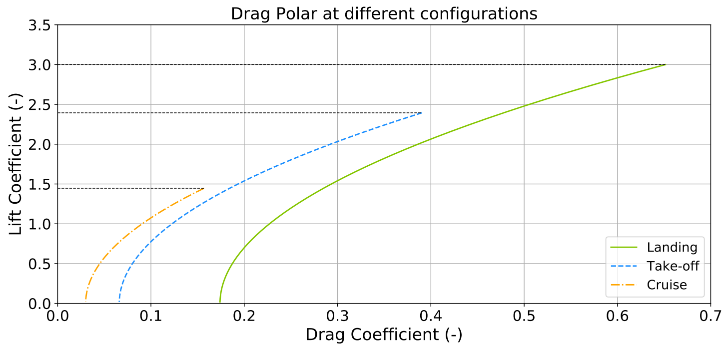

Figure 7.6: Final drag polar in different flight configurations.

at 10km away from the fire. Also, it has been assumed that the UAV will travel for approximately 1km within proximity of the fire, as to locate itself for dropping the payload. These distances had been determined by first investigating several wildfires over the past years, and finding the average distances between the three locations.

Phase Specific Assumptions
There are several assumptions that were made in order to complete the weight estimations, these assumptions were made for a particular phase. The phases of the mission are described in Table 4.1 and visualised in Figure 4.1.

The altitudes at which the phases are performed were initially set to 3km for cruise (phases 5 and 19) and 1km for refill altitude (phases 10 and 14). The dropping altitude is approximately 50m depending on the type of wildfire and fuel, dropping altitudes are further discussed in section 8.3. In the calculations no difference was taken in drop altitude and airport and water body altitude, as this difference was thought to be negligible with respect to duration and fuel consumption for those phases (7, 8, 16 and 17). This was done to reduce complexity within the calculations.

The velocity flown at the cruise phases (5, 10, 14 and 19) was set to be 0.9 of V_{max}, this is not the optimal cruise speed, but as a fast initial attack is of utmost importance, it is assumed to fly faster. The maximum velocity is determined in section 7.1. The maximum rate of climb is achieved at the climb velocity, which has been determined to be 54m/s, as will be further explained in the discussion Figure 7.13. The loiter velocity flown during phases 7, 8, 12, 16 and 17 (all phases during which water is dropped or scooped) was set to 44m/s.

The time spent climbing was found by simply dividing cruise altitude by the average rate of climb. The rate of climb depends on the altitude and velocity flown at, and also the weight of the aircraft. In order to not overcomplicate calculations, an average value of 10m/s has been assumed which is applied throughout the complete mission.

The distances that have to be covered during cruise are reduced by the horizontal distance already travelled during climb (for example 50km is covered by phases 4 and 5). This distance covered is easily found by multiplying the time spent climbing with the climbing velocity (this velocity is assumed to be the horizontal velocity). The descent is not included in the 50km, as it is assumed that the travelled distance during phases 6 and 15 is used to guide the UAV to the correct dropping location at the fire. The time it takes to descent to the required altitude is assumed to be the same as its reverse, so climbing.

It was found that the refill altitude was estimated too high. The horizontal distance covered during phase 13, climb to refill altitude, was 8.5km, leaving only 1.5km to be travelled in cruise if adhering to the design mission. This was not found to be efficient and thus the refill altitude had been reset to 250m. Noting this, it was determined that the altitude of cruise should also be looked at again. A diagram showing the initial attack time, part 1 of the mission, for different cruise altitudes was established. It includes the total time covered until the first drop, climb and cruise time. The altitude was meant to be optimised for fast initial attack, not the fuel consumption, as the purpose of the mission is to fight fires as quickly as possible (section 4.1). From Figure 7.7 it can be noted that for the specific mission (50km to be covered during phase 4 and 5) it is undesirable to climb to a high altitude. Actually, the optimal altitude would be to fly on the ground, as the lower drag, thus faster cruise, at higher altitude does not outweigh the time it takes to climb to that altitude. However, flight can not be performed on the ground, so a cruise altitude of $1km$ is considered. This reduces the time for initial attack by almost $100s$. The cross-over point for faster initial attack by climbing to an altitude of $3km$ is when the fire is located $\pm 250km$ away from the airport.

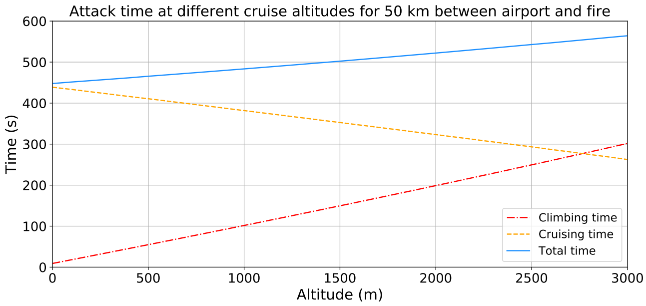

Figure 7.7: Initial attack time at different cruise altitudes, including the time to climb and cruise for a distance of $50km$ between airport and fire. Note, this attack time only includes phases 4 and 5.

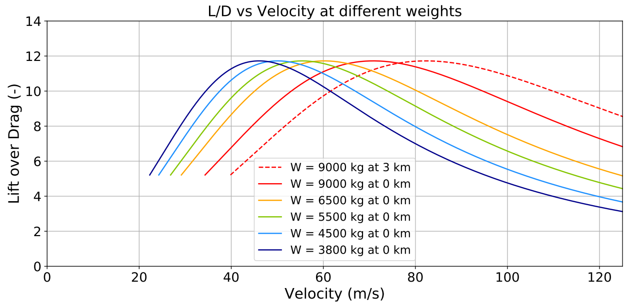

Figure 7.8: Lift over drag curve for different weights and altitudes (densities) of the aircraft.

Weight Fractions for Phases

The initial ratio of payload to maximum take-off weight had been set to 1/3, based on statistical values. As the MTOW has been determined to be $9000kg$, this results in the payload weight to be $3000kg$. An expected empty to maximum take-off weight ratio was determined from existing aircraft. Initially it was thought to use the statistical data provided in part I of Roskam for the amphibious aircraft type [8]. This, however, resulted in very conservative values for the empty weight, due to the fact that the data was outdated. Thus W_E/W_{mto} has been determined from the Air Tractor 802F, as this aircraft is similar to the UAV, with regards to sizing and flight profile; the value was set to 0.41, based on the MTOW for land, as the UAV will not be supplied with skis as the Air Tractor is [2].

The weight fractions of each phase had to be determined in order to find the value of the used fuel during the complete mission. Several of these could be determined from table 2.1 in Roskam part 1 (phases 1-3, 6, 11, 15, 20 and 21) [8]. At first, type 11 was used (amphibious aircraft and flying boats), however, these values were found to be very conservative and the data was again out dated. Thus, it was chosen to use the statistics provided for agricultural aircraft (type 4), although this data was also quite old, this type was assumed to at least have a similar mission profile (this type of aircraft also performs at low altitudes and drops large amounts of payload), and the reference aircraft were also more comparable (engine type and order of weight) than type 11.

The fuel fractions that could not be determined from the statistics provided in Roskam, so the phases in which the UAV climbs or cruises, were determined from rewriting the Breguet equations for endurance and range provided in Roskam part I (equations 2.7 and 2.9) [8]. These equations are given in Equation 7.2 and Equation 7.3, note the values entered should be in the correct set of units.

$$M_{ff,endurance} = \frac{M_{i+1}}{M_i} = \left(e^{\frac{EVcp}{375\eta_p L/D}}\right)^{-1} \tag{7.2}$$

$$M_{ff,range} = \frac{M_{i+1}}{M_i} = \left(e^{\frac{Rcp}{375\eta_p L/D}}\right)^{-1} \tag{7.3}$$

In the above equations, M_{ff} is the fuel fraction for a certain phase, E the endurance given in seconds and R the range given in metres. The endurance equation is used for climb, whereas the range equation is used for cruise. The value for endurance was found by dividing the altitude to be climbed to by the average rate of climb. The range for cruise was found by subtracting the distance covered during climb from $50km$. Initial η_p and c_p values were used from the selection of the engine (subsection 10.1.1). They were set to 0.85 and $75.2 \cdot 10^{-9} kg/J$, respectively. These values were set constant for the complete mission, as to simplify the calculations, such that are no differences for empty or full tank and/or different velocities and altitudes. The lift over drag ratio, L/D, can be found from Figure 7.8. As each phase is executed at a different velocity, this value will differ for the different phases, the weight is taken to be $9000kg$ for all those phases. This

[2] https://janes.ihs.com/JAWAInServices/Display/jau_9269-jau_[cited 11 June 2019]

is assumed, as the fuel fraction is not too sensitive for a slight change in lift over drag.

The used fuel weight can not simply be found by multiplying the fuel fractions of all phases, as then the weight loss and/or gain (by dropping and scooping water) is not considered. The example of a fighter in Roskam [9] is used, as these lose weight during flight as well (they drop bombs, which in essence is the same). An aircraft increasing its weight is not an ordinary thing, thus to account for this, it was treated as a negative amount of water dropped. The fuel fraction after the phase in which weight is lost or gained is corrected by finding intermediate weights. These intermediate fuel usage weights are thus calculated, this is not only useful for the correction, but also provides knowledge about the different parts during the mission, which one uses a lot, why and if it makes sense. It can thus be used as a verification method, which will be discussed in a following subsection.

It has been considered to carry reserve fuel. This has been accounted for by dividing the used fuel weight found for the complete mission by 95%, as the reserve fuel is considered to be 5% of the total fuel weight carried in the aircraft. This percentage is chosen to account for emergencies such as engine failure, unexpected flight conditions, closing of airfields and such.

By multiplying all the (corrected) fuel fractions with the initial take-off weight ($9000kg$) and accounting for the reserve fuel, an estimation for the fuel weight could be made by use of Equation 7.4, in which the factor 0.95 accounts for the reserve fuel.

$$W_F = \frac{9000 - 9000 \cdot M_{ff,total}}{0.95} \tag{7.4}$$

An estimate for the empty weight can be made (Equation 7.5 and this is then compared to the empty weight found using the statistical data from the Air Tractor 802F. If these empty weights are not within 1% of each other, an iteration should take place. Usually the maximum take-off weight would be increased or decreased (depending on which empty weight is larger), however as the MTOW was meant to stay at $9000kg$, the number of refills was altered. This was done, because an increase in number of refills would increase the fuel weight and in turn the MTOW. It was decided not to decrease the MTOW as this would result in iterations to take place within a lot of components of the design, which would not be possible to complete within the amount of time available. For instance this would alter both the power- and wing loading, discussed in section 7.4, which might result in requirements of not being met.

$$W_E = W_{mto} - W_{pl} - W_F \tag{7.5}$$

Results and Findings

The duration of each phase and the (corrected) fuel fractions can be found in Table 7.2. The table is split into the three different parts of the flight. It can be noted that the initial attack time is approximately $800s$, which means that within 15 minutes after starting the engine the first drop of suppressant has been completed. More results with regards to the firefighting performance is discussed in section 8.1. The fuel weights per part of the mission are noted in Table 7.2 as well; the power method for the fuel weight will be discussed in the following section.

The weights of the three different components were determined, after the alteration of the number of refills. As mentioned before, the maximum take-off weight was kept constant at $9000kg$, the empty weight was found to equal $3800kg$, the fuel weight $2200kg$ and payload weight was kept at $3000kg$.

Verification

The method was verified by means of multiple methods. One of which was to implement the provided fighter example explained in part I of Roskam. This particular example was chosen as it also experiences a weight reduction during flight (by dropping bombs, instead of water). It was found that the results from the weight estimation were similar to the values shown in Roskam, slight deviations were present, these were due to the rounding of intermediate values in Roskam. [9]

Not only was the top level verified, but also smaller parts of this weight estimation method were checked. As explained earlier in this section, the altitudes flown in different phases of the flight were verified by means of Figure 7.7.

By calculating the intermediate values of the fuel, which was necessary to account for the weight loss/gain in flight, a sanity check could be done. A sanity check was done; minimal mistakes were found and corrected, as the intermediate values did not add up to the total fuel weight (Equation 7.6) found with the use of Equation 7.4. It was concluded that the

Table 7.2: Duration and fuel fractions for each phase of flight (phases described in Table 4.1) and the fuel usage per part of the mission.

Initial Attack

#	t [s]	FF [-]
1	60	0.996
2	60	0.995
3	30	0.996
4	100	0.9995
5	396	0.995
6	100	0.999
7	30	1.000
8	23	0.999
Total	**799**	**0.9797**

Refill

#	t [s]	FF [-]
9	25	0.9999
10	77	0.999
11	25	0.999
12	30	0.994
13	25	0.998
14	77	0.999
15	25	0.999
16	30	1.000
17	23	0.9999
Total	**337**	**0.9879**

Back to Base

#	t [s]	FF [-]
18	100	0.999
19	396	0.995
20	100	0.999
21	60	0.998
Total	**656**	**0.9910**

	Roskam	*Power*
Part	**W_F [kg]**	**W_F [kg]**
I.A.	182.5	79.4
R	86.2	35.5
B.B.	60.8	58.5

values found were reasonable for the parts of the mission. These fuel weights per part can be found in Table 7.2. Finding the fuel weights for parts of the mission resulted not only in a verification of the method, but also in providing insight into the different phases of the flight. This insight will be further discussed in chapter 8.

$$W_F = W_{F,initial\ attack} + \#drops \cdot W_{F,refill} + W_{F,back\ to\ base} \tag{7.6}$$

Another check was done by calculating the fuel usage of each phase with the use of power settings, efficiency and specific fuel consumption. Specifically, the a setting for the power for each phase was estimated, which was multiplied by the power available and the associated efficiency, Equation 7.7. The index i indicates a phase. The calculations and an explanation for this varying propeller efficiency (η_j) can be found in subsection 10.1.5.

$$P_i = P_{setting} \eta_j P_a \tag{7.7}$$

To find the fuel used per phase, the found power for a phase was multiplied by the specific fuel consumption and the duration of the specific phase, Equation 7.8. Again, the factor 0.95 is applied to account for the reserve fuel.

$$W_{F,i} = \frac{P_i c_p t}{0.95} \tag{7.8}$$

It was found that the fuel fractions used before were rather conservative and it turned out that the UAV is able to complete more refills during one mission than initially expected. The number of refills in one mission was more than tripled, from 23 to 72 refills. The weights of the three components (fuel, payload and empty weight) were unchanged.

To optimise the usage of the fuel weights once more, altering values were used for different phases of the flight. This time distinguishing differences between a full and an empty tank, this can have a difference of up to half of the MTOW. Changing the weight will be especially noticeable in the optimal cruise velocity. However, as the UAV is designed to cruise rapidly, and a cruise speed is set to $0.9 \cdot V_{max}$, this is only leads to very slight changes. The density of the atmosphere was also varied, resulting in different lift over drag curves and rates of climb achievable. But again, the reduction of fuel usage was not significant and thus the simplified method was adhered to.

7.4. Power vs. Wing Loading

A power loading vs. wing loading diagram has been established for multiple reasons. First of all, several flight performance requirements can be checked and iterations can be done if and when those requirements are not met. Also, verifying that the wing surface area and power available from the chosen engine are in an allowed ratio with the maximum take-off weight, can be done by means of this power loading diagram. It will imply certain required ratios for different flight performance parameters. This complete section loosely follows the initial sizing described in part I of Roskam [10].

Assumptions and Estimations

Several estimations and assumptions had to be made, these will be discussed first. The maximum lift coefficient in different conditions had to be estimated first. This was based on table 3.1 of Roskam part I[10], values were taken for the amphibious/flying boat aircraft type (11 in the table), a reference aircraft of this type is the predecessor of the CL-415, the CL-215. The values for C_L for landing, take-off and clean configuration were set to be 2.8, 2.2 ($= 0.8 \cdot C_{L_{max,landing}}$) and 1.5, respectively. This has also been touched upon in section 7.2. Other aerodynamic parameters had to be estimated as well, of which C_{D_0} was initially set to 0.04. The values of the aspect ratio and Oswald factor were also assumed in that section, 7.5 and 0.7, respectively.

The drag polar of the wing could be generated after having assumed the aerodynamic parameters. The lift coefficient is put out against the drag coefficient in Figure 7.6, three different lines are visible, each representing a different configuration of the aircraft. Namely, landing, take-off and cruise configuration. There is a slight change in drag coefficient for each of these configurations as the zero-lift drag coefficient is increased with the use of high lift devices. The deviation of C_{D_0} is 0.036 for take-off and 0.144 for landing, these values are derived from Raymer suggestions for wetted area estimations [11]. It has been assumed that the change of e for the different considerations is to be neglected. Also, the difference between landing gear up or down has been noted to not be significant, thus these configurations are not included in the drag polar.

Performance Parameters

As mentioned before, there are multiple requirements and performance parameters that can be found with the use of the power- vs. wing loading diagram. These parameters are listed and briefly explained and discussed. The imposed requirements on power- and wing loading can be found in Figure 7.9 and Figure 7.10. First the critical power- and wing loading were found for the initial values, and then, based on if the requirement had been met, an iteration for specific parameters could be done.

Stall Velocity

Requirement AF-PERF-01-F states that the stall speed should be lower than $120 km/h$. It can be checked if the requirement is met with the use of Equation 7.9.

$$V_{stall} = \sqrt{\frac{2W}{S\rho C_{L_{max}}}} \tag{7.9}$$

The landing configuration of the aircraft is most critical for this parameter, thus the lift coefficient should be assumed to be $C_{L_{max,landing}}$. The stall speed requirement imposes a constraint on the wing loading, it shows up as a vertical line, as it is not dependent on the power of the UAV. The wing loading should be lower than the value calculated. Calculation is done for different values of $C_{L_{max,landing}}$ in order to compare these values and iterate the aerodynamic parameters.

Cruise

As for the stall velocity, there is a set requirement for cruise, the UAV shall be able to reach $300 km/h$ in cruise (AF-PERF-CRUS-02-F). The cruise power to weight ratio can be determined by the use of Equation 7.10, assumed values for $P_{setting}$ and η_p are 0.8 and 0.85, respectively. These assumptions are discussed insubsection 10.1.1. Also, it is assumed that the aircraft will cruise at an altitude of $3 km$, such that the density at altitude is $0.909 kg/m^3$. Multiple calculations are done for different values of the aspect ratio. The power loading should be lower than the values indicated in the diagram.

$$\left(\frac{W}{P}\right)_{TO} = P_{setting}\eta_p \left(\frac{\rho}{\rho_0}\right)^{3/4} \left(\frac{C_{D_0}\frac{1}{2}\rho V^3}{W/S} + \frac{W}{S}\frac{1}{\pi A e \frac{1}{2}\rho V}\right)^{-1} \tag{7.10}$$

Take-off Parameter (TOP)

It is required that the UAV is able to take off from both land and water within $500 m$ (AF-PERF-TO-03). The value of TOP (the statistics/regulations for CS-23 were used here) is found with this take-off distance requirement and formulae from page 95 of Roskam part 1, namely, Equation 7.11, Equation 7.12 and Equation 7.13 [10]. In these equations, s is the distance in m and σ the ratio of densities at cruise altitude and the ground. It should be noted that these equations are in imperial units. These equations can be rewritten and it can then be concluded that the power loading depends on the wing loading and will thus show up as a curved line in Figure 7.10. A standard atmosphere is assumed, so $\sigma = 1$. For the take-off requirement, again, multiple lines are drawn for different values of $C_{L_{max}}$.

$$s_{TO} = 1.66 s_{TOG} \tag{7.11}$$

$$s_{TOG} = 4.9 \cdot TOP + 0.009 \cdot TOP^2 \tag{7.12}$$

$$TOP = \frac{W}{S}\frac{W}{P}\frac{\sigma}{C_{L_{TO}}} \tag{7.13}$$

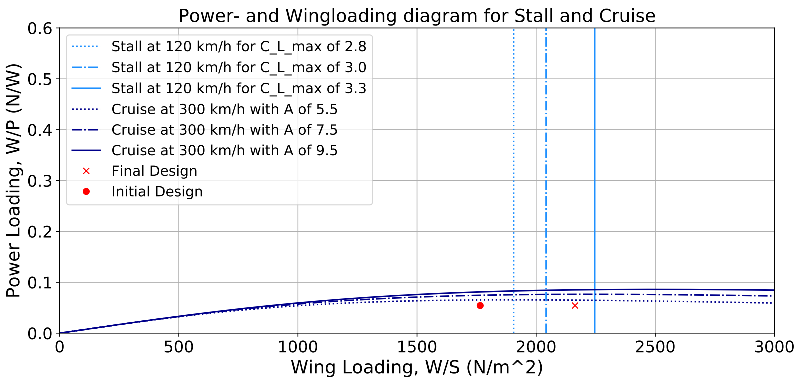

Figure 7.9: Power- vs. wing loading diagram for stall and cruise velocity requirements. The red dot shows the initial values of the UAV, whereas the red cross shows the values of the final design.

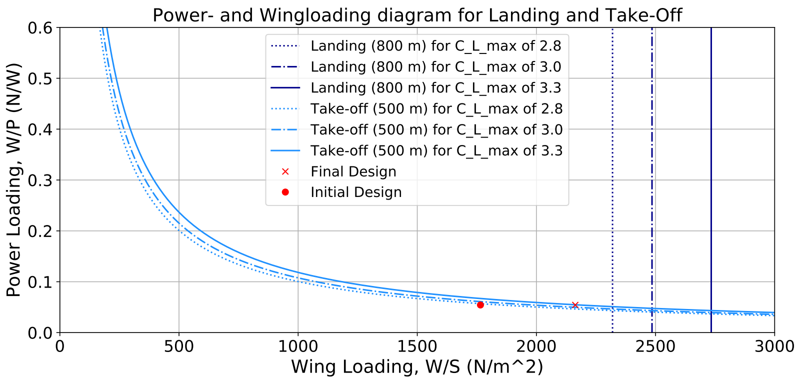

Figure 7.10: Power- vs. wing loading diagram for take-off and landing requirements. The red dot shows the initial values of the UAV, whereas the red cross shows the values of the final design.

Landing

The requirement for the landing distances is to be able to land on both land and water within $800m$ (AF-PERF-LND-02). To check if this requirement is met with the initial values chosen, a statistical method from Roskam is used again. The equations provided in Roskam can be rewritten to SI units and Equation 7.14, Equation 7.15 and Equation 7.16 are the result [10].

$$s_L = 0.5915 \cdot V_{s_{land}}^2 \tag{7.14}$$

$$\left(\frac{W}{S}\right)_{TO} = \frac{C_{L_{max}} \rho V_{s_{land}}^2}{2f} \tag{7.15}$$

$$f = \frac{W_L}{W_{TO}} \tag{7.16}$$

Initially, the landing to take-off weight ratio (f in Equation 7.16) was set to 2/3, although table 3.3 in part I of Roskam suggested otherwise for the amphibious type aircraft (11) [10]. This was done, as the payload is assumed to be more than a third of the maximum take-off weight, thus it is assumed that before a landing, all payload can be dropped and the ratio is then brought to 2/3. This implies that a system should be included that it will always be able to drop the payload for safety reasons (a dropping mechanism will be present, but some sort of alarm could be included to warn if there is still water in the tank), this should be looked at in future design steps. The landing requirement shows up as a vertical line in the diagram, as it is independent of power. It provides the maximum value for wing loading. Several lines are drawn for different values of $C_{L_{max}}$.

Compliance and Iterations

The critical values for the power- and wing loading imposed by the performance requirements to be met, as discussed previously, were calculated for the initial values set. These were plotted in the diagrams (Figure 7.9 and Figure 7.10), also a red dot showing the position of the UAV within the diagram has been plotted (for the initial design of which $S = 50m^2$). From the diagrams it can be checked if requirements are met and iterations followed as several of the requirements were not met (stall speed and take-off distance too large), and aerodynamic properties were altered.

It was decided that the $C_{L_{max}}$ was to be raised by 0.2 to 3.0. This was done in consideration with the determination of the high lift devices, because it had to be ensured that this lift coefficient could be reached. A reduction of the zero-lift drag coefficient to 0.03 resulted in a better performance of the UAV. As there is less drag to be overcome by the UAV and thus the lift over drag ratio increased. This reduction could be done as the initial value of C_{D_0} was found to be rather conservative.

Final Power- and Wing loading and Future Considerations
The final power- and wing loading value is also plotted in the diagrams, it is shown as the red cross. As can be seen, some of the requirements are not met (AF-PERF-01-F and AF-PERF-TO-03). However, these are such small deviations from the requirement that it can be concluded that the flight performance is not significantly reduced. The requirements that are not met are for stall; the UAV has a stall speed of $123.5km/h$, which is only 1% larger than the requirement. Also, the take-off requirement is not met, the UAV will be able to take-off from both land and water within $560m$, if a $C_{L_{max}}$ of 3.0 is used. Both of these requirements are not met as the maximum lift coefficient is not high enough and/or the wing loading is too big. However, as is explored in subsection 10.2.4, a lift coefficient of a value greater than 3.0 might be achievable, because in the final design the propeller will interact with the flow over the wing. This increase in lift coefficient can then result in the UAV being able to take-off within $500m$. Although the MTOW could have been reduced, this was not done, due to the fact that the design had been frozen.

The cruise and landing requirement are both met (AF-PERF-CRUS-02-F and AF-PERF-LND-02). A cruise speed of $300km/h$ can be reached and it was decided to keep the initial selected aspect ratio of 7.5. For the landing requirement, with the landing to take-off weight ratio of 2/3, landing would be possible within $500m$. If this ratio were to be 1, the requirement of a landing distance less than $800m$ is still met. But, being able to land on a shorter runway or water body can only be beneficial, and it is shown that this can be achieved with a ratio of 2/3 for the landing and take-off weight.

All parameters discussed above have been found for a density at sea-level conditions, except for cruise. In future design steps, one might want to consider checking if the requirements are met for densities above fires or at altitude. It was chosen not to this at this stage, as the design was still prone to changes.

7.5. Flight Performance Diagrams

Besides the performance parameters discussed in section 7.4, there are many more, of which some will be discussed in this section, namely the power available and required for different temperatures and banking angles. But also, the rate of climb for these different conditions, this parameter follows from the power diagrams. A figure including the different forces applied to the aircraft at different velocities is included as well.

7.5.1. Power Available and Required

In Figure 7.11, different curves are shown for different atmospheric conditions for the power required. The value of the power available line shown in this graph ($\pm 1600kW$), was determined by the selected engine. This engine was selected based on the required climbing performance of the aircraft and as this relates to both the power available and power required, these have to be found first. The selection of the engine is discussed in more detail in subsection 10.1.1. It is assumed that the available power is constant. It is equal to the sustained power available that the engine is able to provide, this is assumed to be roughly 80 % of the maximum available power. Also, the power required by the internal systems (communications, actuators, etc.) is assumed to be negligible. The power required is found by the use of Equation 7.17, different temperatures of the air relate to different densities, so ρ is altered for each line.

$$P_r = DV = C_D \frac{1}{2} \rho V^3 S \tag{7.17}$$

From the diagram in Figure 7.11, it can also be noted what the maximum reachable velocity is. This is the point where the available and required power are equal, for sea-level conditions this results in $V_{max} = 125m/s = 450km/h$. The stall speed is indicated by the dotted lines, as can be seen from Equation 7.9, this is also variable for different air densities.

The power required to be able to sustain different banking angles is shown in Figure 7.12. The UAV was initially sized to sustain a level banking angle of 30°. From the power diagram it can be seen that this angle can indeed be reached for speeds up to $122 m/s$. Even a banking angle of 60° can be achieved, but only if the velocity of the aircraft is between 50 and $105 m/s$. The required power will increase for both increased temperature and banking angle.

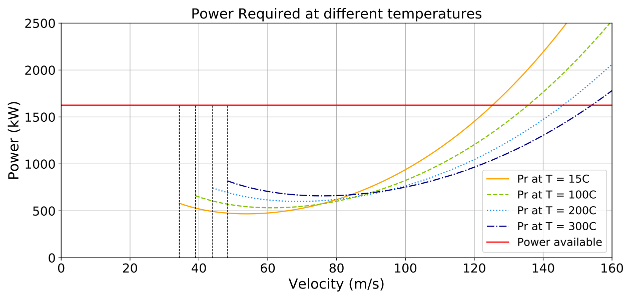

Figure 7.11: Power diagram, showing power available and power required at different temperatures. The dotted lines indicate the stall speed for the specific temperature.

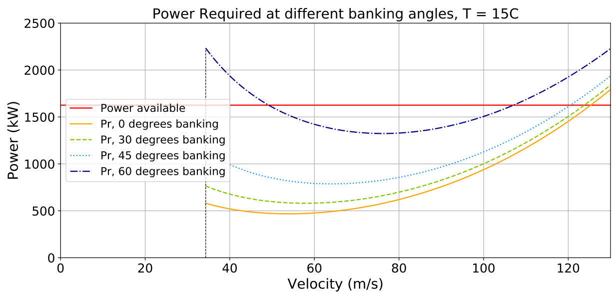

Figure 7.12: Power diagram, showing power available and power required at different banking angles. The dotted line indicates the stall speed for the sea-level temperature.

7.5.2. Rate of Climb

As mentioned before the achievable rate of climb of the aircraft is determined from the power diagram, the formula used is given in Equation 7.18.

$$RC = \frac{P_a - P_r}{W} \tag{7.18}$$

It can be noted that the maximum rate of climb that can be achieved under specific circumstances is at the velocity at which the difference between the available and required power is maximum. The requirement AF-PERF-TO-06, requiring $RC > 10 m/s$, is met as can be seen in Figure 7.13. The achievable rate of climb is lowered as the the temperature or banking angle increases.

Even if the aircraft is banking, it is able to achieve high rates of climb at a large range of the velocity. In Figure 7.14 this is visualised. This figure shows that the UAV is able to perform intense manoeuvres, such as when clearing the surroundings of a water body or when dropping the suppressants. Being able to not only sustain a 60° banking angle, but also climb whilst doing that, shows that the UAV is performing outstandingly. Note that these climbing performances are achieved with maximum take-off weight, which means that is even able to reach higher climb rates after suppressants are dropped or near the end of the mission when a large part of the fuel is used.

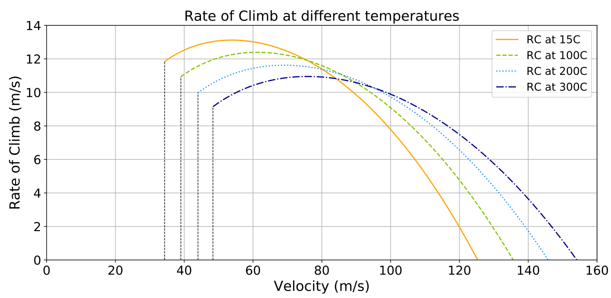

Figure 7.13: Rate of climb performance of UAV for different temperatures. The dotted lines indicate the stall speed for the specific temperatures.

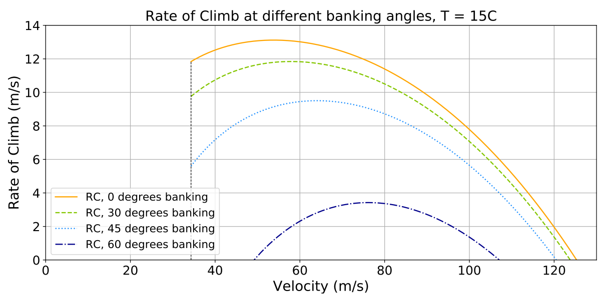

Figure 7.14: Rate of climb performance of UAV for different banking angles. The dotted lines indicate the stall speed for the sea-level temperature.

8
Firefighting Performance

As an aerial firefighting aircraft, there are aspects of the UAVs performance that are exclusive to its mission, such as its ability to perform scoops and drops of suppressant as well as the frequency and time wherein it can do so. The obtained outputs of this chapter, such as payload, fuel weight, and dropping load factors are used in the detailed design of components in chapter 10.

8.1. Versatility of Firefighting Mission

As explained in section 4.1, the main mission Wangari is designed for is to contain wildfires. Hence, the phases of the flight profile that influence the firefighting effectiveness are given special attention. These phases consist of fast cruise to fire, performing a dropping manoeuvre, scooping up water, a quick cruise between the water and fire and returning to the water or base. In section 4.2, it has been discussed what the design mission is. The distances between the three locations of the mission (airbase, fire and water body) were taken as an average from literature study [6]. It was set to $50km$ between the airbase and fire and $10km$ between the fire and water body. The UAV has been designed to complete this firefighting mission as quick as possible.

However, the UAV will not encounter the same design mission each time, thus, to show its versatility, several firefighting performances are analysed and touched upon within this section. The UAV can be versatile in different senses. Firstly, it could be that the fire is closer by or further away than initially expected, or that available water bodies are located at a larger distance. The dropping capability of Wangari is explored for different distances and is visualised in both Figure 8.1 and Figure 8.2.

A wildfire is not only defined by its location; the size and intensity of the wildfire will also determine how Wangari should leave the airbase and what strategy can be applied to best attack the wildfire. Variations could, for example, be made with the payload and fuel weights. It could be decided by the operating crew that initial attack is not as important. A mission might already be in operation for a while, leading to the possibility that the UAV is more effective in terms of dropped amount per hour when it leaves the airbase with no payload and is able to fly more efficiently in cruise. This will of course also depend on the distance to be travelled. A visualisation of this possibility is made in Figure 8.1. In this figure, the performance of the CL-415, the main competitor, is also given to gain insight in Wangari's performance on the market. It must, however, be noted that the design of Wangari is estimated to cost half of that of a CL-415 as given in chapter 19, such that in theory two Wangaris could be deployed for the price of one CL-415.

When a fire is intense, chances are high that Wangari will have to refill at a local body of water to collect new suppressant. The time needed to perform the manoeuvre of cruising to the source of water, scooping up water, and cruising back to the fire, is given in Figure 8.2 for various distances from the fire to a body of water. Again the CL-415 is added to show the market perspective.

Another way in which Wangari is versatile for a firefighting mission, is the interchangeable weight between payload and fuel. Initially it was assumed that the payload would be constant throughout the mission; $3000kg$ of suppressant would be carried to complete all drops within a mission. However, it was found that in total, a larger amount of suppressant can be dropped if the UAV leaves the airbase with partly filled water tank, namely until $2500kg$ instead of the maximum of $4500kg$. As the mission progresses this increases. This is because the weight of the fuel obviously decreases throughout the mission, but as the maximum take-off weight does not, more water can be scooped during each refill, ending up with a final drop of $4500kg$ of suppressant. The evolution of the different weight components throughout the design mission for the variable and constant payload is shown in Figure 8.5.

The dropping capacity of the UAV varies throughout the mission, as was clear from Figure 8.5. However, the dropping capacity per hour also varies depending on the distance of the fire to a source of water. This is visualised in the case

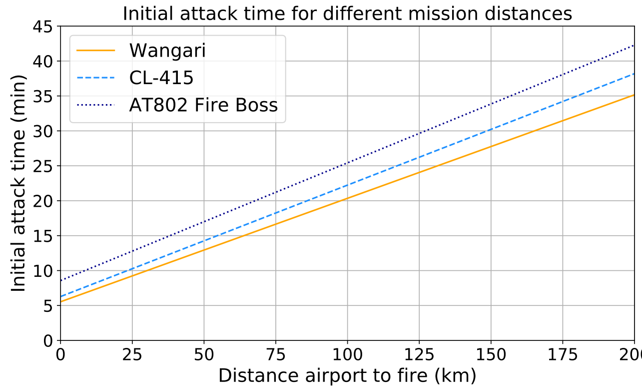

Figure 8.1: Time taken to complete first drop compared to the distance between airbase and fire shown for Wangari and the CL-415.

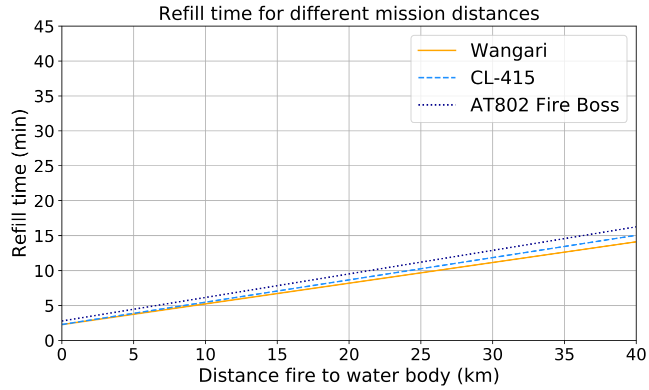

Figure 8.2: Time taken to refill water tank at water body and drop it compared to the distance between fire and water body shown for Wangari and the CL-415.

of 1 or 2 Wangaris and the CL-415 in Figure 8.3. As is visible, one CL-415 is capable of dropping more litres per hour than a single Wangari. However, when two Wangaris are used, which is estimated to cost less than a CL-415, the pair of Wangaris outperforms the CL-415 in terms of dropping capacity. Furthermore, in this figure, the differences due to nightly operations are not incorporated. When the fact that Wangari can do nightly operations and CL-415s cannot is taken into account, the advantage of using the pair of Wangaris instead of the CL-415 will show to be much higher.

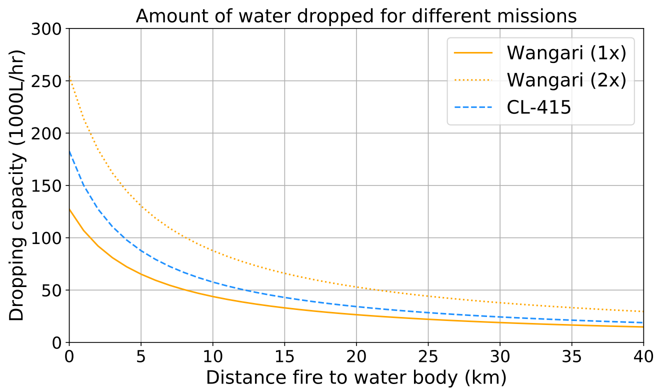

Figure 8.3: Amount of water dropped per hour for different distances between fire and water body.

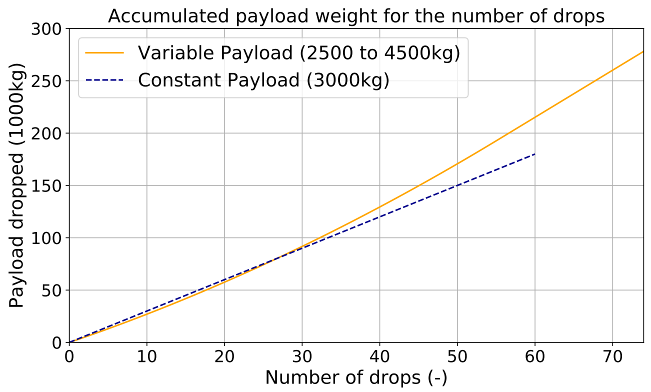

Figure 8.4: Cumulative weight of the suppressant dropped for the design mission for variable (between 2500 and 4500kg) and constant (3000kg) payload.

In Figure 8.4, it can be seen that with an increasing payload throughout the mission, more fuel can be taken by the UAV and thus more refills can be completed, nearly fifteen more. However, it has to be noted that initially less suppressant will be dropped. The accumulation of dropped amount of suppressant can be seen in Figure 8.4. After 26 drops the varying payload will have dropped more suppressant near the fire, resulting in nearly 100,000kg more suppressant dropped per mission compared to when constant payload is taken.

This finding has an effect on several design parameters, for example, the landing distance requirement, as the landing to take-off weight ratio has been increased, this is taken into account in section 7.4. Also, it will affect the internal lay-out of the UAV, a larger water tank should be fitted, holding at least 4500kg of suppressant. The maximum fuel weight is determined to be 2700kg, thus the fuel bladder should be able to contain this amount of fuel as well. This all will influence the control and stability of the UAV, which is discussed in the following sections.

Payload-Range Diagram
By determining the intermediate fuel weights with the power settings, the payload-range diagram could be established, Figure 8.6. The weights of the payload, fuel and maximum take-off are displayed against the range it can achieve carrying

different amounts of fuel and payload. To determine the range, Equation 8.1 is used, in which SFC is the specific fuel consumption.

$$R = V \cdot \frac{W_F}{P_r SFC_{cruise}/\eta_j} \tag{8.1}$$

Different values for each of the critical points are used. It is assumed that Wangari can fly at the optimal lift over drag for cruise, which has a maximum value of 11.7. As can be seen in Figure 7.8, the maximum value is not altered for a variation of altitude or weight. The velocity at which it occurs does change however. The optimal cruise velocity is, therefore, inserted in the range equation. The power required is determined with the use of Equation 7.17, and the efficiency, η_j, is calculated by applying Equation 10.7. The specific fuel consumption is assumed to be constant and equal to $75.2 \cdot 10^{-9} kg/J$. For instance to find the maximum range (ferry range), the UAV will only carry fuel ($2700 kg$), the weight is set to equal $6500 kg$, thus the optimal velocity is found to be $60 m/s$, then the range is found to be $\pm 5600 km$.

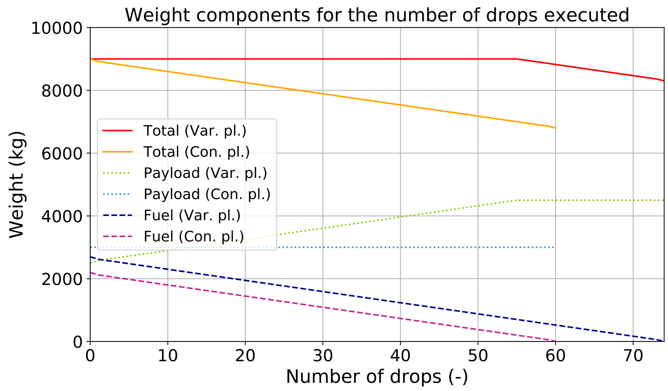

Figure 8.5: Progress of different weight components for the design mission as function of the number of drops. Two scenarios are included, a varying payload throughout flight ($2500 kg$ at first drop and $4500 kg$ at the last) and a constant payload ($3000 kg$).

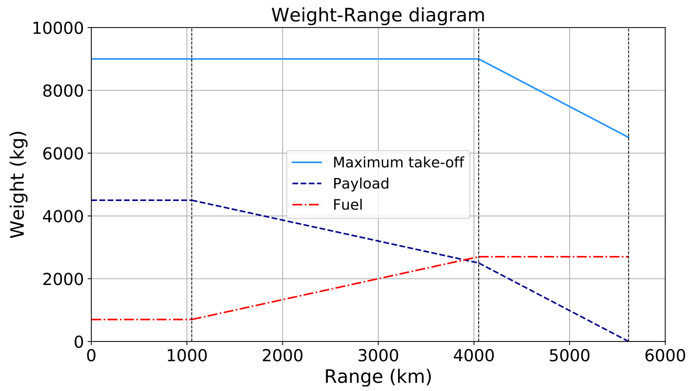

Figure 8.6: Payload-range diagram, fuel and take-off weights are also included.

8.2. Scooping

Scooping up water is a dangerous part of the firefighting mission, especially if high wave heights are present at the water source. The UAV is still in flight mode, extends however scoopers in the water using its forward velocity to bring the water in the tank. By minimising the scooper area, potentially hazardous effects of hydrodynamic drag can be minimised. The stability during scooping is, however, of lesser impact than during landing, take-off and dropping, and has been analysed in subsection 8.3.4 and subsection 10.4.2.

8.3. Dropping

8.3.1. Dropping loads and limits

The UAV is designed for a maximum manoeuvre load factor of 4.4 as is also visible in the flight envelope in Table 7.1. This maximum also impacts the flight performance when dropping suppressant. Analysing Equation 8.2 for the load factor n, it can be observed that a sudden decrease in weight will increase the load factor. This increase in load factor due to dropping impacts the manoeuvres done during dropping. To calculate the maximum load factor of these manoeuvres Equation 8.3 was used.

$$n = \frac{L}{W} \tag{8.2}$$

$$n_{max\ before\ dropping} = n_{max} \cdot \frac{W_{after\ dropping}}{W_{before\ dropping}} \tag{8.3}$$

In Equation 8.3, the assumption was made that during the dropping the lift generated by the UAV does not change. Since there are two extremes in terms of the amount of water the UAV can take along, both allowable load factors are calculated.

For both calculations it is assumed that the UAV is flying at maximum take-off weight before dropping. For the maximum amount of fuel and, thus, the least amount of payload, the UAV can carry 2500 litres of suppressant. Meaning that the maximum allowed load factor due to manoeuvres whilst dropping is 3.17. When the maximum amount of payload is taken, 4500L of suppressant, the maximum load factor due to manoeuvres is 2.2. The allowable load factors for different amounts of payload are also summarised in Figure 8.7

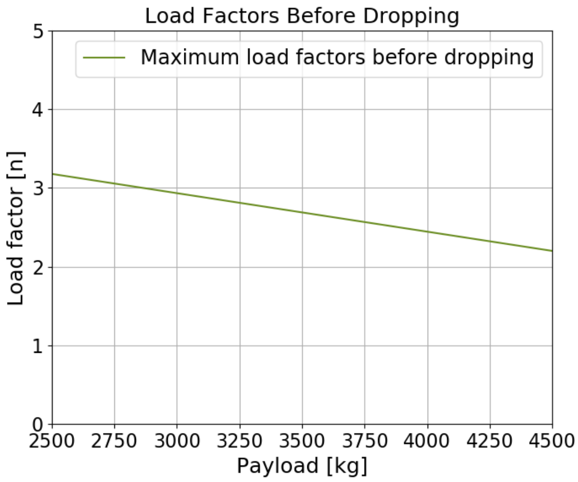

Figure 8.7: Allowed load factors before dropping

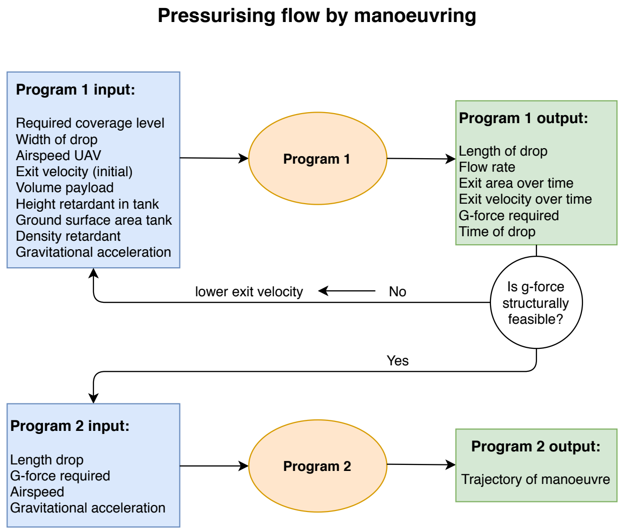

Figure 8.8: Inputs and outputs of the dropping manoeuvre program.

8.3.2. Dropping Mechanism

The dropping mechanism is a crucial aspect of the water bomber, since it determines the dropping characteristics of the suppressant. Optimising the dropping characteristics enhances the effectiveness and efficiency of extinguishing or containing the wildfire. Currently, several mechanisms are used to drop suppressant and their functioning, advantages and disadvantages are described in the following. [1]

Gravity drop system

System with one or more segments filled with suppressant, held in place by doors. If a door opens, all the suppressant in that segment falls out of the tank by gravity. It is very well suited for direct attack and semi-direct attack. It is reliable, because of the low complexity. The system could be used for indirect attack with an accepted efficiency.

Gravity with constant flow doors

Comparable to gravity drop systems, however, the doors open partially. This is done to maintain a constant flow rate (volume of suppressant that flows out of the tank per time) and prevent a large shift in c.g.. The pilot inputs the required coverage level and the total volume to be dropped, after which the computer opens the doors with a certain speed to obtain a constant flow rate over time. The system is also able to perform drops with different coverage levels. For example, when selecting a high coverage level and a huge quantity of product, it can make heavy and decisive direct or semi-direct drops, but using a lower coverage level allows to create thin and long suppressant lines that act like a firebreak.

Pressurised drops

Using a pressurised drop system the suppressant flows more rapidly out of the tank. The advantages of having a pressurised system is that the width of the drop can be made twice as large as compared to those obtained using conventional gravity systems, because of the atomisation and dispersion being more efficient [12]. Besides, because of the higher exit velocity of the suppressant, the suppressant reaches the ground faster. This means that the suppressant will be less affected by high wind speeds and hence the drop will be more accurate. The main disadvantages of a conventional pressurised system is the delay of several minutes on the ground required to pressurise tank and the additional weight carried by the aircraft.

[1] `http://www.marsaly.fr/fred/fire-bombers-drop-systems/` [cited 17 June 2019]

Trade-off dropping mechanism
The objective of the design is to contain the fire and not to extinguish it. Because of the fact that the gravity system is most suitable for (semi-)direct attack, this system will not be used. The constant flow doors have a big advantage by being able to perform drops of constant flow rate and different coverage levels. Having a constant flow rate means that the coverage level over the length of the drop will be constant. Furthermore, being able to make drops with different coverage levels might be very useful when fighting fires with different intensities. For fires with a small intensity, lower coverage levels might be more efficient and vice versa.

On the other hand, a pressurised system has the advantages of being able to perform drops of higher width than a gravity based system and with a higher exit speed such that the drop is less affected by the wind and therefore more accurate.

Therefore, designing a dropping mechanism which is pressurised would be optimal for achieving the objective. A technique, which complies with the aforementioned requirements, that is proposed consists of passively pressurising the suppressant tank by performing manoeuvres in-flight, supplemented by sliding doors which are used to maintain a constant flow rate during the drop. If feasible, the technique will have the advantages of the constant flow mechanism and of the pressurised system, without having to carry additional weight to pressurise the tank and without having a refill delay of several minutes on the ground. Furthermore, since the aircraft is unmanned, the g-forces will not be experienced by a person, however, the loads still need to be supported by the structures in the UAV. The technique is promising and innovative, but needs to be further analysed to check whether it is indeed feasible. This is done in subsection 8.3.3.

8.3.3. Dropping Manoeuvres
In this section the feasibility of the technique described in the previous section is analysed. This is done by calculating the required g-force for several cases. Those g-forces may not exceed the maximum g-force limit determined in subsection 8.3.1. Some assumptions are made during this process, which are listed below:

- Trajectory of the manoeuvre is circular and is performed with a constant velocity.
- The flow in the suppressant tank is incompressible.
- Viscosity and friction in the tank are neglected.
- Coverage level is assumed to be constant over the ground surface.
- Downwards velocity of the suppressant in the tank is assumed to negligible compared to its exit velocity.

Process
Whilst the manoeuvre is performed, a centripetal force is exerted on the UAV, which induces pressure inside the suppressant tank. This pressure is used to push the suppressant out of the tank with a higher exit velocity than when using a gravity-based system. However, in order to calculate the trajectory and the required g-forces, some inputs are needed which are important to determine those outputs. One of them is the so-called coverage level, which expresses the volume of suppressant per area on the ground. For larger fires, a higher coverage level is required and vice versa. In Table 8.1 below an estimate of the coverage level that should be used for different fire behaviour.

Table 8.1: Coverage level required for different types of wildfires, adapted from [13].

NFDRS[2]	Fire Behaviour	Coverage Level $[L/m^2]$	Description
A,L,S	1	0.41	Annual and perennial western grasses, tundra
C	2	0.41	Conifer with grass
H,R	8	0.81	Short-needle closed conifer, summer hardwood
E,P,U	9	0.81	Long-needle conifer, fall hardwood
T	2	0.81	Sagebrush with grass
N	3	0.81	Sawgrass
F	5	1.22	Intermediate brush (green)
K	11	1.22	Light slash
G	10	1.63	Short-needle conifer (heavy dead litter)
O	4	1.63	Southern rough
F,Q	6	2.45	Intermediate brush (cured), Alaska black spruce
B,O	4	2.45	California mixed chaparral, high pocosin
J	12	>2.45	Medium slash
I	13	>2.45	Heavy slash

[2]USA National Fire Danger Rating System

When the required coverage level is determined, the required flow rate can be calculated using Equation 8.4.

$$Q = w v_{UAV} CL \tag{8.4}$$

In which, w, is the width of the drop, v_{UAV}, the velocity of the UAV, and CL, the coverage level.
Another important input is the required exit velocity of the suppressant. The higher the exit velocity, the more efficient the atomisation and dispersion of the drop will be, thus the greater the width of the performed drop can be. Furthermore, when the exit velocity is higher, the suppressant will be less affected by wind speeds, because the suppressant reaches the ground faster, and the drop will, hence, be more accurate. When the exit velocity and the flow rate are determined, these parameters can be used to calculate the initial exit area using Equation 8.5.

$$A_{exit} = \frac{Q}{v_{exit}} \tag{8.5}$$

As mentioned before, to push the suppressant out of the tank with a certain exit velocity, pressure in the tank is required. The magnitude of the pressure required can be determined by making use of Bernoulli's principle stated in Equation 8.6.

$$p_1 + \frac{1}{2}\rho v_1^2 + \rho g h_1 = p_2 + \frac{1}{2}\rho v_2^2 + \rho g h_2 \tag{8.6}$$

In this equation, the variables with subscript 1 are related to the flow of the suppressant in the tank. The variables with subscript 2 are related to the flow of the suppressant exiting the tank. Hence, p_1 is the pressure exerted on the suppressant in the tank and is the variable that has to be determined. Some assumptions are made during this derivation, which are listed below:

- $v_1 = 0$: the velocity of suppressant in the tank is assumed to be negligible compared to the exit velocity.
- $p_2 = 0$: besides the atmospheric pressure, no additional pressure is applied to the flow exiting the tank.
- $h_2 = 0$: the height of the exiting flow is equal to zero.

Using the assumptions and solving for the pressure in the tank, the formula in Equation 8.7 is derived.

$$p_{tank} = \left(\frac{v_{exit}^2}{2g} - h_{suppressant}\right)\rho g \tag{8.7}$$

A sketch of the tank is given in Figure 8.9. The pressure calculated in Equation 8.7 is induced by the centripetal force

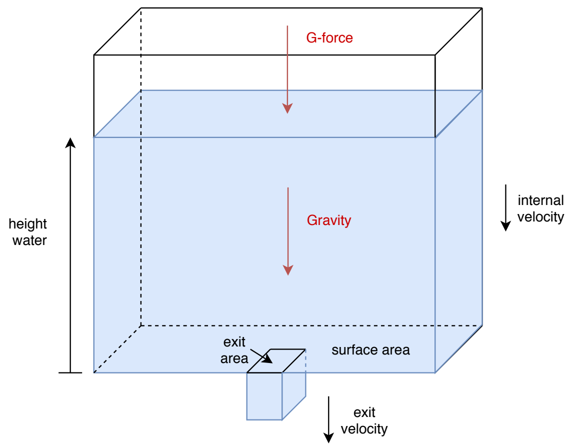

Figure 8.9: Pressurised suppressant flow in the internal tank.

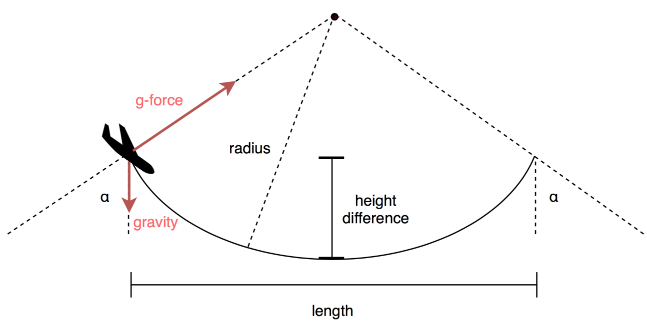

Figure 8.10: Circular trajectory of the UAV during the manoeuvre.

generated by performing the manoeuvre. The g-force experienced by the UAV can be related to the pressure exerted on the suppressant in the tank by Equation 8.8.

$$F_{g-force} = \frac{p_{tank} A_{surface}}{m_{suppressant}\, g} + 1 \tag{8.8}$$

As can be deduced from Equation 8.8, the g-force required depends on the pressure (which depends on the exit velocity, the gravitational acceleration, the height of the water and the density of the suppressant), the surface area of the tank and the mass of the suppressant within the tank. As a circular trajectory was assumed in subsection 8.3.3, the g-force is constant over time, i.e. $\frac{dF_{g-force}}{dt} = 0$. However, some of the parameters will change within the manoeuvre: the height and the mass of the suppressant will change after some suppressant has been dropped. This is why the exit velocity will most likely also change during the manoeuvre, because of that g-force being constant. The height of the suppressant in the tank can be written as $h_0 - v_{tank}t$ and the mass of the suppressant as $m_0 - Q\rho$. Furthermore, the exit velocity can be rewritten as $v_{exit} = \frac{Q}{A_{exit}}$. This is done so that the exit area of the tank can be changed in the equation, to maintain the constant flow rate.

$$F_{g-force} = \Big(\frac{Q^2}{2gA_{exit}^2} - (h_0 - v_{tank}t)\Big)\frac{\rho A_{surface}}{m_0 - Q\rho t} + 1 \tag{8.9}$$

The changing exit area over time is the variable that has to be determined, so that the computer can tell the actuation system how much the sliding doors need to be opened to maintain that constant flow rate. This is why the derivative of Equation 8.9 is taken. Since the g-force is constant over time, its time-derivative is zero. The right hand side of the equation is also differentiated and the derivative of the exit area over time is moved to the left hand side. It is important to keep in mind that the flow rate is hold constant when performing the differentiation. The result is shown in Equation 8.10.

$$\frac{dA_{exit}}{dt} = \Big(\frac{\rho Q}{m_0 - Q\rho t}\Big(\frac{Q^2}{2gA_{exit}^2} - (h_0 - v_{tank}t)\Big) + v_{tank}\Big)\frac{gA_{exit}^3}{Q^2} \tag{8.10}$$

Now $\frac{dA_{exit}}{dt}$ can be determined. However, to determine the exit area at a certain moment, Equation 8.10 has to be integrated. This is done numerically using a programming software. The result is mentioned at the end of this subsection.

Length of drop
The length of the drop is also of importance in efficient firefighting. The length can be determined using Equation 8.11.

$$l_{drop} = \frac{v_{UAV} V_{suppressant}}{Q} \tag{8.11}$$

In which, v_{UAV}, is the velocity of the UAV, $V_{suppressant}$, the volume of the suppressant dropped, and Q the flow rate.
The trajectory of the manoeuvre can eventually be calculated with the constant g-force calculated before. The radius of the circular trajectory will be equal to Equation 8.12.

$$r = \frac{v^2}{(g_{force} - 1)g} \tag{8.12}$$

Having determined the radius, the approach angle can be calculated using Equation 8.13.

$$\alpha = \arcsin\Big(\frac{l/2}{r}\Big) \tag{8.13}$$

Furthermore, the UAV will experience a height difference during the manoeuvre as derived in Equation 8.14.

$$\Delta h = r - \sqrt{r^2 - \Big(\frac{l}{2}\Big)^2} \tag{8.14}$$

A sketch of the circular trajectory is included in Figure 8.10, to help visualise the manoeuvre.

An overview of the inputs and outputs is provided below. Very high g-forces are structurally not allowed. Hence, if the g-force is higher than the maximum g-load plotted in Figure 8.7, the exit velocity of the suppressant has to be lowered and a new iteration should be performed. This should be done until the g-force is structurally feasible.

Results
For a suppressant volume of $3000L$, a dropping width of $30m$ and an airspeed of $40m/s$, the exit velocity at a certain time is depicted in Figure 8.11 for different coverage levels. The initial exit velocity is equal for all coverage levels, as this is set as input. For the three given scenarios, the decrease in velocity is different. The scenario with a higher coverage level has steeper decrease in exit velocity than the scenarios with lower coverage levels. The result shows what was desired, a higher exit velocity than with a gravity-based dropping mechanism is obtained. The initial exit velocity is equal to approximately $8m/s$, while a gravity-based dropping mechanism always has an exit velocity of $0m/s$. This is

favourable because the suppressant will reach the surface earlier and will be less affected by wind. The drops can also be made wider with such an exit velocity. In Figure 8.12, the required exit area over time to maintain a constant flow rate of the suppressant is given for different coverage levels. It shows that the sliding door should keep sliding continuously. For higher coverage levels, the initial exit area (at t=0) is already bigger and the door needs to open faster than for lower coverage levels.

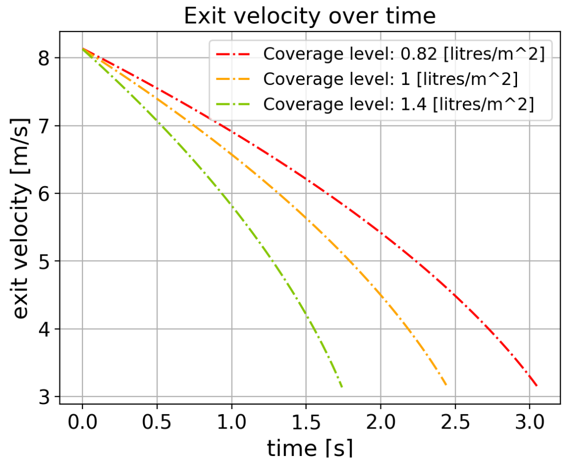

Figure 8.11: Exit velocity over time

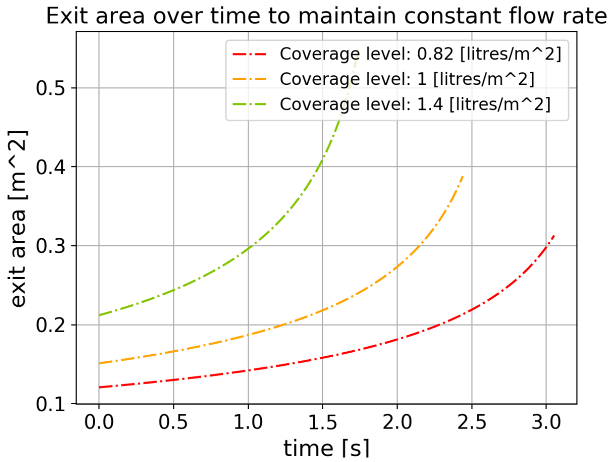

Figure 8.12: Exit area over time

Figure 8.13, Figure 8.14 and Figure 8.15 show the trajectory properties for different coverage levels; the approach angle, the height difference and the length of the drop, respectively. As aircraft have limits on the pitch angle, not all the manoeuvres shown are allowed to be performed. A limit of 45 degrees is set, based on the fact that aircraft also perform manoeuvres with a pitch angle of 45 degrees when doing a zero-gravity manoeuvre. [3] This is depicted by a red dashed line in the graphs below and occurs at a coverage level of $0.81 L/m^2$. Coverage levels lower than $0.81 L/m^2$ need to be obtained with a lower initial exit velocity than 8.15m/s. Hence, for an initial exit velocity of 8.15m/s, the most difficult manoeuvre is performed when a coverage level of $0.81 L/m^2$ is required. The maximum height difference will be 25.6 metres and the maximum length of the drop will be 121.8 metres as can be seen in the graphs.

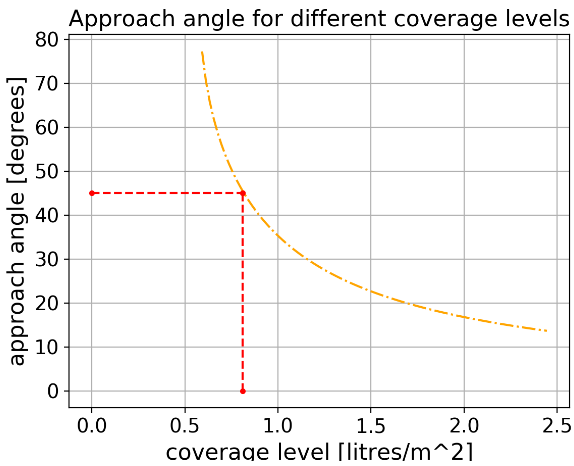

Figure 8.13: Approach angle

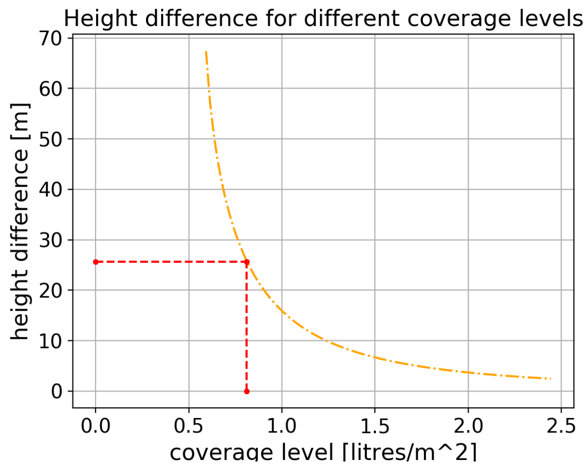

Figure 8.14: Height difference

Finally, Figure 8.16 shows the duration of the drop for different coverage levels. It shows that the duration is longer for lower coverage levels. This is as one would expect, as the flow rate is lower for lower coverage levels, which means that it

[3] https://web.archive.org/web/20090801051003/http://jsc-aircraft-ops.jsc.nasa.gov/Reduced_Gravity/trajectory.html

takes longer to drop all the suppressant. Again, coverage levels lower than 0.81L/m^2 cannot be achieved with an initial exit velocity of 8.15m/s.

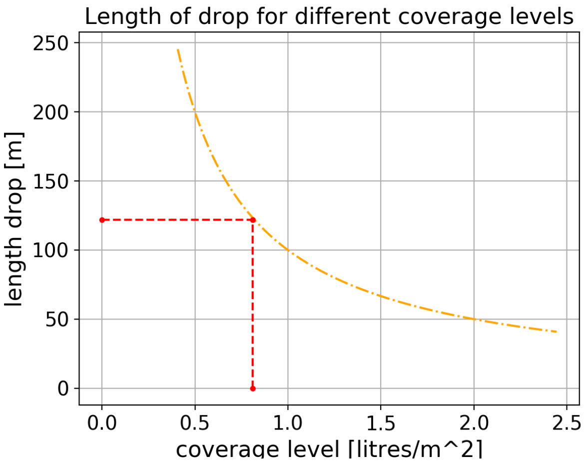

Figure 8.15: Length drop

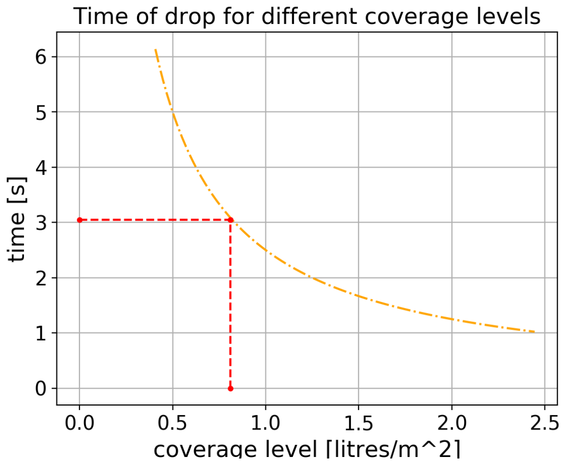

Figure 8.16: Duration drop

8.3.4. Stability During Dropping

A critical aspect of the firefighting performance is ensuring the UAV stays stable and controllable during dropping. During dropping the UAV loses up to 50% of its MTOW, which could lead to a shift in the centre of gravity. The longitudinal c.g. shift caused by dropping the suppressant is regarded as the most important parameter for designing for stability and controllability. A big c.g. shift would mean a big change in the moments caused by the aerodynamic surfaces and propulsion system, which either results in a big pitch up/pitch down moment, or requires large deflections from the horizontal tail surface to counter the moment. It is also a requirement that the UAV should be stable during the dropping of the suppressant.

AF-PERF-STAB-01 The UAV shall be stable during suppressant dropping

As the UAV is designed in such a way that the c.g. of the water tank is at the about same location as the c.g. of the operational empty weight of the UAV, it was achieved to have a maximum horizontal c.g. shift of 7 millimetres. The c.g. shift in x and z direction when dropping the water is shown in Table 8.2.

Table 8.2: The c.g. shift in the x- and z-direction when dropping the water whilst having maximum fuel and whilst having no fuel.

Amount of fuel	**Displacement of c.g. in longitudinal direction (x)**	**Displacement of c.g. in vertical direction (z)**
Full fuel	$0.005m$	$0.38m$
No fuel	$0.007m$	$0.41m$

Only in the vertical direction, a serious shift of the c.g. is observed. However, this has less effect on the longitudinal stability and controllability than the horizontal displacement. This is because the drag components are smaller than the lift components (They are also neglected in constructing the scissor plot in section 10.4). If one was to be interested in general stability and controllability, this can be found in section 10.4.

8.3.5. Retardant Choice

Fighting fires with water only is inefficient as water is prone to evaporation in the air due to shear, heat and wind [14]. Therefore, it is chosen to add a chemical product to the water.

Currently, three retardant options are used in aerial firefighting: long-term retardants, foams and gel enhancers. Of these, only foams can be directly proportioned during flight, for both gels and long-term retardants the mixture must be pre-made on the ground[4]. This would increase the turn-around time and nullify the benefits of the water scooping

[4] `http://airtanker.org/wp-content/uploads/2012/12/Fire-Chemical-Use-Eddie-Goldberg.pdf` [cited 19 June 2019]

capabilities of the UAV. Therefore, foams are chosen to enhance the firefighting effectiveness of the UAV.

Foams consist of both an foaming and wetting agent [15]. The foaming agent creates bubbles that increase insulation and thereby slow evaporation as well as improve the accuracy of the drop. The wetting agent, or surfactant, increases the ability of the mixture to penetrate the fire fuels. Besides the increase in effectiveness of the dropped suppressant itself, the foam helps increasing the effectiveness of the entire firefighting mission by visualising the dropped load using colourants [5]. Due to this, the cameras on the UAVs are able to detect the load both on the ground and in the air, aiding remote pilots of follow-up UAVs to more accurately determine their drop zone.

In the selection process of specific foams is looked at the sustainability of the retardant which is based on the effectiveness of the retardant, as a more effective retardant will reduce the total emissions from the fire; and its environmental toxicity and fate. From the selection process, it has become clear that Class A Foams must be used as they are formulated using environmentally favourable raw materials and are fully biodegradable [5]. The direct environmental impact of the retardant is, however, of lesser importance than its environmental fate as it will be overshadowed by the impact of the fire itself. Research into the environmental toxicity effects of foams has, however, shown that foams by Phos-Check are found to have lower impact on the biodiversity than Fire-Trol and Silvex foam solutions [16]. Phos-Check WD881 is found to be the most concentrated Class A foam product available[6]. This means that for Phos-Check WD881, the lowest amount of water is needed to obtain results, reducing the number of trips needed by the UAV which in turn reduces the emissions and cost. Hence, the retardant tank and injection system is designed to accommodate Phos-Check WD881.

8.4. Night Operations

The optimal time to fight wildfires is at night, because of the reduced temperatures, increased humidity and often lighter winds [3]. However, currently it is not done due to the poor visibility and, therefore, an increased risk for the pilots. Since the Wangari system is unmanned, which means greater risks can be taken, and is equipped with devices and infrared sensors, a nocturnal mission being successful is much more likely than with current aerial firefighting technology. In subsection 11.3.1 all the devices and sensors that are used by the system are described, including the devices and sensors that are useful at night. These consist of four infrared camera's, a navigation system, four strobe lights and eight collision avoidance lights. They will be further explained below, however for all details please refer to subsection 11.3.1.

1. **IR cameras:** The infrared cameras have the same function at night as the normal cameras during the day. They are used to visualise the fire at night and can even see through smoke. Another great advantage of thermal cameras is that they can monitor the fire's spread and detect hot spots [7].
2. **Navigation system:** The navigation system used in the UAVs are designed for air-to-air and air-to-ground operations [8]. This means that pilots at the ground station will know the location of the UAVs at any time and can be used at night to navigate the system to the right location without risking a collision.
3. **Strobe lights:** The strobe lights can be used at night in combination with visual cameras to view its close surroundings at critical moments, for example during scooping. Besides, unforeseen objects, such as power lines, can also be seen and avoided with these lights.
4. **Collision Avoidance lights:** The collision avoidance lights are high-intensity lighting devices used on a UAV to give information on its position, heading and status to other UAVs. It can also be used at night to warn the UAVs if other aircraft and/or UAVs are in proximity. Eight of them are used so that UAVs are always visible, no matter what their relative position is.

Using, these devices, in addition to the regular devices and sensors that Wangari uses described in section 11.3, the Wangari system is able view the situation and spread of the fire at night, to locate all the UAVs at every moment and to see its close surroundings when it is dark. Hence, it is safe to say that the system has a great potential to be used at night to fight wild fires. However, summarising the devices and sensors necessary is definitely not enough and further steps still need to be taken to ensure the UAV is actually able to perform the entire mission, which includes take-off, landing, cruise, scooping and dropping. Furthermore, authorities must still authorise the usage of Wangari in nocturnal operations.

[5] `https://www.fs.fed.us/t-d/programs/wfcs/wfcs/performance/documents/Biodegradability_FoamPlus_110608-Rev.pdf` [cited 19 June 2019]
[6] `https://phoschek.com/product-class/class-a-foam-for-wildland/` [cited 19 June 2019]
[7] `https://www.flir.com/instruments/firefighting/` [cited 24 June 2019]
[8] `https://www.l3commercialaviation.com/avionics/products/tacan/` [cited 24 June 2019]

9
Firefighting Strategies

The project objective includes the use of strategic attacks to fight wildfires. The word strategic is a reference to tactical decisions made to use a fleet of aircraft in order to fight a fire more efficiently than traditional methods. In this case, swarming attacks are investigated as a strategic firefighting method. A firefighting authority has a choice when acquiring a new fleet of aerial firefighters. For the same cost, they can either opt for larger water tankers, or a fleet of smaller aircraft that can operate in swarms to contain fires. The aim of this investigation is to find out if the second option can be advantageous. The problem is thus formulated: "Can several smaller aircraft contain fires more effectively than larger water tankers?"
In order to address the problem, a fire simulation is developed and two different fire scenarios are selected for a case study. The two cases are: a fire that has multiple critical points that are far away from each other, and a case of an intense fire with a persistent fire front line that is hard to slow down and stop. The analysis of these cases in section 9.2 concludes that swarming can be a more effective way to contain fires and limit their spread to smaller burnt areas.

9.1. Fire Simulation

The best way to study firefighting strategies is to predict the behaviour of the fire. Unfortunately, this is not possible since fires, especially wild and forest fires, can spread unpredictably. Too many variables influence fire behaviour. Examples are wind, moisture of objects in the fire path, heat in the area, presence of fire fuel on the fire path, and elevation variation in the forest terrain. The next best option is to either find data on fires that have already occurred, that describes their spreading behaviour, or a simulation tool that has been developed to show the same thing. Attempts to find such data or simulations were not fruitful. No open source simulation was convincing enough as a good model of fire spreading behaviour, and data on past fires often only shows the total burnt area, but not the progression of the fire.

At this stage, the design team decided to make an original fire simulation that can be used as a tool to inform the swarm firefighting investigation. The fire simulation would take inputs of the major fire spreading parameters such as wind and fire fuel density, and output a video simulation showing the way a fire can be expected to spread. The general plan for making and using the simulation is described in section 9.1, before the fire simulation progress is elaborated in subsection 9.1.1 and subsection 9.1.2. Finally, swarm attack analysis is performed and conclusions are drawn using a sample of fire scenarios in section 9.2.

Fire Simulation Plan

For the fire simulation, a plan is developed to envision the different levels of complexity it can incorporate, and what the ideal simulation may look like. Ideally, the envisioned simulation is one that is scientifically accurate, includes the majority of important factors that influence fire spreading behaviour, and an interactive interface that allows the user to change settings easily, create different fire scenarios by randomising inputs, and show fire suppressant drops by the different types of aircraft. This is quite an ambitious vision, and within the time constraints of the project it is a high risk to rely on such a simulation to be completed before drawing conclusions on the possible advantage gained by swarm firefighting. Therefore, a development plan is created for the simulation, where a simple first step of the simulation can already inform the investigation, and the further development of the simulation can contribute by improving and/or verifying the results acquired from the simpler versions.

A description of the different iterations planned is given in Table 9.1. This shows the parameters wished to be incorporated into the fire simulation. The first version of the simulation includes the parameters of the first iteration, and the second and final version includes the parameters from the remaining iterations. At the time of producing this report, the fire simulation development is between the fourth and fifth iterations.

Table 9.1: Fire simulation development plan per iteration

Iterations	Additional incorporated parameters	Features
First iteration	Pre-set probability of a cell catching fire Wind direction Wind speed (low accuracy) Pre-selected clear space (to visualise dropped suppressant)	Basic video Pixelated appearance
Second iteration	Randomised fire fuel density Fire fuel dryness Fire intensity Randomised areas with slopes Higher accuracy for wind speed Evaporation rates of suppressant	Basic video improved colouring
Third iteration	suppressant effectiveness Slanted lines visualising suppressant drops	User experience: Easy to edit inputs Simultaneous multiple simulations Suppressant drops during simulation Better visualised non-sudden slow drop
Fourth iteration	Revised and improved(where necessary) parameters Suppressant drop speed calculated burnt area	Make a user interface Java implemented for faster performance
Fifth iteration	Circular lines visualising suppressant drop more realistically Revised and improved(where necessary) parameters Simulation identifies and carries out optimal drop sequence	Game-like user interface 3-D visuals

9.1.1. Initial Version - v1.0

The first version of the simulation includes only the first iteration shown in Table 9.1. It is a simple version that provides a basis for the analysis. The focus was on creating any kind of simulation to get started with the analysis, after which the further development can start and inform later parts of the analysis. A basic code was found online [1]. This code was altered to suit the purposes of the project.

Model

A grid with cells is created, which can be thought of as a matrix. The size of this grid can be decided, and each cell can be given an initial state. During the simulation, a certain cell can change its state, and cells affect each other's states. Furthermore, the probability of a certain state being the initial state of the cells can be defined. For instance, a probability of 0.7 can be assigned to the state of being fire fuel. This would mean that the fire fuel density of the area is 70%.

Defining the cell states

For this basic version, three states are defined. 0 means that this cell is not fire fuel. This means it is empty and it is not burning, and will not burn in any case. 1 means that this cell is fire fuel. This means that it is not burning (yet) but it is in a state that can burn, provided the right conditions. This is to represent any kind of burnable biomass found in the forest. Finally, 2 means that this cell is on fire.

Defining the interaction between cells

Next, defining how cells influence each other is important. The idea is to say that cells with a state 0 will not burn regardless of what happens to the cells around them. Cells with a value of 1, will burn (turn into state 2) once they identify that one of their immediate neighbours is in state 2. This means that an assumption is made that when a spot is burning, every adjacent spot to it will catch fire as well. Finally, every cell with a state of 2 turns into a state of 0, meaning that after a cell has burned, it is not possible to set it on fire again. This also reflects an assumption, that once a spot has burned, it is completely "spent" and does not contain burnable fuel anymore.

Assumptions

- It is not possible for a cell that has been burned to be set on fire again
- A spot (cell) is set on fire as soon as a neighbouring spot has caught fire
- Fire spreads proportionally to wind speed
- Wind speed is only variable in discrete steps

[1] `https://medium.com/@tetraktyz/how-to-simulate-wildfires-with-python-6562e2eed266` [accessed 23 june 2019]

- Only 3 states exist: Empty(0), fire fuel (1) and on fire (2)
- Fire spread only depends on the neighbouring cells

Parameters
To run the simulation, certain parameters are set by the user, to establish the characteristics of that particular fire.

- **Fuel available:** Cells can have a value of 0 or 1, indicating either an empty cell or a cell with fuel respectively.
- **Wind Direction:** A simple way of modelling wind direction was implemented. This is simply by commanding that if a cell is on fire, multiple cells in a particular direction are set on fire in the next time-step, as opposed to only one. This shows in the simulation as a faster spread in that direction.

Simulation Rules
The states assigned to the cells and how they interact with each other is written in Python code:

```
if states[t-1,x,y] == 2: # if its is on fire
    states[t,x,y] =0 #put it out and clear

    # if there's fuel around the fire, set them on fire
    if states[t-1,x+1,y] == 1:           # cell to the right
        states[t,x+1,y] = 2
    if states[t-1,x-1,y] == 1:           # cell to the left
        states[t,x-1,y] = 2
    if states[t-1,x,y+1] == 1:           # cell above
        states[t,x,y+1] = 2
    if states[t-1,x,y-1] == 1:           # cell below
        states [t,x,y-1] = 2
    if states[t-1,x-2,y] == 1:           # cell to the far left, to model
        states[t,x-2,y] = 2              # wind going to the left
```

The function to clear spaces is written as follows:

```
def clear_spot(grid, shape, position):
grid[0,position[0]:position[0]+shape[0],position[1]:position[1]+shape[1]] = np.zeros(shape=shape)
```

With this, the user can easily choose to clear some spots simply by identifying their coordinates within the grid.

```
#set nonburnable areas
clear_spot(states, (5,50), (30,10))
clear_spot(states, (5,50), (30,42))
clear_spot(states, (5,30), (30,15))
```

Data Structure
All the data is stored inside a ($N_{iterations}$, grid height, grid width) shaped numpy array. Every time step, a copy of the grid is made in which all the results are stored. This is to prevent the program from adapting values in-place, interfering with the simulation.

To generate some visuals for the user, different data is required. Every grid cell needs to have an RGB-value associated with it (a vector of 3 items, each an integer value from 0 to 255). Therefore, every iteration, the colour the cell in question needs to be is calculated and stored inside another numpy array with shape ($N_{iterations}$, grid height, grid width, 3).

Results and Software Verification
This simulation is used as a basis for a more in-depth simulation. A frame from the simulation is shown in Figure 9.2. Wind direction is set to the left of the image.

The lack of parameters available to describe the process of a fire spreading was the main reason for the development of a more advanced simulation. The most up to date version is elaborated in subsection 9.1.2.
No tests were made for this version of the simulation. It was only used as an indication and the plan was to make a new version. Hence, the tests were deemed unnecessary and that time was allocated to working on the new version, which is elaborated in the upcoming subsection 9.1.2.

9.1.2. Final Version - v2.0
The first version of the simulation used a fairly simple model and was useful for its purposes. Since the simulation would be ultimately used to base major design decisions on, a more advanced way to model the fire is developed.
Assumptions

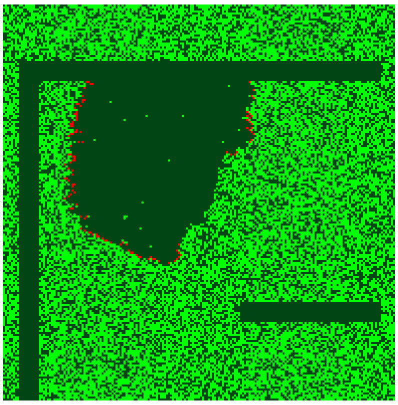

Figure 9.1: Example of a simulation: The fire is contained by simulated suppressant.

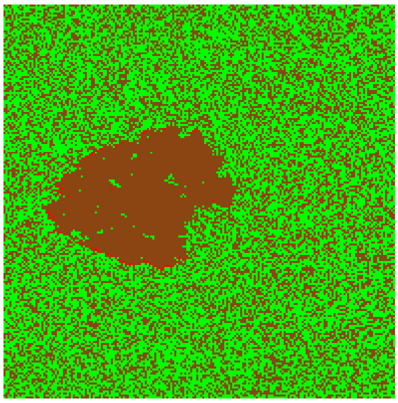

Figure 9.2: Example of a simulation: A fire ignited in the middle and spreading towards the left of the image.

- Suppressant required is approximated to be linearly proportional to the fire intensity, with the slope depending on the suppressant used and the dryness of the fuel [5].
- Suppressant slowly evaporates, even without fire interfering.
- Suppressant base evaporation depends on the amount of suppressant present. More suppressant in a grid cell makes it evaporates slower.
- More arid land will burn faster

Parameters

To run a simulation, there need to be parameters that change and interact with each other and/or themselves. For the forest fire simulation, every grid cell has a certain state. This state consists of 4 main parameters:

- **Fuel Amount, F:** Cells with more fuel should burn and smoulder longer. Cells without fuel cannot support fires for more than 10 iterations, and the fire cannot increase in intensity without fuel present.
- **Suppressant Amount, R:** Cells with suppressant should not be able to catch fire until the suppressant has evaporated.
- **Fire Intensity, I:** Cells with Fire will burn up the fuel present.
- **Fuel Dryness, D:** Cells with a higher dryness factor will have a higher probability of catching fire, and take more suppressant to be extinguished.

These four parameters define the state of the cell. Three other external factors are able to influence the simulation:

- **Wind direction:** Wind direction plays a major role in forest fire spread, and can push a forest fire in a single direction. Wind adds oxygen to the burning fuels, and promotes heat convection and transportation of burning materials such as leaves, which can wreak havoc elsewhere[2].
- **Elevation Levels:** In mountainous areas, forest fires tend to spread faster uphill as the unburnt fuel is more easily accessible for the flames while it receives extra heat through radiation and convection, drying out the fuel before the fire even reaches. Therefore, the fuel will catch fire at a faster rate when the cells are uphill from the reference cell. Figure 10.9 visualises this process.
- **User Defined Suppressant Placements:** The user of the simulation is able to specify at what times, and what positions suppressant needs to be dropped, to emulate the UAVs dropping suppressant. The time, positions, suppressant amounts and aircraft velocity are provided as input.

Simulation Rules

Now that all the relevant parameters are defined, their interactions with one-another can be described. The following pseudo-code pieces are used in the simulation as a basis for the rules of fire spread:

- *Rules For Updating the Fuel*

```
if R_i > 0:                          # If Suppressant is more than 0
    if R_i >= I_i:                   # If suppressant is more than intensity
```

[2]02-06-2019 - https://bit.ly/2Y4Rdjg

```
        F_(i+1) = F_i                # Fuel Doesn't change

    else:
        F_(i+1) = F_i + R_i - I_i    # Fuel minus difference in intensity and suppressant

else:
    F_(i+1) = F_i - I_i              # Else fuel minus intensity

# Any Cells with a value under 0 will be reset to 0
```

- *Rules For Updating the Suppressant*

```
# evap_0 is the base evaporation rate
# Kernel average is the average of a 3x3 kernel of the Intensity grid

if R_i >= I_i:                                        # If the Suppressant is larger than the intensity
    R_(i+1) = (1 - (evap_0 + kernel_average(self.I_grid))) * R_i     # Suppressant will evaporate

else:
    R_(i+1) = 0                                       # Otherwise, suppressant is 0

if t in suppressant_droppings.keys():                  # If the user planned suppressant drops at the
     current time
    for value in suppressant_droppings[t]:
        R_(i+1) += value                              # Add the suppressant drops to the current grid

# Any Cells with a value under 0 will be reset to 0
```

- *Rules For Updating the Fire*

```
delta_fuel = F_(i+1) - F_i                # Amount of fuel burned
delta_suppressant = R_(i+1) - R_i           # Amount of suppressant evaporated

I_avgs = intensity_averages([3, 3])       # Average of the intensity of the 3x3 grid around
                                          # See the Algorithms Section
if F_i > 0:                               # If there was any fuel in the previous iteration
    if I_i > 0:                           # If there's fire present
        I_(i+1) = I_i + I_avgs + \        # Add the average of the 3x3 kernel
                        abs(delta_fuel) + \      # Add the difference in fuel
                        delta_suppressant * suppressant_efficiency # Minus difference in suppressant

    else:
        I_(i+1) = I_avgs - R_i     # If the fire around the cell is high enough it can catch fire

else:
    if I_i > 0:
        I_(i+1) = (I_i + I_avgs)/10       # If theres no more fuel present, smoulder
    else:
        I_(i+1) = 0

# Any Cells with a value under 0 will be reset to 0
```

Derivations

At first, like in subsection 9.1.1, most of the equations were based on very simple rules. However, this did not yield the accuracy desired for the operational analysis of Wangari.

Therefore, a more elaborate set of empirical relationships between the three parameters Fuel, Suppressant and Fire Intensity, were set up and tested. The coefficients were tweaked and yielded decently usable results, however there were still issues with the simulation. Empirical or statistical relationships found in studies were used to describe the model.

Eventually, the equations used for the simulation were mainly based on rough relationships between suppressant, fuel, fire intensity and fuel dryness. Many of these relationships were taken from studies, in particular the study on "The Effectiveness and Efficiency of Aerial Firefighting in Australia" [5]. An example is the linear relationship between suppressant required and fire intensity, as mentioned in the assumptions. This relationship is plotted in Figure 10.8.

To get the simulation as close to real life as possible with the limited resources available for the development of this code, the empirical relationships were tweaked a bit further and then frozen.

[3] http://www.auburn.edu/academic/forestry_wildlife/fire/topos_effect.htm [cited 6 June 2019]

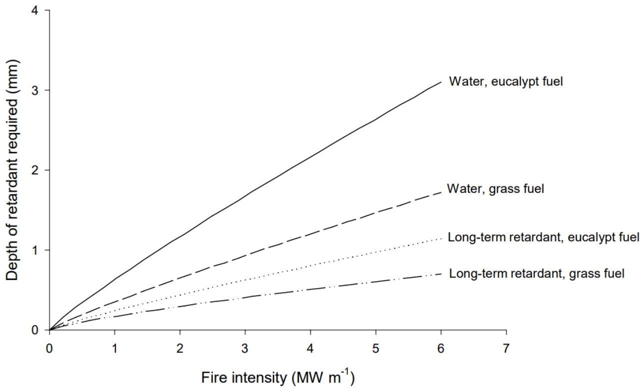

Figure 9.3: Fire Intensity - suppressant Depth Required to hold the fire [5]

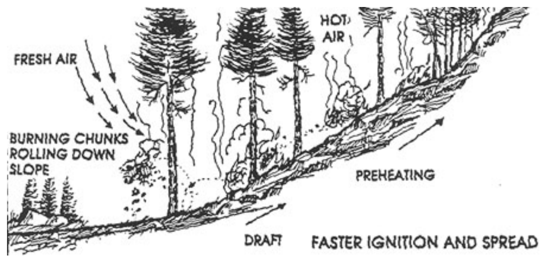

Figure 9.4: Increase in rate of spread for fires spreading uphill [3]

Data Structure
The data of the simulation is stored inside multi-dimensional numpy arrays. The user specifies the length of the simulation in iteration steps, as well as the size of the grid. Since there are 4 parameters to keep track of, the resulting shape will be ($N_{iterations}$, grid height, grid width, 4).

This is however, the array for the final result. Every iteration, temporary arrays are used to perform the calculations on to not have values be changed in-place in the main grid. Changing values in-place will interfere with the results of the simulation depending on the order of the calculations performed. Four temporary arrays are used, one for every parameter in the simulation, each with a size of (grid height, grid width).

A coloured grid is created in a similar fashion, as explained in Data Structure in subsection 9.1.1.

Algorithms
Overall the simulation is not very complex. However, some calculations do require some explanation.

1. Weighted Kernel Calculations
The influence of the elevation and the wind is modelled in the fire spread is done through the I_{AVGS} term as seen in the fire update rules. This average is a weighted average of the (3 x 3) around the cell in question. The weights, when there is no wind nor elevation, are:

$$W_0 = \begin{bmatrix} \frac{\sqrt{2}}{2} & 1 & \frac{\sqrt{2}}{2} \\ 1 & \frac{1}{2} & 1 \\ \frac{\sqrt{2}}{2} & 1 & \frac{\sqrt{2}}{2} \end{bmatrix} \tag{9.1}$$

The corners are a distance of $\sqrt{2}$ further away than the adjacent cells and will therefore have an assigned weight of $\frac{\sqrt{2}}{2} \approx 0.7071$. The centre cell weight is reduced to a half, since the centre value weight is already partially taken into account with the ΔF and ΔR calculations.

Now, assuming a wind direction coming from the north in the simulation, this would add extra values to the cells 'behind' the centre cell, since they would influence the centre cell more as the wind is in their back. Similarly, the cells 'in front' of the centre cell would have a smaller effect on the centre cell burning and will therefore have a reduced weight. The difference in weights for this particular scenario would be:

$$\Delta W = \begin{bmatrix} 1 & 1 & 1 \\ 0 & 0 & 0 \\ -1 & -1 & -1 \end{bmatrix} \tag{9.2}$$

This ΔW matrix changes depending on the wind- and elevation slope direction. ΔW is calculated according to the following formula:

```
def delta_weights(direction: Union[np.array, np.ndarray], magnitude: float):
    """
```

```
    Calculate the delta in the weights for the kernel
    :param direction: 2 by 1 vector
    :return: delta weights matrix
    """

    weights = np.zeros((3, 3))

    for x in range(3):
        for y in range(3):
            weights[x, y] = -direction[0] * (x - 1) - direction[1] * (y - 1)

    return weights*magnitude
```

This formula holds for both wind and elevation. The result of this change of weights, is that fire will spread faster with the direction of the wind, and the fire will spread faster uphill. Therefore, if the wind would go downhill and both magnitudes would be identical, the fire would spread uniformly in all directions.

2. Grid Point Intersection Finder

Since the suppressant will not always be dropped along a single row or column in the simulation, but also along slanted lines, an algorithm to calculate the intersecting cells is required. The code used is specified below:

```
def __intersection_point_finder(grid: Union[np.array, np.ndarray],
                                p_0: Union[np.array, np.ndarray],
                                p_1: Union[np.array, np.ndarray],
                                max_iter: int = 200):

        """
        Function to calculate all cells the line intersects through linear inerpolation
        :param grid: Grid in which the interpolation has to be performed
        :param p_0: starting position
        :param p_2: end_position
        :param max_iter: maximum amount of samples
        :return: [(i0, j0), (i1, j1], ..., (in, jn)]
        """

        indices = []

        length = np.linalg.norm(p_1-p_0)
        v = (p_1 - p_0)/length

        for n in np.linspace(0, length, max_iter):
            p_i = p_0 + n * v

            if 0 <= p_i[0] <= grid.shape[0] and 0 <= p_i[1] <= grid.shape[1]:
                rounded = p_i.round()
                val = tuple(rounded.astype(int))

                if val not in indices:
                    indices.append(val)

            else:
                break

        return indices
```

After all indices are found, around every cell a kernel of shape (m, m) is placed. The value of m is specified by the user, and effectively indicates the width of the suppressant drop. All the cells within these kernels will have suppressant added to them. This is done over multiple time iterations, as this will depend on the velocity of the UAV, and the length of the suppressant line.

3. Randomisation

Predictions can be made for forest fire spreading directions, however there are still many parameters which can be considered random. Wind gusts, distribution of plants and trees, and the distribution of dropped suppressant can all be approximated but in the end there will be a factor of randomisation to the results. This is all modelled using the numpy.random.uniform distributions. These random values are added to the weight matrices of the kernels to simulate terrain irregularities and wind gusts, as well as to the kernels of the suppressant dropping kernels.

Results and Software Verification

The simulation is made with a high level of accuracy given the time available, and the results are similar to real life situations. The resemblance between a recent forest fire in Bandipur, India, February 2019 (shown in Figure 9.5), and the simulation (shown in Figure 9.6), is qualitatively apparent. Naturally, the simulation cannot take every parameter affecting fire-spread into account, and the discretisation is not completely accurate. The grid shown in Figure 9.6 has a shape of 300 x 300 pixels. The main issue with the simulation is the computation time, with an average of 4.8 seconds per time step for a 300 x 300 grid. This means that for 200 time steps, the simulation has a run-time of over 15 minutes, which is not ideal when several scenarios must be investigated. This is due to the fact that it is all written in Python, which is simply a very poorly performing programming language.

Figure 9.5: A clear view on the boundary of a spreading fire.[4]

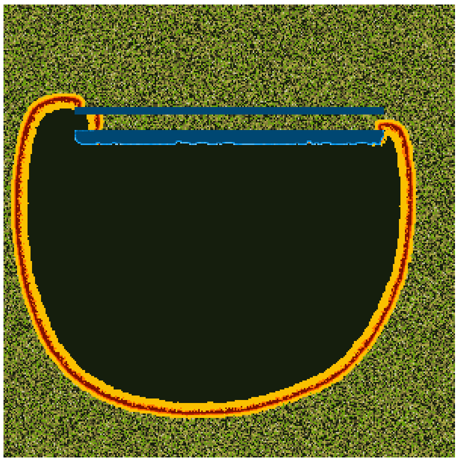

Figure 9.6: Example of a simulation: The shade of blue indicates the amount of suppressant, the shade of green indicates the amount of fuel, red and yellow indicate fire intensities, black indicates lack of presence of any parameter.

For the software verification, unit tests were written for every method in the classes written for the simulation. Due to the software's continuous development and lack of time and resources available for extensive test writing, the line coverage reaches 70% for the final version. This is bound for improvement in the future, as explained in Figure 9.1.2. Due to the random nature of the simulation, a constant seed was always assumed for the numpy randomisation functions during testing to guarantee reproducible results.

Future Plans

As mentioned in 9.1.2, further development of the software is planned. First of all, the simulation run time is sub-optimal. Therefore, it is planned to have a similar version running in Java due to its superior computational performance [5]. Decreasing run time allows for the simulation to be tweaked for better accuracy even more, as it allows for more complex computations, faster. Aside from the run time being decreased by using Java, a more intuitive way of using the simulation is to be implemented, as a graphical user interface. This would make usage of the simulation not only faster but also allows for better tweaking of the simulation parameters, resulting in better strategies for Wangari.

9.2. Swarming Analysis

The goal of this analysis is to compare several smaller aircraft to fewer larger aircraft in containing a fire. For the sake of these comparisons, 2 UAVs (a UAV pair) are compared to one CL-415 since. A UAV costs about a third of a CL-415, but to account for unforeseen costs and sensitivity of the cost estimation method, a margin is introduced and the CL-415 is compared to two UAVs instead of three in this section. Hence, if two UAVs outperform one CL-415, it may be concluded that this is a successful design, as better performance would be obtained for less cost.

Outperforming another aircraft in firefighting ultimately means, being able to save more forest area from being burnt. To find this, the fire simulation is run for different cases with different levels of complexity, starting with a basic fire that spreads equally fast in all directions, and a simple model of containment involving laying straight lines at the expected

[4] https://upload.wikimedia.org/wikipedia/commons/thumb/3/31/Bandipur_fires_2019.jpg/1200px-Bandipur_fires_2019.jpg [cited 15 June 2019]

[5] https://benchmarksgame-team.pages.debian.net/benchmarksgame/fastest/python.html [cited 15 June 2019]

time of arrival of aircraft. The more complex cases involve a later version of the simulation which accounts for several parameters such as random wind directions and wind speeds, evaporation rates, and laying more realistic water lines that are not only horizontal or vertical. For all scenarios, the area within which the fire is contained is computed for both the UAVs and the CL-415 aircraft. Conclusions are made in subsection 9.2.3 to give an overview of the case studies and an overall comparison is presented to show which system is more favourable from a firefighting performance perspective.

9.2.1. Case 1: Fire With Multiple Critical Points

A critical point is a point in the fire progression line whose extinguishing or containing is prioritised. This can be due to its high rate of spread, or due to its proximity to an important area to protect, for example a residential area. This is an important case scenario to study. It is more realistic that fires do not only spread in one main direction, or in all directions. Due to the natural variety of fire fuel density, fire fuel dryness, terrain slopes, and other factors, fire can spread in multiple directions. For instance, if the fire is mostly spreading in the general wind direction, there may be an steep hill in the opposite direction where the fire will keep spreading fast. It is also realistic that fires may be close to residential areas, and even if the fire is spreading slowly in their direction, this fire front will be prioritised, making it critical. This case forms the hypothesis for the swarm attack investigation. This is the main case where attacking the fire with several smaller aircraft promises to be more effective than large air tankers. If multiple aircraft are used, they can simultaneously target the critical areas where the fire spreads fastest. On the other hand, using air tankers can effectively stop the fire from spreading in one direction, but the other critical direction(s) will be neglected until the aircraft has had time to refill and come back, at which point the fire might have escaped beyond control. The following assumptions are made for this scenario:

- The distance from the base to the point at which the the aircraft drops the suppressant is exactly 50 km
- The aircraft can only drop straight lines, due to the limitations of the simulation at this stage
- Differences between the two systems in response times and rotation times are neglected in order to control these variables, and make sure that conclusions on swarming are not attributed to differences in performance, rather than the swarming principle
- Both systems start their attack after 45 iterations after the fire is ignited
- The time to find the correct dropping position and carry out necessary manoeuvres is neglected
- The difference in coverage efficiency between the systems is neglected
- The refill time, including cruise, is 40 iterations
- The difference in maximum cruise speed between the two systems is neglected

Multiple Smaller Aircraft

The multiple, smaller aircraft, forming a swarm, have the ability to create more complex dropping patterns by dropping the loads at separate moments and locations. This is visualised in Figure 9.7 and Figure 9.8. The suppressant lines dropped by the swarm are quite short, one third of the size of the air tanker's, allowing for more flexibility in dropping patterns for the swarm, and this is what is believed to have allowed the swarm to perform so well in this particular scenario.

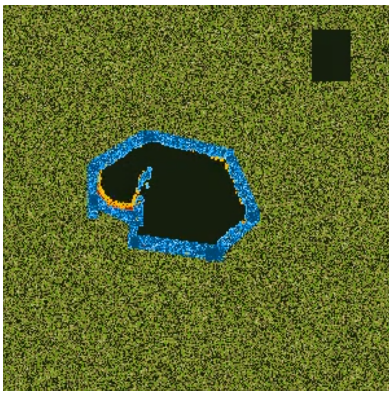

Figure 9.7: Wildfire, contained by smaller aircraft, after 100 Iterations

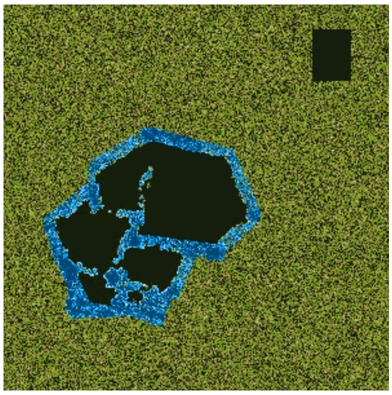

Figure 9.8: Wildfire, contained by smaller aircraft, after 450 iterations

Single Air Tanker

The single larger aircraft performed well, however not as well as the swarm. Due to its inability to make more complex dropping shapes, it was not able to contain all of the fire. It managed to contain the fire and prevent fire spread towards the residential area, however the burned area is rather large.

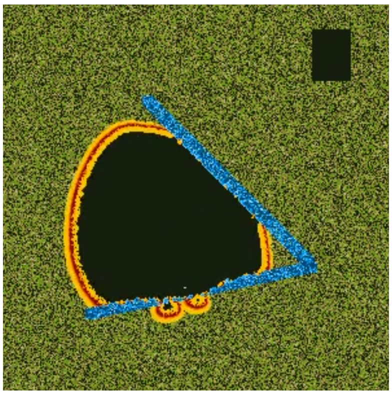

Figure 9.9: Wildfire, contained by a larger aircraft, after 100 Iterations

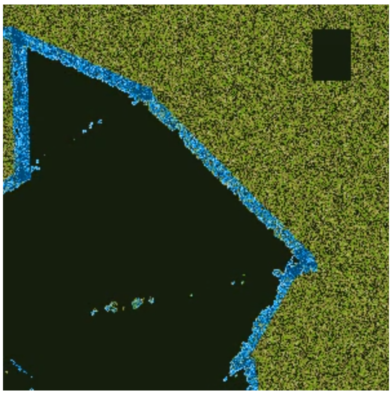

Figure 9.10: Wildfire, contained by a larger aircraft, after 450 iterations

Case results and conclusions

In the case of multiple critical points forming along the fireline, the multiple smaller aircraft outperform the larger aircraft by far. The area saved by the swarm of smaller aircraft is much larger than that of the larger airtanker, and thus more efficient, as that is the goal of aerial firefighters. This is visualized in Figure 9.11 and Figure 9.12, where the graphs represent the average amount of fuel in the grid. The swarm managed to save around 85% of the forest in the grid, while the airtanker only managed to save around 55%. Furthermore it has to be noted that the airtanker could not prevent the fire from crossing the edge of the grid, and therefore the wildfire will rage on outside of the grid if it were reality, and thus the fire would not be extinguished at all yet.

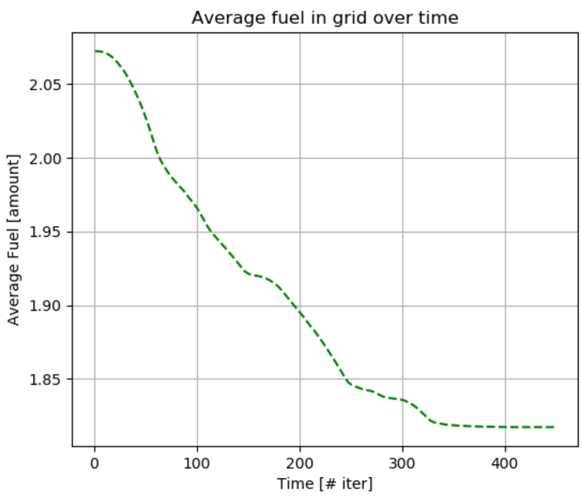

Figure 9.11: Average fuel in the grid over time for the swarm case

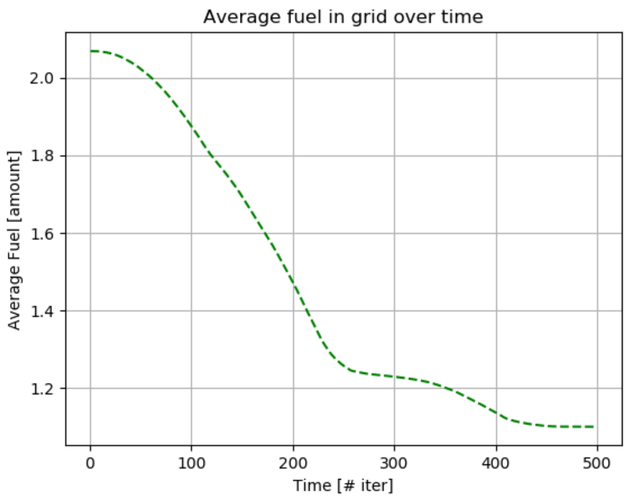

Figure 9.12: Average fuel in the grid over time for the airtanker case

9.2.2. Case 2: An Intense Fire With an Aggressive Front Line

In the case of a highly intense fire, a different set of characteristics is desired in aerial firefighters. An intense fire means that it is difficult to stop or slow down. This kind of fire is fought by laying containment lines some distance ahead of the fire front. The only hope is to contain it within a reasonable perimeter such that the ground crew can safely approach and put out the fire. For this case, it is expected that a single drop of suppressant will not stop the fire. It will have a slowing effect, but the fire is expected to get through the wet area, albeit more slowly.

For this case, the fire terrain is chosen to be a simple rectangle, and the fire is set to spread in one main direction. This allows the control of other variables, in order to focus on the important factor, which is studying how aggressive fire front lines can be stopped.The plan for this simulation is to make the first drop by both systems, and then watch the simulation and take its feedback to decide when and where the second drop should occur. This will depend on how fast the fire gets through the first drops, and how far it will have progressed by the time the UAVs or aircraft are expected to be back on the scene for their second drop. This loop continues until the fire is stopped. 4 Wangari UAVs are used for this simulation, compared to 2 CL-415 aircraft.
The assumptions used in this scenario are

- The distance from the base to the point at which the the aircraft drops the suppressant is exactly 50 km
- The aircraft can only drop straight lines, due to the limitations of the simulation at this stage
- Differences between the two systems in response times before take-off are neglected
- Both systems start their cruise 3 minutes after the fire is ignited
- The time to find the correct dropping position and carry out necessary manoeuvres is neglected
- The difference in coverage efficiency between the systems is neglected
- The distance between the fire and the refilling body of water is 10km
- The aircraft choose to drop water 30m ahead of the fire progression line
- The average speed of fire spread is $0.8m/s$.

The Wangari system
At the time of arrival of the Wangari UAVs to the scene, 10 minutes and 24 seconds after the start of the fire, which is spreading at a speed of $0.8m/s$, the fire front line has reached $500m$ from the ignition point. This is where the simulation is used to see how the fire gets through such suppressant lines. After the fire gets through the first set of drops, and the time calculated for the UAVs to have scooped and come back to the fire, the location of the second drop can be decided to contain the fire. The simulation then does the work and when the fire is contained, the burnt area can be computed.

Figure 9.13: An intense fire approaching an area where 4 Wangari UAVs have dropped water.

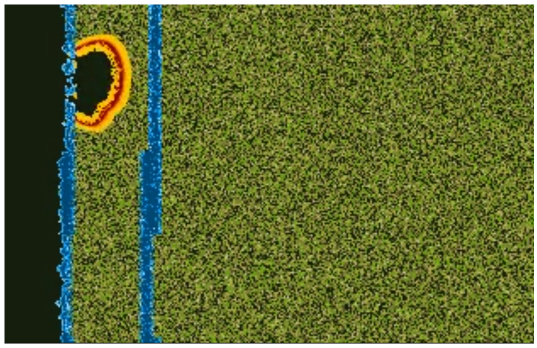

Figure 9.14: An intense fire breaks through the first drops, and approaches the second set of drops.

The CL-415 system
For the CL-415s, it takes 11 minutes and 22 seconds to arrive at the scene. At this time, the fire front line has reached $545m$ from the ignition point. While the lines that the CL-415 aircraft can lay are longer (260m vs Wangari's 195m), they are not wider. Hence, laying two lines at a time is a disadvantage because the fire can penetrate more easily. The simulation shows that the fire escapes the first line of suppressant, and by the time the aircraft are back for the second drop, the fire is at a high intensity again, and escapes the suppressant again. The conclusion therefore is that for this high intensity fire, two CL-415 aircraft are not even able to stop the fire progression.

Case results and conclusions
The Wangari system clearly outperforms the CL-415s as it manages to contain the fire using the line width advantage. The CL-415 can lay longer lines thanks to its higher capacity, but cannot make their lines wider, which is the need in this scenario. As a swarm, flying in an adjacent formation, the laying of multiple adjacent lines gives more width covered on the ground, and is effective at slowing down and ultimately stopping such aggressive fires according to the simulation.

9.2.3. Conclusions
Using several smaller aircraft to contain a fire can be a more effective way to limit the burnt area. The Wangari system

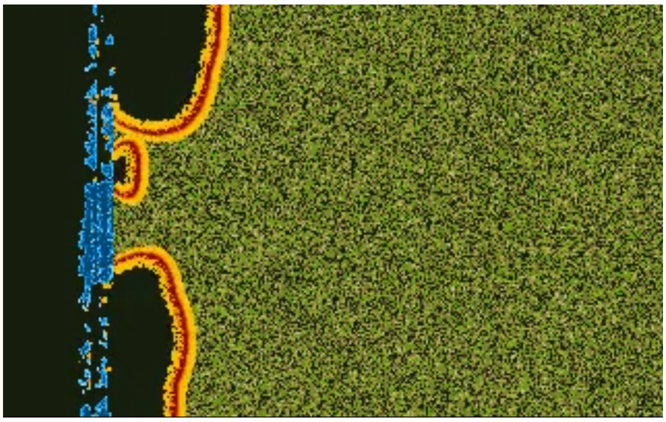

Figure 9.15: The intense fire penetrates and escapes through the water lines laid by the two CL-415 aircraft.

contains fires faster than the CL-415. The fire simulation made to study the effect of swarming UAVs has clear limitations. In every scenario, multiple assumptions are made, which may not be accurate. However, the assumptions are reasonable, and with a low expected impact, and are applied to both systems, yet the Wangari system performs consistently better. The selected fire scenario cases were very different from each other to demonstrate the versatility of this solution. A fire with critical points that are far from each other, and an intense fire whose front line is hard to stop, were both investigated and elaborated upon to see how the system performs across different scenarios. In the first case, the smaller aircraft saved about 85% of the simulation area, while the larger aircraft saved about 55%. In the second case the UAVs managed to slow down the fire on the first drop by using the advantage of the width of the line they can lay by flying in formation, and ultimately stopped the intense fire with their second drop. The comparable two CL-415 aircraft, however, failed to stop the fire.

10 Component Design

In this chapter, the design of the main components influencing the performance of the UAV is discussed. The section on propulsion design presents the sizing of the propeller blades, the engine selection and configuration. The wing design is focused on the wing geometry, aerodynamic performance and the wing box design along with the detachability of the wings. In the discussion of the hull design, the buoyancy of the aircraft, the stability in water and the general hull geometry and strength are analysed. The description of the empennage design is focused on the sizing of the horizontal and vertical tail surfaces such that the aircraft remains stable in air. This is followed by a discussion of the control surfaces and landing gear design which show how the aircraft will remain controllable on the ground and in the air. In the design of the water tank the capacity and anti-sloshing means are described. Finally, in the last section, the weights of all components are listed and discussed.

10.1. Propulsion

10.1.1. Engine Selection

Engine Power & Type

When selecting a propulsion type a turbo shaft or turboprop engine was preferred due to their high specific power output and good low altitude performance. Also, the fast throttle response [17] compared to the alternatives was considered a major benefit in the specific flight conditions in which the UAV will operate. As a turbo shaft engine will be able to go from 0% to 100% throttle within $1 second$ while jet engines require around a significantly longer time [17]. Therefore, to select the right engine for the aircraft a database of multiple turbo shaft and turboprop engines has been downloaded[1]. Both military and civil engines were considered for the selection of the engine. The procedure for selecting the right engine started from the climbing requirement:

AF-PERF-TO-06 The UAV shall have a minimum climb rate of 10 m/s at MTOW.

To be able to achieve this requirement, the engine shall be able to provide a continuous power of around $1600 kW$, as deduced from Figure 7.12. In general, most engines can deliver a continuous power of around 80% of their maximum power available and most propellers will have around an 85% propulsive efficiency [17]. This means that for the engine, a P_{br} of $\frac{1600}{0.8 \cdot 0.85} = 2353 kW$ is desired.

When selecting the exact turbo shaft engine the availability of the engine shall of course also be considered. A readily available engine was preferred as it can directly be implemented and introduces less risks to the design. The list of turbo shaft and turboprop engines in the database[1] showed few engines which met the power requirement. An engine with a P_{br} between 2000 to $2500 kW$ would have been preferred but as shown in Figure 10.1, no engines exist in this range. A good alternative was found to be the General Electric military T700-6TA engine, currently used in the Apache helicopter. Its dimensions and weight are used in further calculations, however, for the performance aspects the shaft power is increased by 50% as the aircraft will preferably be fitted with the newly designed T901 engine from General Electric [2]. General Electric claims that this engine will be able to deliver up to 50% more power and 25% better fuel efficiency than the T700, while maintaining the same dimensions and weight. Due to insufficient information available about the engine for other calculations the specifications from the T700 will be used, only for the performance aspects it is assumed that the engine will be able to indeed produce 50% more power then the T700 6TA engine, to achieve a P_{br} of $2439 kW$. Further research in the specifics of the engine must be conducted to show the effects of fully equipping the aircraft with the T901 engine.

Engine Location

In the process of locating the engine, multiple places on the UAV were considered, as described in chapter 12. Based

[1] `http://www.jet-engine.net/`[cited 23 June 2019]

[2] `https://www.geaviation.com/military/engines/t901-turboshaft-engine`[cited 20 June 2019]

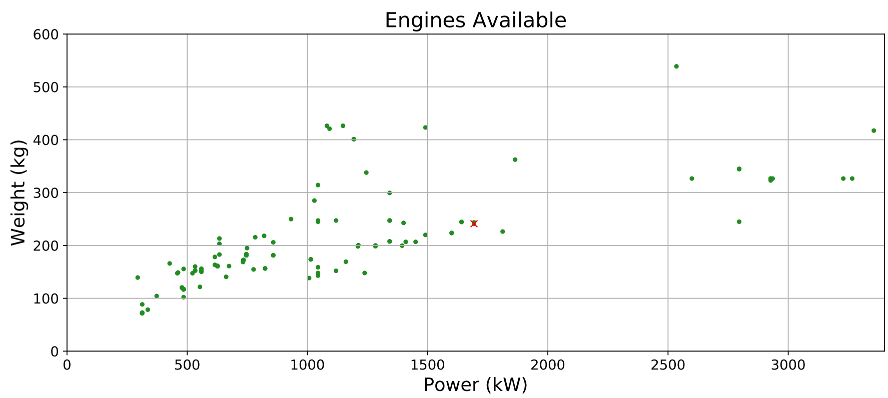

Figure 10.1: Engines available, red cross indicates selected engine

on aerodynamic advantages, described in subsection 10.2.4, it was finally chosen to place the propeller on the wing. This meant that a decision had to be made between having two turboprop engines on the wings or one turbo shaft engine fitted inside the fuselage with a differential and multiple gearboxes connecting it to the two propellers. The main considerations for this were sustainability and the detachability requirement for the main wing. Placement of the engines within detachable wings was not desirable from a structural point of view nor a sustainable option. Hence, the design of the engine would focus on a single engine located within the fuselage. This meant that the required engine would be a turbo shaft engine connected via gearboxes and driveshafts to the propellers. A more detailed explanation of this drivetrain is given in subsection 10.1.4.

10.1.2. Fuel Choice

The selected engine requires JP-5 or JP-4 military grade jet fuel. This does not differ from regular kerosene other than having a higher flash point; 60°C compared to 38°C [3]. This type of jet fuel is mainly used for aircraft stationed on aircraft carriers for safity reasons as it's less volatile. No limiting differences between JP-5 and kerosene are noted, enabling use of regular Jet A(-1) to be used as propellant for the engine [4]. Thus, the UAV can safely operate on general airports around the world as no further special consideration for the UAV have to be made. Using these types of fuel in conventional fuel tanks or bladders, no special pumps are required for the refuelling, meeting the set requirement:

AF-GRND-03 The fuel tank of the UAV shall be fitted with standardised fuel pumps.

Initially, it had been determined that bio-fuels would not be possible to use, mainly due to its lacking infrastructure. However, as is shown in multiple studies [18], adding a slight amount of bio-fuel to fuel usually used in aviation will not alter the performance. Thus, if the bio-fuel infrastructure is to expand and usage can be made of it, so-called 'drop-in' bio-fuels could be used without losing performance in flight. The usage of these bio-fuels will reduce the amount of greenhouse gases emitted by the UAV and thus contributing less to the climate change visible across the globe.

10.1.3. Fuel Tank

During flight the fuel required by the engine is stored in fuel tanks, which will be placed inside the wings to provide bending relief. The tanks can be designed in various ways; they can be an integral part of the wing, or rigid- or bladder-type cells placed in the cavity of the wings.

In the case of integrated tanks, the tanks are made of the same material as the wing. For the Wangari this would mean that they are made of aluminium. However, during its firefighting mission the wings are likely to heat up, which would also heat up the integrated tanks. To keep a constant fuel flow, the integrated tanks would have to be lined with isolated material. This would nullify the weight benefits of the integrated tanks. Therefore, it is chosen to use bladder-type fuel tanks. These will still have some weight saving benefits as they use structural support from the cavities, whilst providing an isolating layer. Furthermore, they can be inspected and repaired easily, when access panels are installed in the wings. All tanks are equipped with sumps and drains, such that in case water or sediment is apparent in the tank it can be

[3] `https://www.globalsecurity.org/military/systems/aircraft/systems/engines-fuel.html`[cited 15 June 2019]
[4] `https://www.globalsecurity.org/military/syste`[cited 15 June 2019]

drained [5]. The bladder tanks will be fully removable,to prevent any accidents with remaining fumes inside the tanks or imploding during drainage.

10.1.4. Drivetrain

The drivetrain for the UAV might seem an unconventional choice for the propulsion of an aircraft, it is however a common solution in helicopter designs. The drivetrain is described in figure 10.2. The main considerations for this unconventional design are the following:

- Weight of the propulsion system.
- Detachability of the wings and complexity of detaching engines.
- Having multiple propellers on the wings for aerodynamic benefits.
- Having one engine for maintenance and sustainability.
- The driveshaft will go through the wing to the propeller with a length of around $2.1m$. This required the driveshaft to be able to bend along with the wing during high loading cases. To mitigate this risk, the helicopter design of the chinook driveshaft will be adopted which incorporates a multistage driveshaft [6].

One of the disadvantages of such a system is the mechanical efficiency related to the multiple driveshafts and gearboxes. Also the throttle response may be influenced by the multitude of linkages, while the throttle response is one of the main considerations for the selection of a turboprop engine. A conventional propeller aircraft would experience around a 98% or 99% mechanical efficiency due to the gearing inside of the engine casing and having only a single driveshaft. In this design, each propeller encounters two driveshafts and two gearboxes before the power is transmitted. Hence, it has double the mechanical linkages compared to a conventional turboprop design which lead to an assumed mechanical efficiency of $.98\%^2 = .96\%$. This efficiency is considered acceptable as the desire for easily detachable wings was provided for.

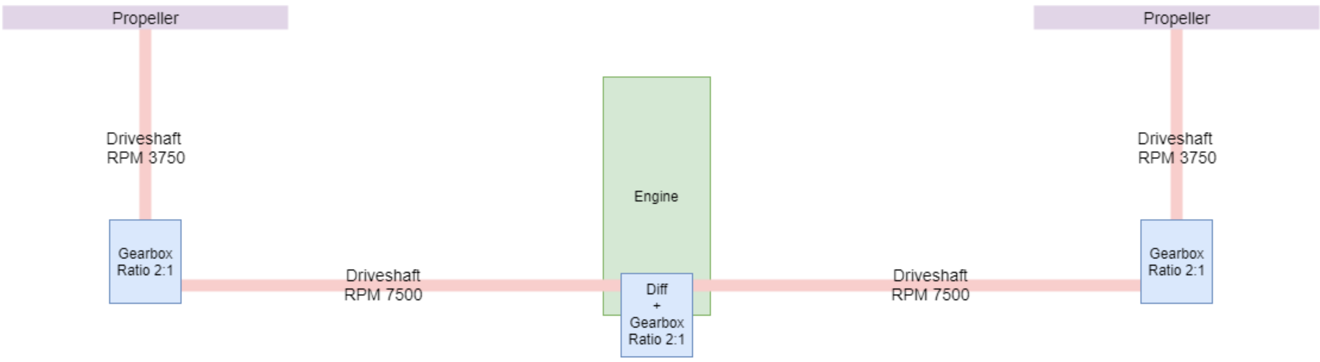

Figure 10.2: Drive train lay-out.

In Figure 10.2 a sketch of the drivetrain layout is given. The differential is required to be able to provide a different amount of power to each propeller. This and a variable pitch on the propeller blades will allow the aircraft to be able to manoeuvre with relative ease during slow speed water manoeuvring. A differential is also desired for the eventuality that one of the driveshafts, gearboxes or propellers fails. Such an event may, for example, occur due to fatigue or a bird strike. In such a case it is desirable to be able to land the UAV while having one engine inoperative. This is also the main design case for the vertical tail of the aircraft as described in section subsection 10.4.3. To improve weight efficiency it is beneficial to have the driveshaft spinning at a higher RPM than the propeller blades such that more rotational energy is generated and less torque. This, in turn, saves weight in the structural design of the driveshaft. A first estimate of the weight of the propulsion system, based on reference systems has been provided in Table 10.1.

To be able to disconnect the wings, the driveshafts will need to be disconnected from the engine gearbox as well. This requires a simple mechanism that can be deduced from existing car designs, such as visible in Table 10.3. Car driveshafts spin at a similar RPM as the driveshaft of the propeller but will only encounter a torque up to $700Nm$, which is less than

[5] http://navybmr.com/study%20material/14008a/14008A_ch4.pdf [cited 21 June 2019]
[6] http://www.chinook-helicopter.com/standards/areas/drive_train.html[cited 24 June 2019]
[7] https://www.2carpros.com/articles/how-to-remove-a-drive-shaft[cited 24 June 2019]

Table 10.1: Propulsion System Weight Overview

Engine [kg]	224
Casing [kg]	50
Struts [kg]	20
Propellers[kg]	50
Gearboxes [kg]	150
Driveshafts [kg]	110
Safety Margin 10%	50
Total Weight [kg]	654

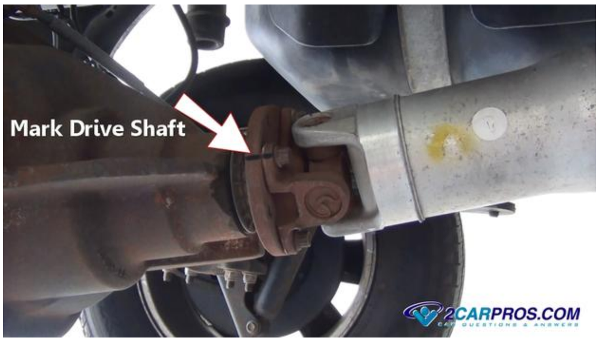

Figure 10.3: Example of a typical driveshaft connection in a car. [7]

the driveshaft of the UAV. Hence, further investigation is required to design specifically for the detachability of the driveshaft.

In the design of the drivetrain and the propellers, it has also been considered to place multiple propellers along the wing to increase the lift augmentation due to the propeller as researched by [19]. Furthermore, this would increase the propeller clearance during water operations. However, this was considered to be mechanically too complex and, therefore, not feasible. This layout for the propellers would be most beneficial for an electrical setup where the small engines could directly drive each propeller. As electrical engines had been eliminated from the design, this was no longer considered an feasible option.

10.1.5. Propeller Blades

General Propeller Blade Considerations

The propeller blades for the aircraft were mainly limited by the clearance required for water landings. When the UAV will land on the water, in the worst case scenario, it will have a draft of 1.3 as described in detail in section 10.3. This meant that the diameter of the propeller was limited with regards to the height of the fuselage and the height of the nacelle. For maximum aerodynamic performance, such that the $C_{L_{max}}$ can be increased, the propeller should not be lifted high above the wing as described in more detail subsection 10.2.4.

In the design process of the propeller blades, it was quickly determined that a variable pitch propeller was desired as the UAV acts within an extreme flight envelope and needs to have maximum thrust available at all possible times. This also means optimisation for cruise flight as quick initial response time is of great importance in firefighting. In general, a pilot of a turboprop aircraft only has the control of one lever which regulates the fuel flow to the engine [17]. In this case, the fuel control operates in conjunction with the pitch control of the propeller blades. In the design of the UAV, it is, however, preferred to separate this direct correlation such that the remote pilot of the UAV has complete control over the thrust available and is able to make quick decisions at any phase of the flight.

Propeller Material Selection

The propeller blades should be as light as possible to both minimise weight and reduce centrifugal loading on other parts of the propeller. This centrifugal force and the aerodynamic loading on the blade are mainly unidirectionally oriented.[20] Therefore, composites, which are light and can be layered to withstand high unidirectional loading, are favoured. A further consideration in the material selection process is fatigue. The propellers basically are rotating fatigue machines, thence the chosen material should have a high specific fatigue strength again favouring composites over metals. Apart from structural considerations, environmental considerations should be taken into account. Although metals would be reusable, their lifetime is significantly shorter than that of composites. Not only due to their lower fatigue strength but also for corrosion reasons. In the case of the amphibious UAV corrosion should be taken even more seriously as the propellers are likely to experience saltwater spray. As carbon fibre composites have excellent fatigue properties, good corrosion-resistance and will have lower maintenance requirements over a longer lifetime than metals as aluminium, these are selected as material for the propeller blades.

Actuator Disk Theory

To translate the performance of the propeller into design parameters actuator disk theory is applied. Using this, the minimum required propeller diameter can be found. Analysing the performance parameters, the propulsive efficiency is found to be described by Equation 10.1.

$$\eta_j = \frac{P_a}{P_{br}} = \frac{TV_0}{P_{br}} \tag{10.1}$$

In which, η_j is the propulsive efficiency, P_a the power available, and P_{br} the shaft power delivered by the engine. T is defined as free-air thrust meaning the thrust generated in absence of an air frame. The main limiting factor in the performance of the propeller blades is the velocity at the tips of the propeller blades. If the tip velocity of the propeller blades approaches a local velocity of around $M = 1$, the efficiency is seriously hindered [17]. In general the magnitude of the propeller tip speed is can be determined using Equation 10.2.

$$V_t = \sqrt{V_0^2 + (\omega R)^2} = \sqrt{V_0^2 + (\pi n_p D)^2} \tag{10.2}$$

In which, R is the blade radius, D, the blade diameter, ω, the angular velocity ,and n_p the revolutions of the propeller per second. The angle between the free-stream velocity and the propeller blade is called the advance angle θ and can be computed using Equation 10.3.

$$\tan\theta = \frac{V_0}{\omega r} = \frac{V_0}{2\pi n_p r} \tag{10.3}$$

To further analyse the tip velocity, rotational velocity, propulsive efficiency, and other factors related to the propeller sizing, Actuator Disk Theory is used, in which the following assumptions are made [21]:

- Both pressure and velocity are uniformly distributed across the disk area.
- The flow passing through the propeller forms a well-defined stream tube.
- The rotation or swirl imparted to the flow as it passes the disk plane can be completely ignored.
- The flow is incompressible.
- The flow passing through the propeller disk can be separated from the rest of the flow by a stream tube.
- Momentum theory is applied at all stages of the design, for both the actuator disk theory and blade element theory.

The thrust is given by the time rate of change of axial momentum, as visible in the relation given in Equation 10.4.

$$T = \rho\frac{\pi}{4}D^2\left(V_0 + V_a\right)V_{a3} \tag{10.4}$$

In which, V_a is the increase in velocity at the actuator disk, and V_{a3} is the increase in velocity to the free-stream by the propeller. Applying Bernoulli's equation, the shaft power may be expressed as the increase in kinetic energy of the air mass flow rate, as given in Equation 10.7.

$$P_{br} = \rho\frac{\pi}{4}D^2\left(V_0 - V_a\right)^2 V_{a3} \tag{10.5}$$

Combining the expressions for thrust 10.4, power 10.5, and propulsive efficiency 10.1, the expression for the propulsive efficiency, as given in Equation 10.6, can be obtained.

$$\eta_j = \frac{2}{2 + \frac{V_{a3}}{V_0}} \tag{10.6}$$

This expression can also be expressed in terms of thrust related to Equation 10.7.

$$\eta_j = \frac{2}{1 + \sqrt{1 + \frac{T}{\frac{1}{8}\pi\rho D^2 V_0^2}}} \tag{10.7}$$

As the diameter of the propeller was required, the equation for efficiency is related back to the relation for the diameter as given in Equation 10.8.

$$D = \sqrt{\frac{8T}{\rho\pi V_0^2\left[\left(\frac{2-\eta_j}{\eta_j}\right)^2 - 1\right]}} \tag{10.8}$$

Using equations 10.7 and 10.8, it can be seen that for a constant thrust, the propulsive efficiency must go down to decrease the minimum propeller diameter. In theory, this means that the propeller can become infinitely small as long as the efficiency also becomes infinitely small. This in turn, means that the exit velocity V_{a3} will become infinitely large. This is of course not possible as creating an exit velocity nearing $M = 3$ would be almost impossible to reach with the tip velocity of the blade. Thus, further research was required to discover the relation between the thrust generated by the propeller, the maximum tip velocity of the blades and the efficiency. Therefore, to determine the required propeller diameter, blade element theory is applied which is discussed in Equation 10.1.5.

Blade Element Theory

The main design scenario for the propeller design is the stall speed, as this is the most critical scenario in terms of power available, power required and efficiency as can been deduced from Figure 10.7 and Figure 10.6. During stall, the propeller must be able to generate the most thrust in case of critical manoeuvres whilst also experiencing the lowest propeller efficiency due to the low free-stream velocity. To conduct the analysis, the blade was divided in multiple sections across its radius such that the local thrust each element generates separately could be analysed. In the analysis, the following assumptions are made:

- The maximum C_L is reached at any element along the blade, meaning an angle of attack of around 5° at any point along the blade radius. This angle of attack may change during cruise for better performance during high speed operations, however, the propeller is mainly designed for climbing. In reality, near the root (hub) and tip of the blade this angle of attack will decrease and not as much thrust will be produced. This assumption will mean a higher thrust is obtained using BET.
- Based on statistical data from [17], the $\frac{C_L}{C_D}$ of the propeller blade is assumed to be 17.5. Due to rotational flow, the lift coefficient could locally increase [22], this increase has not been taken into account hence, the BET will indicate a lower thrust.
- Tip losses and rotational 3D due to Coriolis and centrifugal forces that act on the boundary layer flow over the propeller blades are not taken into account. The total effect is comparable to a favourable pressure gradient [21]. This effect will have a positive influence on the thrust produced, is, however, not taken into account in the BET. Thus, the BET will obtain a lower thrust.
- The propeller shall be able to generate enough thrust at any velocity to meet the thrust output from the engine.
- The induced velocity at the base of the blade is larger than the effective velocity. Due to this negative effect, the thrust generated at the base of the blade is assumed to equal zero. This effect is assumed to occur on the first 15% of the blade radius.
- Wake effects due to multiple blades on a single propeller can be neglected.
- The chord of each blade element, c, is assumed to be equal along the blade. This would in reality vary from the hub to the tip of the blade. This assumption leads to a higher obtained produced thrust.
- The blade is assumed to produce enough thrust within a 15% margin for the most critical case, acceleration at stall speed. In this 15% margin to the required thrust, the exhaust velocity is not taken into account, which in some cases could generate almost 20% of the total thrust [23]. Also, 3D effects are not taken into account meaning a 15% margin is considered sufficient at this point in time.

Using blade element theory, the thrust generated by a single propeller blade can be described by Equation 10.9.

$$T = B\int_H^R dT = B\int_H^R \frac{1}{2}\rho V_e^2 c\big(C_L\cos(\theta_a) - C_D\sin(\theta_a)\big)dr \tag{10.9}$$

In which, B is the amount of blades per propeller, V_e is the effective velocity as shown in 10.5, c is the cord of each blade element, C_L and C_D are the respective lift and drag coefficient of the blade, θ_a is the effective angle of attack and dr is the length of each element. This integration is then conducted starting from the hub, H, and ending at the tip, R. In this, compressibility effects have been taken into account for up to Mach 0.7 using the Prandtl-Glauert [21] correction for both C_L and C_D, given by C_x in Equation 10.10.

$$C_{x_{cor}} = \frac{C_x}{\sqrt{1-M_\infty^2}} \tag{10.10}$$

In Figure 10.5, it can be seen that the tip of the blade has an induced velocity V_i which is dependent on the axial component V_a. This is given by Equation 10.11.

$$V_a = V_i\cos\theta_a \tag{10.11}$$

The effect of V_i, is to reduce the angle of attack, α, to the effective angle of attack, α_e. The effective velocity, V_e, is then given by the relation in Equation 10.12.

$$V_e = \sqrt{V_0^2 + (\omega r)^2 - V_i^2} \tag{10.12}$$

The difficulty in determining the eventual thrust for each blade element using BET, lies in determining the aerodynamic advance angle θ_a. To determine the desired thrust generated by the propeller blade, the acceleration produced by the engine at a certain diameter was determined. For this a program was created that based on an assumed blade diameter reiterated the efficiency and excess thrust until the acceleration that the aircraft is able to achieve at each velocity was determined.

Finally, in the eventual blade sizing, the assumed blade diameter for the generated required thrust was checked to determine whether all conditions are met. First, based on assumptions for C_L, C_D, the number of blades, and the previously determined diameter, the efficiency is determined using Equation 10.1. Then, by dividing the blade in small segments and reiterating the advance angle, the induced velocity is calculated using Equation 10.11. Finally, using Equation 10.9, the thrust generated for each element of the blade is calculated and summed. This value is multiplied with the amount of blades and the amount of propellers which must equal the required total thrust generated by the system. If this requirement was not met or if it was overdesigned, the blade diameter, lift coefficient and/or chord was changed. As a safety measure and to reduce the impact of the assumptions made, the decision was made to design the propellers to generate 10%-15% more thrust then required. The results of this analysis and the final values of the propeller design are given in Table 10.2.

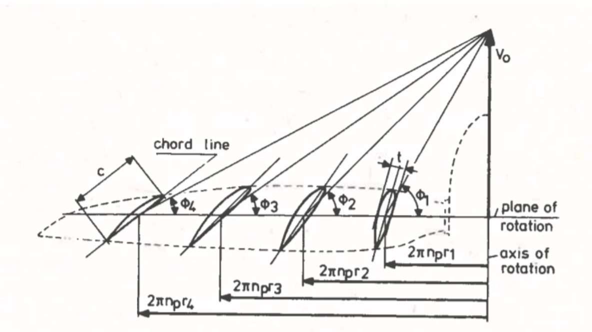

Figure 10.4: Variation of advance angle and blade angle from hub to tip.[17]

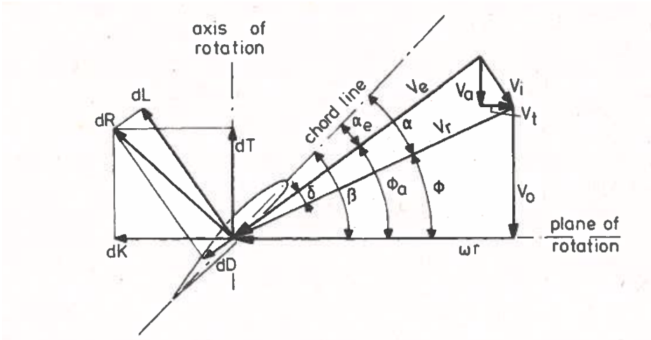

Figure 10.5: Propeller Blade Cross-section.[17]

Table 10.2: Final values for the propeller design.

V_0 **[m/s]**	35.0
$T_{totalreq}$ **[kN]**	34.5
$T_{genprop}$ **[kN]**	39.0
D_{prop} **[m]**	2.20
P_{br} **[kW]**	2439
Efficiency	0.495
V_{a3} **[m/s]**	78.0
Cl_{prop}	1.4
Cd_{prop}	0.08
RPS	38
Chord [m]	0.198
Solidity	22.9%

Effect on Performance

The blade diameter influences the propeller efficiency as during acceleration the ratio $\frac{V_{a3}}{V_a}$ decreases [17], which in turn leads to a decrease in power available. The results of the effect on performance are shown in Figure 10.7. Compared to the theoretical flat line for power available, this efficiency loss at low airspeed can have a significant effect on the low speed performance in terms of rate of climb and acceleration. Although it should be noted that there is quite a significant change, dependent on the thrust that the propeller needs to deliver as is shown in Figure 10.7. In terms of acceleration, the adjusted propeller efficiency also has an influence on the maximum acceleration possible during the different flight speeds. But compared to the acceleration possible for the Canadair CL-415 it is apparent that Wangari is able to accelerate over 60% faster than the CL-415. This result satisfies the goal of outperforming the current market.

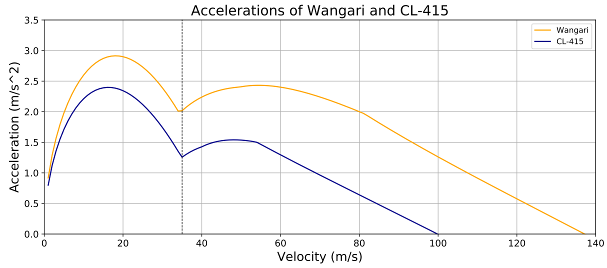

Figure 10.6: Acceleration comparison.

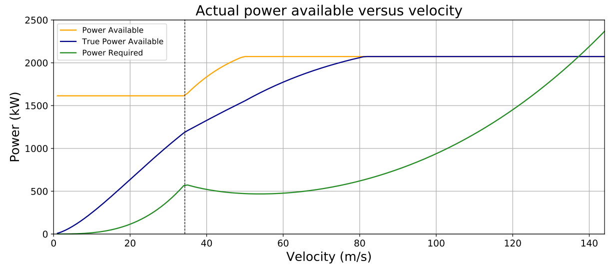

Figure 10.7: True Power Available with propeller efficiency.

10.1.6. Propulsion Design Analysis and Future Steps

Future Improvements

In future design iterations of the propellers, the effects of wake and tip relief should be taken into account. Also, general correction factors due to the assumed incompressibility in the actuator disk theory require further analysis. Furthermore, the C_L and C_D across the length and chord of the blade should be investigated in the future design process. This also allows for including the increase in the local lift coefficient due to the blade rotation. An increase of as much as $1.5 \cdot C_L$ can be witnessed due to this effect [22]. Nacelle effects are also neglected in this preliminary design and the complexity required for having variable pitch propeller blades. Lastly, the thrust generated by the exhaust of the turbo shaft engine is neglected in this conceptual design phase, this could account to up to 20% of the total thrust generated by the aircraft [24] and should hence be properly investigated in future iterations.

Sustainability

In the design of the propulsion system a trade-off between types of propulsion as electrical, hydrogen and a combustion engine was performed. The trade-off between these options was done with regards to the high temperatures of fires and the dangers it may impose on the propulsion system as well as the consequences on the performance of the UAV and the weight and space these configurations would require. Furthermore, the performance of the UAV per engine selection was related to its efficiency of fighting wildfires, which can generate more emissions than the UAV itself [8] [9]. In general, $10.0 kg$ of carbon emissions comes free per squared meter of area burnt by wildfires. This estimate, based on wildfires in different countries [10] [11], does not include the loss of CO_2 emissions that the area could have converted to oxygen using photosynthesis.

In the sustainability analysis, the propulsion system of the UAV is compared to a hybrid aircraft. The Zunum Aero [12] was chosen for the comparison since it is a relatively large aircraft ($5,216 kg$ MTOW) that is mainly powered electrically, and has already flown. For the regular propulsion aircraft it is assumed that around $3.00 kg$ of CO_2 emission is generated per litre of kerosene used by the engine [13].

The following main assumptions and parameters are used for the comparison:

- Both aircraft would need 15 minutes to refuel and/or replace batteries in the event of returning to base
- The relevant parameters of the Zunum Aero are: maximum cruise speed = 151 m/s, range = 1126 km, payload = 1130 kg
- The distance from the fire to the base is 50 km, and from the fire to the water refilling source is 10 km
- All times besides the cruising times between the fire, the base, and the water source are neglected.
- The fire scenario assumed is a fire spreading in a circular shape with a starting speed of 0.1 m/s, and it slows down every half an hour by about 0.01 m/s until it stops naturally 5 hours later.

Although the propulsion system is not as sustainable as a hybrid electric-fuel vehicle, it is holistically more sustainable than the current alternative. The added benefit in performance from regular propulsion aircraft reduces the emissions of the burning forest, thereby outweighing the negative effect of causing more emissions by the aircraft itself.

[8] https://www.bbc.com/news/science-environment-46212844[cited 19 june 2019]
[9] https://www.cbc.ca/radio/quirks/sept-15-2018-summer-science-camping-under-a-volcano-plastic-in-beluga-bellies-and-more-1.4821942/how-do-co2-emissions-from-forest-fires-compare-to-those-from-fossil-fuels-1.4821944[cited 19 june 2019]
[10] https://www.ncbi.nlm.nih.gov/pmc/articles/PMC4874420/[cited 19 june 2019
[11] https://www.hindawi.com/journals/amete/2014/958457/[cited 19 june 2019]
[12] https://zunum.aero/our-charge/ [cited 01 july 2019]
[13] https://www.engineeringtoolbox.com/co2-emission-fuels-d_1085.html[cited 17 june 2019]

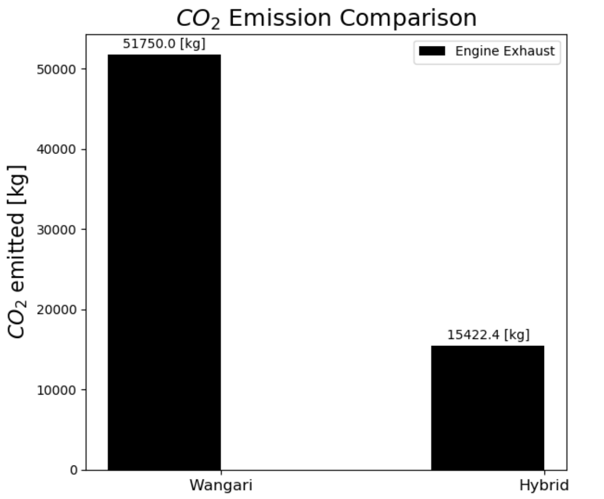

Figure 10.8: Engine exhaust of both propulsion systems in kilograms of CO_2

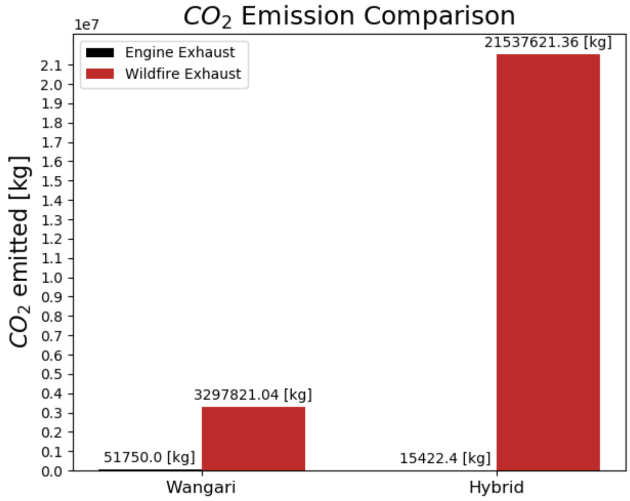

Figure 10.9: Engine- and Wildfire exhaust of both systems in kilograms of CO_2

Sensitivity Analysis

A sensitivity analysis has been performed on the blade element theory described in Equation 10.1.5. In this sensitivity analysis multiple variables have been changed to determine the output of the BET. The main output generated by the BET was the thrust generated by each blade element. Because each element is its own generator of thrust, small changes within this equation were highly sensitive to the thrust that the blade is able to generate. The most sensitive aspect of the BET turned out to be the assumed C_L of the blade and the chord of the blade. A change of 2% within the chord length of the blade is able to create a difference of thrust able to generate of around 20% of the entire thrust required. The same account for the assumed C_L of the blade. A change of this C_L from 1.4 to around 1.2 will cause a 20% decrease in thrust that the blade is able to generate. Also the main contributing factor to the blade performance is the blade diameter. Due to its increase in the efficiency of the propeller and the more elements on the blade. An increase of the blade diameter of 10% will increase the thrust of the propellers by 25%. Also increasing the amount of blades of each propeller is highly sensitive to generate more or less thrust. An increase of propeller blades from 4 blades to 5 blades will increase the thrust by more than 30%.

After all the considerations, it can be assumed that the BET is highly sensitive to many different changes in the design and a significant margin has been taken with the calculation of BET, also within the assumptions stated at the beginning of Equation 10.1.5.

Verification & Validation Procedures

The main calculation for the propeller blade diameter has been verified using example propeller blades from other existing aircraft. The main verification has been created using the blade specification of the CL-415 [14]. The blade diameter, chord and thrust available have been used to create a verification check on the blade element theory as described in section 10.1.5. Through verification of the BET, the values for the blade diameter for the propeller design are assumed to be within a reasonable margin.

In Figure 10.6 a verification of the acceleration figures based on the thrust, propeller diameter and maximum efficiency compared to the Canadair CL-415 has been performed. From this graph it can be noted that the CL-415 reaches an acceleration of 0 at 100m/s which is exactly equal to its maximum speed. This in terms shows the validity of the computations performed and the corresponding relation between thrust required, thrust generated, propeller diameter and propeller efficiency.

Validation procedures required for future design would incorporate wind tunnel testing to validate the actual thrust generated by the propeller. To test all the performance parameters related to the propeller design such as the increase in

[14] `https://airandspace.si.edu/collection-objects/hamilton-standard-propeller-variable-pitch-four-blade-metal`[cited 20 june 2019]

lift augmentation due to the accelerated flow behind the propeller, thrust vectoring and the influence of the air frame behind the propeller, flight tests should be conducted.

Future Risks and Mitigation Strategies
Future risks mainly concern the eventual sizing of the propellers due to the achievable max Cl and l/d values along the propeller blade. Also the complexity of the driveshafts and gearboxes with a differential may cause problems due to complexity and maintenance at later stages in the design. Also an engine location within the fuselage may hinder easy access for maintenance and adjustments when required.

Another risk considered is the eventual development of the GE T901 engine. The performance aspects of the UAV do rely on the performance that the engine is able to deliver. If the engine production is postponed or the performance is less then advertised, this will have a direct influence on the aircraft performance and another aircraft engine may be considered. The closest engine possible for consideration is the Lycoming T55 [15], which is close in performance, size and weight to the GE T901. It may also be considered a risk that the increased lift augmentation due to the accelerated flow of the propeller is not sufficient enough for the wing to created the required $C_{L_{max}}$. This risk may be mitigated by increasing the flapped surface area or adding slats to the wing.

10.2. Wing

10.2.1. Wing Geometry

The main decisions for the wing geometry have been primarily qualitatively based on empirical methods as presented by Raymer[24]. Thorough aerodynamic analyses using CFD software remain time consuming and complex and are hence considered beyond the scope of this design iteration. The aerodynamic choices based on empirical data give the team an initial starting point for the type of geometry to be optimised in a later design stage and have hence been chosen for the initial design presented in this report.

The starting point for the wing geometry bases itself on the wing surface area of $40.8m^2$ which has been previously determined in the concept selection phase[6]. Subsequent decisions on the wing geometry stem from the aircraft's operational constraints and mission profile.

Aspect Ratio
The aspect ratio of a wing can be defined as:

$$AR = \frac{b^2}{S} \tag{10.13}$$

where b is the total span and S the surface area. As the surface area has been predetermined, the decision on the maximum span and hence the aspect ratio has been constrained by the key transportability requirement:

AF-TRNS-01 Two UAVs shall be able to fit in an A400M

A high aspect ratio wing is associated with decreased drag, due to the tips being further apart. This larger spacing will allow for less wing-area to be affected by the tip vortices. Thus, high aspect ratio wings often experience less induced drag and are more lift efficient. Despite this, a higher aspect ratio is also associated with increased wing weight. Later on in a first sensitivity analysis it will be shown what the effect of a different aspect ratio will have on the total wing weight. The effect of aspect ratio on the stall and lifting characteristics of a wing can also be visualised in a guideline by Raymer in Figure 10.10.

In line with the transportability requirement, in order for two wings to longitudinally fit into the A400M cargo bay, the span of the wing is limited to $17.5m$. The maximum possible aspect ratio is then:

$$AR = \frac{17.5^2}{40.8} = 7.5 \tag{10.14}$$

Due to its operations at low altitude and speeds, the UAV is expected to experience more drag compared to normal cruise conditions. Furthermore, high lift coefficients are required in order to facilitate these operations without the use

[15] `https://en.wikipedia.org/wiki/Lycoming_T55`[cited 25 June 2019]

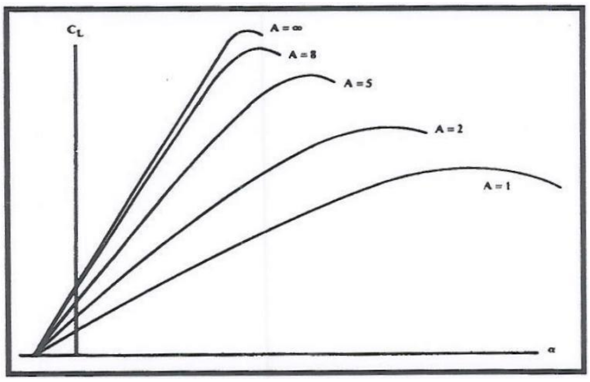

Figure 10.10: Aspect ratio effect on wing lift curve [25]

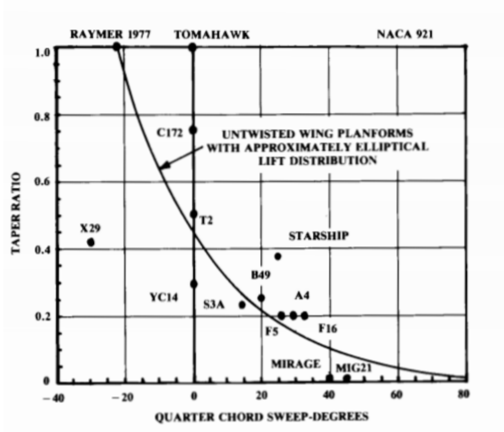

Figure 10.11: Recommended taper ratio for a certain wing sweep angle[26]

of highly complex and heavy high lift devices. Hence, keeping this aerodynamic performance as a driving design parameter, in order to maximise the lift generated and minimise the induced drag, the aspect ratio has been frozen to the highest acceptable of 7.5 in the design iteration presented in this report.

Sweep

Aircraft use sweep in order to primarily minimise the negative effects associated with transonic and supersonic flow. These include aspects such as a loss of lift and increased drag within the transonic region. The UAV will be operating mainly at low speed conditions close to the stall speed of $35.5m/s$. Meanwhile, the cruising speed has been set at $112.5m/s$. This corresponds to a cruise Mach number of 0.33. At this speed from historical empirical data[27], no sweep angle is required as no transonic effects over the wing are expected to occur. Moreover, as increased sweep is also associated with increased wing weight, having no sweep will only be beneficial to the overall structural design.

Taper and Twist

In order to minimise induced drag and hence maximise aerodynamic efficiency, the lift distribution across a wing plan form should be as elliptical as possible. This effect may be achieved by varying the taper ratio as well as the twist distribution along the wing span. An empirical relationship between sweep angle and taper ratio may be visualised from Raymer in Figure 10.11.

For a wing with no sweep, the recommended taper ratio takes a value of 0.45. The values for the root (c_r) and tip chord(c_t) may be determined using Equation 10.15.

$$S = 0.5b(c_r(1+\lambda)) \tag{10.15}$$

This then yields a value of $3.22m$ for the root chord and $1.15m$ for the tip chord. Considering the fact the the total fuselage length takes a value of $9.0m$, a wing root chord taking up 1/3 of the fuselage length was considered unreasonably large.

As mentioned previously, another possibility of optimising the wing for an elliptical lift distribution consists in varying the wing twist along the span. This may also help in minimising the adverse effect of earlier tip stall associated with a lower taper ratio. Despite this, twisting a wing may usually only be successfully done for a certain lift coefficient and has detrimental effects at all other angles of attack. For aircraft designed for cruise where the angle of attack is usually kept constant for the majority of the flight duration, this may be beneficial. Seeing however as this UAV is designed for low speed highly dynamic operations, therefore optimising wing twist for a specific flight condition is not optimal.

Furthermore, as the wing taper and twist distribution both play a significant role in the lift distribution over a wing, there should exist an optimal combination of the two for which the wing may perform best at a given flight condition. Deriving an optimisation method for the such a combination, however, has been considered a topic for the next design iteration. This is not only a consequence of the current time constraint but also of the fact that optimising for a certain flight condition requires a more in depth analysis of the mission and path plan from an operational and performance standpoint.

As increasing the taper ratio above the ideal value of 0.45 for an unswept wing without altering the twist has been shown to have minimal impact on the performance of the wing[26], at this stage in the design the taper ratio has been chosen as 1 with no twist along the wing. Given the final decision on the twist and taper ratio the wing chord can be finalised as:

$$c = \frac{S}{b} = \frac{40.8}{17.5} = 2.33m \tag{10.16}$$

10.2.2. Aerodynamic Parameters

In order to better assess the aerodynamic performance of the aircraft and understand how the wing characteristics will affect the stability and control of the aircraft, various wing induced aerodynamic parameters will be computed.

Wing Lift Gradient

Based on the selected airfoil in section 7.2, a similar lift curve can be drafted for the wing based on its geometry and empirical data. The wing lift gradient may be estimated with the DATCOM method[28] described in Equation 10.17.

$$C_{L_\alpha} = \frac{2\pi AR}{2 + \sqrt{4 + \left(\frac{AR\beta}{\eta}\right)^2 \left(1 + \frac{tan^2\Lambda_{0.5c}}{\beta^2}\right)}} \tag{10.17}$$

where AR is the aspect ratio, Λ the sweep angle, β the Prandtl-Glauert compressibility correction factor defined as $\sqrt{1-M_\infty^2}$ and η the airfoil efficiency parameter defined as $\frac{C_l\beta}{2\pi}$. It can be noted that as the wing has no sweep, the compressibility factor completely filters out of the equation. Inputting the parameters into Equation 10.17, yields a wing lift gradient of $4.81/rad$.

The intercept for zero lift occurs at that of the airfoil and corresponds to an angle of $-6.5deg$. Of course, drafting the lift curve based on the intercept yields an infinitely linear relationship. In order to estimate the stall behaviour of the wing, similar empirical data has been used.

There are two empirical ways to estimate the max lift coefficient of a wing depending on whether the aspect ratio classifies as either high or low. The high aspect ratio method is used in case the condition in Equation 10.18 holds.

$$AR > \frac{4}{(C_1 + 1)\cos(\Lambda_{LE})} \tag{10.18}$$

Where the coefficient C_1 is determined from the curve visualised in Figure 10.12 and is dependent on the taper ratio.

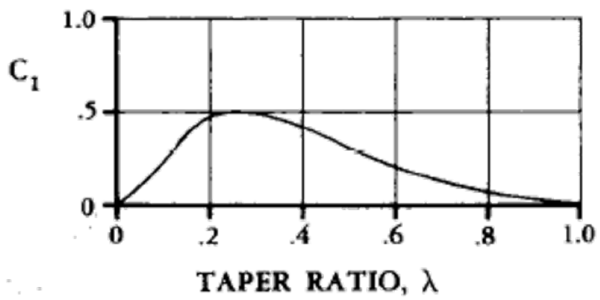

Figure 10.12: C_1 vs taper ratio [28]

With a taper ratio of 1, C_1 in this case is 0 and thus with an aspect ratio of 7.5, the high aspect ratio condition is satisfied. Thus the maximum lift coefficient for the wing can be evaluated using Equation 10.19.

$$C_{L_{Max}} = \left(\frac{C_{L_{max}}}{C_{l_{max}}}\right) C_{l_{max}} + \Delta C_{L_{max}} \tag{10.19}$$

The ratio $\frac{C_{Lmax}}{C_{l_{max}}}$ is also empirically estimated from the curves in Figure 10.13.

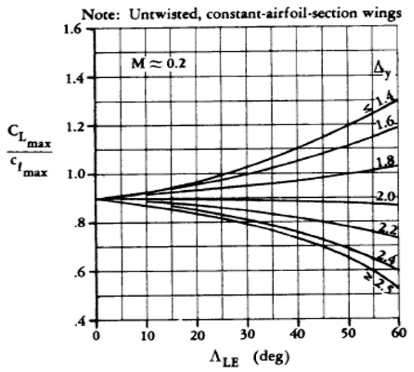

Figure 10.13: $\frac{C_{Lmax}}{C_{lmax}}$ vs taper ratio for multiple sharpness parameters [28]

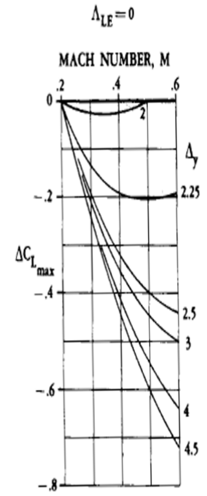

Figure 10.14: $\Delta C_{L_{max}}$ vs mach number for multiple leading edge sharpness parameters [28]

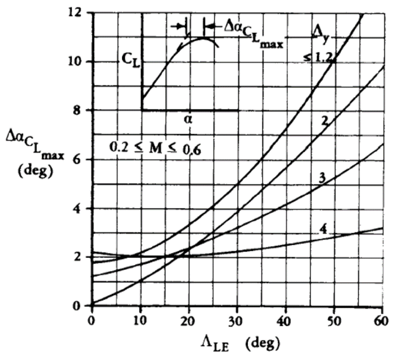

Figure 10.15: $\Delta\alpha_{C_{L_{Max}}}$ vs leading edge sweep for various leading edge sharpness parameters [28]

Furthermore, the sharpness parameter for NACA 64 series airfoil can be estimated as $21.3\frac{t}{c}$[28] and is thus in this case $21.3 \cdot 0.15 = 3.195$. The lift coefficient ratio can hence be determined from the graph for a 0 sweep as 0.9. A similar estimation can be taken for $\Delta C_{L_{max}}$ from the Figure 10.15.

Given the previously calculated Mach number as well as leading edge sharpness parameters, the value of $\Delta C_{L_{max}}$ is taken as -0.18. Inserting these parameters into equation Equation 10.19 yields a value of 1.448 for the maximum wing lift coefficient.

The stall behaviour of the wing can be completed by determining the expected stall angle for the wing. This can be easily computed as using Equation 10.20.

$$\alpha_s = \frac{C_{L_{max}}}{C_{L_\alpha}} + \alpha_{0_L} + \Delta\alpha_{C_{L_{Max}}} \tag{10.20}$$

In which $\Delta\alpha_{C_{L_{Max}}}$ can be estimated from Figure 10.15.

Given the leading edge sharpness parameter, a value of 1.25 has been determined for the difference in the stall angle of attack. Thus, inserting the parameters into Equation 10.20 yields a wing stall angle of 11.96. The finalised lift curve for the wing can be visualised against that of the airfoil in Figure 10.16. The wing will indeed exhibit the same stall shape as the airfoil between the maximum coefficient and the stall angle however for visualisation purposes in this case and to avoid inaccuracies, the maximum lift coefficient as well as the stall angle have been indicated by the light blue and green lines respectively.

Lift gradient tailless aircraft and horizontal tail

From the wing lift gradient, the lift gradients of the tailless aircraft and horizontal tail can be calculated, which are needed to determine to stability of the aircraft.

$$C_{L_{\alpha_{A-h}}} = C_{L_\alpha} \cdot \frac{S_{wing-c\cdot h_b}}{S_{wing}} \cdot 1.07 \cdot \left(1 + \frac{h_b}{b}\right)^2 \tag{10.21}$$

where C_{L_α} can be computed with Equation 10.20, S_{wing} is the wing surface area, c is wing chord, h_b is the width of the hull and b is the wing span.

$$C_{L_{\alpha_h}} = \frac{2\pi AR_h}{2 + \sqrt{4 + \left(\frac{AR_h \cdot \beta}{\eta}\right)^2}} \tag{10.22}$$

where AR_h is the aspect ratio of the horizontal tail, β is Prandtl-Glauert compressibility correction factor as defined

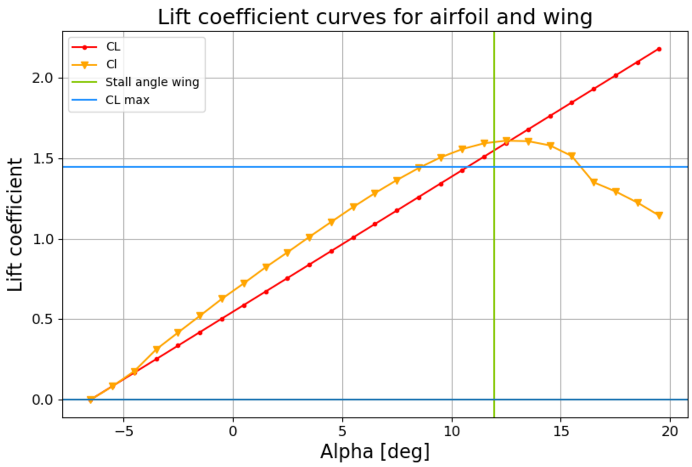

Figure 10.16: Lift curve for airfoil and wing

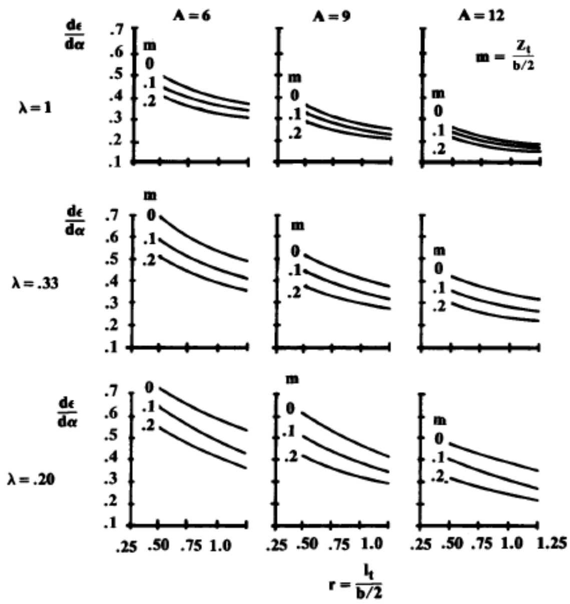

Figure 10.17: Downwash estimation (M=0) [24]

.

above, and η is the airfoil efficiency, also defined above.

Downwash gradient

Aft of the wing, the airflow is pushed downwards due to the wing producing an upwards force, which is called downwash. The gradient of the downwash can be used to calculate the effective angle of attack the horizontal tail sees and is needed to determine the stability of the aircraft. The downwash can be estimated using Figure 10.17 from Raymer. Here λ is the taper ratio, A is the aspect ratio, I_t is the horizontal distance between the wing quarter chord and the horizontal tail quarter chord and Z_t is the vertical distance between. Using this figure, the downwash gradient was estimated to be 0.35.

Moment coefficient

The wing pitching moment about the aerodynamic centre is largely determined by the airfoil pitching moment. It can be computed with the relation in Equation 10.23.

$$C_{m_{ac}} = C_{m_{0_{airfoil}}} \left(\frac{A\cos^2\Lambda}{A + 2\cos\Lambda} \right) \tag{10.23}$$

where $C_{m_{0_{airfoil}}}$ is the moment coefficient of the airfoil at zero angle of attack, A is the aspect ratio and Λ is the wing sweep. $C_{m_{0_{airfoil}}}$ has a value of -0.103 and can be determined from Figure 7.3. $C_{m_{ac}}$ was then computed to be -0.081.

10.2.3. High Lift Devices

Multiple options were considered during the high lift design of the wing. As also mentioned in section 7.4, the following take-off and landing requirements hold:

AF-PERF-TO-05 The UAV shall be able to take off within $500m$ on land at sea level conditions
AF-PERF-TO-06 The UAV shall be able to take off within $500m$ on water at sea level conditions
AF-PERF-LND-02 The UAV shall have a maximum ground landing distance of $800m$ at sea level conditions

As discussed in section 7.4 in order to be able to meet the landing requirement, the UAV shall be capable of achieving a maximum lift coefficient of 3.0. A lift coefficient of 3.0 also would allow the UAV to come close to the take-off requirement with the estimated distance being $560m$. Initially it was attempted to achieve this lift coefficient with the use of both leading edge and trailing edge high lift devices. Keeping a slat as the leading edge device due to its maximum high lift capabilities, the potential increase in lift was investigated for the two extremes of a plain or triple slotted flap. A plain flap has the benefit of requiring a much more simple attachment mechanism and is thus associated with a lower structural weight. A slotted flap is on the other hand associated with significant aerodynamic improvement. In comparison

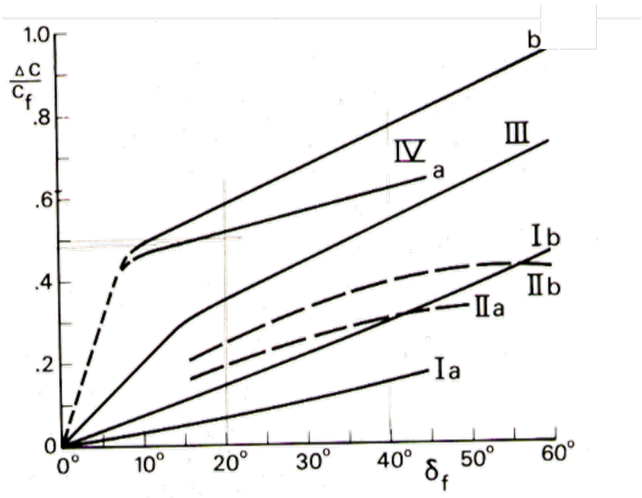

Figure 10.18: Empirical method for estimating the effective change in chord Δc[29]

.

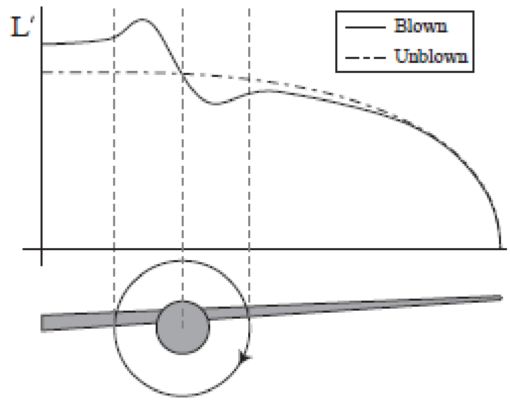

Figure 10.19: Lift Distribution change over the wing due to propeller blowing[19]

.

to the simple flap, it not only allows for increased camber but also increased surface area. In addition, the high-pressure air from underneath the wing is allowed to exit over the top which tends to reduce the tendency of flow separation and hence increases L/D.

From Raymer[29], for an airfoil the change in lift coefficient for a simple flap can be estimated 0.9. Similarly for a triple slotted flap this increase in airfoil lift coefficient is taken as $1.9\frac{c'}{c}$. $\frac{c'}{c}$ can be estimated given that c' corresponds to the change in chord (Δc) added to the original chord (c) length due to the flap deflection. The change in chord may be estimated from Torenbeek using Figure 10.18.
Although typical values for flap deflection do not usually exceed 40° in normal flight conditions, in order to investigate the maximum achievable change in lift an upper limit of 55° is chosen for the eventual flap deflection. This yields a $\frac{\Delta c}{c_f}$ of ≈ 0.9. c_f in this case refers to the portion of the wing that is flapped. Simple flaps usually take up around 25% if the wing chord whilst slotted flaps take up 35% of the chord[29]. For comparison in this case, a standard value of 30% has been assumed. Given the above the change in wing chord for the slotted flap can be calculated as:

$$c' = c + \Delta c = c + 0.9 \cdot 0.3c = 1.27c \tag{10.24}$$

Thus the final ratio $\frac{c'}{c}$ is 1.27 and the maximum achievable change in C_l in a most extremely deflected case from the triple slotted flap is estimated at $1.27 \cdot 1.9 = 2.41$. Given that $C_{l_{max}}$ take a value of 1.5 it appears that for the airfoil, a maximum lift coefficient of 4.0 may be achieved with a triple slotted flap.

This lift augmentation for the airfoil must however be translated to a wing using Equation 10.25.

$$\Delta C_{L_{max}} = 0.9 \Delta C_{l_{max}} \frac{Swf}{S} \cos(\Lambda_{hinge-line}) \tag{10.25}$$

As there is no sweep at the hinge line it is clear that the change in lift for the wing will be limited by Swf which is the portion of the wing actually affected by the high lift device. Limited by the control surface size and placement which is further detailed in section 10.5, the maximum area the flaps can cover is limited to $25m^2$ whilst for the slats the area is limited to $32.6m^2$.

Inserting these parameters into Equation 10.25 yields the results in Table 10.3.

Flap Type	$C_{l_{max}}$	C_{Lmax}
Single	2.5	2.3
Triple Slotted	4.0	3.1

Table 10.3: Maximum achievable lift coefficient with the two flap types and a slat.

The flap analysis has highlighted multiple aspects. Given the available wing area for the high lift devices to cover, the desired maximum lift coefficient of 3.0 is not immediately achievable. Despite the triple slotted flaps potentially able to harness a lift coefficient comparable to the maximum encountered by the CL-415, this is a product of the assumption that the devices will be constantly deflected 55° which is generally unrealistic, primarily given the drag penalty this would induce. Furthermore, the major setback related to the triple slotted flap remains. The mechanism is much more complex and harder to maintain. In addition, given that the lift coefficient requirement will vary quickly during flight, changing the flap settings quickly remains a slower process than for a plain flap. In order to maximise mechanical efficiency and be able to more quickly optimise the UAV at every flight stage, using a more simple/plain flap is ideal.

In consultation with a propulsion expert[16], key to the CL-415's ability to generate a high lift coefficient of 2.8 using plain flaps is the lift augmentation resulting from the interaction between the propellers and the wing. This interaction is also key to the final design configuration chosen by the team and is further explored in subsection 10.2.4.

10.2.4. Propeller - Wing Aerodynamic Interaction

General Background

The aerodynamic behaviour between the slipstream of a propeller and the wing are highly complex. Nevertheless, simplified models have been developed especially in a preliminary stage of the design process in order to get an estimate on the effect of this interaction.

The flow phenomena have been studied by Veldhuis[21] in detail. As a propeller produces thrust, a helical vortex system results behind the propeller, producing a complicated and non-uniform flow field. The velocity at any point in this flow field is predominantly directed either along or tangent to the axis of this propeller. Based on the prime assumption that propeller thrust can be modelled using momentum theory as in subsection 10.1.5, the only useful component of the velocity lies in the axial direction. In order to determine how much the local flow deviates from the purely axial direction it is useful to measure the swirl angle defined as follows:

$$\theta_{swirl} = \tan^{-1}\left(\frac{V_t}{V_\infty + V_a}\right) \tag{10.26}$$

Where V_∞ is the free stream velocity, V_a the axial velocity and V_t the tangential velocity immediately after the propeller. Important to note that although the axial velocity varies, the tangential velocity stays predominantly constant in the slipstream.

As a consequence of this swirl, the angle of attack of the wing sections aft of the upward moving half of the blade tends to increase whilst the opposite happens for the downward moving half of the blade. The apparent velocity over the wing hence varies with peaks and the apparent lift distribution takes the shape visualised in Figure 10.19.
Due to the swirl effect, although the lift does decrease over the downward going section, as the axial velocity increases, it is not equal to the augmented lift on the upward going section. Thus, overall there will be a positive outcome on the lift over the wing.

Assumptions and Used Model

The proposed model in this case is based on an enhanced actuator momentum theory principle. The following assumptions hold from subsection 10.1.5:

- Pressure and velocity are uniformly distributed over the blade area.
- The flow passing through the propeller forms a well defined streamtube and is separated by the from the rest of the flow.
- The rotation of the flow and swirl is ignored.

In addition here, the affect of the nacelle on the wing is also neglected.
The initial model is two dimensional and bases itself on thin wing theory. The airfoil is completely immersed in the flowfield and is represented by the single point vortex of circulation strength Γ placed at the quarter chord point on the zero lift line. The propeller is subject to an inclination angle, i_p with the angle of attack denoted by α_a and the velocity behind the propeller as V_p. The geometry of the problem can be first visualised in Figure 10.20.
The vector diagram of a model of the flow aft of the propeller is then presented in Figure 10.21. V_{ep} is the velocity actually experienced by the airfoil. The point vortex normally induces a downwards velocity w_∞ which then reduces to w_{new} due to the blowing of the propeller.

[16] Joris Melkert, Lecturer, Faculty of Flight Performance and Propulsion, TU Delft

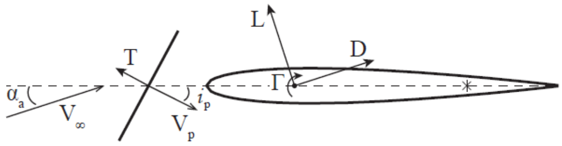

Figure 10.20: Geometry describing the 2D point vortex representation of the airfoil with respect to the incoming freestream velocity and propeller slipstream velocity[19]

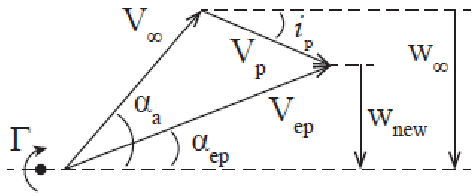

Figure 10.21

.

From the Kutta-Joukowski theorem, the lift per unit span can then be calculated as $L' = \rho V_{ep}\Gamma$. This then allows for the determination of $\frac{\Delta L'}{L'_\infty}$, which represents the change in lift due to the influence of the propeller.

One issue arising from the model is that it can overpredict the lift per unit span due to the implication that the radius of the blade in this case is infinitely large. In order to correct for this, it is hypothesised the velocity experienced by the airfoil may be corrected by a factor β to βV_{ep}.

From Patterson at al.[19], the lift augmentation may be estimated using Equation 10.27:

$$\frac{\Delta L'}{L'_\infty} = \left(1 - \beta\frac{V_p \sin(i_p)}{V_\infty \sin(\alpha_a)}\right)\frac{\sqrt{V_\infty^2 + 2\beta V_\infty V_p \cos(\alpha_a + i_p) + (\beta V_p)^2}}{V_\infty} - 1 \tag{10.27}$$

The efficiency factor β has been estimated by Patterson et al.[19] through CFD simulations based on a propeller actuator disk model placed at various upstream values of a symmetrical airfoil. The simulations were performed for a freestream Mach number of 0.2 with multiple differing values of V_{ep}. Furthermore in this case, although the flow was considered inviscid, compressibility effects were taken into account. The graphical results are summarised in Figure 10.22.

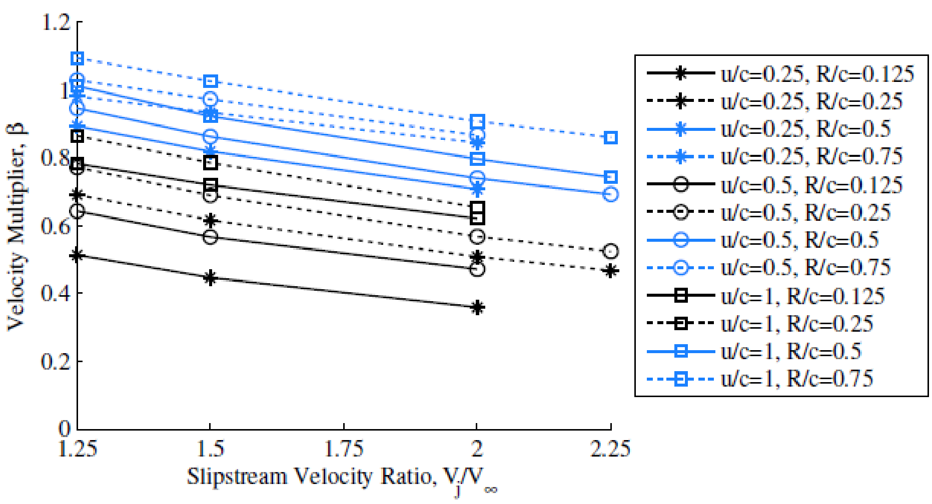

Figure 10.22: Velocity multiplier (β) values as a function of the slipstream velocity ratio for multiple actuator disk heights and upstream distances from the airfoil as a result of the 2D CFD simulations [19]

.

Other than being sensitive to the radius of the propeller, it is immediately apparent that the upstream distance of the propeller relative to the leading edge of the wing also plays a crucial role.

In order to examine the potential effects of the UAVs propellers on the lift augmentation, the most critical lifting condition near near stall is evaluated. At this point the flaps are down and it can be assumed that the UAV is flying close to stall at an angle of attack 11.5°. As this analysis is used to investigate the possible option of employing solely plain flaps, the $C_{l_{max}}$ of the UAV without the propeller is taken as 2.5 according to what was calculated in subsection 10.2.3. The simple airfoil is here considered instead of the entire wing. The lift coefficient for the wing differing from that of the airfoil is a prime consequence of the wing tips. Due to the propeller placement, any wingtip effects may only arise from the difference in velocities within the slipstream and the free stream condition at the edge of the propeller. Nevertheless, they are here considered to be minimal and hence neglected.

In line with the blade element calculations presented in Equation 10.1.5 as well as the finalised dimension of the propeller (R=1.1m) and wing (c=2.33m), the inputs for the model are summarised Table 10.4. V_p has been taken from the velocity induced by the propeller at a critical condition near stall as calculated in section 10.1 when there is no acceleration on the aircraft. Given that this corresponds to an effective velocity ($V_{ep} = V_j$) experienced by the propeller of 68.8m/s, the slipstream velocity ratio $\left(\frac{V_j}{V_\infty}\right)$ used to determine a range of β values from Figure 10.22 is 2.0 assuming V_∞ in this case corresponds to the stall speed.

Table 10.4: Input values for the lift augmentation model at near stall conditions

Parameter	Value
$C_{l_{max}}$	2.5
$C_{L_{max}}$	2.3
V_p $[m/s]$	33.8
V_{stall} $[m/s]$	35
α_a [deg]	11.5
R/c	0.47

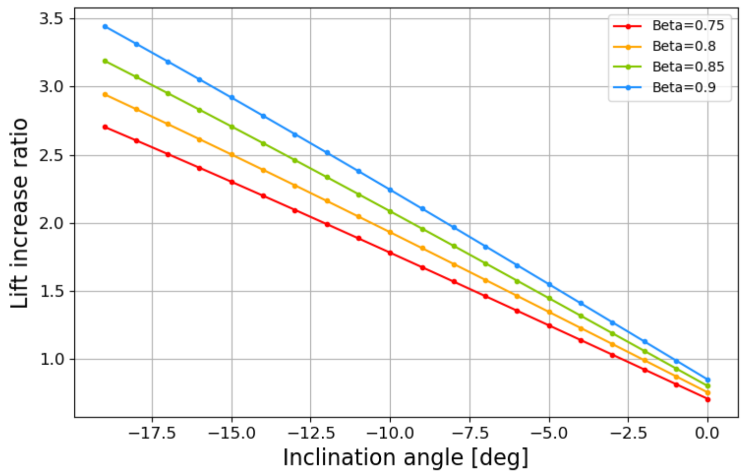

Figure 10.23: Lift ratios for multiple inclination angles of the propeller.

Results

Before the lift ratio results can be interpreted it must first be determined what lift ratio may be required in order to achieve the desired performance of a lift coefficient of 3.0. As the model considers the average effect of the propeller on the lifting performance, it is assumed that only the portion of the wing in the wake of the propeller will experience any change in lift. Additionally, from Figure 10.19, the lifting performance will not be uniform across the entire propeller blade. Finally, in order to account for the tip losses and due to the fact that as explained previously in Equation 10.1.5, not the whole of the blade generated lift, the wingspan here assumed to be positively affected is limited to 75% of the blade radius.
Given the calculated propeller diameter of 2.2m the fraction of the wing span affected by the change in lift is:

$$S_{affected} = \frac{0.75 \cdot 2.2 \cdot 2}{17.5} = 0.19 = 19\% \tag{10.28}$$

Thus, 81% of the wingspan is here assumed to experience a standard lift coefficient of 2.3 as established in subsection 10.2.3.
In order to determine the required lift coefficient in the propeller affected region (x) in order to achieve an effective lift coefficient of 3.0 Equation 10.29 must hold.

$$3.0 = 2.3 \cdot 0.81 + x \cdot 0.19 \tag{10.29}$$

This yields a value of x, the required lift coefficient of the wing in the propeller wake, of 5.02. Given that the airfoil in free stream is expected to generate a lift coefficient of 2.5 this requires a lift ratio of at least 2.0.

The results have been plotted for multiple upstream locations of the propeller in Table 10.23 . As the radius to chord ratio is in this case constant, this corresponds to different values of Beta (β). Important to note is how sharply the lift increases based on the inclination angle of the propeller as originally predicted by Patterson et al.[19].
The results show that a lift ratio of 2.0 may be achievable at relatively low inclination angles for minimal compromise to forward pointing thrust component. Higher ratios resulting in even greater lift coefficients may be also be attainable given a larger inclination angle of the propeller. Of course, due to this inclination, in order to keep the same forward velocity, a slight increase in thrust and additional power will be have to be supplied from the engine. Finally, in order to be able to achieve high β values of over 0.85, these results have also shown the propeller should be placed at least half the wing chord from the leading edge ($\frac{u}{c} = 0.5$).

Verification and Validation
The above analysis is numerically simple. Code verification was done purely by checking a correct implementation of the equation by running values giving certain singularities (such as a division by 0). On the other hand, it makes sense to verify these results against the CL-415 using the following logic. The $C_{l_{max}}$ of the NACA4417 airfoil present on the CL-415 has been determined from X-foil to be 1.3. Applying the same procedure to determine the maximum wing lift coefficient on the CL-415 renders a maximum value of 1.1, considerably less than for the current UAV. Given that the CL-415 also employs simple slotted flaps and that the flapped and slatted area is directly scalable with that of the UAV (60% wetted area for the flaps), this renders an expected maximum lift coefficient of 2.6 for the CL-415 following the exact same design logic presented earlier in this section. Although the effect the CL-415 relies on may be less pronounced, in order to reach its $C_{L_{max}}$ of 2.8, it may still rely on the effect of the propeller. This comparison has addressed the question of whether the above results make sense. True validation of these results may of course only be done with a wind tunnel testing prototype in which the resulting lift coefficient is actually measured.

Result Analysis, Effect of Assumptions and Future Steps
In producing the these results, various sources of error have been introduced, two of which are most significant. The first relates to a complete disregard of the swirl effect in the propeller wake. Despite the model taking into account the overall effect over the entire propeller diameter, in a sense averaging out the two peaks, this may lead to an over prediction of the lift augmentation. The same may be translated into the assumption that the positive effect occurs over 75% of the propeller diameter. In reality, this value may be affected by the both the swirl phenomena as well as the vertical position of the propeller with respect to the wing. In the design, the propeller is slightly elevated due to structural constraints as well as connection to the driveshaft, thus it may be that this again may lead to a a less pronounced effect. Additionally, the assumption of the nacelle providing minimal flow interaction is also debatable. Although it has in the design taken the shape of an airfoil, it may still contribute to aspects such as an increased drag penalty. The inaccuracies introduced will be further discussed in the component risk analysis.

In order to more accurately calculate the affects, in the future it will make sense to consider either a vortex method or thorough full CFD analysis to better model the propeller wing interaction. This may be coupled with an optimisation of the propeller design in order to for example minimise the inclination angle and thus increase the overall performance available from the over the wing configuration. Furthermore, due to the localised increase in lift, it is important to also consider the structural implications this may have on the wing. This however remains subject of the following design iteration.

The above was primarily intended as a complement to the feasibility study presented in this report. Seeing these preliminary results, it has given the team a positive indication that altering the design by placing two propellers on the wing may be highly beneficial to the low speed performance of the aircraft. Finally, the take-off requirement of 500m may even be met as the results show the lifting ratio achieved may be considerably higher than 2.0 provided a higher inclination of the propellers can be achieved without compromising on the required thrust.

10.2.5. Wingbox Design
For the wingbox design, first the wing loading diagrams were made. The first wing loading diagram was based on on the wing without taper and nothing else added on the wing. Then with the wing loading taken from the most extreme case in the flight envelope the wing loading diagram could be made. For this it was assumed that the lift is distributed uniformly over the wing. The assumption was made due to the wing not having any taper or sweep. The result of this assumption is a small overestimation of loads at the wing tips, because normally lift is lost at the wing tips due to tip vortices. The effect this has on the design of the wing is that the wing tips will be slightly over designed and towards the root of the wing probably a slight under estimation of the wing loading is made. The effect is however deemed small enough to

neglect this effect for the design. For the drag the same assumption of a uniform distribution over the wing was made. Lastly a torque diagram was made based on the moment coefficient of the airfoil. Afterwards the propellers were placed on the wing and the effect of these was superpositioned on the already existing load diagrams. The result can be seen in Figure 10.26. The sign convention used is as in Figure 10.25. The origin of the coordinate system is placed at the root chord on the leading edge of the airfoil. Where the positive x-axis is pointing towards the trailing edge of the airfoil, and the y-axis is pointing upwards, and the z-axis finishes the Cartesian right-handed coordinate system. The system used can also be seen in Figure 10.24.

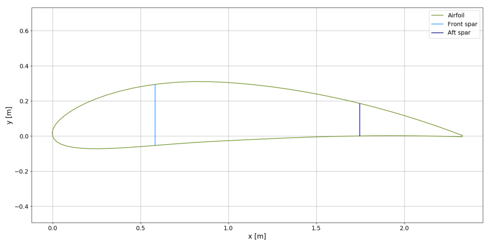

Figure 10.24: Coordinate system used for wing box calculations

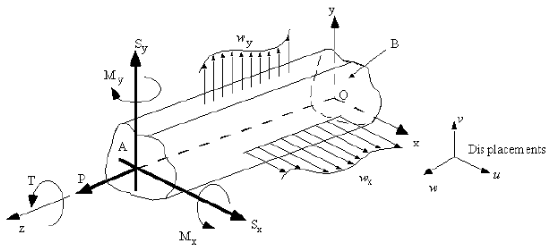

Figure 10.25: Sign convention used as presented in Megson. [30]

Using the coordinate system from Figure 10.24 and the sign convention given in Figure 10.25, the following load cases and corresponding load diagrams visualised in Figure 10.26 could be made. The next step was to define a simple wingbox

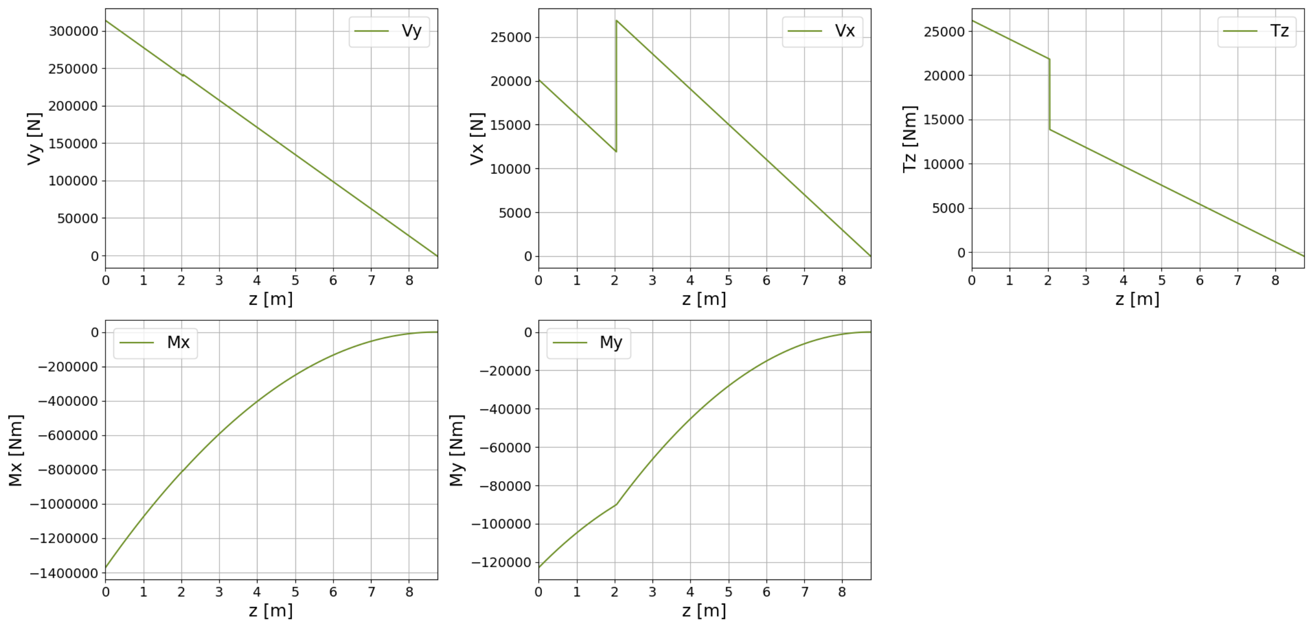

Figure 10.26: Load diagrams for the wing

to get a first estimate of the wing sizing. The decision was made to divide the airfoil into three cells, a cell containing the leading edge, the centre wingbox and the trailing edge. The first step was to determine the location of the spars and the maximum size they could have at that location. The location of the front and aft spar were placed at 25% of the chord and at 75% of the chord, also shown in Figure 10.24, which is in line with the advise given in Raymer[24]. Then the assumption was made that all the load is carried by the centre wingbox, and that the other cells are only there for aerodynamic shape and to put HLDs and control surfaces in. To get a first estimate of the stresses in the wing and the weight of the wing, the calculations were first done for rectangular wingboxes. One wingbox with the height of the biggest spar (the spar placed at quarter chord) and one with the height of the smaller spar (the spar placed at three-quarter chord). Since this is a relatively easy calculation this estimate was also used to verify the code.

Model for wingbox stress calculations
The model that was used for the stress calculations was developed in several steps. The primary inputs it needs are: the

coordinates of the boom locations of the wingbox, the loading on the wing and the dimensions of the wing.
From this starting point, first, the area moments of inertia of the given wingbox are calculated. Using the thin-walled assumption and assuming that any skin between 2 booms is a straight line the centroid of the cross-section can be calculated, and following the centroid, the area moments of inertia can be calculated using Equation 10.30 and the parallel axis theorem, Equation 10.31.

$$I_{xx} = \frac{ta^3 \sin^2\beta}{12} \qquad I_{yy} = \frac{ta^3 \cos^2\beta}{12} \qquad I_{xy} = \frac{ta^3 \sin\beta\cos\beta}{12} \tag{10.30}$$

$$I_{ij}^A = I_{ij}^B + Ac_ic_j \tag{10.31}$$

Where for Equation 10.30, t is the thickness of the skin, a is the length of the piece of skin, β the angle the piece of skin makes with respect to the coordinate system. For Equation 10.31 the i and j are to be substituted for the inertia that is to be calculated, so for I_{xx} both i and j become x, A is the area of the piece of skin and c_i is the distance between the i-centroid of the skin and the i-centroid of the cross-section.
After calculating the moments of inertia of the wingbox the idealisation of the wingbox can be made by calculating the areas that correspond to the booms. This is done according to Equation 10.32

$$B_n = \frac{t_{skin}b}{6}\left(2+\frac{\sigma_{n+1}}{\sigma_n}\right) + \frac{t_{skin}b}{6}\left(2+\frac{\sigma_{n-1}}{\sigma_n}\right) \tag{10.32}$$

Where B_n is the area of the boom to be calculated where n iterates through all booms present in the cross-section. The other variables can be deduced from Table 10.27. The ratio of stresses necessary to calculate the area of the booms is easily calculated in the case that there is a load case consisting out of a pure moment. However due to the fact that the load case consists out of a moment around the x and y-axis the ratio has to be calculated using Equation 10.33, where y and x indicate the location of the point where the stress is calculated and $\bar{y}$ and $\bar{x}$ is the location of the centroid of the cross-section. M_x is the moment around the x axis, and σ_z is the normal-stress in z direction.

$$\sigma_z = \frac{M_xI_{yy} - M_yI_{xy}}{I_{xx}I_{yy} - I_{xy}^2}(y-\bar{y}) + \frac{M_yI_{xx} - M_xI_{xy}}{I_{xx}I_{yy} - I_{xy}^2}(x-\bar{x}) \tag{10.33}$$

After calculating the boom areas it is possible to calculate the shear flows in the skins using Equation 10.34. To do this calculation an imaginary cut is made in the skin and the shear flow is taken as zero at that point. Then going by all booms (we choose a counterclockwise direction, however the direction does not matter) the shear flow of all skins can be calculated.

$$q_s = q_b + q_{s0} = \frac{V_yI_{yy} - V_xI_{xy}}{I_{xx}I_{yy} - I_{xy}^2}\left[\sum_{r=1}^{n} B_r(y-\bar{y})\right] + \frac{V_xI_{xx} - V_yI_{xy}}{I_{xx}I_{yy} - I_{xy}^2}\left[\sum_{r=1}^{n} B_r(x-\bar{x})\right] + q_{s0} \tag{10.34}$$

Finally to close the section the q_{s0} has to be calculated, which is done by taking a moment equilibrium as can be seen in Equation 10.35, where η_0 and $/xi_0$ are the moment arms to the external shear forces, A is the area enclosed by the cross-section, and p is the moment arm to the internal shear flows. If the point the moment is taken around is chosen conveniently η_0 and ξ_0 become 0. For the calculations of the wingbox the point that the aerodynamic forces act through was taken. This was assumed to be at the quarter chord location and at height zero in the coordinate frame of the airfoil.

$$V_x\eta_0 - V_y\xi_0 = \oint pq_b ds + 2Aq_{s0} \tag{10.35}$$

After calculating the shear flow due to the shear forces acting upon the cross-section the shear flows due to the torque can be superimposed on this to obtain the total shear flow. The shear flow due to torque is calculated according to Equation 10.36 where T is the torque acting on the cross-section.

$$q = \frac{T}{2A} \tag{10.36}$$

Now that the shear flow is known the shear stresses in the skins can be calculated according to Equation 10.37. Now that all stresses are known, they are combined using the von mises stress method, as seen in Equation 10.38 and the stress resulting from this is compared to the yield stress of the material to be selected for the wing.

$$\tau = \frac{q}{t} \tag{10.37}$$

$$\sigma_{yield} = \sqrt{\frac{(\sigma_x-\sigma_y)^2+(\sigma_y-\sigma_z)^2+(\sigma_z-\sigma_x)^2+6(\tau_{yz}^2+\tau_{xz}^2+\tau_{xy}^2)}{2}} \tag{10.38}$$

The process described above is what one iteration would look like. To calculate the first estimate of the wing weight the required thickness of the skin was calculated for different positions in the wing. This was done such that the wing can be made lighter since the stress in the wing significantly reduces towards the wing tips. Due to production costs it is not possible to constantly change the thickness to obtain the optimal wing weight. The decision was made to divide the wing up into 9 sections, one in the centre and four on each side. Using the density of aluminium 2024 as discussed in the material selection coming up, the wing weight becomes 9800N.

Verification of the model

To verify the model two things were done, first of all all the functions in the code were unit tested. Next to this an analytic calculation for the non simplified cross-section was done with a simplified load case where there was only one moment acting on the cross-section and only one shear force assumed to go through the shear centre of the cross-section.

$$q_s = q_b + q_{s0} = \frac{V_y I_{yy} - V_x I_{xy}}{I_{xx}I_{yy}-I_{xy}^2}\int_0^s t(y-\bar{y})ds + \frac{V_x I_{xx} - V_y I_{xy}}{I_{xx}I_{yy}-I_{xy}^2}\int_0^s t(x-\bar{x})ds + q_{s0} \tag{10.39}$$

The big difference between the model and analytic solution is the way the shear flow is calculated, for the analytical calculations Equation 10.39 is used. Table 10.5 shows the comparison of stresses for one boom. The biggest difference can be found in the shear stress comparison. The reason for this is the idealisation of the cross-section which was done. This simplification averages out the shear stress for sections of skin, so there are bigger differences in these values, however when in further design the sections between booms get smaller, the shear stresses get more accurate.

Table 10.5: Comparison of the analytical results and the results from the numerical model

	Model	Analytical
Normal Stress (MPa)	174.1	174.4
Shear Stress (MPa)	29.3	26.5
Von Mises Stress (MPa)	181.4	179.9

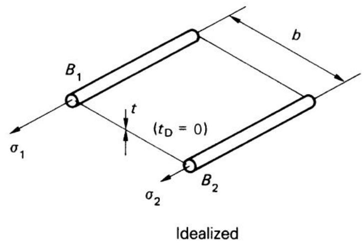

Figure 10.27: Convention of idealising structure into boom and skins as presented in Megson [30].

Next to these tests the calculations were also run for different values to see if the changes made sense, for example that the wing weight would increase with an increase in aspect ratio.

Material choice for the wing

For material selection for the wingbox the main metal that was considered was aluminium. Where the focus was put on the 2xxx and 7xxx series, especially Aluminium 2024 and 7075, commonly used in aerospace products, this can also be found back in literature [31], next to this, when looking through materials in CES Edupack aluminium 2424 was found and selected due to its good performance in terms of fatigue strength. The main characteristics that were looked at for the material choice for the wing were the specific strength of the material, seeing that it is important to keep the OEW as low as possible, as goes almost everywhere in aeronautical engineering. Next to this the cost of the material and the production costs that come along with the type of material should be kept as low as possible. Also the fatigue strength of the material is important, as the mission of the UAV contains a high amount of stress cycles, especially for the wing, due to the drops it does. The last parameters that was looked at was the material's resistance to corrosion, seeing that the aircraft will be operating in and near a lot of (salt) water. The corrosion resistance was however not seen as the most important characteristic of the material, seeing that a lot of protection against corrosion can be done through coatings. The performance of the considered materials can be found in Table 10.6.

Due to the excellent fatigue performance of Aluminium 2424, this would be the first choice for wing material. However after discussion with the tutor, it came to attention that while aluminium 2424 does perform good it is not yet certified for use in aeronautical applications and thus would become too expensive to use. Seeing that the certification process

Table 10.6: Table with material properties taken from CES EduPack 2018

Material	Aluminium 2024-T72	Aluminium 7075-T73	Aluminium 2424-T3
Price [USD/kg]	2.16-2.32	3.98-4.37	2.15-2.31
Specific strength [kNm/kg]	107-127	108-160	96.7-119
Fatigue stength at 10^7 cycles [MPa]	125-147	150-160	190-210
Stress corrosion cracking	Slightly susceptible	Slightly susceptible	Highly susceptible
Maximum service temperature [°C]	170-200	80-100	170-200
CO2 footprint, recycling [kg/kg]	2.49-2.75	2.48-2.74	2.49-2.75

will probably be far outside our budget range. Which leaves us with the standard aerospace aluminium to be used in our aircraft, a combination of aluminium 2024 for the parts of the wing that are mostly in tension, mainly the bottom skin of the wing, and aluminium 7075 for the parts of the wing that are mainly in compression, so for the upper skin of the aircraft and also for the spars.

For the treatment we selected the T7 variant, which means it is solution heat treated and stabilised. This treatment was selected due to its higher stress corrosion cracking resistance, while still maintaining the increase in performance due to the heat treatment.

Since the fatigue performance is an important feature of the wing material and the optimal aluminium is not available, due to it not being certified, also an alternative has been thought of. Should, in later design phases, it become apparent that a better fatigue life is needed out of the wing the aluminium used could be replaced by GLARE, the glass fibre reinforced aluminium laminate also used in the A380. This would come with a significant initial cost increase, but is known to improve fatigue life by a lot. In terms of calculations it can be assumed that it will have the same properties in terms of weight and strength but only performs better in fatigue.

Something that one may think is important but was not considered in the material selection is the maximum service temperature. However it was assumed that the heat would not play as big of a role, seeing that there is a a significant distance between the fire and the aircraft and the strategy of firefighting is about containment of the fire meaning that the temperatures the aircraft experiences will definitely be below the maximum service temperatures of aluminium.

For protection of the aluminium five different coatings are applied to the material, these are the same coatings the CL-415 uses.[17] The coatings consist of an anodising, a dichromate seal, an epoxy primer, a polyurethane topcoat, and a coating of AV-30. Where every layer adds to the corrosion protection of the aluminium.

Fatigue

The fatigue performance of the structure of the wing is very important due to the mission that the UAV is flying. A normal passenger aircraft's wing would normally undergo one big load cycle: Take-off and climb, and the descent and touchdown. This is where Wangari is different. Due to its ability to scoop water, and it doing this up to 70 times per mission Wangari has not one, but 70 major load cycles per flight. To assess the lifetime of the wing, Miner's rule is applied as shown in Equation 10.40.

$$D_t = \frac{n_i}{N_i} \qquad \sum_i^n \frac{n_i}{N_i} = 1 \tag{10.40}$$

Miner's rule is a simple rule of cumulative damage. In this formula D_t is the damage total from one flight, n_i is the amount of occurrences of the load in one flight, N_i is the amount of occurrences it can have until failure, and the sum indicates that when the total reaches 1 that failure will occur. For the calculations it was assumed that every flight 70 times a stress of $147 MPa$ is reached. Which results in having $10e7$ allowable cycles. Calculating when this fraction reaches one results

[17] https://aerialfirefighter.vikingair.com/firefighting/specifications/corrosion-protection [cited 24 June 2019]

in 1.42e5 flights (rounded down to the nearest thousand flights). Then after this due to the method being known for its uncertainty, and the UAV needing to sustain higher loads when necessary a safety factor of 10 is applied leaving the wing with 1.42e4 flights before failure should occur. However seeing that failure is never an option inspection should start earlier already, checking to see if cracks start to form.

10.2.6. Detachability

Since the wing has to be detachable for the UAV to fit inside of the A400m. To achieve this several concepts were thought of, Our first concept was based on the van's RV-12, where the wing is attached to the fuselage by extending the single wing spar through the fuselage for both sides of the wing, and then inside the fuselage the wing spars are locked in place by two pins. The problem with this concept is the different sizing of the wings. The van's RV-12 is a way smaller aircraft which has lower a wing loading compared to the Wangari. This means that the forces acting on the wing of the UAV most likely cannot be transferred effectively to the fuselage by using only one spar. The adaptation to this concept is to extend the complete wingbox instead of only one or two spars. However, after looking through the aircraft hall for other potential solutions the present solution was found. To keep the wing transportable the wing is divided into three parts: the central wingbox which is always connected to the fuselage, and the left and right parts of the wing. The general idea behind the connection can be seen in Table 10.28.. Specific calculations for this part were not performed, but some thought was put into how the part should look, the load paths, and the safety philosophy behind it.

One of the most important things to keep in mind while designing the connection is that the bolts used for assembly and detachment should be accessible such that the wing can be taken off. Several measures have been taken to achieve this. First of all the centre wingbox extends a little bit beyond the fuselage such that the bolts can be accessed both on the upper and lower part of the wing. Next to this cutouts have to be made to have access to to the bolts to fasten and unfasten them.

For the design it is important to think of the failure modes of the connection. General failure modes of bolted connections are: the bolt failing in tension meaning the bolt breaks at the threaded part, there is the case that the bolt fails in shear meaning the bolt breaks in the middle where the two flanges of the connections meet, and then last is failure of the material surrounding the bolt fails due to shear out or the fitting pulling apart due to tension in the plate. For the connection it is important to size it such that it is always the bolts that fail instead of the surrounding material. Seeing that bolts are easy and cheap to replace. In order to transfer the load of the wing to the central wingbox it is important to provide a load path, and seeing that the stringers from the wing cannot be continued a transition will have to be made from a wingbox with skin and stringers to a wingbox consisting solely out of skin and spars such that through the skin the load can be transferred into the bolts and into the centre wingbox. As can be seen if you look carefully at Table 10.28 this is done by increasing the skin thickness in steps such that at the point of connection the skin is thick enough to carry the loads of the wing, and have sufficient strength for the holes needed to put the bolts in such that there will be no shear out. The minimum thickness of the sheet without cutouts can be calculated using the method explained in subsection 10.2.5.

Table 10.7: Wing Characteristics

Characteristic	Value
Surface Area $[m^2]$	40.80
Span $[m]$	17.50
Chord $[m]$	2.330
C_{L_α} $[1/rad]$	4.810
$C_{L_{max}}$	1.448
α_s $[deg]$	11.96
Weight $[N]$	10780

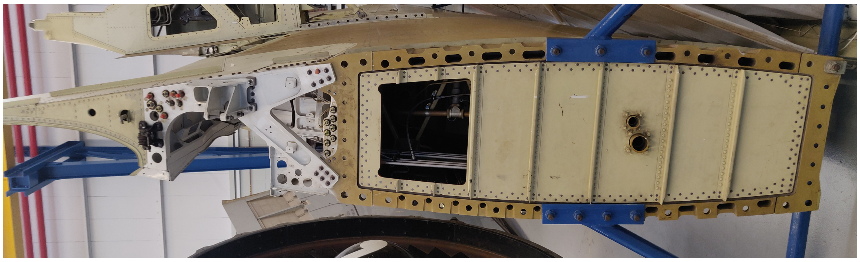

Figure 10.28: Cross-section of the wing of a Fokker VFW-614.

The last part which should be looked at for the detachment of the wings is the added safety. Seeing that the wing is one of, if not the most critical part of any aircraft, we cannot have the wing falling off during flight. Therefore safety factors have to be applied to all components of the wing detachment system. Looking at the failure modes of bolts in [32] and the recommended safety factors on the bolts and surrounding lugs, they range from 25 percent to 150 percent. It is also mentioned that overall it is good design practice to over design the lugs seeing that the increase in weight is relatively small to their importance. This is amplified by the fact that these lugs are literally keeping the wings attached to the aircraft. Therefore, it could be wise to apply a safety factor of at least 2.5 or 150 percent to this part. Next to this the connection should be designed in a fail-safe manner such that a certain amount of the bolts in the connection can fail before complete failure of the wing. This is such that there is ample time to identify failure and should something go wrong the UAV does not lose its wings.

Of course this system has implications on the weight of the wing. Due to the fact that the structure of the wingbox changes from a box with stringers to a wingbox consisting completely out of skin, and because of all the safety factors added. Because the detachment part was not designed in detail it is hard to specifically say what impact it would have on the weight of the wing. However for now it is taken into account by adding 10% of the wing weight adding this safety margin. When adding this safety margin the weight of the wing becomes $10780N$.

Effect of the assumptions and further research
The assumptions that had a big effect on the current results of the structural wing design were the idealised cross-section used and the simplification of the cross-section and this is also where the main opportunities lie for future research and design.

The assumption of having an idealised cross-section averages out the shear flow of the skin between two booms. Since the idealised cross-section for which we did the calculations contains a relatively small amount of booms the shear flow may be severely over- or underestimated. To make sure this becomes an as small as possible influence for now the highest value of shear stress at the booms was used to calculate the Von Mises stresses. This was done to have a conservative estimate of the wing.

The simplified cross-section used for the calculations results in the wingbox having a I_{xx} and a slightly higher I_{yy}. So when sizing the wingbox with the approach that was taken the estimate for the wing weight would be at the lower limit. However, for the actual wingbox a more efficient structure can be designed such that the weight would go more towards this lower limit.

For further recommendations there is a lot to do. One of the first steps would be to do a calculation for a wingbox which is more detailed and also includes stringers and follows the shape of the airfoil. When designing the wingbox with stringers it is also important to take into account the buckling of the skin that is under compression, and also adding ribs to aid the structure of the wing.

The next part that should be looked at in more detail is the connection of the wing to the central wingbox. Here special attention should be paid to the stress concentrations in the cutouts and size the part such that the bolts are the point of failure and that at no point of time there is a failure in the lug. Also the load transfer from the skin to the stringers is a point of attention.

Lastly a recommendation for future upgrades would be to look at the sizing of the wing tip, such that a potential change of the floats becoming floatlets (the combination of a float and a winglet in one) is possible without too big of a design change.

To conclude a summary of the wing design data can be found in Table 10.7.

10.2.7. Sustainability

The main sustainability consideration in the wing is the material choice. Choosing aluminium as material has both its advantages and disadvantages in terms of sustainability. The fact that aluminium is recyclable is a big pro towards sustainability, to put it in numbers: when recycled aluminium 2024 is used the CO_2 footprint per kilogram of aluminium is between $2.49 - 2.75kg$ while for primary production of aluminium 2024 the CO_2 footprint is between $12.4 - 13.7kg$. So huge gains can be made by using recycled material. The downside of using aluminium for the wing is that it is prone to corrosion and the UAV operates in quite a corrosive environment due to the amount of time it spends in (salt)water. Therefore the coatings are applied, which are either bad for the environment, or for the people working with them. However the difference in lifetime that these coatings make is a worthwhile trade-off even in sustainability seeing that less wings have to be produced.

Next to the sustainability in material choice also the propellers on the wing were sized with sustainability in mind. Large propellers were selected because per propeller larger propellers are more efficient than smaller ones. The downside of the propellers chosen is that they do make quite some noise. This could be seen as unsustainable, however for the design perspective of Wangari, Wangari is seen as an emergency vehicle and the performance of the firefighting should be prioritised over the noise it makes. Next to this, the mission of Wangari is fighting wildfires and it will therefore not fly over too many densely populated areas, of course this is partly dependant on the airstrip it operates from.

10.2.8. Risks

A primary risk from the aerodynamic wing design stems predominantly from the uncertainties related to the propeller wing interaction. These risks have been addressed in the analysis through the use of conservative estimates. Nevertheless, a better mitigation strategy consists in as mentioned before, eventual testing of a scale model in order to better study the aerodynamic effects in order to ascertain and eventually also optimise the design. Additionally, the results for the high lift devices have shown that with triple slotted flaps alone, a maximum lift coefficient of over 3.0 may be achievable without using the effect of the propeller. Hence, in case testing shows that the propeller interaction does not provide enough benefit, the possibility always remains of fitting the wing with enhanced slats in order to achieve the desired performance.

The risk for the structural wing design lies in the fact that there are still a lot of calculations to be done. Most calculations were, due to time constraints, done as first estimates, and for the detachment of the wing pretty much no calculations have been done, although the design was based of existing aircraft. The mitigation strategy for this is mainly in the further design of the aircraft where more attention has to be put into the engineering of the structures of the aircraft.
The other risk introduced by the structural design of the wing is that the connection to the most critical component of the aircraft has been made more error prone. Meaning that to prevent the risk of something going wrong in the connection of the wing extra safety factors should be added as mentioned in subsection 10.2.6 and extra attention should be paid to the inspection of the connection and to the correct assembly and disassembly of the wing.

10.3. Hull

The design of the fuselage of an amphibious aircraft is greatly determined by its hydrodynamic characteristics, and therefore often referred to as a hull. In Figure 10.29, key parameters of the hull are illustrated.

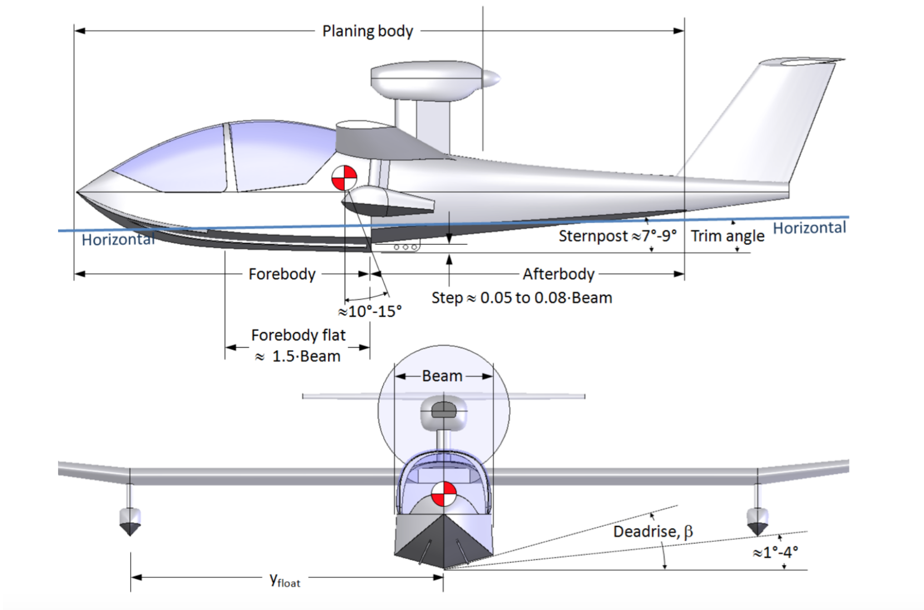

Figure 10.29: Geometric parameters of seaplane design. [33]

10.3.1. Buoyancy

The most important part of the hydrodynamic design has been keeping the UAV afloat. The principles of floating have long been established by Archimedes of Syracuse. His principle states that any object, whether fully or partially submerged in a fluid, experiences an upward buoyant force equal to the weight of the fluid that the object displaces.[18] Using the principle, the buoyant force and submerged volume needed for Wangari to float can be calculated using Equation 10.41.

$$F_{net} \geq F_W - F_{buoy} = mg - \rho_w g \nabla \tag{10.41}$$

In which F_{net} is the floating tendency, if it's smaller than zero the UAV will sink if equal or greater it will float; F_W the weight of the UAV; F_{buoy} the exerted buoyancy force; m, the mass of the UAV; g, the gravitational constant; ρ_w, the density of water and ∇, the submerged volume.

For safety, especially during landing when high impact loading is common, the following requirement is set.

AAF-PERF-COLL-06 The UAV shall have a buoyancy of 1.8· MTOW$_{water}$.

Additionally, the UAV is compartmentalised such that in case of leakage the remaining compartments, auxiliary floats and tires are able to keep it from sinking. As calculating the exact submerged volume of a hull design by hand is very time-consuming, the volume and centre of buoyancy have been monitored using MAXSURF[19] throughout the entire design process.

Normally, in amphibious design, one would start with the determination of the beam width. However, in the design process of Wangari a much more constraining factor was placed on the length of the UAV rather than the width, namely:

AF-TRNS-01 Two UAVs shall be able to fit in an A400M.

Therefore, in the specific design of the Wangari, the length has been taken as starting point, which at the initial design stage was set to equal 9 metres. Using this value, the slenderness ratio of the UAV has been determined. According to literature [33], the slenderness ratio is usually between 5 to 9. A higher ratio will lead to lower aerodynamic and hydrodynamic drag but will at the same time increase water spray during high speed operations. Moreover, a high slenderness ratio will lead to hydrostatic instability and a higher hull weight due to high beam loading. Finally, a ratio of 6 has been chosen, leading to a beam width of 1.5 metres. The beam loading coefficient can then be calculated using equation Equation 10.42,

$$C_\Delta = \frac{\Delta}{g \rho_w B^3} \tag{10.42}$$

in which Δ is the displaced mass, equal to F_buoy, and B, the beam width. According to Wood[34], a desirable range of C_Δ at MTOW$_{\text{water}}$ is between 1 and 2. Having a C_Δ of 1.78, the design of Wangari satisfies this design rule.

10.3.2. Hydrostatic Stability

The lateral or transverse stability of a seaplane is hugely dependent on the configuration chosen. In the early stages of the design, it was already decided that Wangari would be a flying boat. As a flying boat has advantages over a float plane with regards to aerial drag, take-off performance and transportation. This means, however, that stability must be obtained by a single hull instead of two floats.

In the lateral or transverse direction the stability is determined by the distances between the centre of gravity, the centre of buoyancy and the metacentre, as visualised in Figure 10.30. If the metacentre is coincides with the centre of gravity, the UAV is neutrally stable. If the centre of gravity is below the metacentre, the UAV is stable, and if the centre of gravity is above the metacentre the UAV is unstable.[36]

The metacentric height, GM, can then be calculated using Equation 10.43[35].

$$\begin{aligned} BM &= \frac{I}{\nabla} \\ GM &= BM - BG \end{aligned} \tag{10.43}$$

In which I, is the second area moment of the submerged body about the vertical axis, BM, the distance between the centre of buoyancy and the metacentre, and BG, the distance between the centre of buoyancy and the centre of gravity.

[18] `https://www.britannica.com/science/Archimedes-principle` [cited 20 June 2019]
[19] Commercial Integrated Naval Architecture Software by Bentley Systems, Incorporated, ©2016

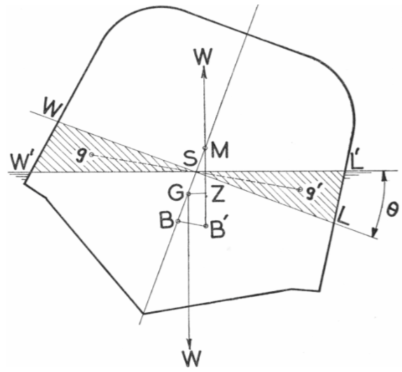

Figure 10.30: Transverse stability visualisation, G is the centre of gravity, B, the centre of buoyancy, and M, the transverse metacentre.[35]

Using MAXSURF[19], the centre of buoyancy and the distance between the metacentre and the centre of buoyancy were found such that stability could be established for small angles of keel of the UAV. Due to the inherently high c.g. location of amphibious aircraft, the lateral stability of the UAV becomes impaired when keeling (rolling) more than 8°. In that case the craft must ensure its lateral stability through auxiliary means. This can be done using stubs or (retractable) tip floats. Stubs generate, however, more aero- and hydrodynamic drag and are heavier as they need to withstand some of the impact landing load[37]. As tip floats would still increase the aerodynamic drag and could lead to dangerous situations under landing impact loads, in the design of Wangari retractable tip floats are chosen.

The volume of each of the tip floats is determined by requiring it to be able to give a restoring moment, RM, of 1.5 times that generated by the keeling mass, when keeling 7° as given in Equation 10.44[36].

$$RM = \Delta GMsin(\theta) \tag{10.44}$$

The restoring moment of the float is given by the force of buoyancy of the entirely submerged tip float at a distance y_{lat} from the centre of gravity. Hence, the float volume can be sized using Equation 10.45. In the case of Wangari, this leads to a tip float volume of $1.35m^3$ and a weight of $50kg$.

$$\nabla = \frac{1.5RM}{y_{lat}} \tag{10.45}$$

In longitudinal direction, a hull on water is always statically stable, according to Pinkster and Bom [38]. However, during the planing phase, in which the forebody rises out of the water, the UAV can become unstable and start porpoising. In

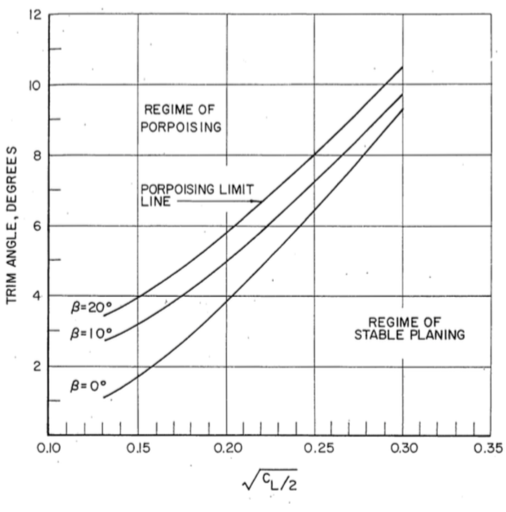

Figure 10.31: Limits for stable porpoising.[39]

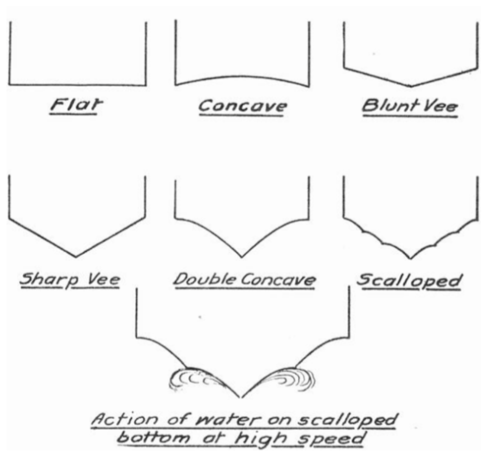

Figure 10.32: The chosen scalloped hull bottom and other existing design options.[36]

Figure 10.31, it can be seen that, in general, a higher deadrise angle decreases the risk of porpoising. To further reduce the risk of becoming dynamically unstable during the planing phase, the forebody of Wangari is kept flat for 1.5·Beam from the step. This reduces the porpoising tendency as the flat plate ensures a more uniform bottom pressure, whereas a curved bottom would result in a varying pressure and lead to a more dynamic response [33]. The flat plate also generates lift and effectively raises the hull out of the water, thereby reducing hydrodynamic drag and shortening the take-off time. Furthermore, the deadrise angle is slightly increased at the forebody as this enables a more favourable trim angle, such that better lift-over-drag ratios can be achieved, whilst staying in the stable planing regime [39].

10.3.3. Spray

Another risk that was identified early on in the design process is the risk of spray hitting the propellers and control surfaces on the wing. To assess the severity of the risk, first, the spray height is determined. This is done using Equation 10.46 [40].

$$z = k_1 \cdot B \frac{C_\Delta^{2/3}}{\frac{l_f}{B}} \tag{10.46}$$

In which, z is the vertical spray height at the point of tangency measured tangent to the keel at the step, k_1 is a constant equal to 2.1, and l_f the length of the forebody. To mitigate the risk of spray, the curvature of the hull between keel and chine of the forebody is flared and warped, also called scalloped, effectively rolling down the water spray as visualised in Figure 10.32. This may reduce the spray height by 21% [41]. Furthermore, on the forebody chine, spray rails have been attached. According to Chicken [37], these spray strips are able to reduce the spray height by another 10%. Chicken based his data, however, on photos from towing tank tests performed in the 1920s, hence, this must be properly validated.

10.3.4. Hull Geometry

The hull of an amphibious aircraft is shaped different than that of a land-based aircraft as it not only has to withstand aerodynamic forces but also hydrodynamic forces. To reduce the hydrodynamic drag several measures are taken, greatly affecting the shape of the hull.

First of all, a step is added, separating the fore- and afterbody of the UAV. Doing this results in the formation of an air pocket behind the step. When increasing the speed, the air will extend out of the pocket towards the stern effectively raising the afterbody out of the water. Thence, less hydrodynamic resistance is experienced. The step, however, adds an aerodynamic drag penalty to the design. The optimal step depth lies therefore between 6 – 10% of the beam [42]. In the Wangari design is chosen for a depth of 8%. The location of the step is also of importance as the step will influence the centre of buoyancy, which during the displacement phase must lie close to the centre of gravity for longitudinal stability, and centre of pressure which must be close to the centre of gravity in the planing phase. Based on the recommendations by Deihl [43] and Gudmundsson [33], the step is positioned at 18° behind the centre of gravity.

Furthermore, the afterbody of the UAV is tapered conform a planing tail design. This configuration is both simpler to manufacture and generates less hydrodynamic drag. The angle at which the afterbody is tapered is called the sternpost angle, σ. Due to this angle, the rear fuselage uplifts earlier such that the transition to planing phase can be reached. Moreover, the sternpost angle reduces the tendency of the UAV to skip on the water during landing [44]. If the angle is set too high, however, the design will generate a large amount of aerodynamic drag. Furthermore, at high sternpost angles less buoyancy will be available, causing the draft and, thus, the hydrodynamic drag to increase. Based on Thurston [45], a sternpost angle of 7° has been set in the design of Wangari.

Finally, the angle of deadrise has been determined. This is important as it influences the ability of the UAV to take off and land on water as well as its stability. A lower deadrise angle allows for quicker take-off as it enhances the planing abilities of the forebody. Moreover, the draft of the UAV will be lowered, reducing the hydrodynamic drag. A higher deadrise angle, on the other hand, allows the UAV to cut through waves easier, deflect spray and very favourably reduces the impact loads during landing. Raymer has, therefore, set Equation 10.47 as guideline for the deadrise angle.

$$\beta \approx \frac{V_s - 8.94}{2} \tag{10.47}$$

In which β is the deadrise angle in degrees, and V_s, the stall speed in $knots$. For Wangari, which has a stall speed of $35.5 m/s$, this would lead to a deadrise angle of 29.7°. To keep the draft at a reasonable level, a deadrise angle of 25° has been selected.

10.3.5. Hull Structure

To be able to stay afloat, the structure of the hull itself must be analysed. The most impactful requirements for the structural hull design are found to be the following:

AF-PERF-TO-01	The UAV shall be able to take off from water.
AF-PERF-LND-04	The UAV shall be able to land on water.

To interpret the impact, the forces acting on the UAV during landing have been analysed as this is the most extreme loading condition of the two. This has been done so under the assumption of zero water payload and from a hydrostatics perspective only.

The reaction force at landing originates from the change of momentum of the water due to the change of velocity of the hull. Besides this impact force, the buoyancy force generates a reaction force. However, this force is in negligible in comparison to the impact force and can hence be neglected [46]. The momentum change is given in Equation 10.48,

$$M = \frac{W}{g} v_{dw} + \frac{1}{2} x^2 \rho_w \pi v = \frac{W}{g} v_0 \tag{10.48}$$

in which M is the momentum, v_{dw} the downward velocity, x, the local beam width, and v_0, the landing speed equalling $1.1 v_{stall}$. The impact momentum is then rewritten to obtain the force of impact, using Equation 10.49 and Equation 10.50.

$$\frac{W}{g} v_{dw}(1 + \frac{\rho_w \pi g x^2}{2W}) = \frac{W}{g} v_0, \qquad \frac{dx}{dt}(1 + \frac{\rho_w \pi g x^2}{2W}) = v_0 cot\beta, \qquad \frac{d^2 x}{dt^2} = \frac{v_0^2 cot^2 \beta}{(1 + \frac{\rho_w \pi g x^2}{2W})^3}(-\frac{\rho_w \pi g x}{W}) \tag{10.49}$$

$$F_{impact} = \frac{W}{g}\frac{d^2 y}{dt^2} = \frac{v_0^2 cot\beta \rho_w \pi x}{(1 + \frac{\rho_w \pi g x^2}{2W})^3} \tag{10.50}$$

According to general aviation regulations[20], a load factor must be placed on the impact force. These differ per location on the hull. As at this stage of the design the radius of gyration and moment of inertia of the total aircraft are unknown, only the loading at the step is considered. This is also the most important condition as (remote) pilots aim to land their amphibian at this location. The load factor at the step is determined using Equation 10.51,

$$n_{sl} = \frac{C_1 V_s^2}{tan\beta^{1/3} W_l} \tag{10.51}$$

in which n_{sl} is the load factor, C_1, a constant equalling 0.012 and W_l, the impact landing weight which can be assumed to equal 1/3 of the maximum landing weight[20].

In the stress analysis of the hull, the hull has been modelled as a sandwich structure. This has been done because a sandwich structure is safer in water operations as it provides an extra barrier against leakage. Moreover, a sandwich structure does not require stringers which would reduce the space available for the internal components.

The stresses on the hull structure have then been calculated by simplifying the hull using boom discretion as visible in Figure 10.33, potential holes for the landing gear and screens for camera vision. In this, only the plates are assumed to withstand the load, the core of Nomex will add additional strength. The stresses in the skin have been calculated using a similar method as in the wing. However, the coordinate system is now centred at boom 1 at the most aft step position.

An additional requirement was set on the seaworthiness of the UAV, namely:

AF-PERF-COLL-05	The UAV shall be able to land on waters with wave heights up to 25cm.

Based on Roskam[47], Wangari is found to be able to safely operate on waters with these wave height. This also reduces the risk of the water being too rough for scooping. As the hull is designed to withstand waves with a height of $1.0m$, the UAV should be able to scoop in rough water conditions on a lake. For rough open water operations the risk must be further analysed.

[20] `https://www.easa.europa.eu/sites/default/files/dfu/CS-23%20Initial%20issue.pdf` [cited 22 June 2019]

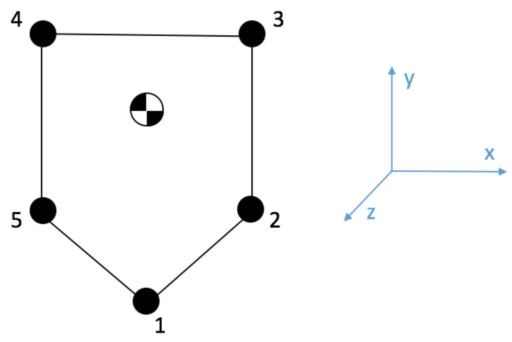

Figure 10.33: Boom idealisation of the hull.

10.3.6. Hull Materials

The hull of the UAV is during its mission often in direct contact with (salt) water. Therefore, the anti-corrosion resistance of the selected material must be excellent. Furthermore, one should take the manufacturability and sustainability into account. The deadrise angle, keel curvature, step and flared chines make the design namely hard to manufacture. Based on the corrosion resistance and manufacturability, composites seem to be a better choice than the arguably more sustainable metals.

For the resin of the composites, three options are commonly used in amphibian and naval hull design; epoxy, vinyl and polyester. Of those vinyl is the strongest, however, vinyl is also the most water absorbent [48]. Therefore, it is chosen to make the design of the Wangari, using the slightly less strong, yet less water absorbent and expensive epoxy. For the fibres, two options were considered; carbon and glass-S fibre. Their characteristics, when in an epoxy matrix, are given in Table 10.8[21].

Table 10.8: Characteristics of the considered composites.[21]

	Carbon Fibre-Epoxy	**Glass Fibre-Epoxy**
Density [kg/m^3]	$1.61\cdot10^3$	$2.0\cdot10^3$
Cost [€/kg]	83.6	22.2
Young's Modulus [Gpa]	50.7	31
Shear Modulus [Gpa]	19.5	11
(Salt) Water Resistance	Excellent	Excellent
CO_2 Footprint [kg/kg]	50.5	5.96
Manufacturability	Acceptable	Good

Due to its ease of manufacturability, cheap cost and low CO_2-emissions, it is chosen to use a glass fibre-epoxy composite for the sandwich structure of the hull. On top of the composite sandwich structure an additional layer of aramid fibre is added to minimise the risk of leakage due to small impacts from, for example, floating objects during water operations [49]. To minimise the established risk of corrosion of the aircraft structures, additional coatings, based on the CL-415 design, are added against (salt)water and alkali: an epoxy primer, a polyurethane topcoat and AV-30.

10.3.7. Hull Design Analysis and Future Steps

In the design for hydrodynamics and stability of the hull, many parameters are dependent on the total weight of the UAV and the location of its centre of gravity. If the c.g. is shifted forwards, the step and centre of buoyancy will also shift forwards. This will result in a higher blister spray height, which can be hazardous to the propeller design, and deeper draft and thus an increase in hydrodynamic drag. An upwards shift of the c.g. could be even more problematic as the lateral stability could be impaired resulting in an unsafe design and increase in tip float size and thus total UAV weight.

[21] Obtained from the commercial CES Edupack software by Granta.

The key parameters of the design of the hull of Wangari have been verified with existing amphibious designs. Those designs were picked based on them having either the same weight class or mission. Overall, the design of Wangari is found to be within the ranges of the existing design. The tip float are slightly larger than the average of the existing designs, which can be explained by the large righting moment required.

Table 10.9: Comparison of existing hull data and those of Wangari.

	MTOW [kg]	**l/b** [-]	β [°]	σ [°]	C_Δ [-]	**Tip Float** [m^3]
Weight Class						
Albatross	12270	6.26	14	6	0.83	-
BV-138	11900	6.27	11	8	0.73	1.24
Finmark	5950	4.93	22	8	0.84	-
Sealand	4128	6.54	25	5	1.06	0.28
Average	8562	6	18	6.75	0.865	0.76
Mission Class						
BE-200	36000	11.98	24	7	2.57	1.29
CL-215	19278	7.54	17	7	1.11	1.09
Average	27639	9.76	20.5	7	1.84	1.19
Wangari	9000	6	25	7	1.78	1.35

In the structural analysis, simplifications of both the hull structure and loading are made to be able to analyse the stresses on the hull. The numerical calculations are verified by performing analytical calculations. However, in future research the exact effect of these simplifications should be further analysed. Furthermore, as at this stage of the design process no values for the radius of gyration and moment of inertia of the entire UAV could be determined, only the static loading for the step landing has been determined. Thence, evaluation of the stresses at bow and stern landing should be analysed in future research, whereby the stress induced by the hydrodynamic drag should also be analysed. To be able to evaluate the hydrodynamic and aerodynamic drag in landing and take-off conditions as well as general displacement on water, towing tank tests should be performed. Finally, the mechanism of the retractable tip floats, which is currently assumed to work like the PBY Catalina mechanism, should be investigated further.

The main risks in the hull design identified before this design iteration consisted of leakage of the hull, hydrodynamic instability and spray. The risk of leakage of the hull has been mitigated by introducing a composite sandwich structure and additional aramid layer against impact. Furthermore, the fuselage has been compartmentalised, such that in the case of leakage, the remaining compartments are able to keep the UAV afloat. The risks of hydrodynamic instability has been reduced by adding a deadrise angle to the hull design and keeping the forebody flat for 1.5·Beam. The risk of spray is also reduced by the introduction of deadrise to the design. Furthermore, the bottom is scalloped to force a downwards roll of the water against the hull, and spray rails are added to the forebody. During the hull design, a new risk became apparent as the performed calculations are based on literature used in existing flying boat designs. This literature, however, stems from the first half of the 20^{th} Century, when the flying boat was still a popular design, and might be outdated.

The main sustainable decisions in the hull design are made in the selection of a glass fibre-epoxy composite as material. The production of which induces significantly less CO_2 emissions than carbon-fibre composites or metals. Also, by doing so, no dichromate seal is needed, which is toxic to the environment. Furthermore, the choice of glass fibre-epoxy resulted in a lighter design than would be obtained using metal, which in turn reduces (hydrodynamic) drag and thus weight.

10.4. Empennage

10.4.1. C.G. Range

The centre of gravity is in terms of aircraft design one of the most important parameters to calculate and keep track of, since its value influences virtually all other parameters of the design. The task of calculating, keeping track of, and updating other departments on the c.g. location rested upon the shoulders of the C&S department, since for C&S the c.g. location is the single most important parameter.

Process

The c.g. on the x and z axis can be determined very straightforwardly once all component weights and positions are known, using Equation 10.52. It is assumed that because of symmetry the c.g. is at $y = 0$ on the y-axis.

$$(\bar{x}_{cg}, \bar{z}_{cg}) = (\frac{\sum \bar{x}_i \cdot w_i}{\sum w_i}, \frac{\sum \bar{z}_i \cdot w_i}{\sum w_i}) \tag{10.52}$$

In Equation 10.52, the bar indicates a coordinate normalised by the mean aerodynamic chord (MAC). Initially very rough component weight estimates were used, but as the design progressed the estimated weights started to converge, and therefore the c.g. The required range of the c.g. was very restricted, since every department had very specific needs for the c.g. position. The Hydrodynamics department required the c.g. to be as far in front as possible for floating ability, while for the aerial stability, the C&S department needed the c.g. to be close to the aerodynamic centre. This required a continuous iterative process, since all component weights would depends on the c.g. position as-well as other parameters.

For the frozen design, the c.g. extremes are located at:

Table 10.10: C.G. locations. X-coordinate is measured from the nose, Z-coordinate is measured from the centreline of the fuselage

Type	**X-Coordinate [m]**	**Z-Coordinate [m]**
Forward	3.287	0.71
Aft	3.294	0.08

As can be seen from Table 10.10, the c.g. has a maximum shift in x-direction of $7mm$. This is extremely low, and very beneficial for the stability of the aircraft during its missions. Since the aircraft will have to collect and drop water continuously, not having a large shift in c.g. will allow for smaller longitudinal stabilising surfaces, such as the horizontal tail surface.[50] Also there won't be the need to implement extensive control loop systems for the stabilisation of the aircraft, as it will be stable and controllable by nature, no matter the loading configuration, as will be further explained in subsection 10.4.2.

Sensitivity c.g. range
The c.g. range is managed to keep within a small horizontal distance of $7mm$. This seems very sensitive, as a component shift would immediately be able to change this to an order of magnitude. However, this is easily countered by shifting another component, and by this again achieving this small horizontal c.g. range. The vertical c.g. range is already significant (almost $0.7m$ for a fuselage with a height of $2.5m$), and this is caused by having a high wing configuration, together with having the c.g. of the water tank in the lower part of the fuselage. This could be made even bigger by moving the c.g. of the water tank down, or having more components at the upper side of the fuselage. This is thus relatively sensitive.

10.4.2. Horizontal Tail Sizing

Longitudinal stability is one of the most important factors when designing an aircraft, if complex control loop systems for stabilisation are not desired. Longitudinal stability is mainly achieved through placement of a horizontal stabiliser. The conventional way is to put this at the tail, but canard configurations can also be used. Even though the canard configuration was removed from the concept selection, it was reconsidered due to the possibility of being able to save weight. And thus, a combination of the horizontal tail and the canard was also considered as a design option.

The main complication with the design was the fact that the c.g. is located very far forward, which is beneficial in terms of tail moment arm, and detrimental for the canard moment arm. This meant that the aircraft with only a canard could not satisfy the stability and controllability requirements without having a unnecessarily large surface area. With regards to the dual configuration (both a canard and tail wing), the same problem applied for the canard and no gains were made in terms of weight reduction, and therefore it was concluded a single horizontal tail plane configuration was the most suitable option.

For the horizontal tail sizing there was no specific requirement set. However, a general desire was present to design an inherently stable aircraft, as this is safer than an unstable system and does not require complex control loop systems, as stated above. It is proven unstable aircraft can fly, as seen in the F-16 Fighting Falcon. However, instability would mean having a lot of redundant systems, with this increasing complexity and weight of the UAV. So, a desire for a stable UAV is present, and is also achieved by sizing the horizontal tail surface for this.

Process
The horizontal tail surface needs to generate moments around the aircraft's c.g. such that the aircraft is, without human interference, stable, while still offering the ability for the pilot to change the attitude of the aircraft. To make an aircraft stable, the horizontal tail needs to be able return to the UAV equilibrium position after a disturbance. To make an aircraft controllable, the horizontal stabiliser needs to be able to generate enough lift to make the aircraft change pitch at the remote pilot's desire, and the aircraft needs to be able to be trimmed.[50]

For both the stability and controllability, a set of equations had to be derived. Since the UAV is an amphibious aircraft, the stability and controllability while while scooping up water, landing, and taking off on and from water, is essential. For the amphibious Stability & Controllability, a simplified analysis is made, to get a estimate for the tail sizing. The various assumptions made for this can be found in **'Assumptions'** below. A more accurate analysis should follow in later stages of the design. During scooping, only the scooping mechanism is in contact with the water. The effect of this mechanism on the Stability & Controllability was also investigated, but as described in **'Scooping stability and control'** below, this effect can be neglected. Two sets of equations for both controllability and stability were derived:

- Aerial Stability & Controllability
- Amphibious Stability & Controllability

All assumptions for the derivations are listed below, and the derivations themselves are explained in the subsequent paragraphs.

Assumptions
All assumptions, their consequence, and their justification are listed below:

1. **ISA Conditions** $\implies \rho = 1.225 \iff$ Due to the nature of the UAV's missions (low speed, low altitude) this simplification can be made.
2. **Negligible Drag Contributions** $\implies C_D = 0 \iff$ Since the drag components are much smaller in magnitude than the lift components and have a much smaller moment arm with the c.g., a.c. and n.p., their contribution can be considered negligible.
3. **Buoyancy Component Negligible** $\implies C_B = 0 \iff$ During scooping, the aircraft will barely have any volume submerged in the water and will therefore experience negligible buoyancy. The buoyancy during take-off and landing will be overshadowed by the aerodynamic lift soon after the aircraft starts the manoeuvre and will therefore not be considered in the equation. Stability on water while stationary is guaranteed as long as the centre of buoyancy is situated directly under the centre of gravity, as seen in subsection 10.3.2.
4. **Centre of Buoyancy remains constant** $\implies (x,z)_{cb} = \text{const.} \iff$ It is out of the scope of the hydrodynamics department to, in this stage of the design, come up with a model to describe the shift of the centre of buoyancy with angle of attack and will therefore be assumed constant.
5. **Thrust has no inclination** $\implies i_p = 0° \iff$ The angle between the centerline of the fuselage and the direction of the thrust, even if present, will not be large and therefore the small angle approximation may be used.
6. **Propeller wake speeds up the air behind itself** $\implies \frac{V_h}{V} \approx 1.3 \iff$ The horizontal tail-plane, which is in the wake of the propeller, will experience an air velocity of about 1.3 times more than the main wing experiences due to the nature of the propeller accelerating air to the back to gain momentum forward.
7. **Aerodynamic Moment of horizontal tail is negligible** $\implies C_{m,ac_h} \lll C_{m,ac_{A-h}} \iff$ The horizontal tail-plane is much smaller and will generate a smaller moment around its aerodynamic centre and will therefore be neglected.
8. **Full Moving Tail** $\implies C_{L_h} = -1 \iff$ Due to the size constraints of the tail, the area of the tail is constrained. Therefore, to get the smallest possible tail area, a lift coefficient of larger magnitude is required to have the controllability required.

Aerial stability and control
For the derivation of Equation 10.57 and Equation 10.58, consider the free-body diagram in Figure 10.34. For this derivation, we will only be considering the contribution of the aerodynamic- and thrust components, not the water buoyancy- and resistance forces. As stated in the assumptions, the drag will be neglected. Furthermore, it is assumed that thrust does not change with angle of attack.

Let us start with the equation for aerial stability. The definition of the neutral point is that in the neutral point, the aerodynamic moment coefficient of the aircraft does not change with angle of attack. When the angle of attack is increased ever

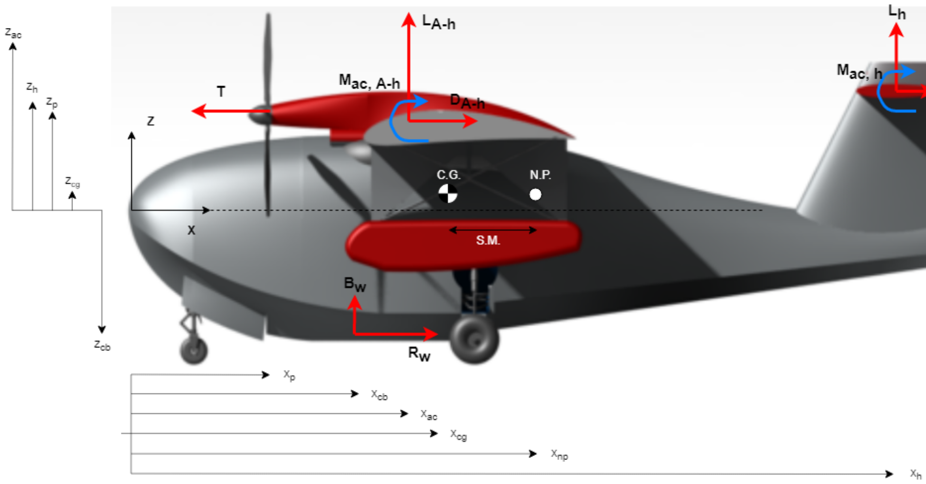

Figure 10.34: Free-Body Diagram used for horizontal tail sizing equations

so slightly with $\Delta\alpha$, the lift and drag on the wing and horizontal tail plane will increase as well. Therefore, in the neutral point, the larger moment generated by the lift in the tail should be cancelled by the larger moment created by the wing. Equation 10.53 is normalised by $\frac{1}{2}\rho V^2 Sc$ to obtain Equation 10.54. The $\frac{S_h}{S}$ term is solved for to obtain Equation 10.57. This is the minimum required tail surface area to be stable, as function of $\bar{x}_{cg}$.

$$\sum \Delta M_{np} : 0 = \Delta L_{A-h}(x_{np} - x_{ac}) + \Delta L_h(x_{np} - x_h) \tag{10.53}$$

$$\therefore 0 = C_{L_{\alpha_{A-h}}}(\bar{x}_{np} - \bar{x}_{ac}) + C_{L_{\alpha_h}}(1 - \frac{d\epsilon}{d\alpha})\frac{S_h}{S}(\frac{V_h}{V})^2(\bar{x}_{np} - \bar{x}_h) \tag{10.54}$$

The equation for controllability is derived in a similar manner, however the control curve is not obtained using a change in angle of attack, but by assuming landing- or loiter conditions, and performing a sum of moments around the aerodynamic centre. See Equation 10.55. The terms are from Figure 10.34. Normalising all terms by dividing by $\frac{1}{2}\rho V^2 Sc$, (Equation 10.56) and isolating the $\frac{S_h}{S}$ term (the size of the horizontal stabiliser with respect to the main wing surface), the minimum surface area required to be able to pitch up or down, can be calculated. The equation describing this requirement is Equation 10.58. Here is $\bar{SM}$ the safety margin, $\frac{d\epsilon}{d\alpha}$ the wing downwash and S the size of the main wing.

$$\sum M_{ac} : 0 = M_{ac_{A-h}} + L_{A-h}(x_{cg} - x_{ac}) - L_h(x_h - x_{ac}) \tag{10.55}$$

$$\therefore 0 = C_{m_{ac}} + C_{L_{A-h}}(\bar{x}_{cg} - \bar{x}_{ac}) - C_{L_h}\frac{S_h}{S}(\frac{V_h}{V})^2(\bar{x}_h - \bar{x}_{ac}) \tag{10.56}$$

$$\left(\frac{S_h}{S}\right)_{\text{stability}} = \left(\frac{S_h}{S}\right)_{\text{stability,aerial}} = \frac{\bar{x}_{cg} + \bar{SM} - \bar{x}_{ac}}{\left(1 - \frac{d\epsilon}{d\alpha}\right)\left(\frac{V_h}{V}\right)^2 \frac{C_{L\alpha_h}}{C_{L\alpha_{(A-h)}}}\left(\bar{z}_h - \bar{z}_{cg}\right)} \tag{10.57}$$

$$\left(\frac{S_h}{S}\right)_{\text{control}} = \left(\frac{S_h}{S}\right)_{\text{control,aerial}} = \frac{\bar{x}_{cg} + \left(\frac{C_{m_{ac}}}{C_{L_{A-h}}} - \bar{x}_{ac}\right) - \frac{T_c}{C_{L_{A-h}}}\frac{2D^2_{prop}}{S}\left(\bar{z}_p - \bar{z}_{ac}\right)}{\frac{C_{L_h}}{C_{L_{A-h}}}\left(\frac{V_h}{V}\right)^2\left(\bar{x}_h - \bar{x}_{ac}\right)} \tag{10.58}$$

The graphs, as functions of the normalised c.g. location along the x-axis, are shown in Figure 10.35. For the aircraft to be stable in the air, the value for $\frac{S_h}{S}$ must at all times lie above the aerial stability curve. To be controllable in the air, the value for $\frac{S_h}{S}$ must be above the control curve at all times. The range of c.g. locations as calculated using Equation 10.52 are shown in the same plot to indicate what values for the c.g. can be expected for the UAV. In this manner, the required values for $\frac{S_h}{S}$ can be read from the graph in Figure 10.35. The lower lines are indicating the aerial control and stability curves, as indicated in the Figure. It can be seen that a value of $\frac{S_h}{S} \approx 0.045$ is required to be stable and controllable while in the air.

Amphibious stability and control

Again consider Figure 10.34. Now the resistance force the water exerts on the aircraft will be included. This means that we will be able to extend the previously defined Equation 10.57 and Equation 10.58 by adding the amphibious contribution term:

$$\left(\frac{S_h}{S}\right)_{\text{stability}} = \left(\frac{S_h}{S}\right)_{\text{stability,aerial}} + \left(\frac{S_h}{S}\right)_{\text{stability,amphibious}} \tag{10.59}$$

$$\left(\frac{S_h}{S}\right)_{\text{control}} = \left(\frac{S_h}{S}\right)_{\text{control,aerial}} + \left(\frac{S_h}{S}\right)_{\text{control,amphibious}} \tag{10.60}$$

Following the same procedure as with the aerial stability and controllability, we sum the change in moments around the neutral point, and the moments about the aerodynamic centre respectively. Both equations are normalised by dividing by $\frac{1}{2}\rho V^2 Sc$.

$$\sum \Delta M_{np} : 0 = \Delta L_{A-h}(x_{np} - x_{ac}) + \Delta L_h(x_{np} - x_h) - \Delta R_w(z_{np} - z_{cb}) \tag{10.61}$$

$$\therefore 0 = C_{L_{\alpha_{A-h}}}(\bar{x}_{np} - \bar{x}_{ac}) + C_{L_{\alpha_h}}(1 - \frac{d\epsilon}{d\alpha})\frac{S_h}{S}(\frac{V_h}{V})^2(\bar{x}_{np} - \bar{x}_h) - C_{R_\alpha}\frac{\rho_w}{\rho}\frac{A}{S}(\frac{V_w}{V})^2(\bar{z}_{np} - \bar{z}_{cb}) \tag{10.62}$$

$$\sum M_{ac} : 0 = M_{ac_{A-h}} + L_{A-h}(x_{cg} - x_{ac}) - L_h(x_h - x_{ac}) + R_w(z_{cb} - z_{ac}) \tag{10.63}$$

$$\therefore 0 = C_{m_{ac}} + C_{L_{A-h}}(\bar{x}_{cg} - \bar{x}_{ac}) - C_{L_h}\frac{S_h}{S}(\frac{V_h}{V})^2(\bar{x}_h - \bar{x}_{ac}) + C_R\frac{\rho_w}{\rho}\frac{A}{S}(\frac{V_w}{V})^2(\bar{z}_{cb} - \bar{z}_{ac}) \tag{10.64}$$

Upon isolating $\frac{S_h}{S}$, the control- and stability curves during scooping, landing, and take-off operations on water are as follows:

$$\left(\frac{S_h}{S}\right)_{\text{stability}} = \frac{\bar{x}_{cg} + S\bar{M} - \bar{x}_{ac}}{\left(1 - \frac{d\epsilon}{d\alpha}\right)\left(\frac{V_h}{V}\right)^2 \frac{C_{L\alpha h}}{C_{L\alpha_{(A-h)}}}\left(\bar{z}_h - \bar{z}_{cg}\right)} + \frac{\frac{\rho_w}{\rho}\frac{A}{S}\left(\frac{V_w}{V}\right)^2 \frac{C_{R\alpha}}{C_{L\alpha_{(A-h)}}}\left(\bar{z}_{cg} - \bar{z}_{cb}\right)}{\left(1 - \frac{d\epsilon}{d\alpha}\right)\left(\frac{V_h}{V}\right)^2 \frac{C_{L\alpha h}}{C_{L\alpha_{(A-h)}}}\left(\bar{z}_h - \bar{z}_{cg}\right)} \tag{10.65}$$

$$\left(\frac{S_h}{S}\right)_{\text{control}} = \frac{\bar{x}_{cg} + \left(\frac{C_{mac}}{C_{L_{A-h}}} - \bar{x}_{ac}\right) - \frac{T_c}{C_{L_{A-h}}}\frac{2D_{prop}^2}{S}\left(\bar{z}_p - \bar{z}_{ac}\right)}{\frac{C_{L_h}}{C_{L_{A-h}}}\left(\frac{V_h}{V}\right)^2(\bar{x}_h - \bar{x}_{ac})} + \frac{\frac{\rho_w}{\rho}\frac{A}{S}\left(\frac{V_w}{V}\right)^2 \frac{C_R}{C_{L_{A-h}}}(\bar{z}_{cb} - \bar{z}_{ac})}{\frac{C_{L_h}}{C_{L_{A-h}}}\left(\frac{V_h}{V}\right)^2(\bar{x}_h - \bar{x}_{ac})} \tag{10.66}$$

The plots of these equations are presented in Figure 10.35.

The values for the water resistance coefficient, C_R and its derivative with respect to α, C_{R_α}, were obtained using a dated, graphical method. This method was taken from a technical notes paper by NASA [51]. Furthermore, the wetted area, A, is determined to be 8.43 m^2 during landing and takeoff, and the area of the scoopers is 0.0093 m^2. Out of both plots, the take-off and landing situations had the highest required $\frac{S_h}{S}$ ratio. The scooping plot is therefore left out of Figure 10.35. From the Figure, it is visible an $\frac{S_h}{S}$ of 0.15 gives a stable and controllable aircraft.

Geometry

With an $\frac{S_h}{S}$ of 0.15 for the horizontal tail and a wing surface area of 40.8 m^2, the horizontal tail area is 6.12 m^2. To keep the span of the horizontal tail at acceptable levels, it was decided to set its taper ratio at 1. The aspect ratio was then set to 4, which is the average value of the aspect ratio for the aircraft category that the UAV falls in [52]. The span of the horizontal tail can then be calculated using Equation 10.67.

$$AR = \frac{b^2}{S} \tag{10.67}$$

Where A is the aspect ratio, b is the span in meters and S is the surface area in m_2. After rewriting the equation for the span, the span of the horizontal tail was computed to be 4.95m. Furthermore, it was decided to keep the sweep at 0°,

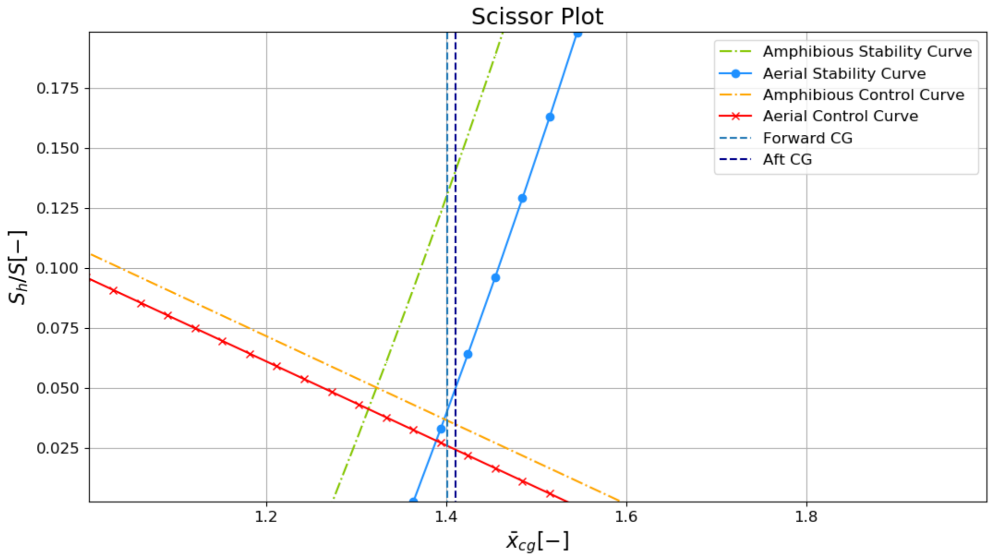

Figure 10.35: Longitudinal Stability Requirement on Horizontal Tail Sizing
Note: X-coordinate is normalised by dividing by chord and the datum is 1 [m] in front of the nose

since for the cruise speed of 112.5$\frac{m}{s}$, shock wave effects do not have to be taken into account[27].

10.4.3. Vertical Tail Sizing

Safety is the main drive for the design of Wangari, and therefore the aircraft must be able to safely operate even during emergency situations, such as drive shaft failure. The drive shaft failure was determined to be the highest risk and thus, the vertical tail was designed to be able to give the aircraft the ability to create a moment large enough to counter the thrust differential which is created when one of the drive shafts fail.

Process

To size the vertical tail, the tasks and functions it needs to be able to fulfil must be generated such that the sizing can be based upon one or multiple of these functions. At the design stage this early, the main function it needs to complete is the directional stability of the aircraft in case of propulsive failure. If one of the propellers fails, the vertical tail must be able to produce enough counter-torque to prevent the aircraft from side-slipping. This was the only function identified in this stage of the design. Therefore, an equation for the required vertical tail area was derived assuming a propeller shaft failure. All other assumptions have been listed below, and the derivation is explained subsequently.

Assumptions

All assumptions, their consequence, and their justification are listed below:

1. **Shaft failure on one side will not affect the other side** $\implies$ One propeller will still be operative when the other propeller's shaft fails $\iff$ Since the shafts will only be interlinked at the engine connection, if one of the shafts fails under the torque applied, the other shaft will still be operative with the same power available and therefore thrust.
2. **Velocity at the tail is the same velocity experienced by the wing** $\implies \frac{V_v}{V} = 1 \iff$ The propeller wakes will not be interfering with the vertical tail and the engine exhaust will be lead around the vertical tail, as the exhaust temperatures would be damaging to the material.
3. **A water rudder is present for steering in water** $\implies$ No sizing for steering in water has to be performed $\iff$ A water rudder is much more efficient to steer at low speeds than a vertical tail, as the vertical tail would have to be extremely large to produce such torques at low speeds, whilst a rudder can be much smaller and therefore weight-saving. Also, since it is not possible to have thrust differentials without a complex gearbox, steering in water will entirely depend on the rudder at low speeds.

Sizing for shaft failure

For the possible situation of one of the shafts failing under the applied torque by the engine, a side-slipping motion would occur. This is not desired and the vertical tail should be able to counteract this torque. Consider Figure 10.36. Equating the Lift multiplied by its moment arm to the thrust multiplied by its moment arm, we obtain Equation 10.68, which can be expanded as Equation 10.69.

$$T_i d_E = L_v l_v \tag{10.68}$$

$$T_{c_i} \rho D_{prop}^2 V^2 d_E = C_{L_V} \frac{1}{2} \rho V^2 S_v l_v \tag{10.69}$$

Normalising Equation 10.69 by $\frac{1}{2}\rho V^2 Sc$, and isolating the term $\frac{S_v}{S}$, we obtain Equation 10.70:

$$\left(\frac{S_v}{S}\right)_{\min} = 2\frac{T_{c_i}\frac{D^2}{S}\bar{d}_E}{C_{L_V}\left(\frac{V_v}{V}\right)^2 \bar{l}_v} \tag{10.70}$$

With T_{c_i} being the thrust coefficient of one propeller when the other one fails, D^2 being the diameter of the propeller, S being the main wing surface, $\bar{d}_E$ the horizontal distance between the working propeller and the centerline of the fuselage, C_{L_V} the lift coefficient of the vertical tail, $\frac{V_v}{V}$ ratio of the air velocity over the vertical tail with the air velocity over the wing and $\bar{l}_v$ the distance between the vertical tail and the centre of gravity.
All terms in Equation 10.70 are either known, or can be designed for. From the general layout of the UAV, aerodynamic properties of the vertical tail and size of the propeller section 10.1 have been obtained, which resulted in a $\frac{S_v}{S}$ of 0.08.

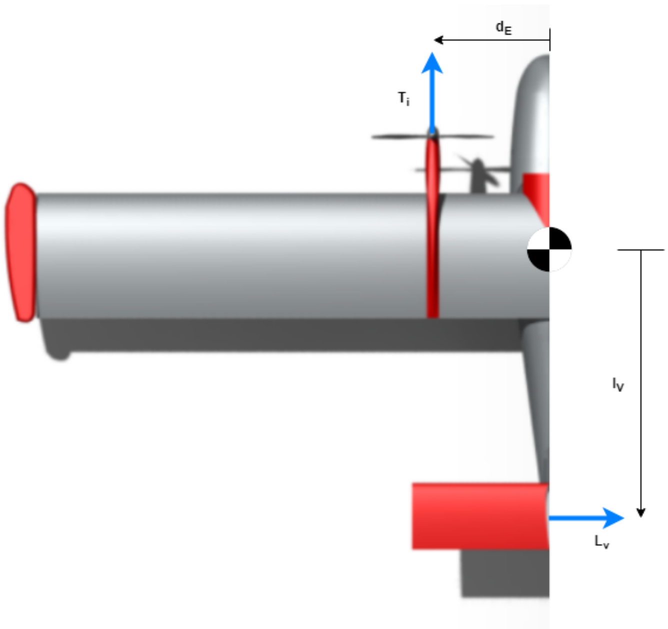

Figure 10.36: Free-Body Diagram used for vertical tail-plane sizing equation

Geometry
With an $\frac{S_h}{S}$ of 0.08 for the vertical tail and a wing surface area of $40.8m^2$, the vertical tail area is $3.264m^2$. Typical vertical tail aspect ratios range between 1.3 and 2.0, whereas the taper ratio ranges between 0.3 and 0.6 [52]. The geometry of the vertical tail was then determined for the four most extreme cases, so $A = 1.3$ $\lambda = 0.3m$, $A = 1.3$ $\lambda = 0.6$, $A = 2.0$ $\lambda = 0.6$ and $A = 2.0 \lambda = 0.6$. It could be concluded that for an aspect ratio of 2.0, the total height of the UAV would exceed the height of the cargo hold of the A400M, so this configuration would not be transportable. According to Raymer, "for a low-speed aircraft, there is little reason for vertical-tail sweep beyond 20° other than aesthetics." Based on this, it was decided to set the taper ratio to the higher end of the spectrum, at 0.6 and the aspect ratio at 1.3. This resulted in a sweep angle of 27°.

10.4.4. Final Tail Configuration

After all the sizing was performed, the final configuration had to be decided. Many parameters, such as $\frac{V_h}{V}$ would be dependent on the configuration. The V-Tail was scrapped first, as it did not have the ability to become a full moving tail, not did it make full use of the propeller wake, which caused the area to be too large. The H-Tail - Crucifix hybrid was considered for its ability to have vertical stabilisers as well as horizontal stabiliser area inside the propeller wake, potentially decreasing the area required. However, it did add more structural weight and was eventually discarded in favour of the T-Tail - Crucifix hybrid. The eventual area ratios can be found in Table 10.11.

Table 10.11: Final size ratios for the stabilising surfaces

Surface	Value
Horizontal, $\frac{S_h}{S}$	0.15
Vertical, $\frac{S_v}{S}$	0.08

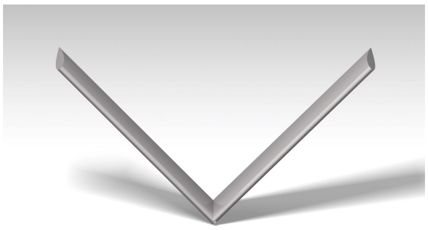

Figure 10.37: V-Tail Configuration

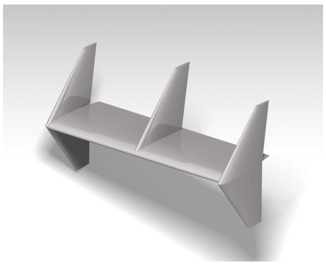

Figure 10.38: H-Tail - Crucifix Hybrid

Figure 10.39: T-Tail - Crucifix Hybrid

10.4.5. Sensitivity Analysis Empennage

As seen in the previous sections, the longitudinal controllability and stability directly relates with the size of the horizontal tailplane. From Figure 10.35 it is visible the size of the horizontal tailplane would increase a lot if the aft. c.g. would shift backwards, so sizing the horizontal tailplane is quite sensitive to changes in the c.g.. However, a forward c.g. shift would not affect the controllability very much, as the control curve's slope is much more gradual.

Another aspect that influences the size of the horizontal tail surface is $\frac{V_h}{V}$. The term is squared in Equation 10.66. As stated above in the assumptions, this is assumed to be 1.3, but if this appears to be smaller in a more detailed analysis, this would increase the horizontal tail surface.

For the vertical tailplane, the size directly scales with the distance of the propellors to the fuselage. As no big changes are expected in this design parameter, the size of the vertical tailplane is not expected to be very sensitive to changes of the design.

10.4.6. Risks

During the calculation and the making of certain assumptions a risk is present that the result is wrong. This could be because of carelessness with the derivation, but also because a wrong assumption is made. The assumptions that could have the biggest effect, if they were to be wrong are assuming the C.o.B. (center of buoyancy) remains constant and the ISA conditions. The C.o.B. not being constant this would change the equations by quite a lot. This risk is however mitigated by stating the hull is always stable in the longitudinal direction, as seen in subsection 10.3.2. The ISA conditions will not hold up when flying above a fire, the temperature will be higher and the density and pressure are both lower. The effect of this is something that has to be taken a look into in a further design phase.

10.4.7. Verification & Validation

For the verification of the code written for the empennage sizing, unit tests were written, with a resulting line coverage of 85%. The unit tests checked for known outcomes for certain combinations of parameters for Equation 10.57 through Equation 10.66.

Aside from unit tests, the derivations for Equation 10.57 through Equation 10.66 were peer reviewed by both C&S department members as well as other members of the Wangari project.

10.5. Control Surfaces

Control surfaces are required to be able to change and control the aircraft's attitude. The primary surfaces are the ailerons (roll), elevator (pitch) and rudder (yaw), and are designed using initial design guidelines by Raymer[53].

The required aileron area can be estimated with Figure 10.40. For this, the total aileron span over wing span is needed. The total span of the wings is $17.48m$. When the hull diameter of $1.5m$ is subtracted from the span and this result is divided by two, the span that can be used for moving surfaces (ailerons, high-lift devices) per wing is computed, which results in an effective wing span of $7.91m$. Since the the high lift devices require a span of $5.36m$ per wing, as described in the section above, this leaves $2.55m$ of span left for the aileron. This results in an aileron span over wing span ratio of 0.29. Then from Figure 10.40, the aileron chord over wing chord was estimated to be 0.32. With a wing chord of $2.33m$, this results in an aileron chord of $0.746m$. Elevators and rudders usually begin at the side of the fuselage and extend to

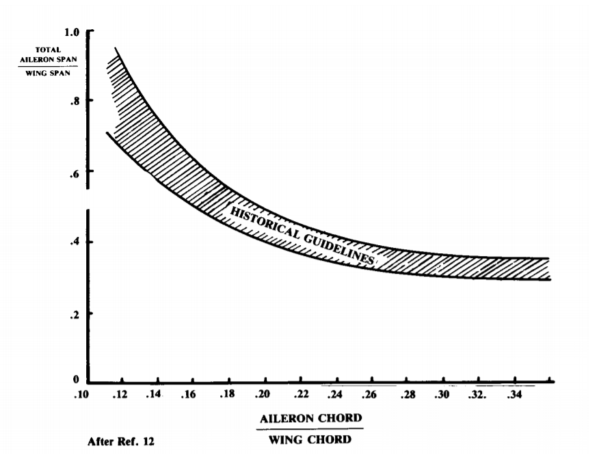

Figure 10.40: Aileron guidelines by Raymer [53]

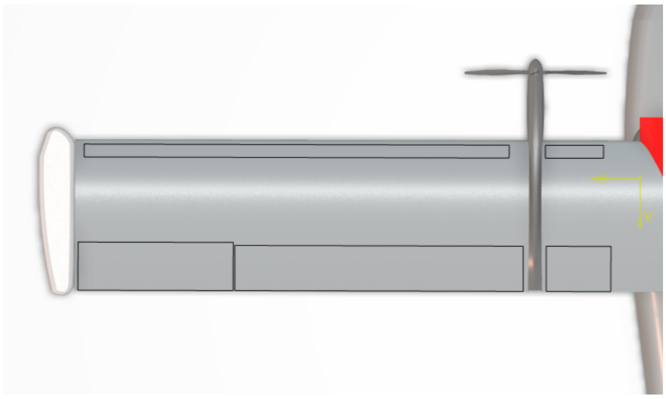

Figure 10.41: Visualisation of the ailerons and high-lift devices. The aileron is positioned near tips of the wing and the high-lift devices near the fuselage.

about 90% of the tail span [53]. The chord length can then be determined using general values for the $\frac{C_e}{C}$ and $\frac{C_r}{C}$ from Raymer. For the aircraft category that the UAV falls in, the general values for the $\frac{C_e}{C}$ and $\frac{C_r}{C}$ are 0.36 and 0.46 respectively [53]. With a horizontal tail chord of 1.237 m and a vertical tail root chord of 1.834 m, the elevator and rudder root chord are 0.445 m and 0.843 m respectively. The final sizes of the control surfaces are show in Figure 10.41 until Figure 10.43.

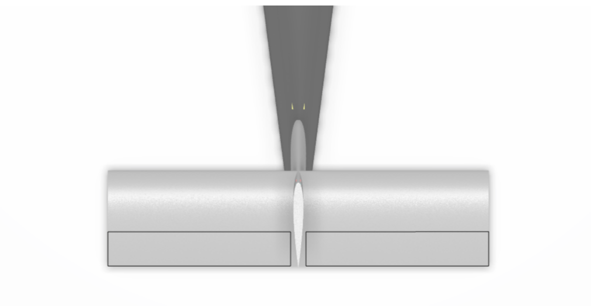

Figure 10.42: Visualisation of the elevator dimensions.

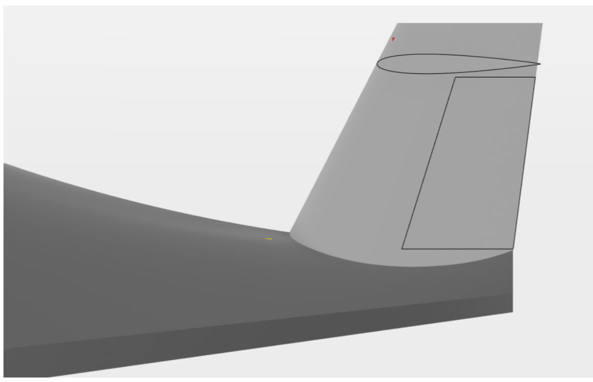

Figure 10.43: Visualisation of the rudder dimensions.

10.6. Landing Gear Placement

To be able to land and take-off on land a landing gear system has to be designed. For this stage of the project only a configuration and location of the landing gear has been determined. In Figure 10.44 various configurations are displayed. The Single main and Bicycle are non-conventional, unstable options, they were not taken into consideration. The Multi-bogey is for big aircraft with a lot of payload, a category in which our UAV does not situate itself. The Quadricycle has a load distribution of 40% on the nose landing gear (NLG) and 60% of the load on the main landing gear (MLG). This configuration is very sensitive to roll, crosswinds, and proper alignment with the runway.[22] This leaves the Tricycle and the Taildragger. As the Taildragger is more prone to a ground loop (because the c.g. is behind the main landing gear) and is less stable during landing in high winds, a Tricycle configuration is chosen.[54]

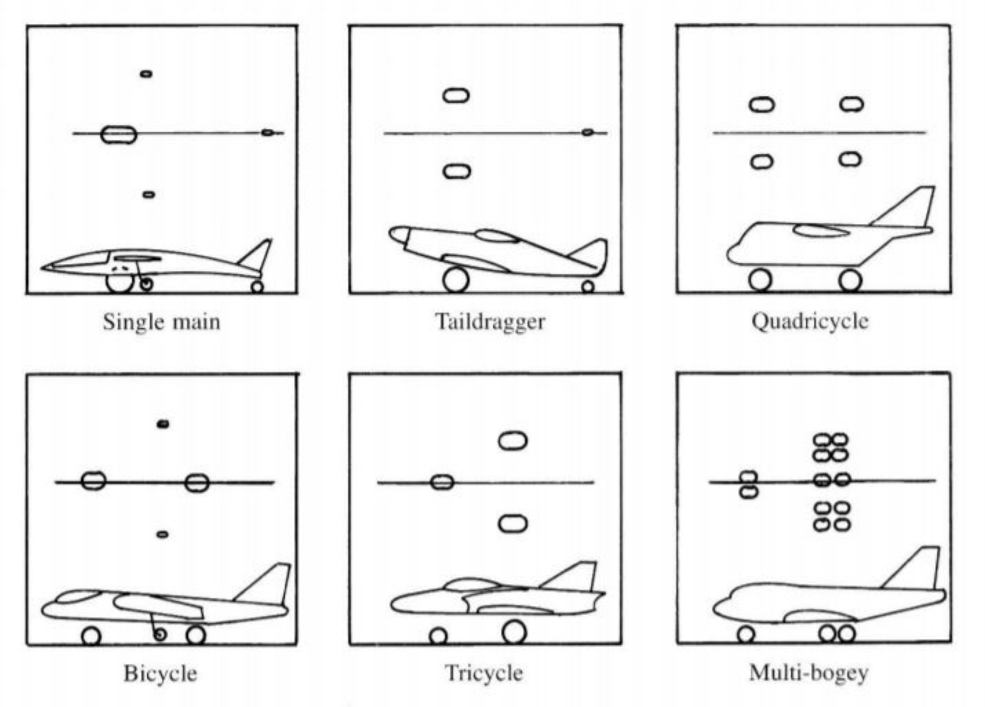

Figure 10.44: Different landing gear arrangements [55]

For the longitudinal placement of the landing gear, first the distance from the main landing gear until the nose of the aircraft is determined. This is dependent on the location of the c.g., the clearance angle, and the tipback angle. A big tipback angle would result in a main landing gear (MLG) far away from the center of gravity. This would mean our nose landing gear would have to carry too much load (>20% of the total load), which is undesirable for steering reasons during taxiing[24]. As advised by the tutor[23], the tipback angle is set at at least 10°. This resulted in the placement, visible in Figure 10.45. The distance from the nose and the load distribution over the landing gears can be found in Table 10.12. As visible from the table, there is some room to add extra weight to the nose landing gear by increasing the tipback angle. This is something that can be applied in the continuation of the project.

Table 10.12: The distance from the nose and the load distribution over the landing gears

	Main landing gear	Nose landing gear
Distance from nose	3.65 m	0.7 m
% of the load on the gear	88%	12%

[22] `http://www.aerospaceweb.org/question/design/q0200.shtml` [cited 18 June 2019]
[23] ir. M.J. Schuurman, Assistant Professor and Senior Air Safety Investigator

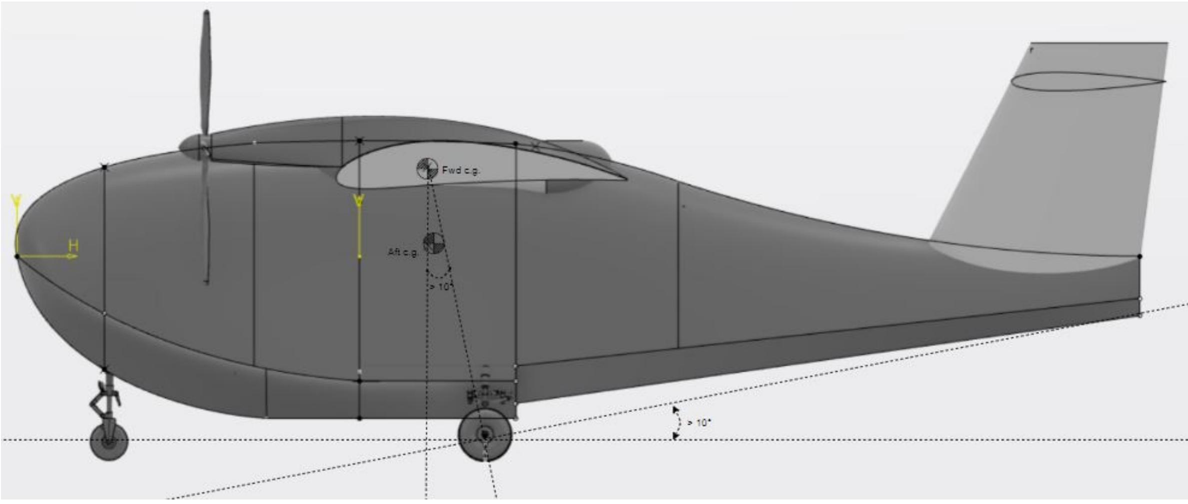

Figure 10.45: The placement of the landing gear with at least 10 degrees of tipback angle.

10.6.1. Lateral Placement of MLG

To have an aircraft that does not tip over while making a turn during taxiing, the lateral placement of the MLG has to be done such that the overturn angle (ψ in Figure 10.46) is smaller than 70°. (This value was also the result of a discussion with our tutor[23]) In the event of a lateral tip-over, the floats attached to the wings would catch the plane, and hereby limit the damage caused to the plane. The risk taken by having a relatively big overturn angle, is thus limited. With Equation 10.71[55], the minimum required y_{MLG} (the horizontal distance between the centreline of the fuselage and the wheel) can be computed. l_n is the distance between the nose landing gear and the c.g., l_m is the distance between the main landing gear and the c.g.. z is the vertical distance between the main landing gear and the c.g., as indicated in Figure 10.46. Using the upper most c.g. from Table 10.10, and Equation 10.71, y_{MLG} is calculated to be at least $0.61m$. The fuselage has a width of 1.5m, so when the landing gear is placed directly next to the fuselage, the requirement of having a y_{MLG} of at least $0.61m$ is achieved.

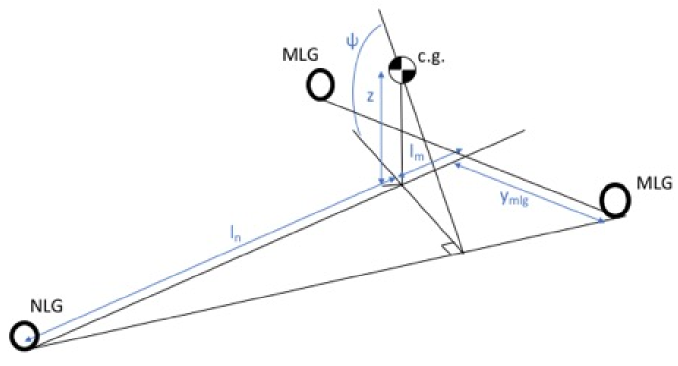

Figure 10.46: Lateral stability for a tricycle landing gear configuration. (adapted from Roskam Part IV)

$$y_{mlg} > \frac{l_n + l_m}{\sqrt{\frac{l_n^2 tan^2(\psi)}{z^2} - 1}} \tag{10.71}$$

10.6.2. Sensitivity Analysis Landing Gear

The location, size and weight of the landing gear is highly dependent on the location of the c.g.. An more aft c.g. would mean the main landing gear would shift backward as well, where in extreme cases the load on the nose landing gear should be taken into account to keep it controllable (>8% of the weight should be on the NLG). As the MLG would move backward just as far as the c.g., this is not very sensitive. The problem with the nose landing gear would also be solved by just moving the NLG more aft.

If the c.g. moves more up, this would also cause the MLG to move more backward (best seen in Figure 10.45) because of the tipback angle. As the most upper c.g. is already quite far up (71 cm from the centerline of the fuselage), it is not expected to move further upward. This means the y_{MLG} is expected not to be increased anymore, just as the main landing gear is not expected to move more backward because of this.

10.6.3. Risk Analysis Landing Gear

The landing gear in the tricycle configuration has as main risks not being controllable by either having too much load on the nose landing gear, or having not enough load on the landing gear. If the nose landing gear carries less than 8% of the load, it has not enough grip to change the direction of the UAV, if it has more than 15% of the load there is a probability the nose landing gear will slip while changing direction or braking.

As visible in Table 10.12 the load on the nose landing gear in the current configuration is 12%. Shifting the c.g. forward or upward increases the load on the landing gear. This could be a risk, as the nose landing gear is already put as far forward as reasonably possible ($0.7m$ from the nose). For the case the c.g. moves aft, the load on the nose landing gear decreases, but this can be countered by shifting the nose landing gear more aft. This does thus not create a risk.

Another risk is having an overturn angle of 70%. A hard turn on while taxiing could cause the UAV to tip over. This is something that has to be taken into account while taxiing with the UAV, and the severeness of the effect is also decreased by the attached floats.

10.7. Water Tank

10.7.1. Dimensions

The internal water tank is one of the most important parts of the design as it determines Wangari's capability to perform the firefighting mission. The maximal amount of suppressant Wangari is able to drop is $4500L$, which coincides with the set requirement:

AF-PERF-COLL-01 The UAV shall have a suppressant capacity of at least 4500L.

The volume of the internal tank needed for the maximal drop is therefore $4.5m^3$. An additional 2% of the volume, equalling $0.09m^3$, is added to account for expansion. The water is divided over two tanks such that these can be part of the fail safe buoyancy philosophy in which the UAV is divided in at least four separate compartments that, in case of leakage of a compartment, are still able to generate enough buoyancy to keep the UAV afloat. Moreover, compartmentalising the tanks has reduces sloshing effects. The design of the tanks was limited by the space available in the small UAV and the desire to control the flow during dropping. The final dimensions of the tanks are visualised in Figure 10.47.

10.7.2. Sloshing

As the suppressant tank is sized for the maximum suppressant volume, the tanks will only be partially filled with suppressant during the first drops. Hence, means to reduce sloshing, which can have negative effects on the stability of the entire fuselage, must be incorporated in the tanks. This can either be done by passive or active means. An active option to reduce sloshing would be to pressurise the tank, however, this would make the passive pressurised dropping system obsolete. Moreover, the pressurised system would introduce extra costs and weight. Therefore, a passive anti-sloshing system is preferred. Two options seemed most feasible: compartmentalisation or the introduction of baffle structures. Further compartmentalisation of the tanks, apart from the two main tanks, was deemed unwanted as this would require a more intricate system for filling of the tanks and dropping. Thence, anti-sloshing by means of baffles was chosen. The baffles are to be made of porous material instead of solid baffles with water ports. Due to the porosity the baffles can be extended over the entire cross-sectional area such that a higher damping of the hydrodynamic waves can be achieved.[56]

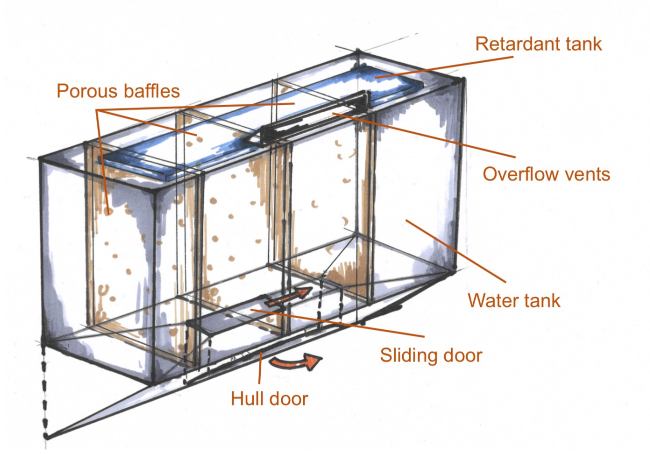

Figure 10.47: Sketch of the internal tank.

10.7.3. Overflow Vents

The design take-off weight may not be overshot by loading of too much water, therefore, an active sensor system PUT IN SYSTEMS is installed. Additionally, in each of the tanks an overflow vent is integrated. These are sized based upon the vent-to-door ratio of 4.4:1 used in the CL-215 and CL-415[57], such that a vent size of $0.07m^2$ is obtained per tank. As well as for disposal of the excess water, these vents can be used for filling of the tanks when taking off from land.

10.7.4. Retardant Tanks

The water tanks are equipped with retardant tanks to mix the water with the chosen enhancer, Phos-Check WD881, as described in subsection 8.3.5. A controlled injection system is implemented in the retardant tanks such that different concentrates of retardant can be added to the water for different mission types. In general the amount of Phos-Check WD881 needed will range from 0.1 to 1% of the water volume [24]. Due to the limited space available in the UAV, the perfect mixture rate will not be available for all 80 drops it's able to make per day. The tanks have thence been sized according to the retardant-over-water volume ratio used in the CL-415[25]. This resulted in a total retardant volume of $18L$. The retardant tanks have been stretched out over the entire length of the water tanks. This allows several connected valves to distribute the retardant better over the water reducing mixing time.

10.7.5. Materials

In the material selection of the internal tanks the most important factor is that the structural integrity of the tanks is not impaired by the (salt) water and chemical foams used as suppressant. Therefore, a fibreglass-epoxy composite which has a high anti-corrosion resistance is chosen. Apart from holding its structural integrity, the internal water tanks should also be designed to not influence the suppressant exit speed. Thus, a coating reducing the ability of the foam to stick to the tank walls should be applied. In future design, research into the exact strength and thickness of the material needed to withstand stresses induced by the (hydrodynamic) loading is required.

10.7.6. Dropping Mechanism

Wangari is designed to excel at performing passively pressurised drops. Therefore, a new dropping mechanism is thought out in which the flow at the exit can be controlled without the need for a heavy and expensive pressurisation system. As explained in subsection 8.3.3, the required flow rate at the exit of the tank is obtained by the use of g-forces and control of the exit area. This control is done using a sliding door in the tank. However, the water needs to be dropped vertically to have the most steady dropping performance, making a sliding door in the angled fuselage skin undesired. Moreover, this would need an extensive structural reinforcement of the skin. Therefore, the sliding door is placed horizontally within the body, with a regular hinged door at the skin, opening wide enough as to not block the water in its way down. The sliding door will be able to open up the maximal required exit area of $0.3m^2$ and will due to its sliding nature be able to create any desired open area below that. Safety measurements are taken into account by establishing a mechanical link between the doors of both tanks such that when one actuator fails the remaining link can still ensure opening and closing of both the tanks.

[24]`https://phoschek.com/product-class/class-a-foam-for-wildland/` [cited 18 June 2019]
[25]`https://www.ovalp.com/en/understand/canadair` [cited 18 June 2019]

10.7.7. Filling Mechanism

The internal tanks of Wangari are designed to not only be filled on land but also by means of scooping up water during the firefighting mission. To do so, the tanks are equipped with scoopers, which can be retracted after scooping to minimise aerial drag. The size of the scoopers is determined by the following requirement:

AF-PERF-COLL-02 The UAV shall be able to scoop up 4500L of water in one single pass.

A single pass is defined as a pass of 10 seconds and the speed at which Wangari is designed to scoop is equal to the loiter speed of 44 m/s. The required opening per scooper, A_{sc} can be determined using Equation 10.72,

$$A_{sc} = \frac{V_{sc}}{2 v_{sc} t_{sc}} \tag{10.72}$$

in which V_{sc}, the required water volume, v_{sc} the design scooping velocity, and t_{sc}, the design scooping time. Inserting the design conditions leads to an area of $0.51 dm^2$ per scooper.

10.8. Mass Budget

After most of the components had been designed, the empty weight of the UAV could be revised. Several of the weights of the components had been found through calculations done in the previous sections, for instance the weight of the wing (subsection 10.2.5. For the other components, masses could not be estimated previously, the mass of those components had to be estimated with the use of a class II weight estimation, the methods described in part V of Roskam were used to do so [58]. These methods were also applied to the components of which the weights were found earlier to check and verify the calculations. The result of the calculations and estimations can be found in Table 6.1.

This section will first elaborate on the method used, which is solely based on methods from Roskam [58]. Known component weights and the verification of those is then discussed. Following that will be the estimations of the weights of all other components with the use of Roskams methods. The end of this section includes a brief discussion on the iteration between the class I and class II weight estimations (section 7.3) and the different departments within the team.

Component Weight Estimation Method

Wangari is said to be of the airplane type general aviation, this is because first of all amphibious aircraft fall under this type, and also the agricultural aircraft, on which the first weight component estimation was based (section 7.3), is of this type. There are multiple methods available for the general aviation type, it is chosen to follow the USAF method. The UAV did not comply with the requirements to use the other methods provided for general aviation, namely the Cessna method (Wangari's speed is not below $200 kts$) and the Torenbeek method (Wangari exceeds the $12500 lbs$ limitation of take-off weight).

Calculated Component Weights

Multiple components of the total weight have been established in the previous sections. First of all, the payload, this includes the water and retardant, is limited to $4500 kg$.The weight of the wing has been estimated in subsection 10.2.5, it has been found to equal $1106 kg$. The tip floats have not been included in this and are estimated to weigh $50 kg$ each. An estimation for power plant was made in Table 10.1, it was said to weigh $654 kg$, this is the sum of different propulsion component weights. The number of batteries required to power the complete UAV will be discussed in chapter 11, each of them weighing $36 kg$, resulting in a total of $288 kg$ (8 batteries). These batteries will for instance provide the power of the instrumentation, avionics and electronics, which will be discussed in the same chapter, these will weigh $87 kg$.

Estimated Component Weights

The weights of all other components still had to be calculated with the use of statistical data, as mentioned, the USAF method will be used to do so. Due to limitations with regards to space in this report, formulae from Roskam ([58]) are not included in this section, but will be referred to (all equations referred to in this section are from Roskam). The components of the empty weight of the aircraft have been divided in three different groups: structure, power plant and fixed equipment, each of which will be elaborated on in this subsection.

Structure

The total weight of the structure of the UAV is made up of the wing, floats, empennage, fuselage and landing gear. The class II weight estimation also provides a method to determine the weights of the nacelle, however, the USAF method includes this in the weight of the power plant. The weights of the wing and floats had been determined earlier, to verify the weight of the wing equation 5.4, values of the parameters in this equation can be found in subsection 10.2.1. It was found that the calculated mass of $1106kg$ was within a 5% margin of the value found using the equation from Roskam, thus this value was verified. There is no method to estimate the weights of the floats in Roskam, but its weight was based on reference aircraft, thus assumed to be in the correct order of magnitude.

The empennage, consisting of both the horizontal and vertical tail, has an estimated weight of $115.5kg$. This has been determined with the use of equations 5.14 and 5.15. The weights of the tails varied largely, as the configuration changed multiple times. Iterations were to be performed with the department of aerodynamics and control and stability, because when the weights changed, the parameters of the control and tail surfaces changed, leading again to a change in weight. Thus this process was continued until the final weight value did not change more than 1% compared to the previous value. section 10.4 discusses the empennage in more detail.

The weight of the fuselage was found with the use of equation 5.25, this weight was multiplied with a factor of 1.65 as the aircraft is amphibious. This increase in weight is due to the fact that the fuselage should be able to handle all loads induced by the impact of the water. This value might be slightly conservative, but was adhered to as the final value of $883kg$ seemed reasonable.

In subsection 10.6.1 the landing gear is discussed. Use is made of equation 5.40 to determine its weight. It was found to equal $152.5kg$, a strut length of $2.5m$ was assumed for this. Iterations had to again be done together with the control and stability department, to ensure that the centre of gravity was still at the correct location.

Propulsion
An initial estimate for the mass of the power plant was made to be $654kg$. The weight of the engine provided by the company's website could not simply be used, because it was decided to add a second propeller to the propulsion system, this is taken into account as can be seen in Table 10.1. The mass of the power plant had to be revised, as this did not account for the fuel system. The mass of the fuel system was estimated by applying equation 6.17. It was found to equal $70kg$, the parameters used where based on the fact that the UAV includes two integral fuel tanks. The two estimated masses were added together and the total weight of the power plant was found to equal $724kg$.

Fixed Equipment
Part of the fixed equipment has been determined with the use of the internal systems required for the UAV, these will be discussed in chapter 11. The list of fixed equipment that the UAV will have is made up of the flight control system, electrical system, and instrumentation, avionics and electronics. All other components listed on page 97 of [58] were not to be calculated, as these will not be present in Wangari.

The weight of the flight controls was found using equation 7.3, the flight controls are powered. The weight of the flight controls was halved, as this includes two sets of flight controls, for both pilots each. But, because Wangari is an unmanned aircraft, it is assumed that only one is required. This results in the flight controls weighing approximately $250kg$

The masses of all sensors, cameras, instruments, etc. are included in the weight of the instrumentation, avionics and electronics. These values were estimated by the operations department, which will be discussed in following sections. There is no way for estimating this weight with the use of the USAF method, thus the weight of $87kg$ has been compared to similar aircraft and was found to be reasonable. The mass of the actuation system is included in this component.

The weight of the fixed equipment is also made up of the electrical systems, this includes, amongst others, all the wiring for the fuel system and the IAE. Its value of $112kg$ was found with the use of equation 7.13.

Iterations Between Estimations and Departments
An overview of all components and their associated weights can be found Table 6.1. Summing all the components of the structure, propulsion and fixed equipment, the empty weight is found to equal $3,818kg$. This final value of the empty weight was found after completing several iterations between the class I and class II weight estimations. This was done as the fuel and maximum take-off weight affect the empty weight, for instance in the weight of the fuel system. An explanation of the class I weight estimation was given in section 7.3. Iterations were stopped once the resulting empty weights of the two estimations were within 0.5% of each other.

As mentioned in section 8.1, the weight of the payload could change for each mission and will even change throughout the mission, the maximum payload the UAV will be able to carry is $4500 kg$. The maximum fuel weight is $2700 kg$. This results in a minimum payload that can be taken along at the start of the mission $2500 kg$ (9000-2800-2700).
These masses of the components were used to consider the controllability and stability of the aircraft. As mentioned before, this introduced several alterations to the design, thus the complete process of estimating the component weights had to be done multiple times. To simplify the process, the maximum take-off weight was kept constant at $9000 kg$, as it was decided to not alter its value any longer due to time constraints. If the empty weight could be reduced, the amount of fuel was increased, keeping the MTOW constant, which means that more refills and thus drops can be performed.

11
Internal Systems

Apart from the general layout and the external design of the UAV the internal systems and layout are also important to have a plan for. Critical functions like communication, actuation and the power system are treated and they are given a preliminary location within the architecture of Wangari.

11.1. Internal Layout

Naturally, the internal layout is largely determined by the volume of the fuselage and the largest components that is has to contain. For the UAV, these components are the water tank, the nose landing gear, the main landing gear, and the engine.

Out of these components, when filled the water tank is the heaviest, so all other components were positioned around it. As the landing gears have to be placed at certain positions to ensure longitudinal and lateral stability, parts of the water tank had to be cut out to make place for the landing gears, whilst ensuring that the total volume of the tanks remained the same. This also applies to the engine, as it had to be placed at a certain position to make the transmission from the engine to the propellers as easy as possible. To do this, the top of the middle water tank was lowered.

Other large components like the batteries, radar and flight recorder were positioned near the nose to shift the C.G. forward. In total, 8 battery packs are placed in the UAV. The power system is elaborated further in section 11.4.

Four strobe lights and visual cameras are located at various positions of the UAV, to allow the drone pilot to observe the fire. One set is positioned at the nose and one set on the vertical tail. Another two sets are placed on the bottom of the hull. The complete layout is presented in Figure 11.1

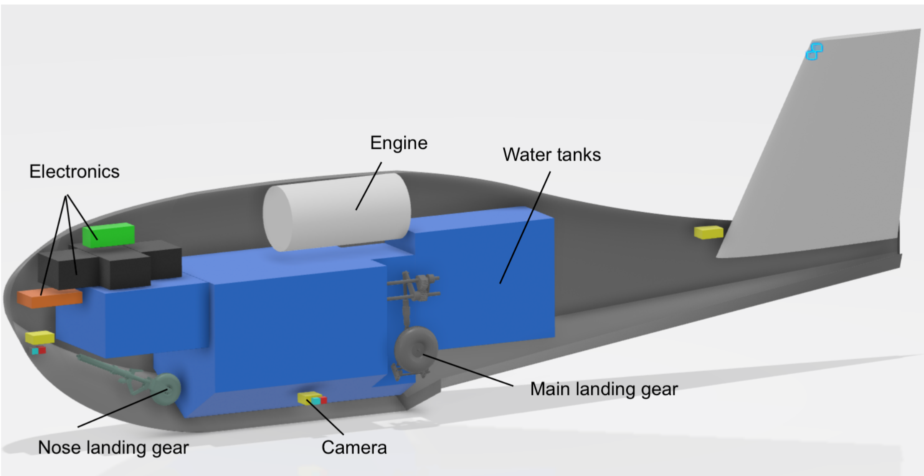

Figure 11.1: Overview of the internal layout. Blue: water tank. White: engine. Green: radar. Black: batteries. Orange: flight recorder. Yellow: Strobe power supplies. Light blue: strobe lights. Red: Visual cameras. Highlighted in the tail is another strobe and camera set.

To be noted is that the fuel tanks are not directly shown in the layout. The fuel tanks take the form of bladders within the wing and are further detailed subsection 10.1.3.

11.2. Hydraulics and Actuation

The actuation of many crucial aircraft components is often accomplished through a hydraulic system. The deployment of flight control surfaces, landing gear, and brakes is done through hydraulics. While hydraulic systems are quite reliable since they have been used extensively in large commercial aircraft, they do have some significant disadvantages. Their complexity is a main issue as they must contain a minimum number of subsystems for redundancy and reliability, and each subsystem has a minimum number of essential components such as a power generating device, a reservoir, an accumulator, filtering systems, and of course the fluid. The complexity of such a system, an example of which is seen in Figure 11.2 comes with unwanted characteristics that clash with the sustainable aims of this project.

Such a complex system adds a lot of weight. Having three different reservoirs (one for the left, one for the right, and a standby system in case either main system fails) and three different connecting lines through the aircraft add unnecessary weight. Extra weight on the aircraft means more fuel is burned, which causes more unwanted emissions.
The complexity of the system also means that there are many interacting parts. This increases the risk of system failure because there are several parts where something can go wrong, for example leakage through the pipes, or fluid contamination, which must be checked regularly. These frequent maintenance checks take a lot of time and resources and are financially unsustainable, as they will incur extra costs throughout the life of the aircraft. Furthermore, many parts will be replaced over the lifetime of the aircraft and thereby many parts are thrown away, which is hazardous for the environment.

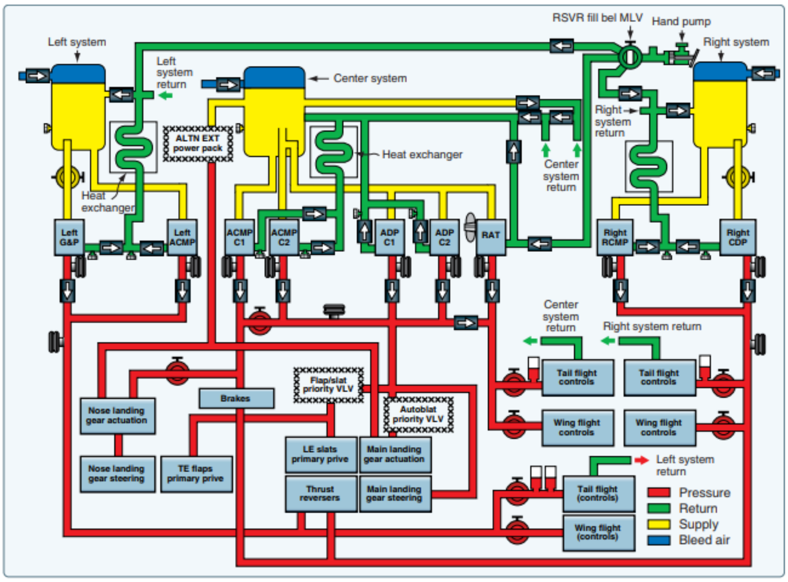

Figure 11.2: Example of a hydraulic system of a large aircraft [1]

Electro-Hydraulic Actuation
Modern aircraft are starting to adapt a power supply system and fly-by-wire flight control system. This means that flight controls are regulated through a computer. The pilot commands are sent electronically to the relevant components, which avoids the need for complex, heavy and high-risk hydraulic lines. Fully electric systems have not yet been tested to a reliable extent, and since the UAV is an emergency response aircraft, it cannot afford pioneering this particular area. A suitable solution is using electro-hydraulic actuators(EHAs). The command is sent electronically to the actuator, which has an inner hydraulic system to perform the actuation. This eliminates the need for a large and heavy and high power consuming central hydraulic system. Because of this EHAs are safer, easier to maintain, and more sustainable. These types of actuators are reliable as they have already been tested successfully by NASA in 1997[59].

Redundant Design
Systems that are critical to be able to land are designed to be fail safe. Those systems are coupled to provide redundancy for each other, for example, the main landing gear has its own EHA, and the nose gear has its own EHA. The two systems

[1] Hydraulic and Pneumatic Systems, `http://www.sweethaven02.com/Aviation/MaintHandbook/ama_Ch12.pdf` [cited 20 June 2019]

are connected, so if one fails, the other is able to actuate both landing gears. The same holds for flaps and elevators. In these cases, where one actuator is used to deploy both surfaces there is the risk that the actuation happens slightly slower, but this risk is acceptable for these systems as they are not time-critical to that degree. For instance, a pilot who is aware of this can start landing gear deployment earlier than usual.

Systems that are time critical are given backup actuation, so there is simply an Electric Backup Hydraulic Actuator (EBHA). If the main EHA fails, the EBHA is used, in the same way that traditional standby hydraulic lines are used. These systems are important to continue a crucial mission, and are time critical. For instance the dropping mechanism doors cannot open too slowly because that will affect the flow of the retardant and the efficiency of the drop.

Systems that are not critical for landing are given a safe life design, so they are regularly checked in maintenance, and are replaced before they fail.

Figure 11.3: Commercially available compact electro-hydraulic actuator with a force of 21.3kN. [2]

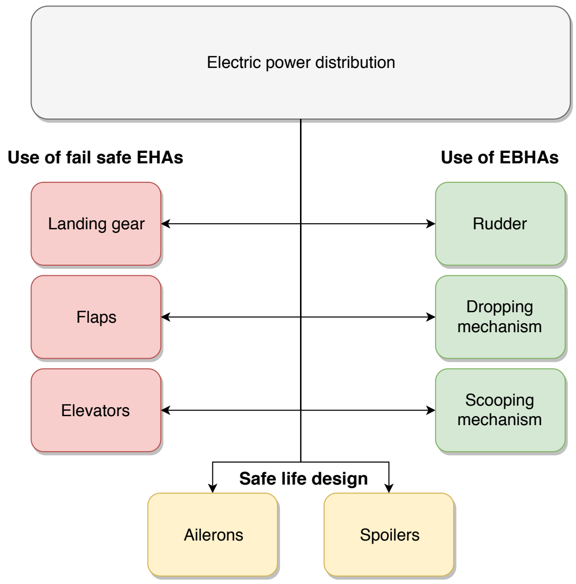

Figure 11.4: Main actuators and their redundancy design.

11.3. Communications

The system that is being designed will consist of unmanned aerial vehicles. This implies that no pilot will be aboard the aircraft. Since the system will not be fully autonomous, the pilots have to be able to remotely control the aircraft from the ground. This requires some form of communication between the ground station and the aerial vehicle. Devices and sensors on the UAVs gather information that has to be sent to the ground station, while the ground station needs to be able to send commands to the UAVs. In the sketch below the interaction between the different units and the internal communication can be seen.

The air attack, equipped with camera's, is flying above the UAVs and is used to better coordinate the system. Besides, it could also be used to complete the communication link through an indirect route when the link between the UAVs and the ground station is blocked, due to smoke or a too large a distance for example. If the air attack can not be reached, because it is not used during that mission for example, the last option for that UAV is to communicate with another UAV which is in direct range with the ground station, so that the link to the ground station could still be completed. Generally two or more UAVs are used in the mission and don't fly too far away from each other, which is why they would be able to communicate mutually most of the time. In the event that the link of one UAV is completely hindered with every unit, by smoke interference for example, the UAV that still has a connection with the ground station should approach the UAV to try and complete the communication link.

[2] https://ph.parker.com/us/en/compact-electro-hydraulic-actuator?cm_re=Search-_-Flyout-_-Series&se=undefined&sr=1[cited 20 June 2019]

The UAVs and the ground station are equipped with devices and sensors in order to gather information, which will be used by the pilots on the ground as well as the air attack coordinator. The devices and sensors used are described in subsection 11.3.1.

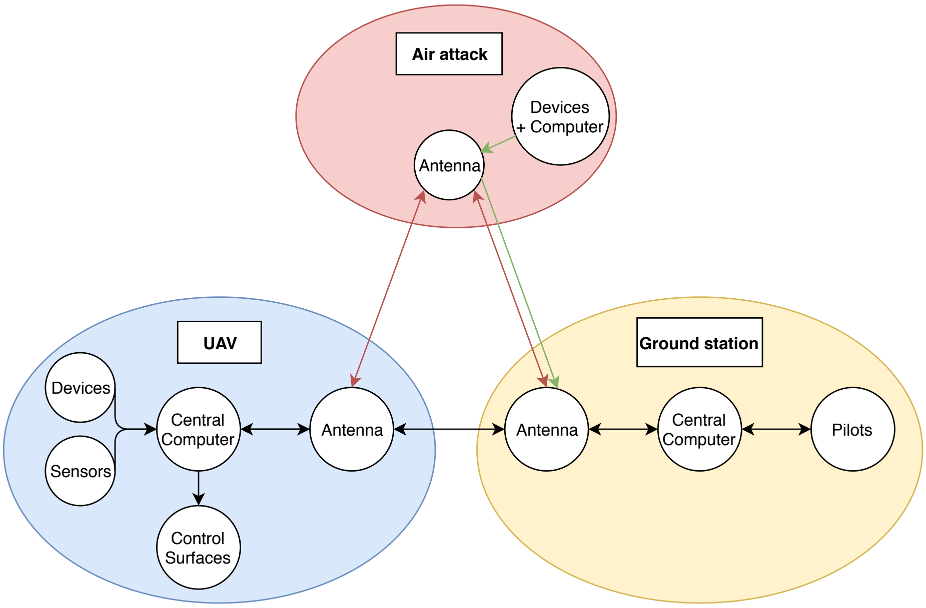

Figure 11.5: Communication flow diagram

11.3.1. Devices and Sensors

In Table 11.1, all the devices and sensors that are placed in the UAV are listed. Next to this, a description of what their function is, the number used, the mass of the device/sensor, the power required per unit and the maximum operating temperature are also mentioned.

Table 11.1: Devices and sensors

Device/sensor	**Description**	**Number**	**Mass per Unit [kg]**	**Power per Unit [W]**	**Max. Operating Temperature [°C]**
Combined Pitot - Static Tube [3]	Pitot Tube + Static Port	1	0.04	0	85
ALT200 Electronic Altimeter [4]	Altitude	1	0.12	0.75 - 4.5	55
VSI200 Electronic Vertical Speed Indicator [5]	Vertical Speed	1	0.12	0.75 - 4.5	55
Kanardia Airspeed Indicator [6]	Airspeed	1	0.21	1.26	85
RCA26 SERIES Electric Attitude Indicator [7]	Attitude (Bank & Pitch)	1	1	16.94 - 33.6	50
TACAN+ Navigation [8]	Position	1	2.36	32.25 - 60.2	71
Model 0861 AOA Transmitter [9]	Angle of Attack	1	1.4	57.5	N.A.
IMPERX C5180 Visual camera [10]	Vision	4	0.390	49.5	85
Fluke RSE 600 IR Camera [11]	Heat Sensor	4	1.04	22.5	50
Orion 650E Collision Avoidance Lights	Light	8	0.12	-	N.A.
Ultrasonic Level Sensor 2UF [12]	Water/Fuel Level	2	0.2	-	105
HDHCF Strobe Power Supply	Power Supply	4	0.95	98	N.A.
Lynx Multimode Radar [13]	Radar	1	37	300 - 1000	55
IMC Industries CSDL [14]	Datalink System	1	0.5	200	N.A.

[3] http://www.uavfactory.com/download/11/Combined_Pitot-Static_Datasheet_V2_0.pdf [cited 20 June 2019]
[4] http://www.aerospacelogic.com/index.php?dispatch=products.view&product_id=246 [cited 20 June 2019]
[5] http://www.aerospacelogic.com/index.php?dispatch=products.view&product_id=244 [cited 20 June 2019]
[6] https://www.kanardia.eu/product/airspeed-indicator/ [cited 20 June 2019]
[7] https://www.kellymfg.com/images/RC%20ALLEN%20Catalog.pdf [cited 20 June 2019]
[8] https://www.l3commercialaviation.com/avionics/products/tacan/ [cited 20 June 2019]
[9] https://utcaerospacesystems.com/wp-content/uploads/2018/04/Angle-of-Attack-AOA-Systems.pdf [cited 20 June 2019]
[10] https://www.imperx.com/cmos-cameras/C5180/ [cited 20 June 2019]
[11] https://dam-assets.fluke.com/s3fs-public/RSE300__umeng0000_0.pdf?WZfokdnNnTKqp2PQzuZ79piHgWBf2P4m [cited 20 June 2019]
[12] https://www.levelsensorsolutions.com/ultrasonic-level-sensor-series-2uf-c-10_4_53.html#2 [cited 20 June 2019]
[13] http://www.ga-asi.com/lynx-multi-mode-radar [cited 20 June 2019]
[14] https://www.imc-mw.com/data-link-systems-2#command-surveillance-data-link [cited 20 June 2019]

The indicators are not used to read of the information on-board, since the aircraft is unmanned, but rather to compute the parameters, send it to the antenna, which then sends it to the ground control station so that the remote pilots can read and use that information. To get an insight in the handling of data within the system and the environment, a data handling block diagram is created. This can be found in Figure 11.6.

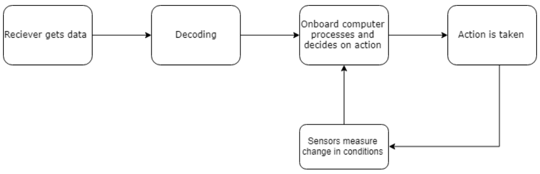

Figure 11.6: The data handling block diagram of the Wangari.

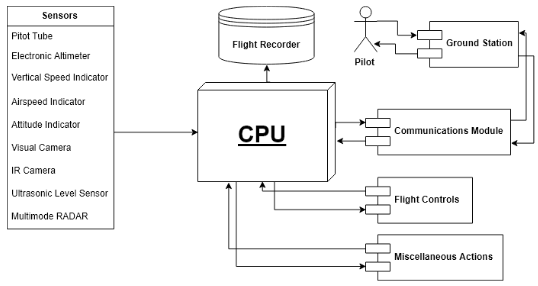

Figure 11.7: The software/hardware interaction block diagram of the Wangari.

11.4. Power System

The devices and sensors need to be powered, which is generally done by the generator in the engines. However, if the engines fail and can't deliver electrical power anymore, the devices need to be powered by a different power source. Furthermore, an additional power source is also required to start the engines. This is done by an auxiliary power unit (APU) in bigger aircraft, because batteries may not provide enough power. However, the engine chosen for the water bomber UAV does not require an APU and can be started easily by only using batteries [15]. For those reasons, batteries are included in the UAV. Different types of batteries are used in aircraft nowadays. They will be analysed and the optimal battery for the mission will be chosen and used in the UAV. The main (dis)advantages are listed below.

- **Lead-acid battery:** If lead-acid batteries are overcharged, they can sometimes vent hydrogen gas which can result in an explosion or lead to a fire. This means that the extreme conditions experienced when fighting fire are not favourable for this type of battery.
- **Lithium-ion battery:** Lithium-ion batteries can be a safety hazard since they contain a flammable electrolyte. If damaged or incorrectly charged this can lead to explosions and fires. There have been several incidents involving lithium-ion batteries on Boeing 787s.
- **Nickel-cadmium battery:** Nickel-cadmium batteries require relatively low maintenance, are reliable and have a wide operating temperature range. Besides, two nickel-cadmium batteries are used in the CL-415 air tanker and show no threat [16].

Regarding the (dis)advantages stated above, the nickel-cadmium batteries will be selected to be used in the UAVs. The properties of the battery are shown in the table below:

Table 11.2: Battery properties.

Battery	Voltage Output [V]	Mass [kg]	Energy [Wh]	Maintenance interval [h]
Ni-Cd Battery	24 DC	36	1056	200-400

Furthermore, if the battery has delivered some power, it can be recharged when power is obtained from the generator in the engines.

11.4.1. Power budget

To determine the number of batteries required, the total power required has to be estimated. Components that require power are lights, sensors, radios, the computer, flaps, control surfaces and the landing gear. Some assumptions have been made before the power estimation could start and are listed below:

- The batteries are used in case of engine failure.

[15] https://www.pwc.ca/en/products-and-services/products/regional-aviation-engines/pw100-150[cited 20 June 2019]
[16] https://aerialfirefighter.vikingair.com/firefighting/specifications/avionics-electrical[cited 19 June 2019]

- The batteries are used to power electrical systems and actuators to support an emergency landing.
- The batteries are used for an accumulated time of 5 minutes of pure actuation time for an emergency landing (moving a flap takes only a few seconds). Actuation includes moving control surfaces, retracting flaps and retracting landing gear.
- The batteries are used for an accumulated time of 45 minutes to power the devices and sensors for an emergency landing. This includes lights, sensors, radios and the computer.
- The batteries may also be used to restart the engine, one battery is assumed enough for this.
- EHAs are assumed to use $8kW$, while their maximum is $10kW$.

The total energy required equals the power required multiplied with the time active for each component. This has to be determined in order to decide how many batteries are required. As can be seen in Table 11.1, some devices or sensors have a minimum and maximum power required. In order to provide enough power for every scenario, the maximum power required is considered for each unit. This means that the maximum total energy required is equal to:

$$E_{required} = \sum P_{device} t_{operative} + \sum P_{actuators} t_{actuation} \tag{11.1}$$

The total energy required by the devices is the sum of the power listed in Table 11.1 multiplied with 45 minutes. The total energy required by the actuation system is $72kW$ ($8kW$ per actuator multiplied by 9 actuators) multiplied by 5 minutes. This results in a total energy required of:

$$E_{required} = 2233.56W\frac{45}{60}h + 72000W\frac{5}{60}h = 7675Wh \tag{11.2}$$

One battery can deliver $1056Wh$ of energy, which means that 8 batteries are required to support the devices, sensors and actuation system in case of emergency. The mass of one battery is equal to $36kg$, as stated in Table 11.2, and hence the total mass of the batteries will be $288kg$.

11.4.2. Architecture

The power sources, i.e. the generator in the engine and the batteries, will be connected to an electrical bus, which provides the power to the devices and actuators. A voltage regulator is used to maintain a constant voltage at varying engine RPM. Furthermore, an ammeter will also be utilised to know whether the batteries or the engines are providing power. Lastly, a load meter is included to be informed how much power the devices and actuators require.
A sketch of the power system is provided below to better visualise the architecture.

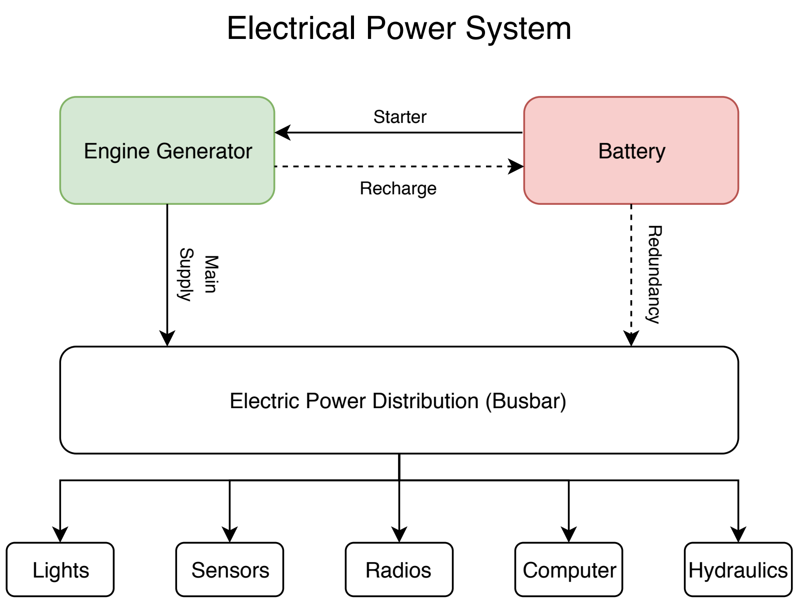

Figure 11.8: Electrical System

12
Design Integration

In a project as large as this, where many iterations are performed based on optimisations for specific parameters, the integration of all parts of the design is of utmost importance. To be able to do so in a structured manner, the group has established an 'Aircraft Parameter Database', described in detail in section 12.1. In here, the current parameters have been stated and were linked to the various code files used for calculations. Older parameters have also been kept such that the evolution of the UAV design could be tracked and unrealistic values could be spotted immediately. The parameters that were influenced by interdepartmental cooperation were found to be the c.g. location and the location of the engine. The cooperation between departments that lead to the changes in these parameters have been described in chapter section 12.2.

12.1. Aircraft Parameter Database

As the detailed design phase began, more and more parameters had to be calculated, tracked and communicated between departments, as miscommunications could have disastrous effects. Therefore, a crude yet effective database was implemented using google drive. Its implementation and usage is explained below.

12.1.1. Implementation

Google drive is free to use with an account, however it also offers an API for developers [1]. The API for the drive of the project was set up, together with a script in Python to extract the data.

Database Layout

The drive contained a large spreadsheet with a page for every department. On every page, the first two columns contained the date of change and a note on what was updated. The rest of the columns were used for storing parameters, such as lift curve slope or aircraft empty weight. Every row represents a design iteration, with trackable changes and design choices made for the changes.

Importing Script

To get the database from the cloud into the source code, a tool was made to request the drive, through the API, to return all desired data. Depending on the needs of the user of the data, different department's pages could be requested. The return of this script is a dictionary containing, for every department requested, a pandas Dataframe [2] with the most up-to-date data.

12.1.2. Usage

All of the team-members made use of the database, and it proved to be effective. Updates were sent out automatically, without having to communicate extensively for every updated parameter. An example snippet of the database from the C&S department is shown in Figure 12.1.

12.2. Design Evolution

Thanks to the database described in section 12.1, a history of all the design changes is readily available, with every iteration having an explanation for the update in parameter values. Furthermore, a date is always attached to every iteration.

12.2.1. Influential Design Parameters & Requirements

Aircraft design depends on many different parameters, however some parameters influence the overall design more than others. Furthermore, requirements are able to significantly influence the evolution of a design. Wangari was no different,

[1] https://developers.google.com/drive/api/v3/about-sdk

[2] http://pandas.pydata.org/pandas-docs/stable/reference/api/pandas.DataFrame.html

1	Date	Notes	CG_fwd	CG_aft	SM	Fuselage	Payload	NLG	MLG	Floats	Engine	Wing	Tail Config
2	13/06/19	Fuselage has heig	[4.287,10.71]	[4.294, 10.08]	0.05	[4,10]	[4.3,9.7]	[1.7, 8.65]	[4.69, 8.65, 1.38]	[3.67, 11, 8.75]	[3.7, 10.5]	[3.67,11]	Crucifix
3	13/06/19	New weights from	[4.27,10.96]	[4.29, 11]	0.05	[4,10]	[4.3,10]	[1.7, 8.45]	[4.75, 8.45, 1.38]	[3.67, 11, 8.75]	[3.7, 11]	[3.67,11.25]	H Tail - Crucifix
4	12/06/19	Changed cg water	[4.36,10.7]	[4.44, 10.9]	0.05	[4,10]	[4.3,10]	[1.7, 8.45]	[4.87, 8.45, 1.38]	[0, 0, 0]	[3.7, 13]	[3.67,11.25]	H Tail - Crucifix
5	12/06/19	Changed cg water	[4.36,10.7]	[4.44, 10.9]	0.05	[4,10]	[4.35,10]	[1.7, 8.45]	[4.87, 8.45, 1.38]	[0, 0, 0]	[3.7, 13]	[3.67,11.25]	H Tail - Crucifix
6	12/06/19	Changed cg water	[4.36,10.7]	[4.44, 10.9]	0.05	[4,10]	[4.35,10]	[1.7, 8.45]	[4.87, 8.45, 1.38]	[0, 0, 0]	[3.7, 13]	[3.67,11.25]	H Tail - Crucifix
7	12/06/19	Added landing ge	[4.18,10.4]	[4.51, 10.9]	0.05	[4.3,10]	[3.9,10]	[1.7, 8.45]	[4.94, 8.45, 1.38]	[0, 0, 0]	[3.7, 13]	[3.67,11.25]	H Tail - Crucifix
8	11/06/19	Shifted CG Back, I	[4.166,10.6]	[4.53, 11.43]	0.05	[4.3,10]	[3.9,10]	[1.7, 8.5]	[5.05, 8.5, 1.38]	[0, 0, 0]	[3.7, 13]	[3.67,11.25]	H Tail
9	11/06/19	Decided Tail Confi	[3.75,10.8]	[4.33, 11.5]	0.005	[4.3,10]	[3.8,10]	[0,0]	[0,0,0]	[0, 0, 0]	[3.6, 13]	[3.4,11.25]	H Tail
10	07/06/19	Added Empennag	[3.75,10.8]	[4.33, 11.5]	0.005	[4.3,10]	[3.8,10]	[0,0]	[0,0,0]	[0, 0, 0]	[3.6, 13]	[3.4,11.25]	Conventional
11	06/06/19	cg@ 33%	[3.75,10.8]	[4.03, 10.8]	0.005	[4.3,10]	[4,10]	[0,0]	[0,0,0]	[0, 0, 0]	[3.9, 13]	[3.4,11.25]	Conventional
12	05/06/19	cg@ 25%	[3.24, 10.8]	[3.24, 10.8]	0.005	[4,10]	[2.6,10]	[0,0]	[0,0,0]	[0, 0, 0]	[5, 13]	[2.6,11.25]	Conventional
13	03/06/19	First Update	[5.8, 10.3]	[5.8, 10.3]	0.005	[4,10]	[3.5,10]	[0,0]	[0,0,0]	[0, 0, 0]	[4, 13]	[3.0,11.25]	Conventional
14	01/01/19	Initialization of da	[0,0]	[0,0]	0.05	[0,0]	[0,0]	[0,0]	[0,0,0]	[0, 0, 0]	[0,0]	[0,0]	Conventional

Figure 12.1: Example snippet of the database

and some of the key parameters and requirements that influenced the design will be discussed here, together with the changes made to the design as a result.

C.G. location

The c.g. location influenced nearly every single department, however the C&S and Hydrodynamics departments were dependent on the c.g. value the most out of all departments. Hydrodynamics needed the overall c.g. at a forward position for buoyancy, while C&S required the overall c.g. to be close to the a.c. and not have the c.g. range to be minimal during all operations. With both of these requirements together, stabilising the aircraft was quite the challenge. The evolution of the forward c.g. is visualised in Figure 12.2. The x-coordinate is measured from the nose, and the y-coordinate is measured from the hull centreline.

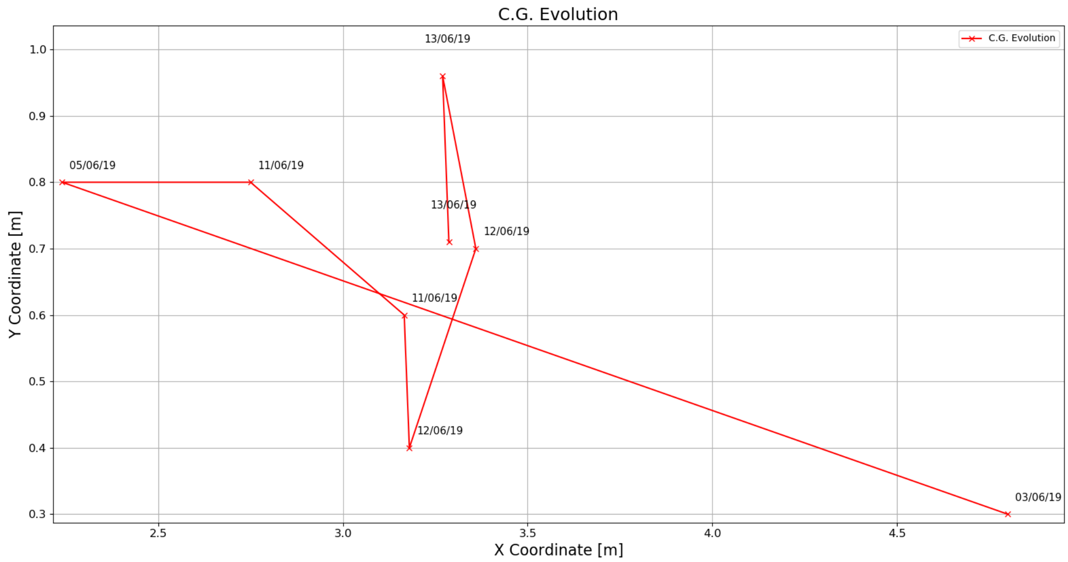

Figure 12.2: Evolution of the c.g. over time

This figure plots the (x, y) position of the forward c.g. for every update, with the dates attached to every iteration. The data corresponds to the values for the forward c.g. column in Figure 12.1.

Engine & Propeller Location

- Prop wakes for empennage - C&S
- Higher CL value for wing - Aero
- Not touching water with blades - FPP
- Lowering Pitch down moment - C&S

The engine location changed the most out of all component positions, since in the initial design concept, the engine was envisioned to be in the tail. However, it became clear very quickly that that was not feasible due to the c.g. constraints laid out by the hydrodynamics department as explained in section 10.3. Therefore, the engine was positioned above the wing to ensure the c.g. is positioned more forward. However, also this was not possible in the end due to the propeller diameter required being too large to have the propeller on top of the fuselage without having a very large pitch-down moment. This pitch down moment would have increased the empennage sizing considerably. Finally, after a certain amount of iterations, it was decided to put two propellers in the wings. Both propellers would be powered by the same engine using drive shafts.

This design choice was ground breaking, as it did not only guarantee a smaller pitch-down moment, but it also allowed for the horizontal tail to be positioned in the wake of the propellers and therefore have a larger effective air velocity, reducing the minimum required surface area. Furthermore, it was essential for the aerodynamics department to have the higher effective air velocity over the wing to obtain the required C_L for the aircraft.

Transportability Requirement
Arguably the requirement influencing the design to the greatest extent was the requirement on transportability. The transportability requirement severely limited the size of the Wangari, and therefore a lot of parameters influencing Wangari's performance. The wing span, chord and thickness were limited as well as the fuselage width and height. Furthermore, the horizontal stabiliser was also limited in span and geometry due to the sizing constraints. Therefore it was decided to make both the wings and the horizontal tail planes detachable, as explained in subsection 10.2.6. Finally, the fuselage had to be adapted by making the fuselage slanted downwards in the back of the aircraft, to have the vertical stabiliser fit inside the A400M, as another detachable surface was not desired. This is better visualised in Figure 10.45.

12.2.2. Inter-Departmental Cooperation
For the most of the major design choices the different departments all have a part in choosing what happens, as it affects all of them. The interaction between these departments will be discussed in this part.

Amphibious stability and controllability
The amphibious stability is dependent on the the hull shape as well as on the sizing of the empennage. When moving slowly on the water, the hull is largely responsible portion of the stability and controllability. Once the speed of the Wangari increases, the wing and tail get a bigger part in the control and stability. The combination of hydrodynamic and aerodynamic properties are illustrative for the interaction between the hydrodynamics and control and stability departments. The hydrodynamic department provided the centre of buoyancy, resulting from the c.g. and shape of the hull of the UAV. This centre of buoyancy is then used for assessing the controllability and stability on the water, and sizing the horizontal tailplane to be controllable and stable. Which then results in a new c.g., again used to determine a new centre of buoyancy, resulting in a new horizontal tailplane size.

Stability and control curves
The C&S department is responsible for the stability and control curves. However, these curves is merely the result of the properties of the aircraft dictated by the other departments. For example the choice of the type of tail has a big effect on the curves, not choosing a full moving tail would shift the curves up, requiring a way bigger horizontal stabiliser. Also the structural changes result in a new c.g. locations, just like the replacement of components by FPP or operations. Most of the updates would require the C&S department to redo all the calculations for the c.g, and therefore the horizontal stabiliser. This would in turn influence the aerodynamic and overall performance of the aircraft, changing the c.g. and therefore amphibious properties, which would have to be redone. Close communication between the C&S department and all other departments is thus crucial.

Aerodynamic and hydrodynamic drag
For the design of the hull both aerodynamic and hydrodynamic properties have to be taken into account. The biggest result of this is the step in the hull. This greatly reduces the hydrodynamic drag, but increases the aerodynamic drag. This has been designed in such a way, that the optimal shape for both use cases has been achieved.

Wing design
The wing has to be designed to generate enough lift to be able to fly and perform all desired manoeuvres. However, the structure inside the wing also needs to be able to withstand all the loads acting on the wing. For both departments, geometry is of high importance. Both departments had to update one another on new parameters, especially regarding geometry of the wing and airfoil. Next to the geometry of the wings the floats at the end of the wing had to be taken into account. Especially seeing that at first there was the idea of combining floats and winglets together in one. For this there

mainly was communication between the hydro department and the aerodynamics department to optimise the buoyancy provided and the aerodynamic performance of the wing. When aero and hydro came to a conclusion, the result was checked by structures to see if the construction would be feasible.

Propulsion unit placement
For the placement of the engine as well as the propeller(s), the Flight Performance & Propulsion department had to work together close with both the aerodynamics and the C&S department. The engine makes up a significant portion of the weight and therefore very influential over the c.g as mentioned in Figure 12.2.1. Furthermore, the aerodynamics department had to design for a certain lift coefficient. This could only be achieved by placing the propellers in front of the wing, causing a part of the wing to be in the wake of the propeller. For all these iterations, all departments had to communicate closely and at a regular basis. The database created allowed for easy and automatic transfer of design parameter values, however it did not warn the user about changes in the database, and therefore every change still had to be communicated to a certain extent.

13
Operations and Logistics

All aircraft operations require an immense amount of planning and killed labour to be able to operate efficiently and safely. Therefore, a plan for all operations regarding ground operations, transportability, maintenance and governmental regulations of the product need to be assessed and planned out, since without these planned operations, operating Wangari would not even be possible.

13.1. Ground operations

Ground operations encompass all tasks needed for the preparation of the system for a mission. This includes the setting up of a ground station as well as making Wangari mission ready.

The ground station that is used is shown in Figure 13.1. It is an advanced cockpit ground control station, which is designed to remotely pilot unmanned aerial vehicles. It offers increased situational awareness and reduced pilot workload [1]. The ground control station only requires electrical power and a base where it can be set up in order to operate in an efficient manner. Because the essential parts of this system are the computers, the monitors and the software, the control station is likely to be transported by an A400M, even with two Wangari UAVs loaded in it. This is a great advantage, since in this way the whole swarm system can be transported fast by the cargo aircraft. Furthermore, the ground station needs to have all the communication systems and interfaces ready before the mission can begin. Setting up the communication system would also include determining, before the mission begins, whether an intermediate link needs to be made between the ground station and the UAVs. If so, the appropriate actions must be taken to ensure connectivity. If this is not possible to do, sending up a communications link with the aerial attack, sending a communications relay with the ground crew or setting up a satellite link are possible solutions.

Getting Wangari mission ready is also part of ground operations. This might include refuelling, refilling the retardant tank, booting up Wangari's communication systems and temporary storage of Wangari inside hangars.

Figure 13.1: Ground station

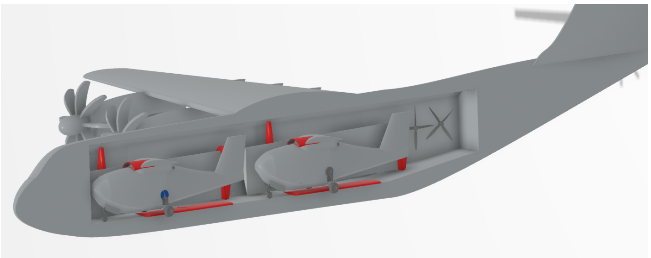

Figure 13.2: Two Wangari UAVs transported in an A400M

[1] http://www.ga-asi.com/advanced-cockpit-gcs[cited 28 June 2019]

13.2. Transportability

Being able to transport multiple UAVs was a major design aspect for Wangari, as it would offer easy access to many more regions around the globe, and this would allow for easier sharing of the Wangari System between nations.
The way the UAVs will be transported is pictured in Figure 13.2. Two Wangaris will fit inside one Airbus A400M, with the wings, horizontal stabilisers and the propeller blades fully detachable and able to be stored beside the UAVs, with space left for ground control system equipment.

For preparing the Wangari for transport, the transport team will first empty out the fuel tanks, in case any was left inside. After the emptying of the fuel, the drive shafts from the engine to the propellers need to be detached, together with the propeller blades. Hereafter, the main wing needs to be detached with a lifting tool, since half a wing weighs 553 kg and needs to be stored inside the cargo aircraft. Following the main wing, the horizontal stabilisers are also detached. One side of the horizontal stabiliser weighs 43.25 kg, which could be manageable by just manpower, however a lifting tool would ensure no man-made damages would be inflicted. The aircraft is then pulled into the transport vehicle with its landing gear extended. This can be done using manpower and enough pulleys, to make sure the tractive force is not too high. After this, the UAV is fastened to ensure the aircraft cannot tumble around in the cargo bay. This process is repeated for the second UAV. For the unloading of the UAVs, the reverse procedure applies.

13.3. Maintenance

Because the mission the UAV performs is not an ordinary mission, Wangari requires a specific sort of maintenance next to the regular inspection. First of all, the aircraft is amphibious, which means that damaging chemical reactions between the water and the hull can occur, especially in the case of missions at coastal areas. A special form of coating is used to reduce effects of potential acidity or alkanility, which needs to be inspected often and repaired if necessary. Furthermore, because the hull is made out of a composite material, the UAV is not extremely susceptible to corrosion. However, corrosion can still occur at the metallic parts of the aircraft, thus inspection for this still needs to occur on a regular basis. Secondly, Wangari experiences high load factors when dropping retardant, which means that it is susceptible to cracks and fatigue. The fact that the wings and horizontal tail are detachable requires the connection bolts to be checked on a regular basis. Lastly, all foam concentrates in the retardant tank have a detergent base. Therefore, cleansing of all plumbing, pumps, tanks, and other exposed surfaces can be expected. This may promote the corrosive actions of water.
Further detail and a more extensive analysis concerning maintenance of the Wangari system is done in chapter 16.

13.4. Regulations

Because the system concerns firefighting and will be deployed to reduce emission of greenhouse gases and to promote safety, it will most likely be possible to request a temporary flight restriction (TFR) for airspace surrounding the wild fire, as is already done for current aerial firefighting missions today [2]. It is extremely important that no other aircraft intrude this space for safety reasons. Regulations concerning unmanned aerial vehicles is generally defined by the national aviation authority of the country and is different for most countries. In the USA, to operate a UAV for non-recreational purposes, the user(s) must obtain a "Certificate of Authorisation" to operate in national airspace. The authorities of the USA may permit the use of UAVs for commercial or business purposes in response to individual exemption requests [60].

[2] https://www.aopa.org/news-and-media/all-news/2017/september/14/wildfire-ahead-check-for-a-tfr

Part III

Project Evaluation

14 Mission Compliance

As defined in chapter 3, the mission of this DSE project was to "tackle the need for a safe and strategic aerial firefighting system" by means of designing "a UAV system that can more safely and strategically attack wildfires" and to do so "within ten weeks by ten students". To assess to what extent the mission and objective have been met, the entire design is evaluated in this chapter in terms of safety and strategy. Due to its unmanned nature and inherent stability, Wangari is found to be a safe design. Wangari's swarming water bombing capabilities during both daily and nightly operations allow for a strategic firefighting tactic whilst also being cheaper than the current competition. However, to give a fair assessment of the mission compliance a sensitivity analysis is added.

14.1. Safe

As became apparent from Figure 4.1, Wangari's mission profile is much more dynamic than that of regular aircraft due to the dangerous manoeuvres performed in aerial firefighting. Not only the manoeuvres of the UAV during and scooping and dropping increase the danger but also the more extreme thermal gusts it has to withstand. Designing for this specific mission has already made Wangari safer to operate than most firefighting aircraft currently in the air, which are often converted and exceed their flight envelopes [61]. The flight envelope [as given in figure INPUT]of Wangari has been properly analysed for both wind and thermal gusts as well as the dangerous firefighting manoeuvres and the wing has been designed to withstand all load factors within the envelope.

Over several design iterations the team has managed to size the tail, hull and auxiliary floats such that stability is guaranteed at every stage of flight and during water operations making it a particularly safe design.

Furthermore, Wangari has been designed under a safety philosophy in which fail-safe and safe-life approaches have been combined. For example, actuation mechanisms have been made fail-safe by creating redundant systems, and safe-life requirements have been set for harder to repair elements. This is described in more detail in chapter 16.

14.2. Strategic

To be a strategic purchase for the customer, Wangari should both be strategic in terms of containing fires better than current alternatives and strategic in terms of being more cost effective than the current alternatives.

Firefighting Effectiveness

The effectiveness at which Wangari is able to fight fires is greatly improved by innovative aspects of the design which include its ability to swarm, execute nightly operations and perform passively pressurised drops. Based on the fire simulation explained in chapter 9, the strategy of a swarm of Wangaris is optimised to fight fires in the most efficient manner by laying containment lines. Due to their small size and high cruise speed the UAVs are able to quickly access small bodies of water and return to the fire to lay more lines, minimising the spread of the fire. Due to the [devices/sensors bladibla] and unmanned nature, Wangari is able to fight the fire not only during the day as current firefighting aircraft do but also during the night. This greatly increases the efficiency of the missions as firefighting at night is more effective as wind speeds and temperatures are lower [3]. Consequently, its ability to perform nightly operations will not only increase the number of litres it can drop per day but also greatly increase the acres saved from wildfire. The passive pressurised drops, made possible by the unmanned state, enable Wangari to be even more efficient as no heavy and costly pressurising system is needed to control the drop flow.

Cost Effectiveness

At this stage of the design it is hard to verify the cost effectiveness as the exact cost of the manufacturing of components can only be estimated. The preliminary cost analysis, as presented in detail in section 19.1, shows that one Wangari UAV, assuming that 60 UAVs will be produced in a 5-year period, costs approximately 10.6 million euros. This gives the

Wangari system a great advantage given that for the cost of its main competitor, the CL-415, two Wangaris are capable of providing up to 1.5 times the payload. The transportability of the design also enables customers to ship the UAV in a cheap and sustainable manner. Lastly, the operating costs are less in comparison to the CL-415 as piloting cost are lower.

14.3. Sensitivity Analysis

To fairly asses the mission compliance a sensitivity study is performed to gauge how realistic the design is and to see how the design is affected should changes be made. The evolution of the c.g. described in section 12.2, and the different solutions of acquiring the required C_L of 3.0 as described in subsection 10.2.3 and subsection 10.2.4, already show a sensitivity analysis that has been performed as part of the design iteration.

Sensitivity of the UAV to c.g. shifts

The first sensitivity analysis that was performed is aimed to gauge how sensitive the layout of the aircraft is to a shift in c.g.. This analysis was included in the design of the stability of the aircraft. The change in c.g. that the UAV underwent is visualised in Figure 12.2. This can have significant effects on, for example, the horizontal tail plane size, as can be deduced from section 10.4. Besides having an effect on the sizing of the empennage, the c.g. location also influences the hull design as can be read in subsection 10.3.4. The third aspect that makes the design of Wangari sensitive to a c.g. shift is the fact that the payload is dropped, meaning that the UAV loses 33% to 50% of its payload within seconds. The difference in c.g. this causes has to be counteracted by the horizontal tail to keep the UAV stable, which was a key qualification of the more safe firefighting design generated.

Sensitivity of the propeller layout

The second sensitivity analysis which was performed during this design iteration was performed by the aerodynamics department and concerns the various ways of reaching the desired C_L of 3.0. In this analysis, the options of introducing complex HLDs, and placing the propellers on the wing to increase lift were explored. The first of these options would create a design very sensitive to changes in C_L required. To elaborate, when the HLD solution is chosen the maximum lift for the current engine and propeller placement is reached. Therefore, when a higher C_L is needed the whole design would have to be changed. On the other hand, when placing the propellers on the wing, an increase in required C_L can more easily be achieved by adding more complex HLD types. Changing HLD has a smaller impact on the design in later phases compared to changing the location of the propulsion system and is hence the chosen option.

Sensitivity of the current design

For the current design the sensitivity is tested in terms of changes in the MTOW, because of the fact that most design changes or uncertainties result in an increase in weight of the UAV.

First the flight performance changes due to an increase in MTOW are assessed. From the curves in (ref to Flight performance graphs) it can be seen that an increase in MTOW results in both the wingloading and the power loading (W/S and W/P) grow larger. In case nothing else is changed about the UAV this could result in the UAV not meeting the stall speed requirement, climb rate, and the take-off and landing requirements. This in turn would have an impact on the firefighting performance of the aircraft. A lower stall speed means a lower efficiency when dropping, and the climb rate, take-off and landing performance has an impact on the time between dropping cycles.

To prevent the reduction of performance changes have to be made to the aircraft. For example to accommodate for a higher weight the $C_{L_{max}}$ can be increased such that the wing loading vs. power loading curves shift to make sure that the design can still reach its performance parameters. The downside of changes like these is that they are almost always accompanied by an increase in weight setting into effect a snowball effect, which is why it is hard to actually perform the sensitivity analysis. Next to paying attention to meeting the performance parameters, also extra attention should be paid to the potential shifts in c.g. these changes could cause, as this was determined to be critical in the previous paragraph.

15 Requirement Compliance

In order to clearly identify which design requirements have been met, compliance matrices are presented here in which the requirements and their verification methods (column titled 'VM' in the table) are shown. The definition for the verification methods is as follows[1]:

- A - Analysis: The requirement is verified using a model and calculations generating a predictive statement of the system behaviour.
- D - Demonstration: The product can be manipulated in order to verify that it fulfils its intended purpose and the results are as planned.
- T- Test: The requirement is verified by giving a specific set of inputs set to produce a specific set of outputs as specified by the requirement.
- I- Inspection: It involves the non-destructive examination of a product using one or more of the five senses.

In the case where two or more verification methods are considered as acceptable, this is also specified in the table. Within the 'check' column, satisfied requirements are shown with a tick whilst those non-satisfied are shown with a cross. A dash represents a requirement which has almost or only partially been met. The requirement abbreviations can be found in section 4.3. Here as well, some requirements have been identified as either killer, driving or key. Requirements labelled with a dash in the 'type' column have been determined to not belong to any of the three previous categories. The requirements have been split up into six overarching sections under which there will be a brief explanation on some of the main requirements which have not been met or for which there is some uncertainty. Performing such an analysis will also help the team within the next step of the design process by identifying the main areas of improvement and analysing some of the impacts of a non-satisfied requirement on the design.

Ground Operations

Reference	**Requirement**	**Type**	**VM[2]**	**Check?**
AF-GRND-01	The UAV shall be mission ready in one hour	Key	D	✓
AF-GRND-02	The UAV shall be able to taxi on an EASA licensed airfield	-	D	✓
AF-GRND-03	The fuel tank of the UAV shall be filled with standardised fuel pumps	-	D	✓
AF-GRND-04	The UAV shall refill on firefighting substances at a rate of 15 kg/s	-	D	✓
AF-GRND-05	The UAV shall be able to taxi on water	-	D	✓

Table 15.1: Requirement compliance for ground operations

As a general note for ground operations, although all these requirements can only verified through demonstrations, they have been directly designed for and are thus considered met. Building a prototype and checking that these indeed hold and the aircraft performs as intended is considered to be part of the validation process.

[1] https://www.modernanalyst.com/Careers/InterviewQuestions/tabid/128/ID/1168/What-are-the-four-fundamental-methods-of-requirement-verification.aspx

[2] Verification Method

Flight Performance

Reference	Requirement	Type	VM	Check?
AF-PERF-01	The UAV shall have a stall speed lower than 120km/h	Driving	A/T	-
AF-PERF-02	The UAV shall have a minimum range of 1000km	Key	A/D	✓
AF-PERF-TO-01	The UAV shall be able to take off on water	Key	D	✓
AF-PERF-TO-02	The UAV shall be able to take off on land	Key	D	✓
AF-PERF-TO-03	The UAV shall be able to take off within 500 m on land at sea level conditions	Key	A/T	-
AF-PERF-TO-04	The UAV shall be able to take off within 500 m on water at sea level conditions	Key	A/T	-
AF-PERF-TO-05	The UAV shall have a payload that is at least 30% of the MTOW	-	D	✓
AF-PERF-TO-06	The UAV shall have a minimum climb rate of 10 m/s at MTOW	-	A/T	✓
AF-PERF-TO-07	The average fuel consumption of the fixed wing UAV shall be lower than 840 l/h	-	A/T	-
AF-PERF-TO-08	The UAV shall be able to climb under an angle of 10° whilst taking off with MTOW from water.	-	A/D	✓
AF-PERF-TO-09	The UAV shall be able to climb under an angle of 10° whilst taking off with MTOW from land.	-	A/D	✓
AF-PERF-LND-01	The UAV shall have a minimum descent rate of 10m/s	-	A/T	✓
AF-PERF-LND-02	The UAV shall have a maximum landing distance of 800m at sea level conidtions	Key	A/T	✓
AF-PERF-LND-03	The UAV shall be able to land on ground	Key	D	✓
AF-PERF-LND-04	The UAV shall be able to land on water	Key	D	✓
AF-PERF-LND-05	The UAV shall be able to descend with a minimum angle of 5° with MTOW.	-	A/D	✓
AF-PERF-CRUS-02	The UAV shall have a cruise speed of at least 300km/h	Key	A/T	✓
AF-PERF-MAN-01	The UAV shall be able to sustain load factor of between 4g and -1g	Key	A/T	✓
AF-PERF-MAN-02	The UAV shall be able to turn with a bank angle of 45 degrees	-	A/T	✓
AF-PERF-MAN-03	The UAV shall be able to turn with a radius less than 250m	-	A/D	✓
AF-PERF-MAN-04	The UAV shall be able to turn 180 degrees within 35 sec with MTOW	-	A/T	✓
AF-PERF-MAN-05	The UAV shall be able to turn 180 degrees within 20 sec with OEW+FUEL	-	A/T	✓
AF-PERF-MAN-06	The UAV shall be able to approach the fire within 30m altitude	-	D	-
AF-PERF-STAB-01	The UAV shall be stable during retardant dropping	-	A/D	✓
AF-PERF-STAB-02	The UAV shall be stable in the wake of fire gusts	-	A/D	-

Table 15.2: Requirement compliance for flight performance

Within flight performance, most of the requirements have been verified by analysis. There remain however some which have been only partially or almost met. The reasons for this and effects on the design are as follows:

- **AF-PERF-01**: The current prediction on the achievable stall speed is $123.5 km/h$. This comes very close to the goal and has minimal impact on the line laying performance during dropping. According to the aerodynamic analysis presented in chapter 10, a slightly higher lift augmentation may still be met such that this requirement could still be easily achieved in the next design iteration.
- **AF-PERF-TO-04, AF-PERF-TO-05**. The current estimation for landing and take-off on water lies at $560m$, with a $C_{L_{max}}$ of 3.0. Just like the previous, this requirement may easily be met in the next design iteration by optimising the aerodynamic interaction between the propeller and the wing. Additionally, the $60m$ extra is expected to have minimal impact on the airfields and water bodies accessible by the aircraft.
- **AF-PERF-MAN-06**: Throughout the design process, it was determined that the best altitude to fly at is over $30m$. Although it is possible to fly at this altitude, it is not actually necessary. Hence, in the future design steps this requirement may indeed be scrapped or changed to what was found to be a more ideal value of $45m$[12].
- **AF-PERF-STAB-02**. The stability in the wake of the fire gusts was not fully considered at this stage. Wangari is however designed to sustain extremely high loads due to the sharp manoeuvres it needs to perform, especially during the dropping manoeuvre. After an initial literature study [7] and having drafted Wangari's flight envelope, it was concluded that the expected loads due to the fire gusts lie within the UAV's flight envelope. Hence, although an investigation should still be done with regards to the controllability and stability in the fire, it may at this stage not be crucial to the design.

Scooping and Dropping Performance

Reference	Type	Requirement	VM	Check?
AF-PERF-BMB-01	The UAV shall be able to deploy the entire payload in a single drop	Key	A/D	✓
AF-PERF-BMB-02	The UAV shall be able to carry out controlled drops	Key	A/D	✓
AF-PERF-COLL-01	The UAV shall have a retardant capacity of at least 4500 L	Key	D	✓
AF-PERF-COLL-02	The UAV shall be able to scoop up 4500L of water in one single pass	Key	A/D	✓
AF-PERF-COLL-03	The UAV shall be able to scoop up water from water surfaces that are at least 1 m deep	Key	A/D	✓
AF-PERF-COLL-04	The UAV shall be able to scoop up water from water surfaces that are at least 30 m wide	Key	A/D	✓
AF-PERF-COLL-05	The UAV shall be able to land on waters with wave heights up to 25 cm	-	A/D	✓
AF-PERF-COLL-06	The UAV shall have a buoyancy of 1.8*MTOW	-	A/D	✓
AF-PERF-COLL-07	The UAV shall be able to turn while on water	-	D	✗

Table 15.3: Requirement compliance for scooping and dropping performance

With regards to the scooping and dropping performance, the one requirement which has not been considered met is **AF-PERF-COLL-07**. It is not necessarily difficult to have the UAV successfully taxi on the water, however this water rudder sizing has not been considered within this report and will be a subject of the next design iteration.

Structures and Materials

Reference	Requirement	Type	VM	Check?
AF-STMAT-MAT-01	The UAV shall be able to withstand temperatures of up to 130 degrees Celsius	Key	T	-
AF-STMAT-MAT-02	The UAV shall have a lifetime of at least 20 years	Key	A/T/I	-

Table 15.4: Requirement compliance for structures and materials

The following can be said for the two primary structures and materials requirements:

- **AF-STMAT-MAT-01**: The materials themselves have been chosen to withstand temperatures of at least of 130°C. However, for the UAV as a whole some aspects have not yet been considered. The sensors for example, will not function at this temperature and an analysis has not yet been done on how these should be protected and how much additional cooling should be required. Should an additional cooling system be required, ths will be developed in the next design stage. This requirement could be simply verified via testing by subjecting the onboard electronics to the expected encountered temperatures.
- **AF-STMAT-MAT-02**: This requirement is difficult to verify. Although an analysis can be done using the fatigue life of the materials based on a current expected number of flights, it is difficult to predict these at this stage. Only throughout the development process, when the number of flights is better estimated, can this requirement be classified as met based on either a predictive analysis, testing or inspection. An inspection may be best in this case, as many of the materials such as the Aluminium in the wings visually show the first signs of fatigue at the surface. Finally, according to the above, in the next design iteration, this requirement should and will be better formulated in terms of flight hours/cycles instead of number of years.

Communications

Reference	Requirement	Type	VM	Check?
AF-CMM-01-A	The UAV communication with air attack shall be uninterruptable by smoke	Key	D	✓
AF-CMM-01-B	The UAV communication with other UAVs shall be uninterruptable by smoke	Key	D	✓
AF-CMM-01-C	The UAV communication with ground control shall be uninterruptable by smoke	Key	D	✓
AF-CMM-02	The maximum control time delay between the pilot and the UAV shall be less than 100ms	Key	T	✗
AF-CMM-03	The range of the signal of the UAV shall be equal to or greater than the half the range of the UAV	Key	D	✗
AF-CMM-04	The UAV shall receive the position of all active UAVs at least every 100ms	Key	A/T	✓
AF-CMM-05	The UAV shall receive the velocity of all active UAVs at least every 100ms	Key	A/T	✓
AF-CMM-06	The UAV shall be able to maintain communication with all other active UAVs during the mission	Key	D	✓
AF-CMM-07	The UAV shall be able to fly autonomously towards the base in case of signal loss, until a signal is found	Key	D	✗
AF-CMM-08	The UAV shall be able to fight the fire at any time of the day	Key	D	✓

Table 15.5: Requirement compliance for communications

For communications, the following requirements have not been met due to the following reasons:

- **AF-CMM-02**: The datasheet of the datalink system states that the time delay is less than 120ms as opposed to 100ms. This will however have minimal impact on the performance of the mission, hence in the future instead of changing the onboard equipment, this requirement may simply change to match the achieved value.
- **AF-CMM-03**: The final ferry range of the UAV is 5617km. The communications data sheet however specifies a maximum range of 250km. Clearly this requirement cannot be met. However, this does not mean to say the UAV will never be able to attain this ferry range as long as it can use different ground stations along the route.
- **AF-CMM-07**: Such a system has not been developed or properly implemented in this design iteration therefore it cannot be stated that this requirement has been met. Such an autonomous system will be a main subject of the next design iteration.

Transportability, Safety, Sustainability and Cost

Reference	Requirement	Type	VM	Check?
AF-TRNS-01	Two UAVs shall be able to fit in an A400M	Driving	A/D	✓
AF-TRNS-02	The UAV shall be loaded onto an A400mM within <tbd> minutes	-	D	✗
AF-SH-SFE-01	The UAV shall be able to detect ground crew and bystanders	Key	D	✓
AF-SH-SFE-02	The UAV shall be able to autonomously avoid ground crew and bystanders	Key	D	✓
AF-SH-SFE-03	The UAV shall be able to autonomously avoid other UAVs in formation flying	Key	D	✓
AF-SH-SFE-04	The UAV shall adhere to AEP-4671 regulations	-	D	✓
AF-SH-SFE-05	The UAV shall comply with flight safety regulations	Key	D	✗
AF-SH-SFE-06	The UAV shall avoid restricted airspace during autonomous flight	Key	D	✓
AF-SH-SFE-07	The frequencies used in the communications shall be compliant with local government regulations	-	A	-
AF-SH-SUS-01	The UAV shall not produce more than 70 dBA of noise	Killer	D	✗
AF-COST-01	A single UAV shall have a maximum cost of 20m dollars (based on 1/3 CL-415)	Driving	A/D	✓

Table 15.6: Requirement compliance for transportability, safety, sustainability and cost

For transportability, safety, sustainability and cost, the following can be said about the requirements:

- **AF-TRNS-02**: This may be a very important aspect in order to enhance the UAV's quick deployability. On the other hand, it is difficult to estimate a value for at the moment. A value for <tbd> will be in the future possibly determined from additional research and literature for existing aircraft using a smililar detachability system and then scaled to the design. The requirement may however only be met through a demonstration in which the UAV may be taken apart and loaded.
- **AF-SH-SFE-05**: As not all safety regulations have been looked into, it cannot yet be said that the design satisfies all. Thus, this requirement has not been met and is part of the further work for operations in the next design stage.
- **AF-SH-SUS-01**: As this is a fire fighting emergency vehicle, the noise aspect has not been considered as a primary concern for the design and it indeed has also not been met. Of course this requirement (although taken directly from the user) will need to be discussed and changed as it is not coupled with a specification on the distance at which this noise level holds.

16
RAMS and Sustainability Analysis

The parameters Reliability, Availability, Maintenance and Safety (RAMS) are crucial for the quality of a system. To assess this, a RAMS analysis is done. This analysis discusses the parameters above for the design of the Wangari. To assess the impact of the system on the environment, an analysis of the sustainability of the system is also provided.

16.1. Reliability

For the reliability of the aircraft the major design choices were looked at, and the risks they pose were taken into account. A slightly optimistic approach has been taken with regards to the risks, it is assumed that, for the reliability of the Wangari UAV, all the risks related to uncertainties in the design due to calculations that were not finished or due to lack of real world validations will be resolved.

Reliability of the drivetrain
Failure of the drivetrain would be catastrophic for the mission. Especially, seeing that the UAV regularly flies at low altitudes or is performing manoeuvres, for example to aid the dropping performance, that could be dangerous in case of a loss of propulsion. Next to this, the risk of a failure in the drivetrain is increased due to the way it is designed with one engine and drive shafts leading to two different propellers. To mitigate the risk of a complete loss of propulsion when one propeller is blocked, a differential was added to the drivetrain such that the other propeller can still provide thrust.

Reliability of the wing and its subsystems
The reliability of the wing in terms of aerodynamic performance is quite high. This high reliability is estimated due to the fact that the HLDs selected are the simplest forms of HLDs, there is not much that can fail. Next to this when aerodynamic performance is lost due to one propeller breaking, the wing still produces enough lift to fly back to base and to safely land the UAV.

Structurally seen, there is a little more risk in the wing. The connection of the wing creates a complex structure so it is more prone to failure. However, with the extra safety factors that are applied and when thorough inspection is applied to the connection there should not be a too large decrease in reliability of the wing. The same goes for the horizontal tail structure.

Reliability of the hull
The hull of the UAV is a critical component in terms of reliability. There are a lot of things in the hull that can go wrong, however already quite some measures have been taken to reduce these risks. First of all, there is the permanent performance decrease when water is absorbed into the sandwich core material. The increase of OEW due to this will decrease the performance of the UAV. To mitigate this, an aramid fibre layer has been added to the composite hull to increase the impact toughness of the hull preventing possible leaks. Next to leaks caused by impact damage also damage to the windows for the cameras and reduce their visibility. The reduced visibility can severely impact the mission performance, however, there is a redundancy in cameras to prevent failure of the mission.

Reliability of the landing gear
Seeing that the UAV uses a fairly simple landing gear, no high impacts on the reliability of the landing gear are expected. The only potential problem identified in the design of the landing gear was a c.g. shift that is big enough to either put too much or too little weight on the nose wheel making the UAV uncontrollable while taxiing. However for this c.g. shift to happen something would have to break-off or something else of catastrophic impact would have to happen in which case it would be optimistic to say a landing is even possible.

Reliability of the instruments
Normally, the reliability of the instruments is a number of operational hours the manufacturer provides. Due to the en-

gine which is placed in the fuselage, however, this number of operational hours may be incorrect. Because the vibrations and/or the temperature of the engine may influence the performance, reliability, and longevity of the instruments. Also no mitigation strategy has been thought of yet, and therefore, for future design this is one of the most important points to improve upon.

16.2. Availability

In terms of availability, it is most important that the UAV is available during the fire-season. The fire-season is, however, moving to a year-round period instead of a certain season which increases the necessary availability. One way the required availability can be more easily met is due to the transportable aspect of the UAV. For example, should there be a high chance of a wildfire occurring somewhere not in range of the current home base of the UAV, it is possible to preemptively move extra necessary UAVs there to match the need of firefighting aircraft at the location at risk. The challenge in having a high availability is aligning it with maintenance. As will be discussed in the next section, the maintenance of some critical parts is intricate, meaning that scheduled inspections and maintenance should be planned wisely for times when no wildfires are expected.
A side effect of the wings being detachable is that they are also easily replaced. This could in turn increase the availability of the aircraft due to it being easily repaired, as long as the supply of new wings does not take too long.

16.3. Maintainability

Maintenance of the hull
Whilst designing the hull the maintenance necessary to keep the hull operation ready was aimed to be kept at a minimum, by for example adding a aramid layer to the outer composite skin of the sandwich panel to increase the impact resistance of the hull. The main inspection and possible maintenance that should be done regularly is the checking of the coating on the hull. Since this coating protects the composite skin from acids, alkalis and from water being absorbed into the laminate. Next to this, the hull should also be checked for impact damages and potential leaks, and be repaired by a lap repair joint when necessary. In terms of performance it is important to try and keep leaks to a minimum. Whilst the UAV is still buoyant when there is a leak in the hull it does increase the empty weight of the UAV because water is absorbed into the core of the sandwich panel.

Maintenance of the wing and its subcomponents
The wing is a critical component of every aircraft and, therefore, should be well maintained. For the wing of Wangari, the bolts used in the connection of the wing to the fuselage are the most important components to keep in good condition. The inspection interval necessary is still to be determined, however, as the most critical components in the system are the bolts used to keep it together and those are relatively cheap. It may, therefore, be wise to replace them when the calculated fatigue life of the bolts is getting near its end and take a safety margin on this time. Another maintenance strategy to apply to the connection of the wings is the overhaul maintenance strategy [62], where all components of a certain type are checked when the aircraft is brought in for repair of a single one of them. So for the case of the bolts, when one of them fails, all the other bolts are also checked for signs of fatigue and if necessary preemptively replaced. This strategy could also be applied to other parts of the aircraft where there are multiple similar components. This reduces the availability, however, it should, if done correctly, reduce the amount of times that the UAV has to be send away for maintenance, meaning that over time it could increase the availability of the UAV. Another critical part to inspect frequently at the detachable system of the wing is the nacelle that covers the bolts. Possible penetrated water could cause corrosion which would rapidly decrease the structural integrity.

Besides the inspection of the detachment part of the wing, of course also the wing itself should be inspected for potential damage, either due to fatigue of due to impact, or any other unforeseen circumstances. Small damage to the wings can be repaired, and should bigger damage occur either due to unforeseen circumstances or because the wing is near the end of its life, the wing could be send in for repair or a new wing could be attached. Next to inspection for regular damage to the wing structure it is also very important to check for damage in the coatings applied to the wing as they prevent corrosion, which would be detrimental to the structure.

Furthermore, for all actuators and other moving parts a regular inspection interval can be introduced to decrease the likelihood of the actuators and other moving parts failing during flight. The main parts to be looked at are the actuators of the ailerons, the actuators of the floats, and the propulsion system (driveshaft, gearbox, and propeller).

Lastly, the fuel system in the wing should be inspected and maintained. Since fuel bladders are used, replacement of one of the bladders is quite easy, so as long as leaks are found in time the UAV should not experience too much downtime due to repairs. The system that takes a little more time is the fuel supply. The fuel lines are detached every time the wing is detached and therefore may break sooner. Hence, a thorough inspection on those, and in time replacement of the fuel lines when necessary may be needed to prevent larger maintenance requirements.

Maintenance of the internal tanks
All foams used in firefighting are based on detergents, which can harm the surfaces exposed to the detergent. Therefore, it is advised to regularly clean the retardant injection system and all other systems or surfaces that are exposed to the foam. One of the advised actions is to flush the pumps exposed to the foam solution for 20 minutes after each shift. The downside of the constant flushing is that the system is constantly exposed to water, making corrosion more likely. Next to this, the flushing of the system also cleans potential dirt or rust from the system which may clog the nozzles used for injecting the foam into the water tank. However, seeing that the foam tank and injection system are only refilled at the airstrip and are closed off from the rest of the system the occurrence of dirt in the tank should be minimal. As the tank is mainly made from an epoxy-glass fibre composite, the internal tanks are expected to require minimal maintenance, as long as proper care is taken, and that nozzles and other choke points are regularly checked for potential clogs due to rust or dirt.[63]

Maintenance on the engine
The big downside of the UAV from a maintenance perspective is the placement of the engine. This is because its placement in the fuselage is hard to access. In the current internal layout the engine is serviced from a service latch that is located directly below the wing. Before having access to the engine first the overflow vent of the water tank has to be removed. This makes maintenance to the engine time consuming to do, whilst this is usually the system that should be easily accessible for maintenance or inspection. To make this a little bit more manageable, in future design one may need to look at additional sensors which can be used to inspect the engine, such that inspection does not require the tedious process of removing parts. Also, these extra sensors could give more information about the engine state and its deterioration such that it becomes easier to predict when maintenance is necessary and, thus, the maintenance can also be planned at convenient times.

16.4. Safety

To ensure the UAV can operate in a safe manner, various safety measures have to be applied. These safety measures are incorporated in the design of the structure and certain policies the UAV has to adhere during flight (dropping water) and on water (scooping, taking off/landing).

16.4.1. Structural Safety Measures

In the structural design of the UAV a certain redundancy philosophy has been applied to safety-critical systems.
In the wing design various redundancy philosophies have been applied. For the detachment of the wing a fail-safe philosophy has been applied, so should one bolt (or more, calculations are still to be done) fail, the rest of the bolts are able to carry the loads to finish the flight. However, as mentioned in the maintenance plan it is also advised to regularly check the bolts and if necessary replace them, such that the safety is maximised. The regular part of the wing is designed with a safe-life design philosophy and its life is mainly limited by the fatigue life of the material the wing is made out of. In future design steps the wing should also be sized for damage tolerance.
The hull of the UAV was designed with a combination of the fail-safe and safe-life design philosophies in mind. Overall in terms of structural strength, the hull was designed with a safe life design philosophy in mind. However, certain fail-safe elements have been implemented, for example, for buoyancy the hull has been divided into several watertight compartments, such that when there is a leak in one part of the hull, the other watertight compartments and the tip floats provide the buoyancy necessary for the UAV not to sink.

16.4.2. Safety During Critical Operations

The critical operations have been identified to be landing/taking off on water, scooping water and dropping water. Each of these operations will be analysed in more depth and their safety will be elucidated.

Water Operations
While not moving on the water, floats are attached to the wings to ensure lateral stability. These are explained in depth in subsection 10.3.2. A danger would be hitting the water with the floats while moving on the water (i.e. landing/take-off

or scooping), and thereby crashing. The floats should therefore be folded in when moving on the water or scooping water.

Dropping Water
During the dropping of the water, the UAV loses between 33% and 50% of its MTOW in a very short time. This does not necessarily introduce a higher wing load seeing that the weight does decrease, it does, however, introduce a transient load. This transient load was not yet taken into account when sizing the structures of the aircraft due to time constraints, but should definitely be taken into account by either defining a maximum amount of drops before replacement (safe-life) or reinforcement of the structures (fail-safe) or, most likely, a combination of both should be implemented. Besides the structural considerations, there is also a risk in having a c.g. shift that very quickly changes the controllability/stability aspects. Losing control of the UAV would be very unsafe. The presence of firefighters on the ground fighting the fire would make a crash possibly lethal. In subsection 8.3.4, the effects of dropping the payload are more elaborated upon. It is concluded that the horizontal c.g. shift is very limited, such that stability and controllability are not jeopardised.

16.5. Sustainability Analysis

Throughout this report the design and the choices made to arrive at the final result have been elaborated on. This section will briefly summarise the sustainability aspects of those decisions, as more extensive explanations have been provided in each section within chapter 10.

16.5.1. Sustainable Decisions Made

Propulsion
Although Wangari is not an electric or hydrogen powered aircraft, it outperforms those types of aircraft in terms of cruise speed, dropping capacity, and other performance parameters. This is necessary as the wildfires produce and emit a lot more greenhouse gases negatively impacting the environment than the firefighting aircraft. The emissions done by the aircraft, even including the production of the system, are almost negligible in comparison to the gases produced by the wildfires. Thus, propulsion based on non-renewable fuels was chosen. Although, bio-fuel could be implemented in the future, this can be done when the infrastructure is available and it is readily accessible. So-called 'drop-in' bio-fuels can be combined with traditional jet fuel without losing performance[64]. Implementing this in the propulsion system reduces the emissions expelled by the aerial firefighter. Further explanation of the sustainability aspect and a comparison of emissions produced by the wildfire and different types of aircraft can be found in subsection 10.1.6.

Materials
In the selection of materials, re-usability and recyclability were determined to be the most important sustainable aspects. However, during the selection of the material it was found that the production and lifetime of the material also play a large role for the material to be sustainable. The lifetime of the aircraft is mainly affected by the fatigue the aircraft experiences. This has, therefore, been touched upon in the material selection of several components subsection 10.1.5, subsection 10.2.7, subsection 10.3.6.

The goal of being able to recycle at least 75% of the materials in weight to be recyclable has not been met. This is due to the fact that it has been decided that the hull will be made out of composites. This will, however, increase the sustainability of the hull in terms of durability. Another reason why the goal has not been met, is because initially the limits of recycling materials that have additional coatings were not been taken into account. This has been further discussed in Table 10.2.5.

Dropping
In order to accurately and efficiently contain the wildfire a pressurised dropping mechanism would be required. However, those mechanisms are often heavy and increase complexity of the aircraft. Hence, a passive pressuring system has been established, this has been done in subsection 8.3.2. Dropping suppressants with a high load manoeuvre improves the containment of the fire, in turn reducing emissions expelled by the fire and reducing the emissions of the aircraft by lowering its weight.

The suppressant that is dropped should also be considered to be sustainable. Research has been done in to different types of retardant and it has been chosen to make use of Phos-Check WD881, this will be combined with water to together make up the fire suppressant. The main reasoning behind the choice follows from is it being highly concentrated and having a minimal impact on the environment. A more elaborate discussion of the retardant choice can be found in subsection 8.3.5.

16.5.2. Future Sustainability Considerations

There are still considerations with regards to sustainability to be made in the future. Mainly due to time constraints, these topics were not investigated thoroughly and are, thus, recommended to be further looked into. This concerns the noise produced by Wangari and formation flying in cruise. Sustainability in manufacturing and assembly will be looked into in chapter 18; limiting cost, and thus considering economic sustainability, is mentioned in chapter 19.

For the further development, production and assembly of the UAV, lean manufacturing should be considered. Costs and usage of resources should be kept to a minimum. This should not only be with regards to the environment, but the manufacturing of the UAV should also not negatively impact the social environment. This concerns the economic sustainability of the aircraft. With regards to economic sustainability, maintenance should also be considered. Reducing the amount of maintenance required and thereby restricting costs and resources would be an added benefit to sustainability of Wangari. Educating the pilots and other people involved in the operations of the system should be informed in a sustainable manner, as set as a goal in the midterm report [6]. This should also be looked into in the future, an idea might be to implement a simulation in the education instead of controlling the actual UAV.

The noise produced by Wangari has not been accurately found. But, noting that it is a propeller powered aircraft, it will probably not meet the initially set requirement for noise pollution, AF-SH-SUS-01. However, as Wangari is an emergency vehicle and typically there are no humans present at the location of a wildfire, this requirement has not been considered as high priority and therefore not been further investigated.

A reduction of fuel usage could be achieved by flying a particular formation during cruise. This topic has not been further investigated due to the limited knowledge of the wake created by the floats located at the tips of the wing. It is expected that reduction could still be achieved, but by how much is unsure.

The load experienced on the ground induced by the dropping of the suppressant has not been investigated. This could be done with the use of tests to research the impact it may have on vegetation and species.

Part IV

Project Outlook

17 Future Design Steps

This chapter aims to set out the steps that need to be undertaken in the future to realise the concept described in part II. This establishes the design and development logic for the future, which includes setting up a validation and production road map, and analysis of future risks. The steps to be undertaken are then included in a Gantt chart. The main goal for the future steps is to produce the UAV as quick as possible due to the necessity of such an aircraft.

17.1. Project Design & Development Logic

The main focus of the feasibility study of the UAV was to be able to produce the UAV as quick as possible and thus no technologies were chosen to be incorporated in the design which were not a proven concept yet or considered to be highly unconventional. To translate the feasibility study into actual production of the Wangari, several steps need to be undertaken. First of all, further detailed design is needed. Although part II is stated to give a detailed design description, this design is still very preliminary. For example, as of now, the wing box design has no stringers and does not follow the shape of the airfoil. These are, however, needed to be able to perform the next step of the development. As final part of the first step, CFD and FEM analysis should be done to verify that the concept works in theory. The next steps for the design team to take are visualised in Figure 17.1.

In the detailed design phase a reiteration on the main subsystems will be performed. This includes a form of verification on each separate component. In the verification and validation phase the entire UAV will be analysed and multiple scale models will be produced to properly test the UAV. After having incorporated the results obtained from the prototype tests, a full size prototype should be produced such that structural performance tests can be done. When these checks are done some adjustments to the design can be made. This phase can be very unpredictable depending on the results of the tests and has a high risk of delaying the production of the UAV. After this a detailed production plan must be created and the certification process must start. It is preferable that the certification starts as soon as possible to get the governing bodies involved in the design as soon as possible to make adjustments early in the design phase to prevent delays. Due to the UAV being a unique vehicle it is important to also get a unique certification such that the vehicle may be optimised to perform as well and safe as possible. An example of the regulations being unclear can be seen in regulations on aircraft flying beyond line of sight, for which none can be found in the USAR [66]. After the certification has been obtained the final flight tests can start after which the production and sales can start. The main risk for the production phase is the production of the hull which will be outsourced due its complexity. If the hull production encounters any delays the entire production of the UAV must be halted which may subsequently cost a lot of money.
During the complete future design process it is important to keep an eye on the main competitor. Vikingair has announced that they are working on a new version of the Cl-415, the CL-515[1]. The emergence of a new alternative on the market could potentially hurt the sales of the Wangari UAV system. When looking at the new CL-515, it is clear that Wangari still precedes the market in terms of pilot safety and performance. However, due to the high necessity of fighting

[1]`https://aerialfirefighter.vikingair.com/aircraft/viking-canadair-515` [cited 25 june 2019]

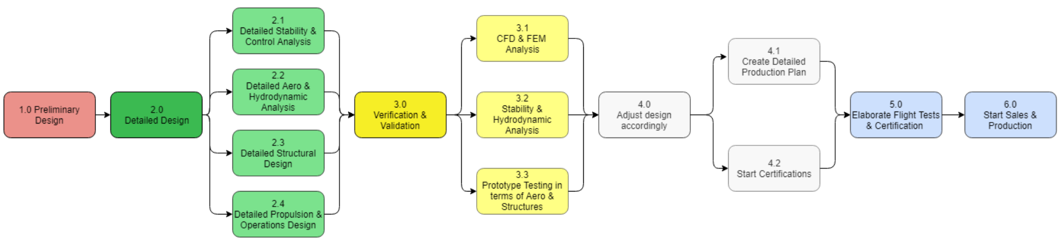

Figure 17.1: Future Design Steps

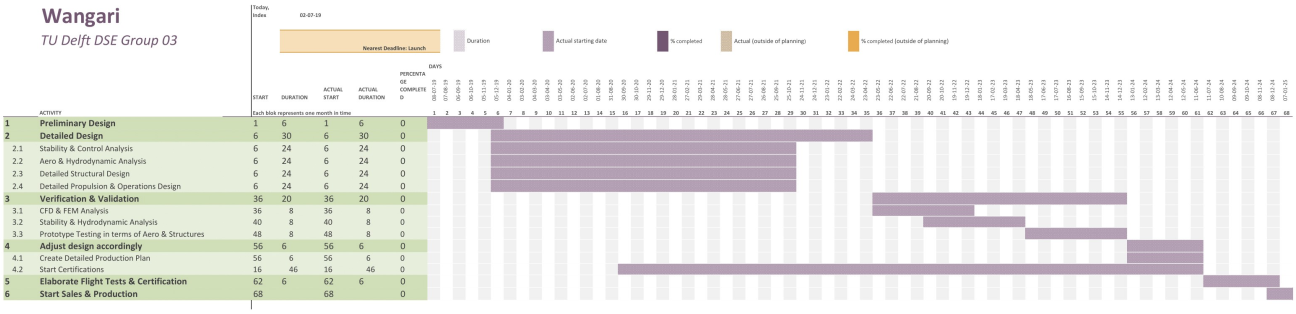

Figure 17.2: Future Gantt Chart

wildfires, potential customers may be forced to pick the best alternative when they need an aerial firefighting aircraft. This is why time to market is very important for the Wangari UAV system and should be done as fast as possible.

17.2. Future Gantt Chart

In the future Gantt Chart, the approach to the following design phases can be seen. During these design phases the design will be further iterated upon whilst simultaneously making sure certification is in order before starting production to ensure maximum security for the design team. The flow of Figure 17.1 has been used for this.

17.3. Recommendations

17.3.1. Technical Recommendations

Given the flow chart for the future steps as presented in Figure 17.1, the recommendations for steps 2 and 3 will be detailed in this section. The detailed design phase will reiterate on the subsystems of the aircraft taking into consideration the four main aspects including stability and control, aero- and hydrodynamics, structures, and propulsion. A next iteration within these aspects will of course also result in an updated performance analysis in order to determine the operational improvement of the UAV.

Control & Stability

With regards to control and stability, as a next step within the design process, the focus will lie on implementing control loops and simulations in order to fully analyse the behaviour of the aircraft to certain inputs both inflight and during the water operations. Additionally, critical to the UAV performance and safety is also the implementation and eventual testing of the autonomous systems for collision avoidance.

Aerodynamics & Hydrodynamics

Within aerodynamics, the next phase will focus on two prime the aspects. The first relies on the possible optimisation of the lifting and control surface geometries for a more critical stage within the mission profile. This will be coupled with an in depth CFD study on the fuselage and floats in order to study how the shape will affect the overall performance (L/D) of the aircraft. Finally, a computational study should also be performed in order to investigate and verify the extent of the effect the propellers may have on the lifting performance of the aircraft.

Within hydrodynamics, there will be an overlap with aerodynamics especially with regards to performing a CFD study in order to investigate to what extent the hull can be altered in order to minimise aerodynamic but most importantly also hydrodynamic drag. Lowering the hydrodynamic drag may greatly improve the water take-off and scooping performance of the aircraft. Moreover, the detailed design of the scooper as well as internal tank will play an important role within the next design iteration.

Structures

Crucial to structures will be a finalisation of the wingbox design. This will include aspects such as determining the number of stringers, ribs as well as accounting for the actual airfoil shape. In addition, as it was determined that the fatigue loading is critical for a UAV performing this type of mission, a focus will be placed on studying the fatigue loading effects on multiple parts of the UAV on subsystems such as the wing as well as the tank door. Finally, there are conceptual aspects of the design which still require preliminary sizing and development. An example for these would be the retractable float mechanism. Although simple, an analysis of the loads experienced is yet to be performed.

Propulsion & Operations

Within propulsion, a direct cooperation with aerodynamics should be present in order to better study the effects of the propeller on the wing through either a CFD analysis or another more detailed numerical method. In addition, the propeller blade itself may also be optimised in a similar manner with regards to its thrust production. Finally, the detailed design of the driveshaft should be looked at in detail to make sure the power is correctly transmitted from the engine to the propeller.

With regards to operations, a main area of focus will lie in the development of the fire simulations to better model the behaviour of the spreading in addition to optimising swarming strategies for different scenarios. In addition, the passively pressurised dropping system should be looked into further especially in terms of the design of the sliding door and its mechanism.

Verification & Validation

Main things to consider for the verification & validation are the design of multiple scale models of the UAV and the eventual production of a prototype. This prototype can be used to to ensure that the design is indeed stable and controllable, especially during scooping and dropping of the suppressant. The amphibious stability has to be analysed in more detail as well during water manoeuvres. Furthermore, the overall stability should be determined in more detail. This contains the determination of the stability derivatives, and using this to establish if the various eigenmotions (e.g. phugoid, spiral) are stable or unstable[65]. When these derivatives are known, a simulation can be made in order to see how the aircraft behaves.
The prototype must eventually validate the structural integrity of the UAV and the wings should be tested for both their ultimate wing loading and the fatigue loading. It should also be taken into account at what happens when the wings are not attached properly such that mitigation measures or guidelines can be created to prevent any accidents occurring related to this. The main critical structural aspect of the UAV is the hull design due to impact loading and the wings due to fatigue loading which is much more prevalent in aerial firefighting aircraft. Main validation procedures for the aircraft can involve wind tunnel testing, ultimate strength tests for the wings and hydrodynamic testing in a towing tank.

17.3.2. Additional Notes

It is recommended that governing bodies are involved in the design of the UAV as soon as possible. Due to the lack of any certifications it is a risk to get the Wangari UAV system certified for operations. Therefore it is recommended to try to involve any authorities as soon as possible. This may also be the case for potential customers to further the develop the UAV to their demand. This will focus on operations however, as the main design parameters have been fixed. It is also recommended that due to the severity of the climate crisis that the UAV will be produced quickly. Also concerning this is the production of a newly developed successor of the Canadair CL-415, the Viking air CL-515. In terms of flight testing, production and sales it is recommended that sales start early on. The market analysis shows that although there is a need for aerial firefighting vehicles, there are not many vehicles sold. In order to keep production costs down, it is very important to be able to sell the recommended amount of UAVs within the given time span of 5 years. This process starts early on in gaining interest from investors and potential customers.

18
Manufacturing, Assembly and Integration

To be truly sustainable, not only the product itself shall be sustainable but also the designing and manufacturing processes shall be done in a sustainable manner. Therefore, the lean manufacturing philosophy shall be implemented. This philosophy strives to eliminate waste in the broadest sense of the word during the complete process.

18.1. Production Process

As the demand of firefighting aircraft is quite low in comparison to commercial aircraft, only 162 firefighting aircraft are currently in use versus over 23600 commercial aircraft [1], the batch per production will also be small. Therefore, it is likely that outsourcing certain parts of the manufacturing process will be cheaper than acquiring the expensive machines needed. The hull, for example, is to be made of over-expanded composites. This will verge complex tooling such as composite freezers and autoclaves, for which the risk and cost could exceed those of ordering and transporting them from renowned aircraft manufacturers. Other parts, like the aluminium wings, can be produced by the Wangari crew such that transportation time, which is classified as waste in the lean manufacturing philosophy can be eliminated.

18.2. Assembly

As in this feasibility study a production plan for exact part manufacturing is premature, focus is instead laid upon the assembly of parts to create the final design. The assembly is performed in several stations along an assembly line, as visualised in Figure 18.1. Into the main assembly line, subassembly lines and parts are fed. Dividing the workload over several stations enables for an efficient production process in which the same crew is responsible for the same task over the entire production period. This way the learning curve of the crew is maximised, thus minimising time and cost. After especially complex stations a buffer station is added to account for delays in the production. The most expensive parts and parts that have to be inspected often, such as the engine and battery cells, are placed at the end of the assembly line to avoid additional costs.

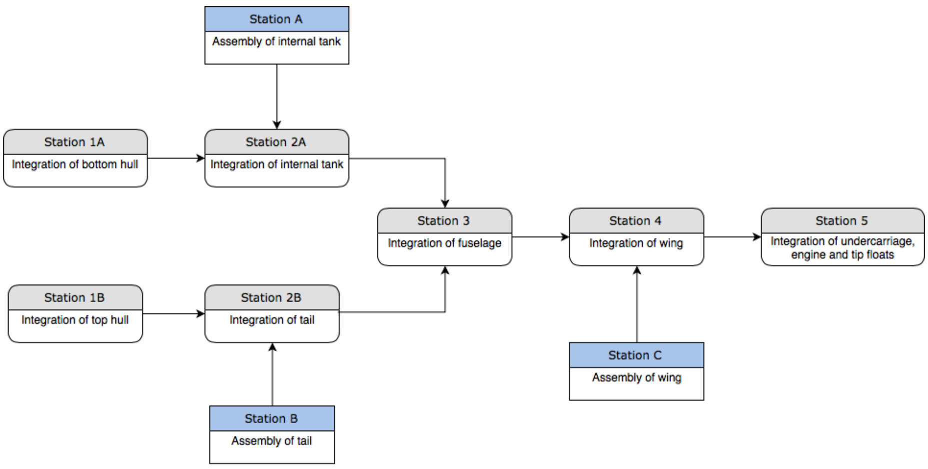

Figure 18.1: Assembly process of the Wangari.

[1] https://www.telegraph.co.uk/travel/travel-truths/how-many-planes-are-there-in-the-world/ [cited 20 June 2019]

19
Financial Analysis

As Wangari is designed to outperform the current market, it is of importance to gain insight in the financial state of the design. Therefore, a financial analysis has been performed to be able to define a strategic sales tactic. In this analysis both a cost breakdown for the future as well as the break-even point in return on profit is determined.

19.1. Cost Breakdown Structure

A cost breakdown is important to be aware of the cost of all the different components of Wangari, but also of the total costs in order to determine a selling price. First of all, the engineering, tooling and manufacturing hours need to be determined, because some costs are related to these working hours. The team assumed that 60 UAVs will be produced during a 5-year period, based on the main competitor, the CL415, of which 95 have been produced from 1993 until 2015. This means that 95 aircraft have been produced during 22 years, however, during the first years more CL-415's have been produced than at the end. The number of planned aircraft to be produced is important because the more UAVs produced, the less the cost per UAV. This is because components generally get less expensive per unit when more of it is used and because the engineers gain experience, which means that their performance increases with increasing UAVs that get produced. All the costs are in American dollars, since the formula's used are using this currency, but will be converted to euro's at the end.

19.1.1. Labour Hours

Engineering Hours

Engineering hours represent the number of man hours to design an assumed number of UAVs over a period of 5 years.

$$H_{ENG} = 0.0396 \cdot W_{\text{airframe}}^{0.791} \cdot V_H^{1.526} \cdot N^{0.183} \cdot F_{\text{CERT}} \cdot F_{\text{CF}} \cdot F_{\text{COMP}} \cdot F_{\text{PRESS}} \tag{19.1}$$

In which, $W_{airframe}$ equals the weight of the structural skeleton, V_H the maximum level airspeed, N the number of planned aircraft to be produced over 5-year period (60 units assumed), F_{CERT} equals 1 for more costly certifications, F_{CF} equals 1 for a simple flap system, $F_{COMP} = 1 + f_{comp}$ a factor to account for the use of composites in the air frame; f_{comp} is assumed to be 0.4, and F_{PRESS} equals 1 for an unpressurised aircraft.
The exponent of the number of planned UAVs is less than one as can be seen in the equation, because of what was explained above. The engineers gain experience after having designed the UAVs, hence the hours per unit decrease with increasing number of UAVs. After inserting the parameters, the engineering hours is found to be 377287 hours, which is equal to 15720 days or 43 years.

Tooling Hours

Tooling hours represent the number of working hours to design and produce necessary tools, such as jigs and molds, to support the production process.

$$H_{TOOL} = 1.0032 \cdot W_{\text{airframe}}^{0.764} \cdot V_H^{0.899} \cdot N^{0.178} \cdot Q_m^{0.066} \cdot F_{\text{TAPER}} \cdot F_{CF} \cdot F_{\text{COMP}} \cdot F_{\text{PRESS}} \tag{19.2}$$

In which, Q_m equals the estimated production rate in number of aircraft per month, F_{TAPER} equals 0.95 for a constant-chord wing.
Again, the tooling hours are related to the number of planned aircraft with an exponent smaller than one. Once more because of the gained experience. After filling in the parameters, the tooling hours is found to be 241360 hours, which is equal to 10057 days or 27.5 years.

Number of Manufacturing Labour Man-hours

$$H_{MFG} = 9.6613 \cdot W_{\text{airframe}}^{0.74} \cdot V_H^{0.543} \cdot N^{0.524} \cdot F_{\text{CERT}} \cdot F_{CF} \cdot F_{\text{COMP}} \tag{19.3}$$

Also for the manufacturing hours, the number of planned aircraft in the equation have an exponent smaller than one. The more material that is used, the less expensive it will be per unit. After inserting the parameters, the engineering labour man-hours is found to be 949364 hours, which is equal to 39557 days or 108 years.

19.1.2. Costs

Now that the labour hours have been determined, the different costs during the whole project can be calculated. All the empirical formula's for the cost estimation are obtained Gudmundsson [33].

Total Cost of Engineering

The engineering costs include the wages that the engineers receive for designing the Wangari system.

$$C_{ENG} = 2.0969 \cdot H_{ENG} \cdot R_{ENG} \cdot CPI_{2012} \tag{19.4}$$

In which, R_{ENG} equals the rate of engineering labour in US dollars per hour (assumed 92 \$/hour), and CPI_{2012} the consumer price index relative to the year 2012, when this method and its assumed costs were originally made. The total engineering costs equals 85.5 million dollars for the 60 UAVs planned to be produced over a 5-year period.

Total Cost of Development Support

The developments costs are the costs that make sure that the design gets developed to the appropriate stage, which includes building prototypes for example.

$$\begin{aligned} C_{DEV} = 0.06458 \cdot W_{\text{airframe}}^{0.873} \cdot V_H^{1.89} \cdot N_P^{0.346} \cdot CPI_{2012} \\ \cdot F_{\text{CERT}} \cdot F_{\text{CF}} \cdot F_{\text{COMP}} \cdot F_{\text{PRESS}} \end{aligned} \tag{19.5}$$

In which, N_P equals the umber of prototypes, 2 assumed, and $F_{COMP} = 1 + 0.5 \cdot f_{comp}$. The total developments costs are estimated to be 5.1 million dollars for the production of 60 UAVs.

Total Cost of Flight Test Operations

This includes the development and certification of flight-testing.

$$\begin{aligned} C_{FT} = 0.009646 \cdot W_{\text{airframe}}^{1.16} \cdot V_H^{1.3718} \cdot N_P^{1.281} \\ \cdot CPI_{2012} \cdot F_{\text{CERT}} \end{aligned} \tag{19.6}$$

The total flight test costs are estimated to equal 0.9 million dollars.

Total Cost of Tooling

The tooling cost represent the total costs to design and produce necessary tools, such as jigs and molds, to support the production process.

$$\mathrm{C}_{\text{TOOL}} = 2.0969 \cdot H_{\text{TOOL}} \cdot R_{\text{TOOL}} \cdot \mathrm{CPI}_{2012} \tag{19.7}$$

Where R_{TOOL} equals the rate of tooling labour in US dollars per hour (61 \$/hour assumed). This is estimated to be 34.9 million in total.

Total Cost of Manufacturing

The manufacturing cost represent the total costs to manufacture and produce the assumed 60 UAVs.

$$C_{\text{MFG}} = 2.0969 \cdot H_{\text{MFG}} \cdot R_{\text{MFG}} \cdot CPI_{2012} \tag{19.8}$$

In which, R_{MFG} is the rate of manufacturing labour in US dollars per hour (53 \$/hour assumed). The manufacturing cost forms the largest part of the total costs and is estimated to equal 119.2 million dollars for 60 UAVs.

Total Cost of Quality Control

Quality control is done to assure certain standards in manufactured products by testing a sample of the UAV against the specifications, for example.

$$C_{QC} = 0.13 \cdot C_{MFG} \cdot F_{CERT} \cdot F_{COMP} \tag{19.9}$$

The quality control costs are estimated to be 18.6 million dollars for the assumed 60 UAVs.

Cost of Materials

This includes the cost of all the raw materials to make the aircraft, not only such as aluminium sheets for the wing or composites for the hull, but also landing gear and avionics.

$$C_{MAT} = 24.896 \cdot W_{\text{airframe}}^{0.689} \cdot V_H^{0.624} \cdot N^{0.792} \cdot \text{CPI}_{2012} \cdot F_{\text{CERT}} \cdot F_{\text{CF}} \cdot F_{\text{PRESS}} \tag{19.10}$$

This is estimated to equal 7.5 million dollars for 60 UAVs.

Cost of Landing Gear
The cost of landing gear is already assumed in the coefficients of the model. In case the landing gear is not retractable, a subtraction of 7500$ is appropriate. However, since the landing gear of Wangari is indeed retractable, this cost does not require any adjustments.

Cost of Engine and Propellers
The engine used is commercially available and costs 837.445 $. The propellers are assumed to cost 15% of the engine cost each. This percentage is based on statistics of other aircraft.

Cost of Avionics
The cost of the avionics for an unmanned aerial vehicle is difficult to estimate, because it is heavily related to the mission of the aircraft. The cost of the avionics for the "General Atomics MQ-9 Reaper", which is a surveillance UAV may be completely different than the costs for a firefighting UAV. Besides, the avionics of a UAV system are a lot more complex and expensive than for a manned aircraft, so also not comparable. Therefore it is difficult to estimate this, but the team assumes that the avionics costs will be approximately 20% of the total costs. This because the Wangari system will be equipped with complex sensors and devices, both in the ground control system and in the UAV itself, required to operate in a strategic and safe manner.

Below a summary of the costs is shown in a table, which also groups the fixed costs and the variable costs. The fixed costs are costs that are independent of the number of UAVs produced. They remain constant throughout the production process. The variable costs are dependent on the number of UAVs produced. After the total cost has been determined, the total cost including liability insurance can be calculated, which equals the total cost per UAV (sum of fixed cost per UAV and variable cost per UAV) multiplied by 0.17. As the total cost per UAV equals 6.2 million$, the liability insurance costs equals 1.05 million $ per UAV. This liability costs is distributed over the fixed and variable costs according to their contribution to the total costs per UAV. The fixed costs make up 30% and the variable costs make up 70% of the total costs per UAV. This means that 30% of the liability insurance costs will be added to the fixed costs and that 70% of the liability insurance costs will be added to the variable costs.

Table 19.1: Cost breakdown

	Costs [mil. dollars]	**for 60 UAVs**	**per UAV**
Fixed Costs	Engineering	85.8	1.4
	Development	5.1	0.1
	Flight Test	0.9	0.01
	Tooling	34.9	0.6
	Total Fixed	**126.7**	**2.1**
	Total Fixed Incl. Liability	**150.3**	**2.5**
Variable Costs	Manufacturing	119.2	2
	Quality Control	18.6	0.3
	Material	7.5	0.1
	Engines	75.4	1.3
	Propellers	22.6	0.4
	Avionics	92.5	1.54
	Total Variable	**335.8**	**5.6**
	Total Variable Incl. Liability	**391**	**6.5**
	Total Costs	**541.2**	**9.0**

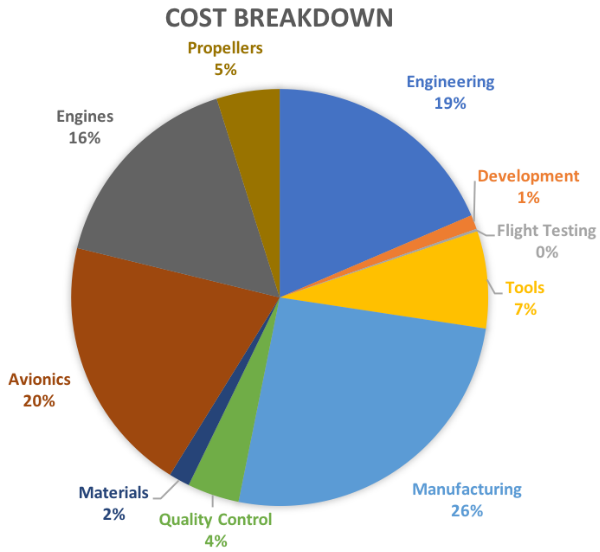

Figure 19.1: Cost breakdown

19.2. Return on profit

The return on profit point is the point at which the total expenses equal the total revenue. If this point is set on 28 UAVs, the selling price of single UAV would equal 12 million$, or 10.6 million euros. The total revenue/expenses is equal to 330 million$ at this point.

The point is determined by looking at the intersection between the line which visualises the expenses and the line that visualises the revenue. The total expenses are equal to the sum of the total fixed costs and the total variable costs per UAV multiplied by the number of UAVs produced. The fixed costs are the costs that are independent of the number of UAVs produced which are, in this case, the engineering costs, the developments costs, the flight test costs and the tooling costs. These remain the same regardless of how many UAVs have already been produced and are estimated to be 150.3 million $ in total including liability insurance costs. The variable costs are the costs dependent on the number of UAVs that are produced and are stated in Table 19.1 and is estimated to equal 6.5 million$ including liability insurance costs. The total revenue equals the selling price, which is 12 million$ multiplied by the number of UAVs sold. All of this is shown in Figure 19.2.

Figure 19.2: Return on profit

19.3. Sales Strategy

The Wangari system does not consist of a single UAV, but rather of multiple UAVs, controlled by pilots located at a ground station, and possibly assisted by an air attacker. The whole design is based on cooperation of all the different units in the system. Only utilising a single UAV would hence not be an efficient manner to fight wildfires and therefore it would not make sense to sell individual UAVs to customers. Instead, a different sales strategy will be used, consisting of packages including multiple UAVs, a ground station and systems for the air attack. The reason that the air attacker itself is not included in the package, is because the aircraft that the team designed has performance characteristics that are optimal for a water bomber, but not for an air attacker. The UAVs are amphibious, are able to scoop water and have a large water tank inside the fuselage, which are all features that are not required for the air attack. Besides, the air attack needs to be designed for endurance, to stay as long as possible in the air to coordinate the situation, which is definitely not the case for the water bomber UAVs. Hence, only the systems that an air attack requires are included in the package, so that an available aircraft could be used as an air attacker by making use of those systems. The different units will be explained below in further detail.

1. UAV: a number of UAVs, depending on what the customer wants. If the system has to be transported by cargo aircraft and the customer buys a multiple of 2 UAVs, he/she has to pay less per unit than when the customer buys an odd number of UAVs. This is because with an odd number of UAVs, the cargo aircraft will not be filled completely, because it has space for 2 UAVs. Not making optimal use of payload capacity costs money.
2. Ground station: the ground station is essentially the remote-pilot cockpit. This includes monitors which show information, computers, a control system and an antenna to send feedback to the UAVs. Although the exact dimensions of the remote-pilot cockpit are unknown, the team assumes it fits in the empty spaces in the A400m, because it is also able to fit in a truck [1].
3. Systems for air attack: even though the air attacker itself is not provided in the package, systems for the air attacker are included. As mentioned in section 11.3, the air attack is used to coordinate the UAVs, with the use of camera's. It can also be used to complete the communication link through an indirect route whenever the link between the UAVs and the ground station is blocked. In order to perform those two functions, the air attack needs to be equipped with camera's, with a computer and with an antenna. Hence, those are included in the package.

This will make sure that the system can be used in the way that it is designed for, i.e. cooperation of all the different units included in the package. Another great advantage of having this package with 2 UAVs is that it all fits in a single A400m. Figure 13.2 shows that 2 UAVs are able to fit in the cargo aircraft, with even having additional space for other loads. This will be enough to transport the ground station and the systems necessary for the air attack along with the UAVs. If a customer decides to buy more than 2 UAVs and the system has to transported by cargo aircraft, multiple cargo aircraft need to be used to carry the system to the customer. It is difficult to recommend a general number of UAVs to a customer, because it depends on a lot of factors, e.g. the type of fire, the budget of the customer, proximity to residential area, etc.

[1] `http://www.ga-asi.com/advanced-cockpit-gcs`

20 Conclusions

The objective of this project was assessing the feasibility for a UAV system which aims at revolutionising firefighting with innovations such as tactical swarm attacks, night firefighting and passively pressurised fire-retardant drops. In developing the design, the focus was placed on determining the right payload, quick deployment, safety, low speed performance, dropping efficiency, sustainability and cost and will hence form the main focus of this conclusion. The final selected concept consists of a single engine, twin propeller amphibious aircraft with a high wing, cruxifix/T-tail hybrid configuration.

Based on a developed firefighting simulation, an analysis of different scenarios showed that having several smaller UAVs may be an advantage to having fewer larger aircraft. In consultation with firefighting experts, taking into account the evaporation rate of the retardant and water during the dropping, it was determined the UAV shall be able to carry a minimum payload of $2500L$. The final UAV is able to carry a payload of up to $4500L$ of suppressant.

In line with the goal of quick deployability, the wing and horizontal tail are both detachable such that at least two UAVs fit in an A400M cargo aircraft (cargo hold dimensions of $17.71x4.00x3.85m$). With regards to safety, as the aircraft is remotely piloted, the on-board pilot risk is completely removed. The UAV is also equipped with an autonomous system able to detect ground crew as well as other other vehicles. For the moment however, this system has not been fully developed and is the subject of a future design stage. Finally, an additional safety consideration has been taken into account with regards to the retractable floats of the aircraft. Aside from providing stability during water taxiing, the retractability of the floats decreases the risk of catching the water at fast speeds during scooping.

The large surface area of the wings coupled with a high payload-to-maximum-take-off-weight ratio and the placement of the propeller over the wings allows for the UAV to achieve excellent low speed performance and with a stall speed of $35.5m/s$. The powerful engine coupled with a low MTOW also allows for much higher cruising speeds of $112.5m/s$, which is considerably higher than the current firefighting aircraft. This gives Wangari the additional benefit of very short initial attack times. Finally, controllability and stability is maximised at low speeds due the minimal c.g. shift during the dropping.

In order to maximise the dropping efficiency, through the development of the fire simulation, it has been shown that the dropping pattern and number of UAVs required may be optimised based on the fire scenario. In addition, a passively pressurised drop system has been developed. This makes use of the manoeuvres by translating the encountered loading the force required for the water dropping. A sliding door allowing for a variable exit area enables control of the rate at which the water leaves the tank.

This aforementioned passive dropping system goes directly in line with the sustainability considerations present throughout the entire design process. An actively pressurised system would induce additional weight and cost into the system. Keeping the MTOW weight as low as possible resulting in a reduction in fuel consumption was also reflected in choosing the single engine over the twin engine aircraft. Sustainable materials were chosen for each of the components throughout the entire design and in addition, a hybrid electro-hydraulic system was implemented in order to avoid the additional weight and induced complexity coupled with an entirely hydraulic system. Finally, the UAV may also fit in a shipping container and not just the A400M cargo aircraft, in order to facilitate the possibility of more sustainable deployment.

The current UAV is also highly cost-competitive with the current market leaders such as the CL-415. A conservative estimate prices a single UAV at 10.6 million euros, which is just under half the price of a single CL-415. This gives the Wangari system a great advantage given that for the same cost, two Wangaris are capable of providing up to 1.5 times the payload.

A risk analysis performed at an early stage following the concept selection identified the main risks to be mainly directed to the water operations. A critical aspect amongst these, is the sloshing within the water and retardant tanks during the manoeuvre as well as the instability effects due the the shift in the centre of gravity during scooping. The sloshing risk may be mitigated through the implementation of anti-sloshing baffles within the water tanks whilst the shift in the c.g. has been designed to be minimal, when full or empty, through the placement of the water tank.

In order to finalise the feasibility assessment of the design, the requirement compliance in chapter 15 showed most of the requirements have been met. Those that have not, are either primarily related to the detailed development of the autonomous and communication system (to be developed in detail in the next design phase) or not considered at this stage critical to the performance of the UAV. Finally, in combination with the mission compliance in chapter 14, it was determined that the main pillars mentioned here within the first paragraph were overall satisfied.

For recommendations into the technical details of the next design iteration as well as the global design process, the interested reader is referred to chapter 17 which details the project outlook.

Bibliography

[1] World Meteorological Organization, "WMO Statement on the State of the Global Climate in 2018", WMO-No. 1233, 2019.

[2] Butler, C. R., O'Connor, M. B. and Lincoln, J. M., "Aviation-Related Wildland Firefighter Fatalities - United States, 2000-2013", Weekly, Volume 64, No. 29, 2015, pp. 793-796.

[3] Hayes, G. L., "Differences in Fire Danger with Altitude, Aspect, and Time of Day", Journal of Forestry, Vol. 40, No. 4, 1942, pp. 318-323.

[4] Jane, F. T., "Jane's All the World's Aircraft, Upgrades", McGraw-Hill, New York, 2019.

[5] Plucinski, M., Gould, J., Mccarthy and G., Hollis, J., "The Effectiveness and Efficiency of Aerial Firefighting in Australia part 1", Bush re Cooperative Research Centre, 2007, p. 27.

[6] DSE Group 03, "Midterm Report, Aerial Firefighting UAVs", unpublished, 2019.

[7] Bramlette, R. B., "Exploratory flight loads investigation of the P-2V aircraft in aerial firefighing operations," Master Thesis, Dept. of Aerospace Engineering, Wichita State University, Wichita, KS, 2008.

[8] Roskam, J., "Part I: Preliminary Sizing of Aircraft", DARcorporation, University of Kansas, Lawrence, 2003, pp. 5-48.

[9] Roskam, J., "Part I: Preliminary Sizing of Aircraft", DARcorporation, University of Kansas, Lawrence, 2003, pp. 60-68.

[10] Roskam, J., "Part I: Preliminary Sizing of Aircraft", DARcorporation, University of Kansas, Lawrence, 2003, pp. 89-170.

[11] Raymer, D. P., "Aircraft Design: A Conceptual Approach", 4th edition, USA, 2006.

[12] Legendre, D., Becker, R., Alméras, E. and Chassagne, A., "Air tanker drop patterns", International Journal of Wildland Fire, CSIRO Publishing, Vol. 23, no. 14, 2014, pp. 272-280.

[13] Jordan, C. and Solarz, P., "Ground Pattern Performance of the Neptune P2V-7 Airtanker", United States Department of Agriculture and Forest Service, September 2000.

[14] Suter, A., "Drop Testing Airtankers, A Discussion of the Cup-and-Grid Method", USDA Forest Service, Missoula, Montana, 2000.

[15] Rakowska, J., "Best Practices for Selection and Application of Firefighting Foam", MATEC Web Conf. 247 00014, 2018.

[16] Poulton, B., Hamilton, S., Buhl, K., Vyas, N., Hill, E. and Larson D., "Toxicity of Fire Retardant and Foam Suppressant Chemicals to Plant and Animal Communities", Interagency Fire Coordination Committee, Boise, Idaho, 1997.

[17] Ruijgrok, G.J.J., "Elements of airplane performance", 2nd edition, Delft, 2009.

[18] Air Transport Action Group, "Beginner's Guide to Aviation Biofuels", Ed. 2, 2011.

[19] Patterson, M. D., Derlaga J. M. and Borer, N. K., "High-Lift Propeller Configuration Selection for NASA's SCEPTOR Distributed Electric Propulsion Flight Demonstrator", NASA Langley Research Center, Hampton, Virginia, June 2016.

[20] Cantor, B., Assender, H., and Grant, P., "Aerospace Materials", Taylor & Francis Group, LLC, 2001.

[21] Veldhuis, L. L. M., "Propeller Wing Aerodynamic interference", Delft University of Technology, Faculty of Aerospace Engineering, 2005.

[22] Himmelskamp H., "Profiluntersuchungen an einem Umlaufenden Propeller", Max-Planck Institut für Strömungsforschung, Göttingen, Germany, 1945.

[23] Raymer, D. P., "Aircraft Design: A Conceptual Approach", 4th edition, USA, 2006, Chap 13, p.385 - p.387

[24] Raymer, D. P., "Aircraft Design: A Conceptual Approach", 4th edition, USA, 2006, Chapter 6, p.151.

[25] Raymer, D. P., "Aircraft Design: A Conceptual Approach", 3rd edition, USA, 1999, Chap 4, p.58.

[26] Raymer, D. P., "Aircraft Design: A Conceptual Approach", 3rd edition, USA, 1999, Chap 4, p.65.

[27] Raymer, D. P., "Aircraft Design: A Conceptual Approach", 3rd edition, USA, 1999, Chap 4, p.60.

[28] Oliviero, F., "Aerospace Design and Systems Engineering Elements II Course Slides, Lecture 2: Aircraft Aerodynamic Analysis - Lift & Drag" TU Delft, Delft, The Netherlands, 2017.

[29] Oliviero, F., "Aerospace Design and Systems Engineering Elements II Course Slides, Lecture 3: Aircraft Aerodynamic Analysis -Mobile Surfaces on the Wing" TU Delft, Delft, The Netherlands, 2017.

[30] Megson, T. H. G., "Aircraft Structures for Engineering Students", 5^{th} ed., Oxford, 2013.

[31] Mouritz, A. P., "Introduction to aerospace materials", 1^{st} ed., Woodhead Publishing Limited, Cambridge, England, UK, pp. 173-187.

[32] Bruhn, E. F., "Analysis and Design of Flight Vehicle Structure", Jacobs Publishing Inc., Indianapolis, USA, 1973, pp. D1.4-D1.6.

[33] Gudmundsson, S., "General Aviation Aircraft Design: Applied Methods and Procedures", Butterworth-Heinemann, Oxford, UK, 2014, App. C3.

[34] Wood, K. D., "Aircraft Design, Aerospace Vehicle Design Volume 1", Johnson Publishing Company, 1968.

[35] Nelson, W., “Seaplane Design”, McGraw-Hill Book Company, Inc., New York, NY, 1934.

[36] Canamar, L. and Alan, L., "Seaplane conceptual design and sizing", Glasgow, UK, 2012.

[37] Chicken, S. H., "Conceptual Design Methodologies for Waterborn and Amphibious Aircraft", Air Vehicle Technology Group, Cranfield University, Cranfield, UK, 1999.

[38] Pinkster, J. and Bom, C. J., "Hydromechanica 2, Deel 2 Geometrie en Stabiliteit", TU Delft, Delft, The Netherlands, 2006.

[39] Savitsky, D., "Hydrodynamic Design of Planing Hulls.", Marine Technology, Vol. 1, No. 1, 1964, pp. 71-95.

[40] Knowler, H., "The Future of the Flyingboat", Journal of the Royal Aeronautical Society, Vol. 56, No. 497, 1952, pp. 322-354.

[41] Ridland, D. M., "The Effect of Forebody Ways on Stability and Spray Characteristics", ARC CP203, 1955.

[42] Stinton D., "Anatomy of the Airplane", Granada, London, UK, 1980.

[43] Deihl, W. S., "A Discussion of Certain Problems Connected with the Design of Hulls of Flying Boats and the Use of General Test Data", NACA TN 625, 1938.

[44] Hugli, W. C., Jr. and Axt, W. C., "Hydrodynamic Investigation of a Series of Hull Models Suitable for Small Flying Boats and Amphibians", NACA TN-2503, 1953.

[45] Thurston, D. B., "Design for Flying", TAB Books, division of McGRaw-Hill, Inc., Blue Ridge Summit, PA, 1995.

[46] Karman, T. von, "The Impact of Seaplane Floats During Landing", NACA TN-321, 1929.

[47] Roskam, J., "Part 3: Layout Design of Cockpit, Fuselage, Wing and Empennage: Cutaways and Inboard Profiles", DARcorporation, University of Kansas, Lawrence, 2003, p44.

[48] Miller, P. H., "Durability of Marine Composites: A Study of the Effects of Fatigue on Fiberglass in the Marine Environment", Marine Technology and Management Group Civil and Environmental Engineering, University of California, Berkeley, 2000.

[49] Park, R. and Jang, J., "Impact Behavior of Aramid Fiber/Glass Fiber Hybrid Composites: The Effect of Stacking Sequence", Seoul National University, Seoul, Korea.

[50] Oliviero, F., "Systems Engineering and Aerospace Design Course Slides, Lecture 5: Requirement Analysis and Design principles for A/C stability & control (Part 2)" TU Delft, Delft, The Netherlands, 2019.

[51] Locke, F. W. S., Jr., "A Graphical Method for Interpolation of Hydrodynamic Characteristics of Specific Flying Boats from Collapsed Results of General Tests of Flying-Boat-Hull Models", NACA TN-1259, 1948.

[52] Raymer, D. P., "Aircraft Design: A Conceptual Approach", 4th edition, USA, 2006, Chap 6, p.84.

[53] Raymer, D. P., "Aircraft Design: A Conceptual Approach", 4th edition, USA, 2006, Chap 6, p.123 - p.126.

[54] Macdonald, M., S., "From the Ground Up", Aviation Publishers Co. Limited, 2017, p.11

[55] Raymer, D. P., "Aircraft Design: A Conceptual Approach", 4th edition, USA, 2006, Chap 11, p.229.

[56] Cho, I. H., and Kim, M. H., "Effect of Dual Vertical Porous Baffles on Sloshing Reduction in a Swaying Rectangular Tank", Ocean Engineering, Vol. 126, Oct. 2016, pp. 364-373.

[57] Blakely, A. D., George, C. W., and Johnson, G. M., "Static Testing to Evaluate Airtanker Delivery Performance", Intermountain Forest & Range Experiment Station, Ogden, Utah, 1982.

[58] Roskam, J., "Part V: Component Weight Estimation", DARcorporation, University of Kansas, Lawrence, 2003.

[59] Navarro, R., "Performance of an Electro-Hydrostatic Actuator on the F-18 Systems Research Aircraft", Dryden Flight Research Center, NASA, Edwards, California, October 1997.

[60] Sabatini, N., "Unmanned Aircraft Operations in the National Airspace System ", Department of Transportation Federal Aviation Administration, Washington DC, February 6, 2007.

[61] Scott, W. B., "Safety Concerns Ground Aerial Firefighting Tankers," Aviation Week and Space Technology, Vol. 157, No.25, 16 Dec. 2002, pp. 65-66.

[62] IATA, "Best Practices for Component Maintenance Cost Management", IATA, Montreal, 2015.

[63] Foam Task Group, "Foam vs Fire Class A Foam for Wildland Fires", National Wildfire Coordinating Group, Oct. 1993.

[64] Yilmaz, N. and Atmanli, A., "Sustainable alternative fuels in aviation", Energy, Vol. 140, Part 2, 2017, pp. 1378-1386.

[65] J.A. Mulder, "Lecture Notes AE3202 Flight Dynamics", TU Delft, 2013

[66] NATO, "Unmanned Aircraft Systems Airworthiness Requirements (USAR)," Ed. B, Ver. 1, NATO STANDARDIZATION OFFICE (NSO), April 2019

[67] Scott, W. B., "Safety Concerns Ground Aerial Firefighting Tankers, Aviation Week & Space Technology, Boise, Idaho, 2002, p. 65.

[68] George, C. W., "Fire Retardant Ground Distribution Pattern from the CL-215 Airtanker", Intermountain Forest & Range Experiment Station, Ogden, Utah, 1975.

[69] European Aviation Safety Agency (EASA), "THE EUROPEAN PLAN FOR AVIATION SAFETY (EPAS) 2018-2022", November 2017.

[70] Oliviero, F., "Systems Engineering and Aerospace Design Course Slides" TU Delft, Delft, The Netherlands, 2019.

[71] Gawron, B. and Bialecki, T., "Impact of a Jet A-1/HEFA Blend on the Performance and Emission Characteristics of a Miniature Turbojet Engine", International Journal Environmental Science Technology, Vol. 15, No. 7, 2018, pp. 1501–1508.

[72] `https://www.flightglobal.com/news/articles/flight-test-bombardier-415-the-superscooper-331305/`.

[73] Cantor, B., Assender, H. and Grant, P., "Aerospace Materials", Institute of Physics Publishing, Bristol, 2001.

[74] Shen, H., Perkins, N.H., Lin, K. and Zarmehr, A., "Energy-Saving Formation Flight: A Review of the Past, Present, and Future", International Journal of Innovative Research in Technology & Science, Vol. 4, No. 3, May 2016.

[75] National Interagency Fire Center, "Interagency Standards for Fire and Fire Aviation Operations", Boise, Idaho, USA, February 2019

[76] Cernan, J., Hocko, M. and Cuttuva, M., "Safety Risks of Biofuel Utilization in Aircraft Operations", Transportation Research Procedia, Vol. 28, 2017, pp. 141-148.

[77] Zhou, L., Liu, Z. and Wang, Z., "Numerical Study of Influence of Biofuels on the Combustion Characteristics and Performance of Aircraft Engine System", Applied Thermal Engineering, Vol. 91, 2015, pp. 399-407.

[78] Yang, J., Xin, Z., He, Q., Corscadden, K. and Niu, H., "An Overview on Performance Characteristics of Bio-jet Fuels", Fuel, Vol. 237, 2019, pp. 916-936.

[79] Hitchcock, D., "Ready for Takeoff? Aviation Biofuels Past, Present, and Future", Atlantic Council, 2019

[80] Weick, F. E., "Propeller Design. Practical Application of the Blade Element Theory I", NACA TN-235, 1926.

[81] Reede, C.H., "Verzameling van schroefgegevens", Technische Hogeschool Vliegtuigbouwkunde, 1957.

[82] Martínez-de Dios, J. R., Merino, L., Caballero, F. and Ollero, A., "Automatic Forest-Fire Measuring Using Ground Stations and Unmanned Aerial Systems", NCBI, June 2011.

[83] U.S Department of Transportation, Federal Aviation Administration, "Instrument Flying Handbook", FAA-H-8083-15B, 2012.

[84] Weick, F. E., "Aircraft Propeller Design", NACA, McGraw-Hill Book Company inc., London, UK, 1930.